Biocompatible nanosystems for innovative applications of small therapeutic molecules

Ilaria Andreana

N°d'ordre 2022LYSE1001

THESE de DOCTORAT DE L'UNIVERSITE DE LYON
opérée au sein de
l'Université Claude Bernard Lyon 1
en co-tutelle avec:
l'Università degli Studi di Torino

Ecole Doctorale EDISS 205
(Ecole Doctorale Interdisciplinaire Sciences-Santé)

Spécialité de doctorat : Sciences Pharmaceutiques et Biomoléculaires

Soutenue à huis clos le 21/07/2022, par:

Ilaria ANDREANA

Biocompatible nanosystems for innovative applications of small therapeutic molecules

---

Devant le jury composé de:

MATRICARDI, Pietro, Professeur, Università di Roma "La Sapienza"	President
HILLAIREAU, Hervé, Professeur, Université Paris-Saclay	Rapporteur
NICOLI, Sara, Professeure associée, Università di Parma	Rapporteure
BRIANCON, Stéphanie, Professeure, Université Claude Bernard Lyon1	Examinatrice
DE ROSA, Giuseppe, Professeur, Università di Napoli "Federico II"	Examinateur
STELLA, Barbara, Professeure associée, Università di Torino	Directrice de thèse
KRYZA, David, Maître de conférences, Université Claude Bernard Lyon1	Directeur de thèse
LOLLO, Giovanna, Maître de conférences, Université Claude Bernard Lyon1	Co-Directrice de thèse

Università degli Studi di Torino

Dottorato in

Scienze Farmaceutiche e Biomolecolari

Tesi svolta presso il

Dipartimento di Scienza e Tecnologia del Farmaco
in co-tutela con:
Université Claude Bernard Lyon1

CICLO XXXIV

Biocompatible nanosystems for innovative applications of small therapeutic molecules

---

Tesi presentata da: **Ilaria ANDREANA**

TUTORS:
Prof.ssa Barbara STELLA, Università degli Studi di Torino
Dr. David KRYZA, Université Claude Bernard Lyon1
Dr. Giovanna LOLLO, Université Claude Bernard Lyon1

Coordinatore del dottorato: **Prof.ssa Roberta Cavalli**

Anni accademici**: 2018-2022**

Settore Scientifico-disciplinare di afferenza:
Farmaceutico Tecnologico Applicativo

Alla mia Famiglia

La forza non deriva dalle capacità fisiche,
ma da una volontà indomita.
(Mahatma Gandhi)

Acknowledgments

Defining the period of Ph.D. can be complicated. It is a long journey that challenges you. In the last three years and a half, I felt a lot of emotions: from joy to discouragement, from enthusiasm to depression, and finally to conquest. I believe that a Ph.D. means conquest. A personal conquest that has allowed you to get to know yourself a little bit more.

The people that I have met on my journey are a lot, maybe also because of the co-tutorship of this Ph.D. project. First, I would like to express my sincere thanks to my thesis advisors. From the Italian side, Pr. Barbara Stella, who contacted me in March 2018 letting me know about the opportunity of a Ph.D. At that moment, the Ph.D. seemed to be an important opportunity to be seized. You followed me with constancy and kindness, allowing me to gain experience and become more aware of myself. You persuaded me that science is a cool challenge, and that the final satisfaction is the best price. I would like to thank Dr. David Kryza and Dr. Giovanna Lollo from the French side. Both of you made it possible for me to be an Italian student in Lyon. Dr. David Kryza, with your kindness and understanding, managed to make me feel welcome. I will always be grateful to Dr. Giovanna Lollo. Although the beginning in Lyon was hard, you never gave up on me and tried to find a way to make me love the lab and the city. I know that dealing with me can be complicated because of my tears, but you tried, and you won. My period in Lyon was simply scientifically and humanely amazing.

I would like to acknowledge all the people that I met on my way. I would say thank you to Pr. Silvia Arpicco. I started to learn about science when you send me to Paris for my Erasmus period. Your enthusiastic approach to science made me believe that this is the most beautiful job in the world. A special thank goes to Pr. Dosio, Dr. Milla and Pr. Rolando for your time to collaborate with me and your professional input. Thanks to Yves and Claire for the opportunity to collaborate with you and for all your time considering my data. All your suggestions pushed me to consider my work from different perspectives. To Gaetan Juban and Remi Mounier, who gave me the opportunity to learn about biology and understand that it is complicated but really interesting. Thanks to Jaqueline, the moments all together with a lot of mice are always on my mind. Thanks to Delphine, Cynthia, Geraldine, Jean-Pierre, and Maria, who always asked me “Ça va, Ilaria?” and tried to understand my personal French vocabulary. I am grateful for the enthusiasm of all the people that crossed my way.

Many people are an important part of my life now. When I started my thesis in Turin, I found a wonderful team that changed over the years but always kept its positive vibes. And this is thanked to Valeria, firstly a simple colleague and now an incredibly good friend. You always

listen to me, in the best and the worst moments, saying that we can do everything together. I am starting to believe it.
Silvia, we started together with our incredible experience abroad. You have been my “ferry” toward Lyon, and you have been there since the beginning to help and listen to me.
A special thank goes to the French lab, which made me feel welcomed: Analisa, Serena, Chiara, Giulia, Tiffanie, and Valentine. All of you were there during sad and funny moments that I will bring with me forever. A particular thank is for Mathieu and Valentina. First, we were just officemates but now we are friends. I must tell you “thank you” and “I’m sorry.” You have put up with me in the worst times, but it is only thanks to you that I am a better person now. I grew up. Thank you for all the laughs, the coffees, the cokes, the apero, and the running times and to let me spend my time with you.
Another special thank is to all the people that were there before this period and shared with me a part of their life. Elisa, you are the most strange and special person that I know. I think in another life we could have been in love. You are the person with that I chose to share all my adventures. Together we are extraordinary. Thanks to Giulia, my lifelong friend. You are there even when life makes it challenging. We will always be friends because you made me the person that I am now. Thanks to all the people who enrich my life: Rabi, Deni, Robi, Ale, and Sara are sincere friends who make me believe that I am special.
I am incredibly lucky because my life is full of special people. This is possible thanks to my family. Mamma. Thank you for your unconditional love. You are always ready to listen to me and help me to be a better person. You remember me that I am special because you can see something that I cannot. Papà. Thank you for being my Papi. You always help me without asking and are always present. Thank you for your unconditional love because I know that it often can be hard dealing with me, but you always tried to do your best to make me feel happy. Thank you to my nonna, you are the only one and I hold you in my heart forever. To Flavio, my brother. It seems we come from two different universes, but your universe made the best choice to send you to me. Thank you for being how you are because when I am with you, the world and life seem easier.
Lastly, I thank the person who started with me this full-emotional period and is still here. Marco, I believe in you as you believe in me. Your love and patience make me feel lucky. Thank you for standing for me, for encouraging me every time that I thought it was too hard, and for celebrating by my side every single day. You make me feel extraordinary.
And at the end, I would thank the seven years old-Ilaria. I hope you can be proud of me because I realized your dream to be “the person who works in a lab”.

Tables of contents

Abstract

Nanomedicine is a potential strategy to improve the clinical applicability of active molecules through the formulation of drug delivery systems (DDSs). One of the main hurdles for developing DDSs lies in their potential toxicity. The aim of the present work was the development of biocompatible nanoparticles (NPs) for innovative applications of small therapeutic molecules. Lipid and polymer-based nanocarriers were designed to improve the therapeutical applicability of pentamidine (PTM) as repurposed anticancer drug, avoiding drug derivatization and exploiting the classical nanoprecipitation technique. However, manufacturing limitations opened the way to the development of innovative production processes. To address challenges in NP formulation, the microfluidic technology has been proposed for its advantages. Thus, a manufacturing translation study of poly(lactic-*co*-glycolic acid) (PLGA)-based NPs from conventional nanoprecipitation to the microfluidic process was set up, choosing a model drug, namely 991. Moreover, biological evaluation of 991-loaded NPs, as a potent activator of AMP-kinase protein involved in reducing inflammation and fibrosis in Duchenne muscular dystrophy, was assessed. Biological findings demonstrated a reduction in a pro-inflammatory cytokine in presence of drug in fibrotic macrophages cells. *In vivo* administration of loaded NPs resulted in a 10% of fibrosis reduction in muscular cells, suggesting an improvement of muscular homeostasis.

In the last part of the project, stearoyl-L-carnitine (SC) was used to actively target polymer NPs toward muscular specific receptors, namely OCTN2. *In vitro* tests on C2C12 cell line demonstrated a higher expression of OCTN2 receptor on myotubes than myoblasts, occurring in increased NPs internalization. In the frame of drug repurposing, PTM has been efficiently encapsulated into SC-associated NPs to enhance drug delivery toward muscular cells.

Overall, this thesis provided an extensive investigation of lipid and polymer-based DDSs to improve the therapeutic applicability of two small molecules and underlined the importance of the manufacturing technique for NP features.

Sommaire

La nanomédecine est une stratégie efficace pour améliorer le potentiel clinique de molécules actives par la formulation de systèmes d'administration de médicaments (DDSs). L'un des principaux obstacles au développement de ces systèmes réside dans leur toxicité éventuelle. L'objectif de ce travail était de développer des nanoparticules (NPs) biocompatibles pour des applications innovantes de petites molécules thérapeutiques. Des NPs à base de lipides et de polymères ont été conçus pour améliorer le potentiel thérapeutique de la pentamidine (PTM) en tant que médicament anticancéreux, en exploitant la technique classique de nanoprécipitation. Cependant, les difficultés de fabrication ont ouvert la voie au développement d'un processus de production innovant. Pour relever les défis de la formulation des NPs, la technologie microfluidique a été proposée pour ses avantages. Ainsi, une étude de transposition de la nanoprécipitation classique au processus microfluidique pour la fabrication de NPs à base d'acide poly(lactique-*co*-glycolique) (PLGA) a été mise en place, en choisissant un médicament modèle, à savoir le 991. En outre, l'évaluation biologique des NPs chargées de 991, en tant qu'activateur puissant de la protéine AMP-kinase impliquée dans la réduction de l'inflammation et de la fibrose dans la dystrophie musculaire de Duchenne, a été évaluée. Les résultats biologiques ont démontré une réduction d'une cytokine pro-inflammatoire, en présence du médicament dans les cellules macrophages fibrotiques. L'administration *in vivo* de NPs chargées a entraîné une réduction de 10% de la fibrose dans les cellules musculaires, ce qui suggère une amélioration de l'homéostasie musculaire.

Dans la dernière partie du projet, la stéaroyl-L-carnitine (SC) a été utilisée pour marquer les NPs polymériques et cibler activement des récepteurs musculaires spécifiques, à savoir OCTN2. Des tests *in vitro* sur la lignée cellulaire C2C12 ont démontré une plus grande expression du récepteur OCTN2 sur les myotubes que sur les myoblastes, ce qui a entraîné une plus grande internalisation des NPs. Dans le cadre du repositionnement de médicaments, le PTM a été efficacement encapsulé dans des NPs marquées avec de la SC pour améliorer l'administration de médicaments aux cellules musculaires.

Dans l'ensemble, cette thèse a permis d'étudier de manière approfondie les DDS à base de lipides et de polymères pour améliorer l'efficacité thérapeutique de deux petites molécules et a également souligné l'importance de la technique de fabrication sur les caractéristiques des NPs.

Riassunto

La nanomedicina è considerata una strategia per migliorare l'applicabilità clinica di molecole farmacologicamente attive attraverso la formulazione di sistemi di rilascio dei farmaci (DDSs). Uno dei principali ostacoli allo sviluppo dei DDSs risiede nella loro potenziale tossicità. Lo scopo del presente lavoro è stato lo sviluppo di nanoparticelle (NPs) biocompatibili per applicazioni innovative di diversi principi attivi. Nanoparticelle a base lipidica e polimerica sono state progettate per migliorare l'applicabilità della pentamidina (PTM) nella terapia antitumorale, evitando la derivatizzazione del farmaco e sfruttando la tecnica classica della nanoprecipitazione. Tuttavia, alcuni limiti formulativi delle NPs hanno reso necessario lo sviluppo di processi produttivi innovativi. A questo scopo la tecnologia della microfluidica è stata proposta per i suoi vantaggi: è stato quindi proposto uno studio di traslazione della produzione di NPs a base di acido poli(lattico-*co*-glicolico) (PLGA) dalla nanoprecipitazione convenzionale al processo microfluidico, incorporando un farmaco modello chiamato 991, potente attivatore della proteina AMP-chinasi coinvolta nella riduzione dell'infiammazione e della fibrosi nella distrofia muscolare di Duchenne. Successivamente, è stata effettuata una valutazione biologica delle NPs caricate con 991. I risultati hanno dimostrato una diminuzione di una specifica citochina pro-infiammatoria, in presenza di farmaco nelle cellule macrofagiche fibrotiche. La somministrazione *in vivo* di 991 incorporato nelle NPs ha determinato una riduzione del 10% della fibrosi nelle cellule muscolari, suggerendo un miglioramento dell'omeostasi muscolare.

Nell'ultima parte del progetto la stearoil-L-carnitina (SC) è stata utilizzata per indirizzare attivamente le NPs polimeriche verso recettori muscolari specifici, in particolare OCTN2. I test *in vitro* sulla linea cellulare C2C12 hanno dimostrato una maggiore espressione del recettore OCTN2 nei miotubi rispetto ai mioblasti, con conseguente aumento dell'internalizzazione delle NPs. Sulla base di dati in letteratura riguardanti un possibile *repurposing* della PTM, questa molecola è stata incapsulata in modo efficiente in NPs associate a SC per migliorare la veicolazione di farmaci verso le cellule muscolari.

Complessivamente, questo lavoro ha fornito un'analisi approfondita sui DDSs a base di lipidi e polimeri per migliorare l'applicabilità terapeutica di due diversi principi attivi, sottolineando l'importanza del processo produttivo per le caratteristiche delle NPs.

List of Figures

State of the art

Review – Nanotechnological approaches for pentamidine delivery

Review– Nanomedicine for gene delivery and drug repurposing in the treatment of muscular dystrophies

Fig. 4 Strategies and accurate models to explore MD treatments. Broad in vitro, ex vivo and in vivo MD models to promote the translation on nanomedicine-based therapies (MD, muscular dystrophies; X-MET, ex vivo-vascularized muscle engineered tissue).

Chapter I

Fig. 1 Chemical structures of SQ-COOH (a) and PTM-B (b).

Fig. 2 Aggregation process of SQ-COOH (SQA) and PTM-B (PTM) molecules during MD simulations. Each row corresponds to a simulation, the number of SQ-COOH and PTM-B molecules is reported in brackets. Frames were extracted at the beginning ($t = t_0$), at half ($t = ½ t_1$) and at the end ($t = t_1$) of the simulation time. Molecules are depicted as capped sticks, in cyan (PTM-B) and beige (SQ-COOH). Each aggregate is labelled according to the SQ-COOH/PTM-B ratio.

Fig. 3 Cryo-TEM images of SQ-COOH/PTM-B 3:1 (V_e/V_w 0.2:1) nanoparticles.

Fig. 4 PTM-B release from SQ-COOH/PTM-B 3:1 (V_e/V_w 0.2:1) nanoparticles as a function of time in PBS pH 7.4 or acetate buffer pH 5.0 at 37 °C.

Fig. 5 Expression of LDLR in different cancer cell lines. Whole extracts and plasma-membrane associated extracts from breast cancer MCF7 and MDA-MB-231 cells, prostate cancer LNCap and PC-3 cells, hepatoma HepG2 cells, cultured 24 h in medium with (+) or without (-) 10% v/v FBS, with (+) or without (-) 10 μM simvastatin (SIM) were analyzed for the expression of LDLR. β-tubulin and pancadherin were used as control of equal protein loading. The figure is representative of 1 out of 3 experiments.

Fig. 6 Dose- and time-dependent cytotoxicity of SQ-COOH/PTM-B 3:1 (V_e/V_w 0.2:1) nanoparticles. LDLR-positive (MDA-MB-231, PC-3 and HepG2) and LDLR-negative (MCF7 and LNCap) cell lines were incubated for 24, 48 or 72 h, in the absence (0) or in the presence of free PTM-B (PTM) or SQ-COOH/PTM-B 3:1 (V_e/V_w 0.2:1) nanoparticles (SQ-PTM-NP) at 10^{-7}, 10^{-6}, 10^{-5} M, in a medium with (+) or without (-) 10% v/v FBS. Before the incubation, SQ-COOH/PTM-B 3:1 (V_e/V_w 0.2:1) nanoparticles were maintained 30 minutes in complete medium containing 10% v/v FBS. Cell viability was measured in triplicates using a chemiluminescence-based assay. Data are presented as means $\pm$ SD. *$p<0.05$: *vs*. the respective untreated (0) cells; °$p<0.05$: SQ-COOH/PTM-B 3:1 (V_e/V_w 0.2:1) nanoparticles *vs.* PTM-B.

Fig. 7 Effects of simvastatin and FBS deprivation on the cytotoxicity of SQ-COOH/PTM-B nanoparticles. MCF7, PC-3 and HepG2 cell lines were incubated for 24 h in the absence or in the presence of 10 μM simvastatin (SIM), then washed and cultured for 72 h, in the absence (0) or in the presence of free PTM-B (PTM) or SQ-COOH/PTM-B nanoparticles (SQ-PTM-NP) at

10^{-7}, 10^{-6}, 10^{-5} M, in a medium with (+) or without (-) 10% v/v FBS. Before the incubation, SQ-COOH/PTM-B nanoparticles were maintained 30 minutes in complete medium containing 10% FBS. Cell viability was measured in triplicates using a chemiluminescence-based assay. Data are presented as means ± SD. *p<0.05: *vs*. the respective untreated (0) cells; °p<0.05: SQ-COOH/PTM-B nanoparticles *vs*. PTM-B; $^{\#}$p<0.05: SIM-treated cells *vs*. SIM-untreated cells.

Fig. 8 Effect of LDLR silencing on the cytotoxicity of SQ-COOH/PTM-B nanoparticles. HepG2 cell line was treated with a non-targeting scrambled siRNA pool (scr) or with a siRNA pool targeting LDLR (siLDLR), in medium with (+) or without (-) 10% v/v FBS, in the absence or in the presence of 10 μM simvastatin (SIM) for the last 24 h. **A.** The expression of LDLR in whole extracts and plasma-membrane associated extracts was analyzed by immunoblotting 48 h after the transfection. β-tubulin and pancadherin were used as control of equal protein loading. The figure is representative of 1 out of 3 experiments. **B.** Cells treated as reported in A were cultured in the absence (0) or in the presence of SQ-COOH/PTM-B nanoparticles at 10^{-7}, 10^{-6}, 10^{-5} M. After 72 h, cell viability was measured in triplicates using a chemiluminescence-based assay. Data are presented as means ± SD. *p<0.05: *vs*. untreated (0) cells; °p<0.05: siLDR cells *vs*. scr cells.

Suppl. Fig. 1 Intracellular cholesterol after FBS deprivation and simvastatin treatment. Breast cancer MCF7 and MDA-MB-231 cells, prostate cancer LNCap and PC-3 cells, hepatoma HepG2 cells, cultured 24 h in medium with (+) or without (-) 10% v/v FBS, with (+) or without (-) 10 μM simvastatin (SIM), were radiolabeled with 1 μCi/mL [^{3}H]-acetate for 24 h. Then, lipids were extracted, separated by TLC and the amount of synthesized cholesterol was measured by liquid scintillation. Data are presented as means ± SD. *p<0.05: SIM-treated *vs*. SIM-untreated cells; °p<0.05: FBS-deprived medium *vs.* FBS-containing medium.

Chapter II

Fig. 1 Chemical structure of PTM.

Fig. 2 Representative cryo-TEM images of (a) unloaded PLGA 75:25 nanoparticles; (b) PTM-B-loaded PLGA 75:25 nanoparticles; and (c) PTM-B-loaded PLGA 75:25/PEG_{2000}-PLGA 1:0.5 nanoparticles. Bar, 200 nm.

Fig. 3 Representative cryo-TEM images of (a) unloaded liposomes; (b) Lipo PTM-C; and (c) Lipo PTM-S. Bar, 200 nm.

Chapter III

Fig. 1 TEM images of PLGA nanoparticles prepared by microfluidic procedure.

Fig 2 Turbidity variation in function of salt additions at increasing concentrations of NaCl. (A) Nanoprecipitation and (B) microfluidic technique. (C-D) Stability ratio *versus* NaCl and *CCC* calculation. (C) Nanoprecipitation and (D) microfluidic technique.

Fig. 3 Turbidity variation in function of salt addition in presence of Pluronic F68. Neither nanoparticles prepared by nanoprecipitation technique (A), nor nanoparticles prepared by microfluidic process (B) showed aggregation after salt addition.

Chapter IV

Fig. 1 Schematic representation of the microfluidic micromixer.

Fig. 2 Release profile of drug-loaded PLGA NPs in PBS medium at 37 °C.

Fig. 3 TEM images of (A-B) PLGA NPs and (C-D) loaded NPs prepared by microfluidic technique.

Fig. 4 Contour plots of the response surface for EE and DL at FRR 1:5 (a), 1:3.5 (b) and 1:2 (c).

Fig. 5 Characterization of drug-loaded NPs after freeze-drying. (A) Stability study (size, and PDI) upon resuspension of loaded freeze-dried nanoparticles. (B) TEM images of freeze-dried loaded-PLGA NPs after resuspension.

Chapter V

Fig. 1 (A) Scheme of the experimental design. (B) Intracellular uptake of PLGA nanoparticles in fibrotic BMDMs. Confocal fluorescence microscopy of BMDMs (I-VI) that have been incubated with nanoparticles for 2 h (I, II), 4 h (III, IV) and 24 h (V, VI). PLGA nanoparticles were loaded with DiD (red fluorescence) and cell membranes are counterstained with Cy3 fluorophore (green fluorescence). Hoechst 33258 (blue fluorescence) staining depicts nuclei. (C, D) BMDMs were treated with free and loaded 991 (NPs 991-PLGA) for 6 h, and the phosphorylation of ACC (p-ACC) was quantified by immunoblotting (C-D). (C) Representative immunoblots showing p-ACC, total ACC, and β-actin as a loading control (NT, non-treated). (D) Quantification of the ratio of phosphorylated and total ACC protein. (E) $TGF\beta_1$ production of BMDMs incubated overnight with free drug, PLGA nanoparticles, and drug-loaded PLGA nanoparticles at a concentration of 10 μM. (F) Annexin V/DAPI staining of fibrotic BMDMs. The cells were incubated for 24 h with free 991 and 991-loaded nanoparticles at a concentration of 20 μM. Data are presented as means $\pm$ SEM. **$p<0.01$, *** $p<0.0005$.

Fig. 2 (A) Scheme of the experimental design. (B) Organ ex vivo biodistribution of DiD-loaded PLGA nanoparticles, at selected time points. (C) Quantification of mean fluorescence intensity

in fluorescent organs. (D) Quantification of mean fluorescence intensity in diaphragm. (E) Quantification of cells which internalized fluorescent-PLGA nanoparticles by FACS analysis in diaphragm cells. (F) Quantification of cells which internalized fluorescent-PLGA nanoparticles by FACS analysis in gastrocnemius cells. Data is shown as mean ± SEM (n =3).

Fig. 3 991-PLGA nanoparticles treatment ameliorates dystrophic muscle phenotype. (A-F) D2.mdx mice were treated every other day for three weeks, and diaphragm and gastrocnemius were harvested. (A) Scheme of the experimental design. (B-C) FACS analysis of the surface marker CD45+ and CD64+ in gastrocnemius for sample treated with PLGA nanoparticles (B, left) and 991-PLGA nanoparticles (B, right). (C) Percentage of positive macrophages in gastrocnemius. (D-E) Muscle sections were immunostained for Coll1. (D) Representative images of Coll1 immunostained in the diaphragm. (E) Percentage of Coll1 area in the diaphragm. (F-G) Muscle mass normalized to mouse body weight for diaphragm (F) and (G) gastrocnemius.

Chapter VI

Fig. 1 Cellular uptake of SC-PLGA nanoparticles: functionalized nanoparticles bind to OCTN2 receptor on cell membrane, forming a complex that is then internalized into the cell.

Fig. 2 PTM-B release from 5% SC-nanoparticles as a function of time after incubation in PBS pH 7.4 at 37 °C.

Fig. 3 C2C12 cell viability evaluated by MTT test after 2 h (A), 24 h (B), 24 h + 24 h recovery (C) treatment in presence of 5% SC-nanoparticles. Data are given as mean SEM, representative of three independent experiments. * $p< 0.03$ *vs* control (CTR) sample.

Fig. 4 TEM analysis of 5% SC-nanoparticles uptake and intracellular fate. TEM images of a C2C12 myoblast incubated for 2 h with 5% SC-nanoparticles (A-B). Two nanoparticles (arrows) are entering the cell by endocytosis (A). A nanoparticle (arrow) is escaping an endosome (B). TEM images of a C2C12 myoblast incubated for 24 h with 5% SC-nanoparticles (C-E). Two nanoparticles (arrows) occur free in the cytosol (C). Three nanoparticles (arrows) occur inside secondary lysosomes (D-E).

Fig. 5 Fluorescence microscopy micrographs of a myoblast (A) and a myotube (B) immunolabelled for OCTN2 (green); counterstaining with phalloidin (red). Note the high number of receptors in the myotube

Fig. 6 (A) Confocal fluorescence microscopy analysis of myotubes that have been incubated with (A-a) untargeted nanoparticles and (A-b) 5% SC-conjugated PLGA nanoparticles. Nanoparticles are loaded with Nile Red (red fluorescence) and cells are counterstained with

phalloidin conjugated with Alexa488 (green fluorescence). Hoechst 33342 (blue fluorescence) staining depicts cell nuclei. (B) Morphometric analysis of C2C12 myoblasts for nanoparticles (NPs).

Discussion

Fig. 1 Schematic representation of self-assembled NPs by electrostatic interactions.

Fig. 2 Comparative analysis of nanoprecipitation and microfluidic technique.

List of Tables

Table 2 Cytotoxic activity (IC_{50}) on human tumor cell line A2780 at 24, 48, and 72 h. The values are arithmetic means of 3 determinations (N=3; SD<10% for all values).

Chapter III

Table 1 Mean diameter, ζ potential and critical coagulation concentration (CCC) of PLGA nanoparticles prepared by two different techniques.

Chapter IV

Table 1 Selected experimental factors and their coded levels in the 2^3 full factorial design.

Table 2 Physicochemical characterization of blank and loaded PLGA NPs prepared by nanoprecipitation (N) and microfluidic technique (M). Values are given as mean ± SD (*n*=3). NPs nanoparticles; PDI: polydispersity index.

Table 3 Experimentation plan built according to a 2^3 full factorial design (runs 1 to 8) with two additional center points (runs 9 and 10) with the corresponding responses.

Table 4 Physicochemical characterization of loaded-PLGA NPs prepared by microfluidic technique, before and after freeze-drying.

Chapter VI

Table 1 Physicochemical characteristics (mean diameter, PDI and zeta potential) of nanoparticles.

List of abbreviations

AB: antibody
Abs: absorbance
ACC: acetyl-CoA-carboxylase
AMPK: AMP-protein kinase
ASO: antisense oligonucleotides
BBB: blood brain barrier
BMDMs: bone marrow derived macrophages
BSA: bovine serum albumin
CCC: critical coagulation concentration
CFM: confocal microscopy
CMC: critical micellar concentration
Coll1: collagenase 1
CSA: cross-sectional area
CY: cyanine
DAPI: 4′,6-diamidino-2-phenylindole
DDS: drug delivery system
DiD: 1,1′-dioctadecyl-3,3,3′,3′-tetramethylindodicarbocyanine, 4-chlorobenzenesulfonate salt
DL: drug loading
DLS: dynamic light scattering
DLVO theory: Derjaguin, Landau, Verwey and Overbeek theory
DM1: Dystrophia Myotonica 1
DMD: Duchenne muscular dystrophy
DMEM: Dulbecco's Modified Eagle Medium
DMSO: dimethyl sulfoxide
DoE: design of experiments
ECM: extracellular matrix
EDTA: ethylenediamine tetraacetic acid
EE: encapsulation efficiency
EGTA: ethylene glycol-bis(beta-aminoethyl ether)-N-tetraacetic acid
ELISA: enzyme-linked immunosorbent assay
EMA: European Medical Agency
EPR: enhanced permeation and retention effect
Ex: excitation
FACS: fluorescence activated cell sorting
FBS: fetal bovine serum
FDA: Food and Drug Administration
FITC: fluorescein-5-isothiocyanate
FNP: flash nanoprecipitation
FRR: flow rate ratio
GA: glycolic acid
GI: gastrointestinal track
GMP: good manufacturing practice
I.M.: intramuscular
I.V.: intravenous injection
LA: lactic acid
LDL: low density lipoproteins

LDLR: low density lipoprotein receptor
LNCs: lipid nanocapsules
LNPs: lipid nanoparticles
LP: lipoproteins
LTBP4: latent-TGF-β-binding protein
MD: molecular dynamics
MTT: (3-(4,5-dimethylthiazol-2-yl)-2,5-diphenyltetrazolium bromide) tetrazolium
NMD: neuromuscular diseases
NPs: nanoparticles
NT: untreated
OCTN2: organic cation/carnitine transporter
OD: optical density
PBS: phosphate buffer saline
PDI: polydispersity index
PEG: poly(ethylene glycol)
PLGA: poly(lactic-*co*-glycolic) acid
PMSF: phenylmethanesulfonyl fluoride
PTM: pentamidine
PTM-B: pentamidine free base
PVA: poly(vinyl alcohol)
RBC: red blood cells
S.C.: subcutaneous
SC: stearoyl-L-carnitine
SCR: scrambled siRNA
SLC22: Solute Carrier Family 22
SLNs: solid lipid nanoparticles
SQ: squalene
SQ-COOH: squalenic acid
TA: tibialis anterior
TEM: transmission electron microscopy
TFA: trifluoracetic acid
TFR: total flow rate
TGFβ: transforming growth factor-beta
TLC: thin layer chromatography
UHPLC: ultra high performance liquid chromatography

Thesis overview

Nanomedicine is a potential strategy to improve the clinical applicability of several active molecules through the formulation of nanosystems, namely drug delivery systems (DDSs). Over the last decades, DDSs have been extensively studied for designing more effective and safer treatments with significant applications against many pathologies, such as cancer, brain disorders, and immune diseases. One of the main hurdles for developing DDSs lies in their potential toxicity. On these bases, the aim of the present work was the development of biocompatible nanoparticles (NPs) for innovative applications of small therapeutic molecules. In particular, lipid and polymer-based nanocarriers were designed to improve the therapeutical applicability of pentamidine (PTM). PTM is an old antiprotozoal drug, whose repositioning for its anticancer activity and application in muscular dystrophy treatment has been recently proposed. Therefore, in the first part of this thesis, a squalene derivative (SQ-COOH) and poly(lactic-*co*-glycolic) acid (PLGA) were selected as biocompatible materials to efficiently encapsulate PTM free base (PTM-B), thus avoiding drug derivatisation. Electrostatic interactions between the positively charged amidine groups of PTM-B (pKa=12) and negatively charged lipid or polymer vehicle (pKa=4.5) occurred to stabilize the loaded nanosystems. For SQ-COOH-based NPs, the maximization of drug loading (DL) was achieved working at SQ-COOH/PTM-B molar ratio 3:1 and 0.2 volume ratio ($V_{ethanol}/V_{water}$) during the preparation procedure. The formulation of PTM-B into polymer NPs led to system stabilization by electrostatic interactions between the drug and acid-terminated PLGA. Both nanosystems were designed to test the anticancer activity of PTM-B *in vitro*, confirming the internalization of NPs in cancer cell lines and the pH-depend drug release profile. Lipid and polymer-based nanocarriers were formulated by exploiting the classical nanoprecipitation technique. However, manufacturing limitations, such as batch-to-batch variability, control of NP physicochemical characteristics and the need to scale up the process, opened the research to the development of innovative production processes. To address these current challenges in NP formulation, microfluidic technology has been proposed for its advantages. Thus, in the second part of this thesis, a manufacturing translation study of PLGA NPs from conventional nanoprecipitation to the microfluidic process was set up, choosing a small benzimidazole molecule as the model drug, namely 991. By setting microfluidic parameters (*e.g.*, total flow rate - TFR - and flow rate ratio - FRR) we obtained sub-100 nm NPs with high DL. NP translation was optimized with the aid of a design of experiments (DoE), which checked the influence of FRR, polymer and drug concentration in the organic phase on encapsulation efficiency and DL. Our findings demonstrated how FRR (1:5) plays a key role in improving the nanosystem drug content.

The third part of this project was focused on the biological evaluation of the 991-loaded NPs, as a potent activator of AMP-kinase (AMPK) protein involved in reducing inflammation and fibrosis in Duchenne muscular dystrophy (DMD). Biological findings demonstrated a reduction in transforming growth factor-β ($TGF\beta_1$) expression, a pro-inflammatory cytokine, in presence of free or loaded drug in fibrotic bone marrow-derived macrophages (BMDMs) cells. *In vivo* administration of loaded PLGA NPs resulted in a 10% of fibrosis reduction in muscular cells of the diaphragm and gastrocnemius, the most representative muscles in DMD mouse model. The preliminary *in vivo* results suggested an improvement of muscular homeostasis by 991-loaded nanocarrier administration.

The last part of the research project gave preliminary results to develop an active targeting strategy to increase muscular tropism. Stearoyl-L-carnitine (SC) was used to precisely target PLGA NPs toward muscular specific receptors, namely Na^+- organic/cation transporter 2 (OCTN2). Two different concentrations of SC (5% and 10% w/w) were assessed to find the balanced ligand density. *In vitro* tests on C2C12 cell line demonstrated a higher expression of OCTN2 receptor on myotubes than myoblasts, occurring in increased NPs internalization. In the frame of drug repurposing, PTM-B has been efficiently encapsulated into SC-associated PLGA NPs to enhance drug delivery toward muscular cells.

Overall, this thesis provided an extensive investigation of lipid and polymer-based DDSs to improve the therapeutic applicability of two small molecules. The critical analysis of the manufacturing process underlined the importance of the technique and formulative parameters which might influence NP features. Moreover, these small molecules have been assessed for alternative applications, highlighting drug repositioning in cancer therapy and treatment of muscular diseases.

General introduction

Controlled drug delivery technology has progressed over the last years as reflected by the exponential growing of publications and preclinical/clinical studies showing the importance of micro- and nano-carriers. Innovation has been developed by the formulation of systems that are able to deliver molecules of different nature (*e.g.* essential oil, drugs, antimicrobial molecules, etc.) and even target specific tissue [1–3]. These innovative systems may have a different nature including polymer, lipidic and inorganic structures and they are referred as drug delivery systems (DDSs) [4–6]. The application of DDSs to human health identifies a large and interesting field of study called nanomedicine. Nanomedicine gives the tools to overcome many drawbacks related to the therapeutic and pharmacological issues of many drug molecules. Mean advantages arise from the properties of technological carriers and the ability to encapsulate molecules, modulating their physicochemical characteristics [7]. In this frame, the use of nanoparticles (NPs), particularly lipidic and polymer NPs, proved to be a promising strategy to improve drugs administration and delivery in therapeutic approaches. By leveraging the mechanism of passive (endocytosis, extravasation into inflamed tissue, enhanced permeation and retention effect - EPR) or active targeting by the modification of the surface of DDSs (selective ligands, peptides, antibodies), a variety of nanocarriers have been developed. Among polymer DDSs, poly(lactic-*co*-glycolic acid) (PLGA) NPs are attractive candidates because of their biocompatibility and biodegradability, and their ability to encapsulate hydrophobic as well as hydrophilic molecules [8]. PLGA is considered one of the most successfully biodegradable polymers, approved by Food and Drug Administration (FDA) and European Medicine Agency (EMA) for human parental administration [9]. PLGA is able to spontaneously form NPs upon dispersion in an aqueous phase, resulting in a stable colloidal dispersion. The formulation of polymer NPs involves a large range of methods; among them, solvent displacement or nanoprecipitation is the simplest and most commonly used laboratory procedure [10,11].

Despite several technological advances, some biological challenges, improvable drug loading, modulation of drug release, active targeting toward a precise site of action, and off-target effects, are still preventing these delivery strategies from complete application in clinics [12]. In this context, the application of nanomedicine is a key point in research activity due to the enormous advantages that a nanotechnological approach can provide.

References

1. Park, K. Controlled Drug Delivery Systems: Past Forward and Future Back. *J Control Release* **2014**, *190*, 3–8, doi:10.1016/j.jconrel.2014.03.054.
2. Jain, K.K. An Overview of Drug Delivery Systems. *Methods Mol Biol* **2020**, *2059*, 1–54, doi:10.1007/978-1-4939-9798-5_1.
3. Nirmala, M.J.; Durai, L.; Gopakumar, V.; Nagarajan, R. Preparation of Celery Essential Oil-Based Nanoemulsion by Ultrasonication and Evaluation of Its Potential Anticancer and Antibacterial Activity. *Int J Nanomedicine* **2020**, *15*, 7651–7666, doi:10.2147/IJN.S252640.
4. Stella, B.; Andreana, I.; Zonari, D.; Arpicco, S. Pentamidine-Loaded Lipid and Polymer Nanocarriers as Tunable Anticancer Drug Delivery Systems. *J Pharm Sci* **2020**, *109*, 1297–1302, doi:10.1016/j.xphs.2019.11.011.
5. Cosco, D.; Tsapis, N.; Nascimento, T.L.; Fresta, M.; Chapron, D.; Taverna, M.; Arpicco, S.; Fattal, E. Polysaccharide-Coated Liposomes by Post-Insertion of a Hyaluronan-Lipid Conjugate. *Colloids and Surfaces B: Biointerfaces* **2017**, *158*, 119–126, doi:10.1016/j.colsurfb.2017.06.029.
6. Peretti, E.; Miletto, I.; Stella, B.; Rocco, F.; Berlier, G.; Arpicco, S. Strategies to Obtain Encapsulation and Controlled Release of Pentamidine in Mesoporous Silica Nanoparticles. *Pharmaceutics* **2018**, *10*, E195, doi:10.3390/pharmaceutics10040195.
7. He, Y.; Liang, S.; Long, M.; Xu, H. Mesoporous Silica Nanoparticles as Potential Carriers for Enhanced Drug Solubility of Paclitaxel. *Mater Sci Eng C Mater Biol Appl* **2017**, *78*, 12–17, doi:10.1016/j.msec.2017.04.049.
8. Danhier, F.; Ansorena, E.; Silva, J.M.; Coco, R.; Le Breton, A.; Préat, V. PLGA-Based Nanoparticles: An Overview of Biomedical Applications. *J Control Release* **2012**, *161*, 505–522, doi:10.1016/j.jconrel.2012.01.043.
9. Sartor, O. Eligard: Leuprolide Acetate in a Novel Sustained-Release Delivery System. *Urology* **2003**, *61*, 25–31, doi:10.1016/s0090-4295(02)02396-8.
10. Fessi, H.; Puisieux, F.; Devissaguet, J.Ph.; Ammoury, N.; Benita, S. Nanocapsule Formation by Interfacial Polymer Deposition Following Solvent Displacement. *International Journal of Pharmaceutics* **1989**, *55*, R1–R4, doi:10.1016/0378-5173(89)90281-0.
11. Almoustafa, H.A.; Alshawsh, M.A.; Chik, Z. Technical Aspects of Preparing PEG-PLGA Nanoparticles as Carrier for Chemotherapeutic agents by Nanoprecipitation Method. *International Journal of Pharmaceutics* **2017**, *533*, 275–284, doi:10.1016/j.ijpharm.2017.09.054.
12. Wicki, A.; Witzigmann, D.; Balasubramanian, V.; Huwyler, J. Nanomedicine in Cancer Therapy: Challenges, Opportunities, and Clinical Applications. *Journal of Controlled Release* **2015**, *200*, 138–157, doi:10.1016/j.jconrel.2014.12.030.

State of the art

I.1 Current state-of-art of nanotechnology applications

Nanotechnology and nanoscience play a key role in the field of medicine, mainly due to the limitations affecting the conventional medical agents, older formulations and delivery systems. Nanomedicine is highly active field, which involves several production devices and systems with innovative properties and functions. The design of nanomaterials in nanometer size range for medical applications is aimed at the identification of a sort of shuttle that transports active substances (*e.g.*, genetic materials, probes, small molecules) specifically to the intended target, reducing off-target effects and enhancing pharmacological activity, overcoming biological barriers. Over the years, pieces of evidence have confirmed the ability of several nanomedicines (both non-targeted and targeted) to improve active payload concentrations at the target site (*e.g.* tumor environment) [1,2], as well as to reduce toxicity [3] and enhance therapeutic efficacy compared with free drugs in preclinical studies [4]. Moreover, clinical studies in humans underlined the importance of nanotechnology in biomedicine for the diagnosis and therapy of many human diseases [5–7]. There are currently over 50 nanomedicine and nanotechnology-based medical products approved for a variety of clinical indications (Tab. 1) [8]. When administered, the fate of DDSs in the human body can be modulated by changing their surface chemistry or their physicochemical features to improve the accumulation into the target tissues or avoid rapid clearance (Fig. 1). The possibility to personalize treatments and address the therapies needed to increase the promising shift within the nanomedicine field involving cardiovascular [9], autoimmune [10] and genetic and rare disorders [11].

Notably, in cancer therapy, the application of DDSs led to the commercialization of doxorubicin-loaded PEGylated liposomes in the treatment of solid tumors (Doxil®) [12]. Thanks to the EPR effect, liposomes easily accumulate into tumors, delivering doxorubicin and avoiding adverse effects and high doses. The development steps of the Doxil® formulation evidenced the importance of the cross-talk between physicochemical, nanotechnological and biological principles to reach a final commercialized product. Furthermore, the importance of nanotechnology to improve pharmacological efficacy compared to the free drug was achieved by Abraxane® (albumin-bound paclitaxel NPs). It showed its superior efficacy to conventional paclitaxel for the treatment of solid cancers [13]. The 2018 FDA and EMA approval of the first RNA interference NPs treatment (Onpattro®) defined a shift in the market of nucleic acid therapies [14]. Messenger RNA vaccines development for the Sars-CoV-2 has gained emergency use authorization by international agencies. Indeed, BioNTech/Pfizer and Moderna vaccines are based on lipidic DDSs able to deliver genetic material and stimulate immune response towards virus infection [15,16]. The development of lipid nanoparticles (LNPs) has

become the gold standard in the non-viral delivery of genetic material. The study of LNPs morphology and lipid composition has crucial application in the prevention and treatment of infectious diseases *via* LPN-mRNA vaccines [17,18], opening the possibilities for new approaches to diseases prevention.

However, challenges are involved in the clinical development of nanomedicines, making difficult their clinical applicability. The translation of nano-strategies from the research level into the market product faces several challenges, which include characterization of physicochemical properties, process and quality control, biocompatibility and nanotoxicity, scalability-related issues and improvement of production scale as well as reproducibility [19]. Although the constant research and application of nanotechnology in the treatment of human diseases increased the interest in overcoming the drawbacks related to nanotechnology application, the continuous advances in preclinical studies do not correspond to the implementation of universally standardized practice and regulatory guidelines to easily promote clinical translation [20,21].

Although some aspects of the critical points of nanomaterials need to be put into perspective, it is undoubted that the overall poor transferability of nanoparticulate concepts into clinical applications calls for fundamental improvement [22]. While numerous nanoparticulate systems have already reached marketability, it is also clear that the current nanomedicine research, therefore, needs to rethink implementations of nanocarriers development [23].

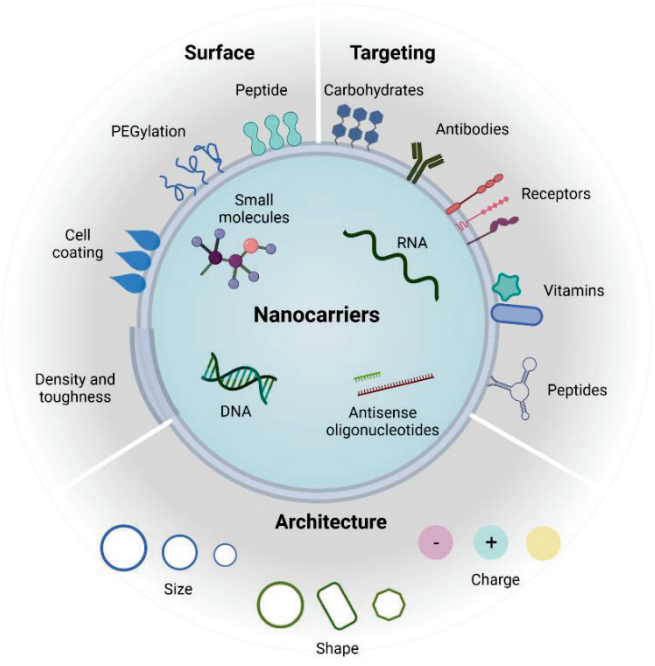

Fig. 1. Characteristics of DDSs that can be altered in intelligent design to tailor the platform to a specific application

Table 1 Examples of nanomedicines approved by FDA

	Formulations	Product names	Indications	Characteristics	Approval year
Polymer NPs	PLGA microparticles and leuprolide acetate	Lupron®	Central precocious puberty/endometriosis	Drug sustained release	1995
	Leuprolide acetate and polymer PLGA	Eligard®	Prostate cancer	Drug sustained release	2002
	PEGylated INF alpha-2a protein	Pegasys®	Hepatitis B and C	Improved protein stability by PEGylation	2002
	PEGylated anti-VEGF aptamer (vascular endothelial growth factor) aptamer	Macugen®	Decreased vision	Improved stability by PEGylation	2004
	Polymer-protein conjugate (PEGylated IFNbeta-1a)	Plegridy®	Multiple sclerosis	Improved protein stability by PEGylation	2014
	Polymer-protein conjugate (PEGylated factor VIII)	ADYNOVATE	Hemophilia	Improved protein stability by PEGylation	2015
Liposomal	Liposomal doxorubicin	Doxil®/Caelyx™	Karposi sarcoma, ovarian cancer, multiple myeloma	Increased tissue accumulation and decreased system toxicity	1995
	Liposomal daunorubicin	DaunoXome®	Karposi sarcoma	Increased tumor accumulation and decreased systemic toxicity	1996
	Liposomal amphotericin B	AmBisome®	Fungal infection	Reduced renal toxicity	1997
	Liposomal morphine sulphate	DepoDur®	Loss of pain	Prolonged drug release	2004
	Liposomal vincristine	Marqibo®	Acute lymphocytic blood clot	Increased tumor accumulation and decreased systemic toxicity	2012
	Liposomal irinotecan	Onivyde®	Pancreatic cancer	Increased tumor accumulation and decreased systemic toxicity	2015
Lipid NPs	siRNA lipoplexes	Onpattro®	Hereditary transthyretin amyloidosis	Improved stability of genetic material	2018
	mRNA-vaccine	Comirnaty®	Prevention of Sars-CoV-2 serius illness	Improved stability of genetic material	2020
	mRNA-vaccine	Spikevax®	Prevention of Sars-CoV-2 serius illness	Improved stability of genetic material	2020
Protein NPs	Engineered protein combining L-2 and diphtheria toxin	Ontak®	T-Cell lymphoma	T cell selective targeting	1999
	Albumin-bound paclitaxel NPs	Abraxane®	Breast cancer, non-small cell lung cancer, pancreatic cancer	Improved drug solubility and tissue accumulation	2005

I.2 Polymer-based drug delivery systems

Many different DDSs have been developed for a large number of applications in human diseases. Among the most used nanosystems, polymer-based DDSs have dominated the nanomedicine field, due to their ability to modulate their properties by combining different materials in a wide variety of macromolecular architectures. They are usually referred to as NPs and considered solid and spherical structures, produced adopting natural or synthetic polymers that can be either lipophilic or hydrophilic [24–26]. Polymer NPs offer drug protection from degradation, increased water solubility for hydrophobic molecules and allow a targeted administration to specific organs or cells. They are easily internalized by cells, partly through fluid-phase pinocytosis and also through clathrin-mediated endocytosis [27]. Their surface is generally considered thicker, stronger, and more stable than other DDSs (*e.g.* liposomes), thus opening additional interest for clinical applications. The wide range of polymers used for their preparation identifies polymer NPs as excellent candidates for molecules of different natures. Moreover, polymer-based DDSs can be administered by different administration routes, being suitable for intravenous injection (i.v.) due to their size of around 100-200 nm.

I.2.1 Classification of polymer-based drug delivery systems

Recent advances in nanotechnology provided a wide range of polymers able to be formulated into nanoparticulate carriers for various active molecules. The most adopted polymer-based nanocarriers for drug delivery comprise polymer micelles, polymersomes, dendrimers and polymer NPs (Fig. 2).

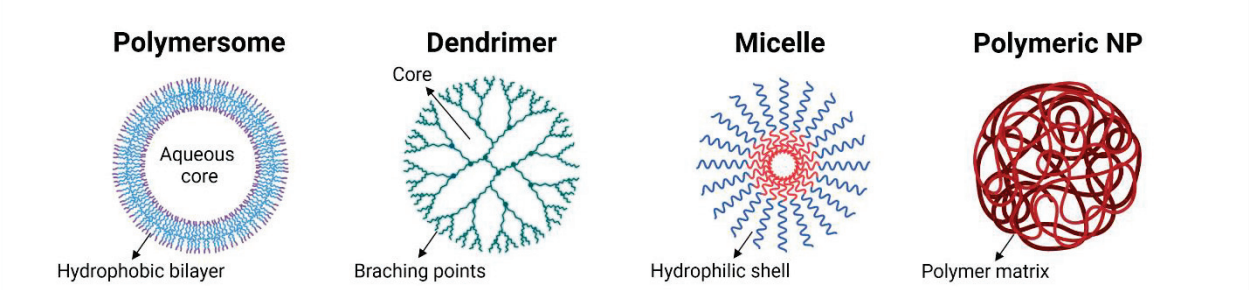

Fig. 2. Polymer DDSs

Polymersomes are spherical nanostructures made up of amphiphilic block copolymers, in which a hydrophobic bilayer encloses an aqueous core. Thanks to their nature, polymersomes are considered the only type of polymer DDSs that can physically encapsulate in the same NPs hydrophilic drugs in their aqueous core and/or hydrophobic agents within their lamellar membranes [28]. This characteristic represents the most important advantage of using

polymersomes. Despite this, the scalability of the production processes is still challenging, as well as storage and sterilization methods limit their application [29].

Dendrimers are polymer-based macromolecules with highly branched three-dimensional architecture whose monomers can impact both the surface and internal properties. The dendrimer architecture is characterized by void space for molecular encapsulation, branching points and surfaces groups [30]. Poly(amidoamine) (PAMAM) dendrimers were the first reported dendrimers and are commercially available with different surface groups [31], a strategy to encapsulate molecules with different chemical natures. Despite their versatility and flexibility as DDSs, dendrimer-based therapies are not available on the market.

Polymer micelles are considered a relevant part of polymer-based DDSs. They are obtained from surfactant or block copolymers that can self-assemble in water above their critical micellar concentration (CMC). Their hydrophilic part is exposed on the surface and in contact with aqueous phase. The formation of polymer micelles is thermodynamically driven and their disruption occurs once below their CMC [32].

Unlike micelles, polymer NPs require physical or chemical processes for their formulation, using natural or synthetic polymers as main components [33,34]. NPs can be easily coated on their surface to efficiently control their superficial and physicochemical features. Moreover, active targeting agents can be associated onto their surface to improve cellular uptake in target tissues. For example, surface functionalization by hyaluronic acid can enhance cellular uptake in CD-44 overexpressed tissues [35]. Among the polymers used for NPs formulation, biodegradable and biocompatible molecules are preferentially selected to limit the nanocarrier toxicity. Different chemical structures of polymers are used to guarantee the encapsulation of hydrophobic as well as hydrophilic drug molecules, making them the best candidates for drug delivery. The possibility of tuning their characteristics leads to increased colloidal stability and improved administration and storage [36].

I.2.2 Polymer nanosystems in the clinic

Despite the plethora of different polymer nanosystems reported in the literature, only a few formulations reached the clinical phase and/or have been marketed (Tab. 2).

Table 2 Polymer NP-based formulations currently on clinical trials

Product name	Particle	Drug	Indication	Clinical Trials
BIND-014	PMSA targeted PEG-PLGA or PLA-PEG particle	Docetaxel	Prostate, metastatic, cervical or lung cancers	4 trials completed
Genexol-PM®	PEG-poly(D,L-lactide)	Paclitaxel	Head and neck or breast cancer	1 trial completed 2 new trials
NC-600 4 Nanoplatin	Polyamino acid, PEG micellar nanoparticle	Cisplatin	Solid tumor, lung, biliary, pancreatic cancers	3 new trials
CriPec®	mPEG-methacrylates micelles	Docetaxel	Solid tumors, ovarian cancer	1 trial completed 2 new trials
CRLX101	Cyclodextrin-polyethylene glycol co-polymer	Camptothecin	Ovarian, renal cell, small cell lung or rectal cancers	9 new trials

Translation of polymer NPs into clinics is limited due to their recent discovery and development, compared to liposomal formulations [37]. More frequently, commercialized polymer nanomedicines refer to free drugs attached to a hydrophilic polymer to improve drug circulation or modify its chemical properties [38]. The most well-established polymer is poly(ethylene glycol) (PEG), which increases the molecule half-life (*e.g.* for antibodies, growth factors, etc.) in plasma thanks to its stealth effect [39]. Recently, the formulations of polymer NPs for clinical application are moving toward the study of hydrophobic or hydrophilic materials that facilitate the controlled release of the active molecule. This aim is achieved by using slowly degradable compounds that lead to a kinetically driven release of the drug. Among the different polymers, PLGA had significant success for drug encapsulation for its biocompatibility and biodegradability [40].

I.2.3 Poly(lactic-*co*-glycolic) acid (PLGA)

PLGA is one of the most successfully used biodegradable polymers to develop a nanomedicine approach. PLGA hydrolysis leads to the production of biodegradable metabolites, lactic (LA) and glycolic acid (GA), easily metabolized into cells *via* the Krebs cycle, making PLGA a biocompatible polymer (Fig. 3).

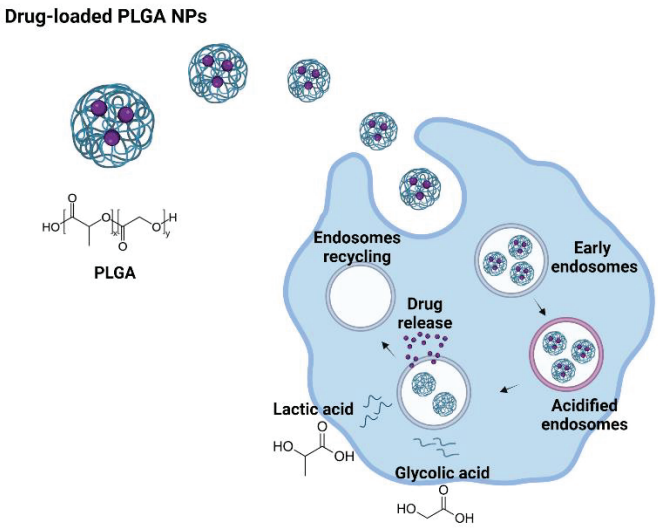

Fig. 3. Schematic representation of PLGA NPs internalization in cells. Hydrolysis of PLGA leads to the formation of LA and GA, monomers constituting PLGA polymer

PLGA is approved by FDA and EMA for its low toxicity in medical applications and is suitable for human parental administration [41]. Chemically, PLGA, an aliphatic polyester *co*-polymer, is randomly constituted of LA and GA. The hydrolysis rate of PLGA can be modulated by changing the monomer ratio and/or molecular weight [42].

PLGA is able to spontaneously form NPs upon dispersion in an aqueous phase, achieving a colloidal dispersion [43]. The simple production methods of polymer NPs made PLGA a promising carrier for the nanotechnological approach. Hundreds of published articles and patents reported different applications of PLGA DDSs, such as NPs, microparticles, implants, nanogels [44–46]. Moreover, PLGA DDSs can load cargos of different chemical nature, ranging from small molecules to large proteins, hydrophilic to lipophilic drugs, as well as amphiphilic molecules [47–49]. Among the advantages of polymer nanosystems, PLGA-based carriers can protect the drug from degradation, sustain and control drug release, and modify cargo pharmacokinetics. A recent application of PLGA attracted the attention of the research community, concerning the role of LA in its pharmacological contribution. Lactate plays a key role as fuel for cells and as a chemical messenger [50]. For example, the effect of exogenous lactate was tested for wound healing. Studies reported the effect of lactate derived from PLGA NPs, which enhanced re-epithelialization, collagen deposition and angiogenesis [51]. Ongoing studies are devoted to evaluating the importance of lactate, released from PLGA NPs, in biological processes. New clinical potential applications and mechanisms related to PLGA polymer may be deeper investigated to understand the role of PLGA NPs, not only as DDSs.

I.3 Lipid-based drug delivery systems

Lipid-based DDS is a wide-ranging designation for formulations containing a dissolved or suspended drug in lipid excipients. Lipid NPs are considered one of the most appealing delivery tools for genetic material and drug delivery. This class includes various subset structures, sharing a typical spherical organization of one lipidic bilayer surrounding at least one internal aqueous compartment. As polymer NPs, lipid nanocarriers have many advantages, such as formulation simplicity, biocompatibility, self-assembly properties and the ability of high drug encapsulation [52,53]. For these reasons, lipid-based NPs are the most common class of FDA-approved nanomedicines together with more and more undergoing clinical trials [54]. Their composition includes phospholipids of several natures, which influence physicochemical properties and surface charge. After being administered, they are rapidly taken up by the reticuloendothelial system. For this reason, lipid-based DDSs include surface modification to increase their blood half-life and prolong circulation [55].

I.3.1 Classification of lipid-based drug delivery systems

Lipid-based nanosystems can be classified on the basis of their internal structure (Fig. 4). Among lipid DDSs, liposomes are the best known ones. Since their discovery, liposome-based DDSs have been exploited as biocompatible and simply modifiable nanosystems. Liposomes are composed of phospholipids, which can form unilamellar or multilamellar vesicular structures. Drug encapsulation strategy exploits their double chemical nature, allowing the aqueous core to contain the hydrophilic drugs and the phospholipid bilayer to localize lipophilic drugs [56]. Furthermore, the surface-modification process increases their blood circulation and tunes drug delivery [57].

Another remarkable subset of lipid-based DDSs is commonly referred to as lipid nanoparticles (LNPs). They are characterized by a liposome-like structure and are currently mostly used for genetic material delivery [58,59]. Ionizable phospholipids constitute the base structure of LNPs allowing the complexation with nucleic acid and exploiting their pH sensitivity to promote endosomal escape [60]. Another class owing to lipid nanocarriers is nanoemulsions. Nanoemulsions are thermodynamically unstable colloidal dispersions consisting of two immiscible liquids, with one of the liquids dispersed as small spherical droplets in another liquid (oil-in-water, O/W, or water-in-oil, W/O). Lipids/oils used in nanoemulsions are chosen by considering the solubility of the drug to encapsulate [61]. The term lipid-based nanocarrier also includes the solid lipid nanoparticles (SLNs) and lipid nanocapsules (LNCs). SLNs represent a colloidal dispersion of non-polar lipids such as triglycerides, fatty acids or phospholipids, which

are solid at room temperature as well as body temperature. An advantage of SLNs is the non-toxic nature of nanocarrier itself, as they made up of safe excipients. There are different preparation methods which generally include the formation of an emulsion, followed by size-reduction using methods such as homogenization and ultracentrifugation [62].

LNCs are vesicular nanocarriers constituted by an oily phase and an aqueous phase, stabilized by surfactants and a polymer shell. The polymer shell has a relevant impact on nanocarrier properties (*e.g.* surface charge, hydrophilicity). The preparation methods are based on two main steps: the formulation of a nanoemulsion and then, the formation of the polymer shell through different methods, which include interface polymerization or interfacial deposition. LNCs are very tempting due to their easiness of formulation, small size and high encapsulation efficiency of hydrophobic or amphiphilic drugs [63].

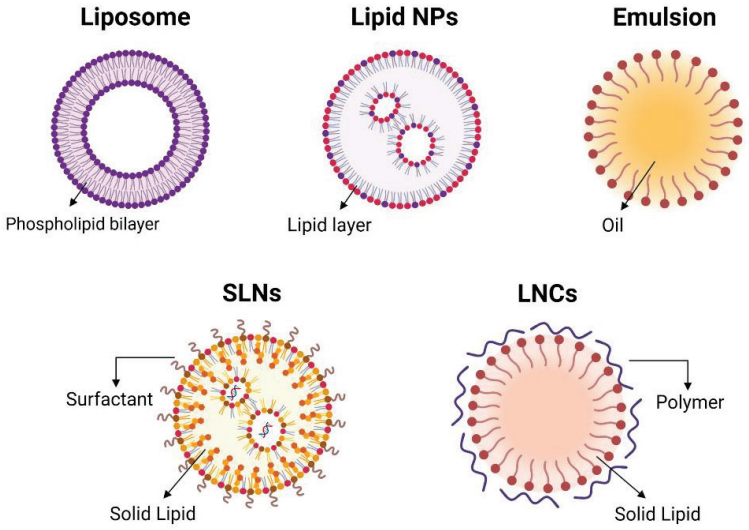

Fig. 4. Lipid DDSs

I.3.2 Lipid nanosystems in the clinic

The versatility of lipid-based nanosystems in terms of their composition, particle size and surface charge allows the marketing of several nanomedicines. Doxil® was the first liposome-based therapeutic approach FDA-approved for cancer treatment (Tab. 1) [12] and over the years even more nano-therapeutics were clinically approved and marketed. Although the cancer nanomedicine field has exponentially grown in recent years and the vast majority of nanomedicines currently in preclinical and clinical trials target malignant tumors [64], the application of nanomedicine to noncancer conditions increased [65,66]. Indeed, a breakthrough in the development of pharmacologically acceptable lipid formulations was the advent of ionizable cationic lipids, guaranteeing the fusion process with endosomal membranes to nucleic

acid delivery. One prominent example is the recent approval of Onpattro®, the first gene-silencing product using cationic lipids as carriers for siRNA in the treatment of hereditary transthyretin amyloidosis [67]. Similar compositions are still used for many mRNA-based vaccines, which can be used to enhance immune stimulation in the case of infectious diseases. mRNA-based COVID-19 vaccines (Comirnaty® and Spikevax®) are based on lipid NPs which underlined the flexibility and swiftness of the production of mRNA vaccines [68,69]. The efficacy of the nucleic acid delivery along with their simple synthesis, small size and serum stability have made lipid NPs a suitable platform for the delivery of genetic material [70].

I.3.3 Squalene

Loading drugs into nanocarriers could require different approaches. Couvreur *et al*. have pioneered the exploitation of squalene, a metabolic precursor of cholesterol, as DDS [71]. Squalene has been chemically conjugated to compounds from several therapeutic classes to improve their biological applications [72–75]. The bioconjugation of squalene (squalenoylation) with drug molecules induces an auto-assembly in aqueous media to form NPs without adding surfactant or other co-formulants. Furthermore, squalene derivatives changed the delivery of therapeutic molecules safely and more efficiently. Thus, squalene and its modified subsets can be considered as bricks for the preparation of different lipid NPs. Moreover, it is a biomimetic carrier that interacts with low-density lipoproteins (LDL) [71], counting as an efficient indirect targeting agent towards cells that overexpress LDL receptor [76,77]. Finally, squalene and its conjugates are well tolerated after intravenous or oral administration [78]. A different strategy to exploit squalene derivatives to form lipid NPs will be a part of the subject of this thesis.

I.4 Formulation methods

Depending on the type of drug to be loaded and the chrematistics required for a selected administration route, diverse manufacturing processes can be selected for NPs production [79]. In particular, the classical methods for polymer NPs preparation include solvent evaporation emulsification, solvent diffusion, salting-out [80] and nanoprecipitation [81]. Each procedure counts an organic solution that dissolves the polymer and hydrophobic drugs and an aqueous or water phase. Organic solvents can generate toxicity problems, reducing *in vitro* and *in vivo* applications. Thus, solvent residues must be removed from the final suspension.

I.4.1 Nanoprecipitation

The nanoprecipitation method, also called solvent displacement, was firstly developed by Fessi *et al*. [81]. It requires a water/buffer phase and a water-miscible solvent as the organic solution that can be easily eliminated from the final nanosuspension. This technique is based on the displacement of organic solvent from a lipophilic solution to an aqueous phase [82]. The most used solvents in nanoprecipitation process are ethanol, acetone and acetonitrile, which can be added to lyophobic excipients. Practically, the organic solution of the polymer and the hydrophobic drug is added dropwise into an aqueous phase, under moderate magnetic stirring, to promote drug encapsulation into the polymer matrix (Fig. 5). The fast spontaneous diffusion of the polymer solution into the water phase induces the instantaneous formation of NPs. The driving force of NPs constitution is the attempt of polymer solution to avoid contact with water molecules. Indeed, the mutual contact of water and solvent phases leads to interfacial turbulence which causes the insolubility of particle-matrix and the formation of NPs [83]. Nanoprecipitation is based on four steps, which include the generation of supersaturated spots, nucleation, growth and coagulation. Every single step could affect the physicochemical characteristics of NPs such as size, polydispersity and drug encapsulation. The supersaturation rate is the main step to determining NPs size, where a higher rate decreases particle diameter. Then, the nucleation step promotes the thermodynamical stability of the colloidal system until a critical point characterized by improved stability than NPs dissolution. Each nucleus starts to grow by surface deposition of solute molecules into the matrix.

Although it was firstly proposed for polymer NPs [84], the manufacturing process was then adapted to formulate lipid NPs and polymer-hybrid NPs [85,86]. The solvent displacement technique was widely studied for the encapsulation of hydrophobic drugs that were dissolved in the organic miscible-water solvent. However, the encapsulation of hydrophilic drugs by nanoprecipitation was investigated [87]. Nanoprecipitation is widely considered as a simple, low-cost, environmentally friendly, quite reproducible technique, obtaining submicron particle sizes with narrow size distribution using low energy. Moreover, either nanocapsules or nanospheres can be produced by nanoprecipitation with good stability properties.

Based on its feasibility, nanoprecipitation has important applications for pre-clinical and clinical studies. However, the employment of organic solvents during the NP preparation steps is considered a limit of this technique. Several methods are currently used to eliminate organic solvent residuals to obtain a suitable preparation for *in vitro* and *in vivo* tests [88].

The simplicity of the nanoprecipitation technique is the key point in the scaling-up process. Its success depends on the mixing way of the aqueous and organic phases. At lab-scale, the

procedure conditions can be easily controlled to obtain stable colloidal suspensions. However, the translation from batch to industrial production requires a large amount of both phases. On these bases, the scale-up process needs a critical investigation of industrial equipment to optimize formulation and operative parameters. Indeed, the feasibility of nanoprecipitation depends on the way the organic and aqueous phases are mixed. At lab-scale, the mixing rate is suitable for the small amounts of the two solutions (mL), reaching stable conditions for the whole process. However, the industrial scale needs a larger amount of both phases and continuous production, which do not guarantee stable conditions during the nanoprecipitation process: the continuous addition of the organic phase can lead to transient supersaturation due to solvent diffusion and therefore repeated nucleation. For this reason, nanosuspension in industrial production can be characterized by an increased polydispersity index [89]. To overcome the potential scale-up issues, an ultra-rapid one-step antisolvent precipitation process termed flash nanoprecipitation (FNP) has been developed for polymer NPs production [90]. Flash nanoprecipitation is a modified technique based on stimulating supersaturation conditions required, using a jet mixer to mix the two phases [91]. Such rapid mixing induces a homogeneous supersaturation state that initiates the precipitation process, reducing the size and polydispersity of NPs compared to the classical nanoprecipitation procedure [92]. FNP can be considered an advanced version of the simple nanoprecipitation process which could lead to more precise and reproductive nanosuspensions. Moreover, FNP is proposed as the first method that can be run at a laboratory scale with small amounts of the solution but that opens the opportunity for industrial scale-up [93].

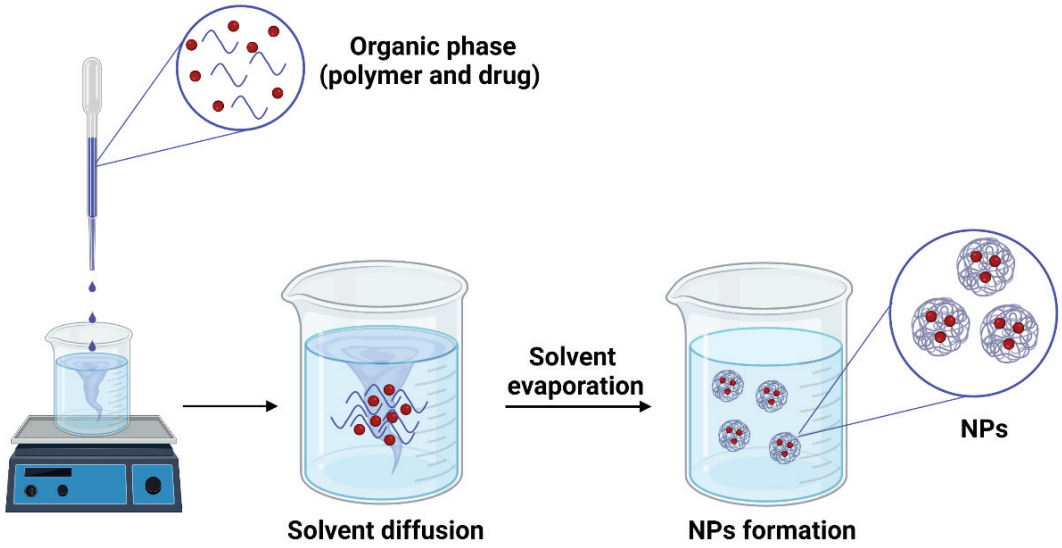

Fig. 5. Nanoprecipitation schematic representation

I.4.2 Microfluidic technique

Conventional methods for NPs preparation regularly result in particles with a broad size polydispersity, leading to problems of reproducibility, biodistribution, encapsulation efficiency, drug loading and release profile. Recently, manufacturing developments addressed these issues improving NPs production. Microfluidic technique is a new field that deals with fluid contact at the micro- and nanoscale and has been exploited as a promising tool to boost the formulation of DDSs, based on the classical solvent displacement method [94,95]. The microfluidic approach takes advantage of the channel geometry and architecture of microfluidic devices, to generate a turbulent flow that guarantees high mixing efficiency, not possible using conventional methods [96]. Microfluidic devices include a network of microchannels, inlets to inject fluids, micropumps and outlets to remove fluids and are based on enhanced mixing and precise fluid control. Important formulation and operative parameters, such as total flow rate (TFR) and flow rate ratio (FRR), need a precise control to modulate NPs features. TFR is considered as the total speed of the two phases within the channels. Generally, polymer NPs are characterized by a size lower than 100 nm as higher the TFR and higher FRR, that is the ratio between aqueous and organic phases [97]. The speed of the mixing process in microchannels is generally faster than the nucleation step of NPs, leading to controlled size with a narrow polydispersity index [98,99]. Other variables that can influence the physicochemical characteristics of NPs include the composition of the mixing solutions, the polymer and drug concentration, the nature of organic solvents or surfactant concentration [100,101]. Furthermore, by tailoring the inner structure of microfluidic devices, the size, the payload and the release profile can be tuned [102]. Different mixing structures are commercialized for microfluidic-assisted NPs preparation. For example, the staggered herring-bone micromixer contains patterned micro-ruts of different shapes and angles which generate a turbulent chaotic stirring in a very short time, 5-10 ms [103]. This device has been adopted for the formulation of polymer and lipid NPs to modulate size and encapsulation efficiency [100,104]. However, the multi-dimensional variables and the limitation on the size of the herring-bone features limit the achievement of the Good Manufacturing Practice (GMP) standards in terms of final product volume. To overcome these issues, an innovative microfluidic device has been projected, based on a toroidal mixer design (Fig. 6). The inner circular structure guarantees an efficient inner mixing process at high fluid speeds. This design induces a chaotic flow, increasing the number of chaotic vortices and centrifugal forces [105,106].

The growing interest in microfluidic technologies led to the commercialization of a great variety of microfluidic devices with different shapes, inner architecture and geometry, to address the formulation of different DDSs (Fig. 6). Microfluidic process is able to answer the urgent need to scale up the NPs production, moving from a batch to an industrial level. Indeed, the constant continuous flow provides the same mixing quality during all the process, obtaining very reproducible NPs over time and limiting the batch-to-batch variability of classical methods [107]. As already mentioned, the possibility to control particle size changing FRR or TFR parameters is an important advantage of microfluidic technique compared to classical methods. Indeed, the particle smaller size improves the cellular uptake and therapeutic effectiveness [108]. The production of mRNA-based vaccines represents the most important application of the microfluidic process, exploiting its important advantages for a continuous and reproducible production of mRNA lipid NPs [109].

While microfluidic technologies have many advantages, one key disadvantage is the volumetric throughput. The very small dimension of microchannels limits the amount of volume production. This issue remains one of the main challenges for some microfluidic devices to be translated into large-scale production. To address this challenge and the large amount of time needed to produce a significant amount of NPs, new innovative devices have been engineered to operate in parallel [110].

Therefore, microfluidic offers new opportunities for the production of highly reproducible nanomedicines which guarantee the same critical quality across different productions. It provides a rapid and direct production of loaded DDSs and accurate control over synthetic conditions for a clinical translation.

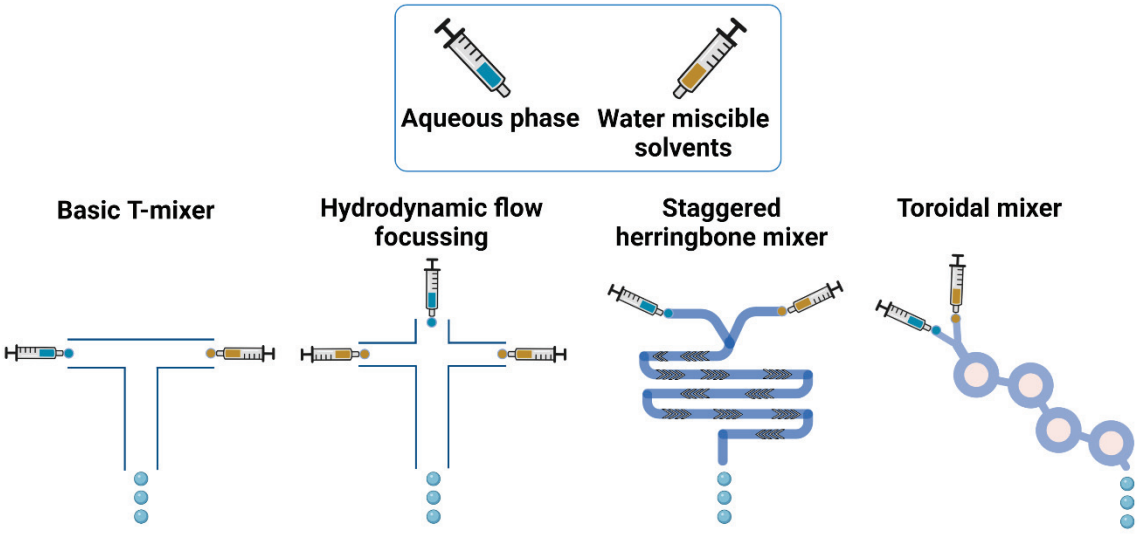

Fig. 6. Design of microfluidic devices for NPs formulation

References

1. Battistella, C.; Klok, H.-A. Controlling and Monitoring Intracellular Delivery of Anticancer Polymer Nanomedicines. *Macromolecular Bioscience* **2017**, *17*, 1700022, doi:10.1002/mabi.201700022.
2. Garbayo, E.; Pascual-Gil, S.; Rodríguez-Nogales, C.; Saludas, L.; Estella-Hermoso de Mendoza, A.; Blanco-Prieto, M.J. Nanomedicine and Drug Delivery Systems in Cancer and Regenerative Medicine. *Wiley Interdiscip Rev Nanomed Nanobiotechnol* **2020**, *12*, e1637, doi:10.1002/wnan.1637.
3. Irvine, D.J.; Dane, E.L. Enhancing Cancer Immunotherapy with Nanomedicine. *Nat Rev Immunol* **2020**, *20*, 321–334, doi:10.1038/s41577-019-0269-6.
4. Zhao, M.; van Straten, D.; Broekman, M.L.D.; Préat, V.; Schiffelers, R.M. Nanocarrier-Based Drug Combination Therapy for Glioblastoma. *Theranostics* **2020**, *10*, 1355–1372, doi:10.7150/thno.38147.
5. Wei, G.; Wang, Y.; Yang, G.; Wang, Y.; Ju, R. Recent Progress in Nanomedicine for Enhanced Cancer Chemotherapy. *Theranostics* **2021**, *11*, 6370–6392, doi:10.7150/thno.57828.
6. Kinnear, C.; Moore, T.L.; Rodriguez-Lorenzo, L.; Rothen-Rutishauser, B.; Petri-Fink, A. Form Follows Function: Nanoparticle Shape and Its Implications for Nanomedicine. *Chem Rev* **2017**, *117*, 11476–11521, doi:10.1021/acs.chemrev.7b00194.
7. Chen, L.; Wang, Y.; Sun, L.; Yan, J.; Mao, H.-Q. Nanomedicine Strategies for Anti-Inflammatory Treatment of Noninfectious Arthritis. *Adv Healthc Mater* **2021**, *10*, e2001732, doi:10.1002/adhm.202001732.
8. Choi, Y.H.; Han, H.-K. Nanomedicines: Current Status and Future Perspectives in Aspect of Drug Delivery and Pharmacokinetics. *J Pharm Investig* **2018**, *48*, 43–60, doi:10.1007/s40005-017-0370-4.
9. Liu, C.; Chen, L.; Ma, Y.; Hu, K.; Wu, P.; Pan, L.; Chen, H.; Li, L.; Hu, H.; Zhang, J. Pulmonary Circulation-Mediated Heart Targeting for the Prevention of Heart Failure by Inhalation of Intrinsically Bioactive Nanoparticles. *Theranostics* **2021**, *11*, 8550–8569, doi:10.7150/thno.61875.
10. Kim, T.W.; Kim, Y.; Jung, W.; Kim, D.E.; Keum, H.; Son, Y.; Jon, S. Bilirubin Nanomedicine Ameliorates the Progression of Experimental Autoimmune Encephalomyelitis by Modulating Dendritic Cells. *J Control Release* **2021**, *331*, 74–84, doi:10.1016/j.jconrel.2021.01.019.
11. Huang, D.; Yue, F.; Qiu, J.; Deng, M.; Kuang, S. Polymeric Nanoparticles Functionalized with Muscle-Homing Peptides for Targeted Delivery of Phosphatase and Tensin Homolog Inhibitor to Skeletal Muscle. *Acta Biomater* **2020**, *118*, 196–206, doi:10.1016/j.actbio.2020.10.009.
12. Barenholz, Y. (Chezy) Doxil® — The First FDA-Approved Nano-Drug: Lessons Learned. *Journal of Controlled Release* **2012**, *160*, 117–134, doi:10.1016/j.jconrel.2012.03.020.
13. Yuan, H.; Guo, H.; Luan, X.; He, M.; Li, F.; Burnett, J.; Truchan, N.; Sun, D. Albumin Nanoparticle of Paclitaxel (Abraxane) Decreases While Taxol Increases Breast Cancer Stem Cells in Treatment of Triple Negative Breast Cancer. *Mol Pharm* **2020**, *17*, 2275–2286, doi:10.1021/acs.molpharmaceut.9b01221.
14. Park, H.; Otte, A.; Park, K. Evolution of Drug Delivery Systems: From 1950 to 2020 and Beyond. *Journal of Controlled Release* **2022**, *342*, 53–65, doi:10.1016/j.jconrel.2021.12.030.
15. Tenchov, R.; Bird, R.; Curtze, A.E.; Zhou, Q. Lipid Nanoparticles─From Liposomes to MRNA Vaccine Delivery, a Landscape of Research Diversity and Advancement. *ACS Nano* **2021**, *15*, 16982–17015, doi:10.1021/acsnano.1c04996.

16. Zhang, N.-N.; Li, X.-F.; Deng, Y.-Q.; Zhao, H.; Huang, Y.-J.; Yang, G.; Huang, W.-J.; Gao, P.; Zhou, C.; Zhang, R.-R.; et al. A Thermostable MRNA Vaccine against COVID-19. *Cell* **2020**, *182*, 1271-1283.e16, doi:10.1016/j.cell.2020.07.024.
17. Paloncýová, M.; Čechová, P.; Šrejber, M.; Kührová, P.; Otyepka, M. Role of Ionizable Lipids in SARS-CoV-2 Vaccines As Revealed by Molecular Dynamics Simulations: From Membrane Structure to Interaction with MRNA Fragments. *J Phys Chem Lett* **2021**, *12*, 11199–11205, doi:10.1021/acs.jpclett.1c03109.
18. Eygeris, Y.; Patel, S.; Jozic, A.; Sahay, G. Deconvoluting Lipid Nanoparticle Structure for Messenger RNA Delivery. *Nano Lett* **2020**, *20*, 4543–4549, doi:10.1021/acs.nanolett.0c01386.
19. Zingg, R.; Fischer, M. The Consolidation of Nanomedicine. *Wiley Interdiscip Rev Nanomed Nanobiotechnol* **2019**, *11*, e1569, doi:10.1002/wnan.1569.
20. Liu, X.; Tang, I.; Wainberg, Z.A.; Meng, H. Safety Considerations of Cancer Nanomedicine-A Key Step toward Translation. *Small* **2020**, *16*, e2000673, doi:10.1002/smll.202000673.
21. Csóka, I.; Ismail, R.; Jójárt-Laczkovich, O.; Pallagi, E. Regulatory Considerations, Challenges and Risk-Based Approach in Nanomedicine Development. *Curr Med Chem* **2021**, *28*, 7461–7476, doi:10.2174/0929867328666210406115529.
22. Hua, S.; de Matos, M.B.C.; Metselaar, J.M.; Storm, G. Current Trends and Challenges in the Clinical Translation of Nanoparticulate Nanomedicines: Pathways for Translational Development and Commercialization. *Frontiers in Pharmacology* **2018**, *9*.
23. Metselaar, J.M.; Lammers, T. Challenges in Nanomedicine Clinical Translation. *Drug Deliv Transl Res* **2020**, *10*, 721–725, doi:10.1007/s13346-020-00740-5.
24. Osmałek, T.; Froelich, A.; Jadach, B.; Tatarek, A.; Gadziński, P.; Falana, A.; Gralińska, K.; Ekert, M.; Puri, V.; Wrotyńska-Barczyńska, J.; et al. Recent Advances in Polymer-Based Vaginal Drug Delivery Systems. *Pharmaceutics* **2021**, *13*, 884, doi:10.3390/pharmaceutics13060884.
25. Wang, B.; Wang, S.; Zhang, Q.; Deng, Y.; Li, X.; Peng, L.; Zuo, X.; Piao, M.; Kuang, X.; Sheng, S.; et al. Recent Advances in Polymer-Based Drug Delivery Systems for Local Anesthetics. *Acta Biomaterialia* **2019**, *96*, 55–67, doi:10.1016/j.actbio.2019.05.044.
26. Idrees, H.; Zaidi, S.Z.J.; Sabir, A.; Khan, R.U.; Zhang, X.; Hassan, S.-U. A Review of Biodegradable Natural Polymer-Based Nanoparticles for Drug Delivery Applications. *Nanomaterials (Basel)* **2020**, *10*, E1970, doi:10.3390/nano10101970.
27. Adinolfi, B.; Pellegrino, M.; Tombelli, S.; Trono, C.; Giannetti, A.; Domenici, C.; Varchi, G.; Sotgiu, G.; Ballestri, M.; Baldini, F. Polymeric Nanoparticles Promote Endocytosis of a Survivin Molecular Beacon: Localization and Fate of Nanoparticles and Beacon in Human A549 Cells. *Life Sci* **2018**, *215*, 106–112, doi:10.1016/j.lfs.2018.11.007.
28. Zhou, D.; Fei, Z.; Jin, L.; Zhou, P.; Li, C.; Liu, X.; Zhao, C. Dual-Responsive Polymersomes as Anticancer Drug Carriers for the Co-Delivery of Doxorubicin and Paclitaxel. *J Mater Chem B* **2021**, *9*, 801–808, doi:10.1039/d0tb02462g.
29. Klermund, L.; Castiglione, K. Polymersomes as Nanoreactors for Preparative Biocatalytic Applications: Current Challenges and Future Perspectives. *Bioprocess Biosyst Eng* **2018**, *41*, 1233–1246, doi:10.1007/s00449-018-1953-9.
30. Abbasi, E.; Aval, S.F.; Akbarzadeh, A.; Milani, M.; Nasrabadi, H.T.; Joo, S.W.; Hanifehpour, Y.; Nejati-Koshki, K.; Pashaei-Asl, R. Dendrimers: Synthesis, Applications, and Properties. *Nanoscale Res Lett* **2014**, *9*, 247, doi:10.1186/1556-276X-9-247.
31. Kheraldine, H.; Rachid, O.; Habib, A.M.; Al Moustafa, A.-E.; Benter, I.F.; Akhtar, S. Emerging Innate Biological Properties of Nano-Drug Delivery Systems: A Focus on PAMAM Dendrimers and Their Clinical Potential. *Adv Drug Deliv Rev* **2021**, *178*, 113908, doi:10.1016/j.addr.2021.113908.

32. Biswas, S. Polymeric Micelles as Drug-Delivery Systems in Cancer: Challenges and Opportunities. *Nanomedicine (Lond)* **2021**, *16*, 1541–1544, doi:10.2217/nnm-2021-0081.
33. Obinu, A.; Rassu, G.; Corona, P.; Maestri, M.; Riva, F.; Miele, D.; Giunchedi, P.; Gavini, E. Poly (Ethyl 2-Cyanoacrylate) Nanoparticles (PECA-NPs) as Possible Agents in Tumor Treatment. *Colloids Surf B Biointerfaces* **2019**, *177*, 520–528, doi:10.1016/j.colsurfb.2019.02.036.
34. Wilson, B.K.; Prud'homme, R.K. Processing Chitosan for Preparing Chitosan-Functionalized Nanoparticles by Polyelectrolyte Adsorption. *Langmuir* **2021**, *37*, 8517–8524, doi:10.1021/acs.langmuir.1c00990.
35. Nicolas, J.; Mura, S.; Brambilla, D.; Mackiewicz, N.; Couvreur, P. Design, Functionalization Strategies and Biomedical Applications of Targeted Biodegradable/Biocompatible Polymer-Based Nanocarriers for Drug Delivery. *Chem. Soc. Rev.* **2013**, *42*, 1147–1235, doi:10.1039/C2CS35265F.
36. Zhang, X.; Chau, L.Y.; Chan, H.W.; Weng, J.; Wong, K.W.; Chow, S.F.; Chow, A.H.L. Physical Stability and in Vivo Brain Delivery of Polymeric Ibuprofen Nanoparticles Fabricated by Flash Nanoprecipitation. *Int J Pharm* **2021**, *598*, 120224, doi:10.1016/j.ijpharm.2021.120224.
37. Judson, I.; Radford, J.A.; Harris, M.; Blay, J.Y.; van Hoesel, Q.; le Cesne, A.; van Oosterom, A.T.; Clemons, M.J.; Kamby, C.; Hermans, C.; et al. Randomised Phase II Trial of Pegylated Liposomal Doxorubicin (DOXIL/CAELYX) versus Doxorubicin in the Treatment of Advanced or Metastatic Soft Tissue Sarcoma: A Study by the EORTC Soft Tissue and Bone Sarcoma Group. *Eur J Cancer* **2001**, *37*, 870–877, doi:10.1016/s0959-8049(01)00050-8.
38. White, J.T.; Crossman, M.; Richter, K.; Berman, M.; Goyal, J.; Subramanyam, M. Immunogenicity Evaluation Strategy for a Second-Generation Therapeutic, PEG-IFN-β-1a. *Bioanalysis* **2015**, *7*, 2801–2811, doi:10.4155/bio.15.197.
39. Fam, S.Y.; Chee, C.F.; Yong, C.Y.; Ho, K.L.; Mariatulqabtiah, A.R.; Tan, W.S. Stealth Coating of Nanoparticles in Drug-Delivery Systems. *Nanomaterials (Basel)* **2020**, *10*, E787, doi:10.3390/nano10040787.
40. Danhier, F.; Ansorena, E.; Silva, J.M.; Coco, R.; Le Breton, A.; Préat, V. PLGA-Based Nanoparticles: An Overview of Biomedical Applications. *J Control Release* **2012**, *161*, 505–522, doi:10.1016/j.jconrel.2012.01.043.
41. Sartor, O. Eligard: Leuprolide Acetate in a Novel Sustained-Release Delivery System. *Urology* **2003**, *61*, 25–31, doi:10.1016/s0090-4295(02)02396-8.
42. Li, J.; Stayshich, R.M.; Meyer, T.Y. Exploiting Sequence to Control the Hydrolysis Behavior of Biodegradable PLGA Copolymers. *J Am Chem Soc* **2011**, *133*, 6910–6913, doi:10.1021/ja200895s.
43. Operti, M.C.; Bernhardt, A.; Grimm, S.; Engel, A.; Figdor, C.G.; Tagit, O. PLGA-Based Nanomedicines Manufacturing: Technologies Overview and Challenges in Industrial Scale-Up. *International Journal of Pharmaceutics* **2021**, *605*, 120807, doi:10.1016/j.ijpharm.2021.120807.
44. Gu, B.; Sun, X.; Papadimitrakopoulos, F.; Burgess, D.J. Seeing Is Believing, PLGA Microsphere Degradation Revealed in PLGA Microsphere/PVA Hydrogel Composites. *J Control Release* **2016**, *228*, 170–178, doi:10.1016/j.jconrel.2016.03.011.
45. Yu, Z.; Ma, S.; Wu, M.; Cui, H.; Wu, R.; Chen, S.; Xu, C.; Lu, X.; Feng, S. Self-Assembling Hydrogel Loaded with 5-FU PLGA Microspheres as a Novel Vitreous Substitute for Proliferative Vitreoretinopathy. *J Biomed Mater Res A* **2020**, *108*, 2435–2446, doi:10.1002/jbm.a.36995.
46. Manna, S.; Donnell, A.M.; Faraj, R.Q.C.; Riemann, B.I.; Riemann, C.D.; Augsburger, J.J.; Correa, Z.M.; Banerjee, R.K. Pharmacokinetics and Toxicity Evaluation of a PLGA and

Chitosan-Based Micro-Implant for Sustained Release of Methotrexate in Rabbit Vitreous. *Pharmaceutics* **2021**, *13*, 1227, doi:10.3390/pharmaceutics13081227.
47. Stella, B.; Andreana, I.; Zonari, D.; Arpicco, S. Pentamidine-Loaded Lipid and Polymer Nanocarriers as Tunable Anticancer Drug Delivery Systems. *J Pharm Sci* **2020**, *109*, 1297–1302, doi:10.1016/j.xphs.2019.11.011.
48. Fan, S.; Zheng, Y.; Liu, X.; Fang, W.; Chen, X.; Liao, W.; Jing, X.; Lei, M.; Tao, E.; Ma, Q.; et al. Curcumin-Loaded PLGA-PEG Nanoparticles Conjugated with B6 Peptide for Potential Use in Alzheimer's Disease. *Drug Deliv* **2018**, *25*, 1091–1102, doi:10.1080/10717544.2018.1461955.
49. Kumari, A.; Yadav, S.K.; Yadav, S.C. Biodegradable Polymeric Nanoparticles Based Drug Delivery Systems. *Colloids Surf B Biointerfaces* **2010**, *75*, 1–18, doi:10.1016/j.colsurfb.2009.09.001.
50. Descalzi, G.; Gao, V.; Steinman, M.Q.; Suzuki, A.; Alberini, C.M. Lactate from Astrocytes Fuels Learning-Induced MRNA Translation in Excitatory and Inhibitory Neurons. *Commun Biol* **2019**, *2*, 247, doi:10.1038/s42003-019-0495-2.
51. Chereddy, K.K.; Her, C.-H.; Comune, M.; Moia, C.; Lopes, A.; Porporato, P.E.; Vanacker, J.; Lam, M.C.; Steinstraesser, L.; Sonveaux, P.; et al. PLGA Nanoparticles Loaded with Host Defense Peptide LL37 Promote Wound Healing. *J Control Release* **2014**, *194*, 138–147, doi:10.1016/j.jconrel.2014.08.016.
52. Hammoud, Z.; Kayouka, M.; Trifan, A.; Sieniawska, E.; Jemâa, J.M.B.; Elaissari, A.; Greige-Gerges, H. Encapsulation of α-Pinene in Delivery Systems Based on Liposomes and Cyclodextrins. *Molecules* **2021**, *26*, 6840, doi:10.3390/molecules26226840.
53. Yun, P.; Devahastin, S.; Chiewchan, N. Microstructures of Encapsulates and Their Relations with Encapsulation Efficiency and Controlled Release of Bioactive Constituents: A Review. *Compr Rev Food Sci Food Saf* **2021**, *20*, 1768–1799, doi:10.1111/1541-4337.12701.
54. Filipczak, N.; Pan, J.; Yalamarty, S.S.K.; Torchilin, V.P. Recent Advancements in Liposome Technology. *Adv Drug Deliv Rev* **2020**, *156*, 4–22, doi:10.1016/j.addr.2020.06.022.
55. Janeczek, A.A.; Scarpa, E.; Horrocks, M.H.; Tare, R.S.; Rowland, C.A.; Jenner, D.; Newman, T.A.; Oreffo, R.O.; Lee, S.F.; Evans, N.D. PEGylated Liposomes Associate with Wnt3A Protein and Expand Putative Stem Cells in Human Bone Marrow Populations. *Nanomedicine (Lond)* **2017**, *12*, 845–863, doi:10.2217/nnm-2016-0386.
56. Guimarães, D.; Cavaco-Paulo, A.; Nogueira, E. Design of Liposomes as Drug Delivery System for Therapeutic Applications. *Int J Pharm* **2021**, *601*, 120571, doi:10.1016/j.ijpharm.2021.120571.
57. Grad, P.; Gedda, L.; Edwards, K. Effect of Gangliosides on Structure and Integrity of Polyethylene Glycol (PEG)-Stabilized Liposomes. *J Colloid Interface Sci* **2020**, *578*, 281–289, doi:10.1016/j.jcis.2020.05.120.
58. Kulkarni, J.A.; Darjuan, M.M.; Mercer, J.E.; Chen, S.; van der Meel, R.; Thewalt, J.L.; Tam, Y.Y.C.; Cullis, P.R. On the Formation and Morphology of Lipid Nanoparticles Containing Ionizable Cationic Lipids and SiRNA. *ACS Nano* **2018**, *12*, 4787–4795, doi:10.1021/acsnano.8b01516.
59. Cullis, P.R.; Hope, M.J. Lipid Nanoparticle Systems for Enabling Gene Therapies. *Mol Ther* **2017**, *25*, 1467–1475, doi:10.1016/j.ymthe.2017.03.013.
60. Maugeri, M.; Nawaz, M.; Papadimitriou, A.; Angerfors, A.; Camponeschi, A.; Na, M.; Hölttä, M.; Skantze, P.; Johansson, S.; Sundqvist, M.; et al. Linkage between Endosomal Escape of LNP-MRNA and Loading into EVs for Transport to Other Cells. *Nat Commun* **2019**, *10*, 4333, doi:10.1038/s41467-019-12275-6.

61. Singh, Y.; Meher, J.G.; Raval, K.; Khan, F.A.; Chaurasia, M.; Jain, N.K.; Chourasia, M.K. Nanoemulsion: Concepts, Development and Applications in Drug Delivery. *J Control Release* **2017**, *252*, 28–49, doi:10.1016/j.jconrel.2017.03.008.
62. Ekambaram, P.; Sathali, A.A.H.; Priyanka, K. Solid lipid nanoparticles: A review. *Sci Rev Chem Commun* **2012**, *2*, 80–102.
63. Huynh, N.T.; Passirani, C.; Saulnier, P.; Benoit, J.P. Lipid Nanocapsules: A New Platform for Nanomedicine. *International Journal of Pharmaceutics* **2009**, *379*, 201–209, doi:10.1016/j.ijpharm.2009.04.026.
64. van der Meel, R.; Sulheim, E.; Shi, Y.; Kiessling, F.; Mulder, W.J.M.; Lammers, T. Smart Cancer Nanomedicine. *Nat Nanotechnol* **2019**, *14*, 1007–1017, doi:10.1038/s41565-019-0567-y.
65. Miller, M.R.; Raftis, J.B.; Langrish, J.P.; McLean, S.G.; Samutrtai, P.; Connell, S.P.; Wilson, S.; Vesey, A.T.; Fokkens, P.H.B.; Boere, A.J.F.; et al. Inhaled Nanoparticles Accumulate at Sites of Vascular Disease. *ACS Nano* **2017**, *11*, 4542–4552, doi:10.1021/acsnano.6b08551.
66. Pinheiro, R.G.R.; Granja, A.; Loureiro, J.A.; Pereira, M.C.; Pinheiro, M.; Neves, A.R.; Reis, S. Quercetin Lipid Nanoparticles Functionalized with Transferrin for Alzheimer's Disease. *Eur J Pharm Sci* **2020**, *148*, 105314, doi:10.1016/j.ejps.2020.105314.
67. Adams, D.; Gonzalez-Duarte, A.; O'Riordan, W.D.; Yang, C.-C.; Ueda, M.; Kristen, A.V.; Tournev, I.; Schmidt, H.H.; Coelho, T.; Berk, J.L.; et al. Patisiran, an RNAi Therapeutic, for Hereditary Transthyretin Amyloidosis. *N Engl J Med* **2018**, *379*, 11–21, doi:10.1056/NEJMoa1716153.
68. Polack, F.P.; Thomas, S.J.; Kitchin, N.; Absalon, J.; Gurtman, A.; Lockhart, S.; Perez, J.L.; Pérez Marc, G.; Moreira, E.D.; Zerbini, C.; et al. Safety and Efficacy of the BNT162b2 MRNA Covid-19 Vaccine. *N Engl J Med* **2020**, *383*, 2603–2615, doi:10.1056/NEJMoa2034577.
69. Jalkanen, P.; Kolehmainen, P.; Häkkinen, H.K.; Huttunen, M.; Tähtinen, P.A.; Lundberg, R.; Maljanen, S.; Reinholm, A.; Tauriainen, S.; Pakkanen, S.H.; et al. COVID-19 MRNA Vaccine Induced Antibody Responses against Three SARS-CoV-2 Variants. *Nat Commun* **2021**, *12*, 3991, doi:10.1038/s41467-021-24285-4.
70. Dammes, N.; Goldsmith, M.; Ramishetti, S.; Dearling, J.L.J.; Veiga, N.; Packard, A.B.; Peer, D. Conformation-Sensitive Targeting of Lipid Nanoparticles for RNA Therapeutics. *Nat Nanotechnol* **2021**, *16*, 1030–1038, doi:10.1038/s41565-021-00928-x.
71. Desmaële, D.; Gref, R.; Couvreur, P. Squalenoylation: A Generic Platform for Nanoparticular Drug Delivery. *J Control Release* **2012**, *161*, 609–618, doi:10.1016/j.jconrel.2011.07.038.
72. Brusini, R.; Dormont, F.; Cailleau, C.; Nicolas, V.; Peramo, A.; Varna, M.; Couvreur, P. Squalene-Based Nanoparticles for the Targeting of Atherosclerotic Lesions. *Int J Pharm* **2020**, *581*, 119282, doi:10.1016/j.ijpharm.2020.119282.
73. Dormont, F.; Brusini, R.; Cailleau, C.; Reynaud, F.; Peramo, A.; Gendron, A.; Mougin, J.; Gaudin, F.; Varna, M.; Couvreur, P. Squalene-Based Multidrug Nanoparticles for Improved Mitigation of Uncontrolled Inflammation in Rodents. *Sci Adv* **2020**, *6*, eaaz5466, doi:10.1126/sciadv.aaz5466.
74. Boutary, S.; Caillaud, M.; El Madani, M.; Vallat, J.-M.; Loisel-Duwattez, J.; Rouyer, A.; Richard, L.; Gracia, C.; Urbinati, G.; Desmaële, D.; et al. Squalenoyl SiRNA PMP22 Nanoparticles Are Effective in Treating Mouse Models of Charcot-Marie-Tooth Disease Type 1 A. *Commun Biol* **2021**, *4*, 317, doi:10.1038/s42003-021-01839-2.
75. Gobeaux, F.; Bizeau, J.; Samson, F.; Marichal, L.; Grillo, I.; Wien, F.; Yesylevsky, S.O.; Ramseyer, C.; Rouquette, M.; Lepêtre-Mouelhi, S.; et al. Albumin-Driven Disassembly of Lipidic Nanoparticles: The Specific Case of the Squalene-Adenosine Nanodrug. *Nanoscale* **2020**, *12*, 2793–2809, doi:10.1039/c9nr06485k.

76. Sobot, D.; Mura, S.; Rouquette, M.; Vukosavljevic, B.; Cayre, F.; Buchy, E.; Pieters, G.; Garcia-Argote, S.; Windbergs, M.; Desmaële, D.; et al. Circulating Lipoproteins: A Trojan Horse Guiding Squalenoylated Drugs to LDL-Accumulating Cancer Cells. *Mol Ther* **2017**, *25*, 1596–1605, doi:10.1016/j.ymthe.2017.05.016.
77. Sobot, D.; Mura, S.; Yesylevskyy, S.O.; Dalbin, L.; Cayre, F.; Bort, G.; Mougin, J.; Desmaële, D.; Lepetre-Mouelhi, S.; Pieters, G.; et al. Conjugation of Squalene to Gemcitabine as Unique Approach Exploiting Endogenous Lipoproteins for Drug Delivery. *Nat Commun* **2017**, *8*, 15678, doi:10.1038/ncomms15678.
78. Coppens, E.; Desmaële, D.; Naret, T.; Garcia-Argote, S.; Feuillastre, S.; Pieters, G.; Cailleau, C.; Paul, J.-L.; Prost, B.; Solgadi, A.; et al. Gemcitabine Lipid Prodrug Nanoparticles: Switching the Lipid Moiety and Changing the Fate in the Bloodstream. *Int J Pharm* **2021**, *609*, 121076, doi:10.1016/j.ijpharm.2021.121076.
79. Crucho, C.I.C.; Barros, M.T. Polymeric Nanoparticles: A Study on the Preparation Variables and Characterization Methods. *Mater Sci Eng C Mater Biol Appl* **2017**, *80*, 771–784, doi:10.1016/j.msec.2017.06.004.
80. Lee, B.K.; Yun, Y.; Park, K. PLA Micro- and Nano-Particles. *Adv Drug Deliv Rev* **2016**, *107*, 176–191, doi:10.1016/j.addr.2016.05.020.
81. Fessi, H.; Puisieux, F.; Devissaguet, J.Ph.; Ammoury, N.; Benita, S. Nanocapsule Formation by Interfacial Polymer Deposition Following Solvent Displacement. *International Journal of Pharmaceutics* **1989**, *55*, R1–R4, doi:10.1016/0378-5173(89)90281-0.
82. Martínez Rivas, C.J.; Tarhini, M.; Badri, W.; Miladi, K.; Greige-Gerges, H.; Nazari, Q.A.; Galindo Rodríguez, S.A.; Román, R.Á.; Fessi, H.; Elaissari, A. Nanoprecipitation Process: From Encapsulation to Drug Delivery. *Int J Pharm* **2017**, *532*, 66–81, doi:10.1016/j.ijpharm.2017.08.064.
83. Zhao, C.; Melis, S.; Hughes, E.P.; Li, T.; Zhang, X.; Olmsted, P.D.; Van Keuren, E. Particle Formation Mechanisms in the Nanoprecipitation of Polystyrene. *Langmuir* **2020**, *36*, 13210–13217, doi:10.1021/acs.langmuir.0c02071.
84. Han, F.Y.; Liu, Y.; Kumar, V.; Xu, W.; Yang, G.; Zhao, C.-X.; Woodruff, T.M.; Whittaker, A.K.; Smith, M.T. Sustained-Release Ketamine-Loaded Nanoparticles Fabricated by Sequential Nanoprecipitation. *Int J Pharm* **2020**, *581*, 119291, doi:10.1016/j.ijpharm.2020.119291.
85. Godara, S.; Lather, V.; Kirthanashri, S.V.; Awasthi, R.; Pandita, D. Lipid-PLGA Hybrid Nanoparticles of Paclitaxel: Preparation, Characterization, in Vitro and in Vivo Evaluation. *Mater Sci Eng C Mater Biol Appl* **2020**, *109*, 110576, doi:10.1016/j.msec.2019.110576.
86. Iqbal, A.; Zaman, M.; Wahab Amjad, M.; Adnan, S.; Abdul Ghafoor Raja, M.; Haider Rizvi, S.F.; Mustafa, M.W.; Farooq, U.; Abbas, G.; Shah, S. Solid Lipid Nanoparticles of Mycophenolate Mofetil: An Attempt to Control the Release of an Immunosuppressant. *Int J Nanomedicine* **2020**, *15*, 5603–5612, doi:10.2147/IJN.S255636.
87. Surwase, S.S.; Munot, N.M.; Idage, B.B.; Idage, S.B. Tailoring the Properties of MPEG-PLLA Nanoparticles for Better Encapsulation and Tuned Release of the Hydrophilic Anticancer Drug. *Drug Deliv Transl Res* **2017**, *7*, 416–427, doi:10.1007/s13346-017-0372-9.
88. Dikpati, A.; Mohammadi, F.; Greffard, K.; Quéant, C.; Arnaud, P.; Bastiat, G.; Rudkowska, I.; Bertrand, N. Residual Solvents in Nanomedicine and Lipid-Based Drug Delivery Systems: A Case Study to Better Understand Processes. *Pharm Res* **2020**, *37*, 149, doi:10.1007/s11095-020-02877-x.
89. Li, F.; Chen, Y.; Liu, S.; Qi, J.; Wang, W.; Wang, C.; Zhong, R.; Chen, Z.; Li, X.; Guan, Y.; et al. Size-Controlled Fabrication of Zein Nano/Microparticles by Modified Anti-

Solvent Precipitation with/without Sodium Caseinate. *Int J Nanomedicine* **2017**, *12*, 8197–8209, doi:10.2147/IJN.S143733.
90. Johnson, B.K.; Prud'homme, R.K. Mechanism for Rapid Self-Assembly of Block Copolymer Nanoparticles. *Phys Rev Lett* **2003**, *91*, 118302, doi:10.1103/PhysRevLett.91.118302.
91. Valente, I.; Stella, B.; Marchisio, D.L.; Dosio, F.; Barresi, A.A. Production of PEGylated Nanocapsules through Solvent Displacement in Confined Impinging Jet Mixers. *J Pharm Sci* **2012**, *101*, 2490–2501, doi:10.1002/jps.23167.
92. Chen, K.; Fu, Z.; Wang, M.; Lv, Y.; Wang, C.; Shen, Y.; Wang, Y.; Cui, H.; Guo, X. Preparation and Characterization of Size-Controlled Nanoparticles for High-Loading λ-Cyhalothrin Delivery through Flash Nanoprecipitation. *J Agric Food Chem* **2018**, *66*, 8246–8252, doi:10.1021/acs.jafc.8b02851.
93. Chen, Z.; Fu, Z.; Li, L.; Ma, E.; Guo, X. A Cost-Effective Nano-Sized Curcumin Delivery System with High Drug Loading Capacity Prepared via Flash Nanoprecipitation. *Nanomaterials (Basel)* **2021**, *11*, 734, doi:10.3390/nano11030734.
94. Liu, D.; Zhang, H.; Cito, S.; Fan, J.; Mäkilä, E.; Salonen, J.; Hirvonen, J.; Sikanen, T.M.; Weitz, D.A.; Santos, H.A. Core/Shell Nanocomposites Produced by Superfast Sequential Microfluidic Nanoprecipitation. *Nano Lett* **2017**, *17*, 606–614, doi:10.1021/acs.nanolett.6b03251.
95. Salerno, A.; Levato, R.; Mateos-Timoneda, M.A.; Engel, E.; Netti, P.A.; Planell, J.A. Modular Polylactic Acid Microparticle-Based Scaffolds Prepared via Microfluidic Emulsion/Solvent Displacement Process: Fabrication, Characterization, and in Vitro Mesenchymal Stem Cells Interaction Study. *J Biomed Mater Res A* **2013**, *101*, 720–732, doi:10.1002/jbm.a.34374.
96. Valencia, P.M.; Farokhzad, O.C.; Karnik, R.; Langer, R. Microfluidic Technologies for Accelerating the Clinical Translation of Nanoparticles. *Nature Nanotechnology* **2012**, *7*, 623–629, doi:10.1038/nnano.2012.168.
97. Operti, M.C.; Dölen, Y.; Keulen, J.; van Dinther, E.A.W.; Figdor, C.G.; Tagit, O. Microfluidics-Assisted Size Tuning and Biological Evaluation of PLGA Particles. *Pharmaceutics* **2019**, *11*, E590, doi:10.3390/pharmaceutics11110590.
98. Kimura, N.; Maeki, M.; Ishida, A.; Tani, H.; Tokeshi, M. One-Step Production Using a Microfluidic Device of Highly Biocompatible Size-Controlled Noncationic Exosome-like Nanoparticles for RNA Delivery. *ACS Appl Bio Mater* **2021**, *4*, 1783–1793, doi:10.1021/acsabm.0c01519.
99. Gimondi, S.; Guimarães, C.F.; Vieira, S.F.; Gonçalves, V.M.F.; Tiritan, M.E.; Reis, R.L.; Ferreira, H.; Neves, N.M. Microfluidic Mixing System for Precise PLGA-PEG Nanoparticles Size Control. *Nanomedicine: Nanotechnology, Biology and Medicine* **2022**, *40*, 102482, doi:10.1016/j.nano.2021.102482.
100. Chiesa, E.; Dorati, R.; Modena, T.; Conti, B.; Genta, I. Multivariate Analysis for the Optimization of Microfluidics-Assisted Nanoprecipitation Method Intended for the Loading of Small Hydrophilic Drugs into PLGA Nanoparticles. *Int J Pharm* **2018**, *536*, 165–177, doi:10.1016/j.ijpharm.2017.11.044.
101. Streck, S.; Hong, L.; Boyd, B.J.; McDowell, A. Microfluidics for the Production of Nanomedicines: Considerations for Polymer and Lipid-Based Systems. *Pharm Nanotechnol* **2019**, *7*, 423–443, doi:10.2174/2211738507666191019154815.
102. Zhou, J.; Zhai, Y.; Xu, J.; Zhou, T.; Cen, L. Microfluidic Preparation of PLGA Composite Microspheres with Mesoporous Silica Nanoparticles for Finely Manipulated Drug Release. *Int J Pharm* **2021**, *593*, 120173, doi:10.1016/j.ijpharm.2020.120173.
103. Xu, Z.; Lu, C.; Riordon, J.; Sinton, D.; Moffitt, M.G. Microfluidic Manufacturing of Polymeric Nanoparticles: Comparing Flow Control of Multiscale Structure in Single-

Phase Staggered Herringbone and Two-Phase Reactors. *Langmuir* **2016**, *32*, 12781–12789, doi:10.1021/acs.langmuir.6b03243.

104. Riewe, J.; Erfle, P.; Melzig, S.; Kwade, A.; Dietzel, A.; Bunjes, H. Antisolvent Precipitation of Lipid Nanoparticles in Microfluidic Systems – A Comparative Study. *International Journal of Pharmaceutics* **2020**, *579*, 119167, doi:10.1016/j.ijpharm.2020.119167.
105. Shepherd, S.J.; Issadore, D.; Mitchell, M.J. Microfluidic Formulation of Nanoparticles for Biomedical Applications. *Biomaterials* **2021**, *274*, 120826, doi:10.1016/j.biomaterials.2021.120826.
106. Webb, C.; Forbes, N.; Roces, C.B.; Anderluzzi, G.; Lou, G.; Abraham, S.; Ingalls, L.; Marshall, K.; Leaver, T.J.; Watts, J.A.; et al. Using Microfluidics for Scalable Manufacturing of Nanomedicines from Bench to GMP: A Case Study Using Protein-Loaded Liposomes. *Int J Pharm* **2020**, *582*, 119266, doi:10.1016/j.ijpharm.2020.119266.
107. Liu, D.; Zhang, H.; Fontana, F.; Hirvonen, J.T.; Santos, H.A. Current Developments and Applications of Microfluidic Technology toward Clinical Translation of Nanomedicines. *Adv Drug Deliv Rev* **2018**, *128*, 54–83, doi:10.1016/j.addr.2017.08.003.
108. Nakamura, T.; Kawai, M.; Sato, Y.; Maeki, M.; Tokeshi, M.; Harashima, H. The Effect of Size and Charge of Lipid Nanoparticles Prepared by Microfluidic Mixing on Their Lymph Node Transitivity and Distribution. *Mol Pharm* **2020**, *17*, 944–953, doi:10.1021/acs.molpharmaceut.9b01182.
109. Shepherd, S.J.; Warzecha, C.C.; Yadavali, S.; El-Mayta, R.; Alameh, M.-G.; Wang, L.; Weissman, D.; Wilson, J.M.; Issadore, D.; Mitchell, M.J. Scalable MRNA and SiRNA Lipid Nanoparticle Production Using a Parallelized Microfluidic Device. *Nano Lett* **2021**, *21*, 5671–5680, doi:10.1021/acs.nanolett.1c01353.
110. Shan, H.; Lin, Q.; Wang, D.; Sun, X.; Quan, B.; Chen, X.; Chen, Z. 3D Printed Integrated Multi-Layer Microfluidic Chips for Ultra-High Volumetric Throughput Nanoliposome Preparation. *Front Bioeng Biotechnol* **2021**, *9*, 773705, doi:10.3389/fbioe.2021.773705.

Aim of the work

The main aim of this work was to design drug-loaded polymer and lipid nanosystems for biomedical applications of small molecules. Firstly, we assumed that the chemical characteristics of lipid and polymer NPs could be exploited to formulate loaded DDSs. Indeed, the structure of SQ derivatives and PLGA could allow the electrostatic interaction with positively charged drug molecules and/or the hydrophobic interaction for an efficient drug encapsulation avoiding a covalent linkage between the drug and the polymer. Such biocompatible and biodegradable nanoparticulate systems could increase drug stability and bioavailability, minimizing side effects.
Secondly, we hypothesized that by embedding selected ligands able to specifically recognize receptors overexpressed by cells DDSs cellular uptake could be increased. After screening in literature possible targeting molecules, a small zwitterion compound has been selected for muscular active targeting.

Therefore, the project was divided into different parts: i) formulation of drug-loaded SQ and PLGA NPs, selecting an old drug in the frame of drug repurposing for anticancer applications, ii) encapsulation of a novel therapeutic molecule able to act on pro-inflammatory macrophages involved in muscular diseases (MDs) physiopathology, iii) association of PLGA NPs to specific agents directed toward muscular cells.

To reach this aim, specific objectives were:

1. to prepare, optimize and physicochemically characterize pentamidine free base (PTM-B)-loaded PLGA and SQ NPs and test the anticancer activity
2. to prepare, optimize and physicochemically characterize 991-loaded PLGA NPs produced by the microfluidic technique
3. to evaluate the *in vitro* activity of 991-loaded PLGA NPs on fibrotic bone marrow-derived macrophages (BMDMs) to reduce inflammation and fibrosis
4. to study the *in vivo* biodistribution and activity of 991-loaded PLGA NPs after intravenous administration to MDs mouse model
5. to associate a derivative of carnitine to PLGA NPs, thus allowing the targeting of carnitine receptor overexpressing muscular cells
6. to evaluate the preferential uptake of actively targeted PLGA NPs by muscular cells.

The manuscript is divided into two parts: a general overview of nanomedicine and its applications and an experimental section that is further divided into 6 chapters (Chapter I, II, III, IV, V and VI).

A bibliographical section included a general introduction about the main DDSs, their applications and manufacturing processes.

Then, a description of PTM as a repurposed drug for different biological applications is highlighted by a published review in Pharmaceutics, doi: 10.3390/pharmaceutics13020278. Moreover, a focus on nanomedicine application in inflammatory status of muscular dystrophies is provided by a published review in Drug Delivery and Translational Research, doi: 10.1007/s13346-022-01127-4

Chapter I is dedicated to the formulation of lipid SQ NPs. The process of NPs preparation, optimization and physicochemical characterization is presented. A formulation study on the feasibility of SQ NPs obtained by electrostatic interactions is provided. On the bases of the chemical characteristics of the drug, PTM-B-loaded SQ NPs were prepared studying the influence of different formulation parameters on nanosuspension physicochemical properties (submitted original research article).

Chapter II is dedicated to the formulation of PLGA NPs. The study of the preparation of polymer NPs, the optimization and physicochemical characterization is presented. A proof-of-concept of the PTM-B anticancer activity is reported. The results of this part have been published in Journal of Pharmaceutical Sciences, doi: 10.1016/j.xphs.2019.11.011.

Chapter III describes a physicochemical analysis of PLGA NPs colloidal stability in presence of different stabilizers and media (original research article in preparation).

Chapter IV is devoted to the design and development of PLGA NPs for 5'-AMP-activated protein kinase (AMPK) activator molecule encapsulation. A small benzimidazole molecule, termed 991, has been selected as a model drug. The work presents the process of the conventional formulation method and the microfluidic manufacturing process. The optimization of translated formulation and physicochemical characterization is reported (original research article in preparation).

Chapter V includes the *in vitro* evaluation of the 991-loaded nanosystem activity on BMDMs. The *in vivo* biodistribution of PLGA NPs in superior Duchenne muscular dystrophy (DMD) mouse model (D2.mdx) is described. Then, the activity of encapsulated 991 has been studied *in vivo* to evaluate the positive effect on fibrosis and inflammation that characterize *mdx* mouse model (original research article in preparation).

Chapter VI focuses on the design of PLGA NPs actively targeted towards muscular cells. To this aim, a derivative of L-carnitine has been added to NPs and a formulation study of has been set up to optimize the nanosystem. Results concerning the *in vitro* evaluation of preferential uptake of targeted NPs are presented.

Reviews

Review

Nanotechnological approaches for pentamidine delivery

I. Andreana, V. Bincoletto, P. Milla, F. Dosio, B. Stella, S. Arpicco

(Published in 2022)

Drug Delivery and Translational Research
https://doi.org/10.1007/s13346-022-01127-4

ORIGINAL ARTICLE

Nanotechnological approaches for pentamidine delivery

Ilaria Andreana[1] · Valeria Bincoletto[1] · Paola Milla[1] · Franco Dosio[1] · Barbara Stella[1] · Silvia Arpicco[1]

Accepted: 31 January 2022

Abstract
Pentamidine (PTM), which is a diamine that is widely known for its antimicrobial activity, is a very interesting drug whose mechanism of action is not fully understood. In recent years, PTM has been proposed as a novel potential drug candidate for the treatment of mental illnesses, myotonic dystrophy, diabetes, and tumors. Nevertheless, the systemic administration of PTM causes severe side effects, especially nephrotoxicity. In order to efficiently deliver PTM and reduce its side effects, several nanosystems that take advantage of the chemical characteristics of PTM, such as the presence of two positively charged amidine groups at physiological pH, have been proposed as useful delivery tools. Polymeric, lipidic, inorganic, and other types of nanocarriers have been reported in the literature for PTM delivery, and they are all in different development phases. The available approaches for the design of PTM nanoparticulate delivery systems are reported in this review, with a particular emphasis on formulation strategies and in vitro/in vivo applications. Furthermore, a critical view of the future developments of nanomedicine for PTM applications, based on recent repurposing studies, is provided.

Keywords Pentamidine · Drug delivery · Liposomes · Nanoparticles · Repurposing

Introduction

Nanocarrier-based drug delivery has gained ever increasing amounts of attention in recent decades thanks to the characteristics that it can provide: increased drug solubility, modified pharmacokinetics, sustained release, tissue targeting, reduced toxicity, biosafety, and the ability to bypass biological barriers, which result in higher drug efficacy and bioavailability [1–3]. A plethora of different nanocarriers have been proposed for different diseases, such as cancer, central nervous system–related disorders, immune diseases, and, more recently, viral infections [4–7]. Proposed drug nanocarriers differ in their composition (mainly lipid, polymeric, or inorganic) and their structure (matrix or vesicular systems, including those with an aqueous, lipid, or gas core) and several incorporation strategies have been adopted, both for lipophilic and, sometimes, hydrophilic compounds, which is even more challenging [8, 9]. Among the molecules that have been considered for nanoencapsulation, we can find pentamidine (PTM), which is a drug that was initially developed as a synthetic analogue of insulin and is now a Food and Drug Administration (FDA)– and European Medicines Agency (EMA)–approved molecule for the treatment of a range of parasitic infections (Table 1) [10, 11].

PTM [1,5-bis(4-amidinophenoxy)pentane] (CAS Registry number 100–33-4) (Fig. 1) is an aromatic diamidine, which has been marketed in the form of two salts, isethionate [bis(2-hydroxyethane-1-sulfonic acid)] and mesylate [bis(methanesulfonic acid)], and is administered via the intravenous (i.v.) and intramuscular routes (i.m.) and via inhalation [12, 13]. Its chemical and physical properties indicate that PTM is a solid (melting point 186 °C, decomposes) that is completely water soluble at 25 °C (0.0236 mg/mL, predicted) with a logP of 4 (experimental) and a pKa of 12.13 (predicted) [14]. At physiological pH, both amidine groups are positively charged, meaning that PTM has poor oral bioavailability [15, 16]. Consequently, PTM is used i.v. in the treatment of trypanosomiasis, leishmaniasis, and *Pneumocystis pneumonia* (PCP), and is usually inhaled in aerosol form to prevent PCP in high-risk, HIV-infected patients [17–19].

Although PTM is widely used, its application as a curative strategy for infectious diseases and in new therapeutic options urgently requires approaches to improve its therapeutic efficacy, to overcome drug resistance, and to reduce the complications that are caused by its associated adverse

✉ Barbara Stella
barbara.stella@unito.it

[1] Department of Drug Science and Technology, University of Turin, Via P. Giuria 9, 10125 Turin, Italy

Published online: 25 February 2022

Table 1 Commercially available products containing pentamidine isethionate

Name	Physical description	Dosage as active ingredient (mg)	Company
Nebupent®	Powder for solution	300	Fresenius Kabi, APP Pharmaceuticals
Pentacarinat®	Lyophilized powder	200/300	Aventis Pharma, Lepetit
Pentam®	Powder for solution	300	Fresenius Kabi, APP Pharmaceuticals
Pneumopent®	Lyophilized powder	60	Fisons Pharmaceuticals
Pentamidine isethionate	Powder for solution	200/300	Mayne Pharma, David Bull Laboratories, Taylor Pharmaceuticals, Avet Pharmaceuticals, Seton Pharmaceuticals, Abbott Laboratories

Administration route: by inhalation or i.v. injection

effects [20]. The objective of this review is to discuss the advanced strategies that have been adopted to improve PTM delivery. Two different approaches have been developed to overcome the issues inherent in PTM use. The first is the synthesis of new PTM derivatives to provide compounds with better pharmaceutical activity, higher lipophilicity, and lower cytotoxicity. The most promising compounds have been tested in in vitro and in vivo models. This approach is out of the scope of this review. However, papers by Porcheddu et al. and Soeiro et al. provide a full description of the chemical modification methods and synthetic routes used to obtain PTM derivatives [21, 22]. The second approach involves nanotechnology and is the topic of this review. Although not reported in this paper, microcapsules have also been proposed as a means to encapsulate PTM [23–26]; in these preliminary formulation studies, PTM was used as a model drug to analyze the influence of various preparation parameters on the physico-chemical characteristics of drug-loaded poly(lactide-*co*-glycolide) (PLGA) microparticles.

Herein, we will initially explore the previously approved and newly proposed therapeutic applications of PTM, focusing on its repurposing in cancer, as well as in brain and muscular disorders (Fig. 2). Secondly, we will consider the most relevant nanomedicine-based strategies that make use of the physico-chemical properties of PTM to overcome its drawbacks and increase its therapeutic compliance. An in-depth analysis of structure, composition, features, benefits, and uses has been conducted for these systems.

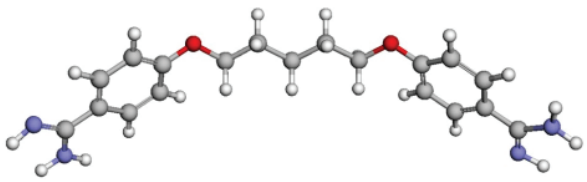

Fig. 1 Ball and stick representation of PTM structure (carbon atoms are gray, oxygen red, nitrogen light blue, hydrogen white) [14]

Applications of PTM

Current PTM applications

PTM was first synthesized in the late 1930s as a hypoglycemic drug against trypanosomes as it was observed that the parasites require glucose for their in vitro maintenance [12]. PTM has been used since the 1940s and is still one of the most frequently used drugs for the treatment of the first stage of human African trypanosomiasis and other neglected diseases, such as malaria and leishmaniasis [27]. Moreover, aerosolized PTM was approved for use in prophylaxis against PCP in HIV-infected patients who are at high risk when infected [28]. It has been reported that the benzamidine moiety is the essential pharmacophore of several commercially available drugs for the treatment of parasitic and fungal diseases; these compounds are characterized by a symmetrical structure in which the aromatic rings are separated by a short acyclic linker [29, 30].

Leishmaniasis and human African trypanosomiasis are infective and endemic diseases that affect the population the world over. Leishmaniasis incidence occurs mainly in three geographical regions (South-East Asia, Latin America, and East Africa) with a total number cases of up to 1.2 million [31, 32]. The parasites are transmitted to humans in the bites of infected female phlebotomine sandflies as a flagellated, metacyclic promastigote, which is phagocyted by host macrophages and then differentiates into non-flagellated, replicative amastigotes, culminating in the expression of clinical disease [33, 34]. Leishmaniasis is characterized by several different clinical manifestations: ulcerative skin lesions that develop at the site of the sandfly bite, multiple non-ulcerative nodules, destructive mucosal inflammation, and disseminated visceral infection [35]. The development of the disease is determined by the parasite's characteristics, vector biology, and host factors, such as immune response [33], and affects organs including the liver and spleen. Pentavalent antimonials, which have a narrow therapeutic index and whose use has largely been limited, are still the first-line

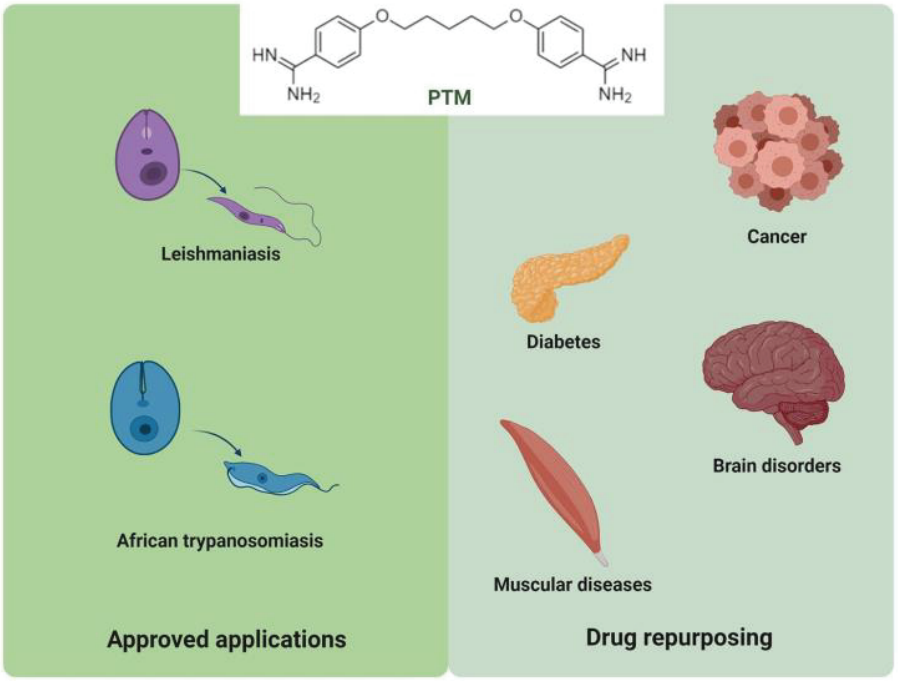

Fig. 2 Approved and proposed therapeutic applications of PTM (created with BioRender.com)

drugs in several parts of the world [36]. As a second choice, amphotericin B, PTM, and paromomycin are considered to be curative strategies. Amphotericin B is a highly efficacious antifungal drug, whose associated side effects are ameliorated in its liposomal formulation [37]. Over the years, paromomycin, an aminoglycoside antibiotic, has been used for the topical treatment of leishmaniasis, showing positive results in disease resolution [38]. Many clinically resistant cases have recently been found and treatment failure is an increasing problem. Technological and therapeutic approaches are urgently required if clinical outcomes are to be reached [39, 40]. Although PTM has poor oral bioavailability and pharmacokinetic issues, it can be successfully used for drug-resistant leishmaniasis.

Despite the pharmaceutical drawbacks of PTM, it is also used in the treatment of African trypanosomiasis. Human African trypanosomiasis, also known as sleeping sickness, is considered a neglected disease. It is caused by infection with protozoan parasites that belong to the genus *Trypanosoma*, which is widespread in 23 African countries [41–43]. Trypanosomes are surrounded by a surface glycoprotein that is recognized by the host's immune system. Nevertheless, a few of the parasites have changed their surface protein to continue proliferating unnoticed by the immune system [44]. It is transmitted via the bite of the blood-sucking tsetse fly, which is a viviparous insect that deposits a fully developed larva, which then needs to become an adult fly and feeds on an infected mammalian host in order to evolve into the infective form. Only about 0–1% of flies carries a mature infection that can be transmitted to another host [45]. The early stage of the pathology is characterized by headaches, weight loss, fever, and lymphadenopathy, which evolve into more serious symptoms that potentially involve the nervous system when the parasite crosses the blood–brain barrier (BBB) [46], producing neurological disturbances including sleep disorder, tremor of the hands, and motor weakness, and can lead to death if untreated [47]. The first-line therapeutic strategy in the early stage currently consists of suramin, melarsoprol, or PTM, although the application of PTM is limited because of its well-known side effects. In particular, hypoglycemia and hyperglycemia are the most common consequences of PTM therapy in patients affected by African trypanosomiasis [41, 48]. Hypoglycemia, with possible progression to insulin-dependent diabetes mellitus, has been reported in HIV-infected patients [49]. Moreover, PTM treatment may be accompanied by a prolongation of the QT interval on electrocardiograms and hypotension [50–52]. Other PTM side effects include abscesses at the site of intramuscular injection, abnormal liver function, pancreatic complications, nephrotoxicity, leucopoenia, thrombocytopenia, and hypocalcaemia [53–56].

PTM repurposing

As PTM is widely used in clinics and can be readily repurposed, it is the most studied member of the diamidines series, which is a class of compounds that can interfere

with many biomolecular targets, meaning that they have been studied as potential drugs for the treatment of a variety of diseases, such as parasitic diseases, tumors, brain disorders (Alzheimer's and Parkinson's diseases), hypertension, diabetes, and muscular dystrophy [57]. Indeed, PTM has been investigated, alone and in combination with approved drugs (to foster the discovery of new antimicrobial synergies), in several screenings for the targeting of fungal, Gram-negative, and other pathogens [58–63]. In addition, PTM has recently been identified as a potential blocker of the SARS-CoV-2 3a-channel in a library of 2839 approved-for-human-use drugs, although PTM activity is still to be tested on the whole virus [64].

The mechanism of action of PTM is not well understood despite all of these studies. It has been shown experimentally to interfere with numerous cellular processes [65]. PTM can act as an N-methyl-D-aspartate (NMDA) receptor antagonist, and thus displays neuroprotective effects [66, 67]. It is actively transported into trypanosomes and binds to DNA within the nucleus and kinetoplasts. Additionally, PTM interferes with polyamine synthesis, RNA polymerase activity, enters protozoan cells and binds to transfer RNA, and prevents the synthesis of proteins, nucleic acids, phospholipids, and folate. It is also known to be an antagonist of histone acetyltransferase and calmodulin [68, 69].

Recently, PTM has been reported to exhibit anticancer properties and has shown antiproliferative effects on various human cancer cell types, such as melanoma, prostate, ovarian, colon, breast, lung, and cervical cancers in in vitro and in vivo models. In these studies, several different sites of action were proposed for PTM, but the mechanism of its anticancer activity still remains elusive [70–78].

In another research field, PTM was the first small molecule proposed for the treatment of *Dystrophia myotonica* type 1 (DM1); it gave interesting initial results as it is able to reverse the splicing defects associated with myotonic dystrophy. Indeed, DM1 is a genetic disorder of autosomal dominant inheritance caused by pathological expansions of small DNA sequences ($(CTG)_n$) of the DMPK gene. The expanded DNA sequences are transcribed into RNA triplets which aggregate in specific structures called nuclear foci. The unstable structures sequestrate the muscleblind protein (MBNL) in the nucleus, resulting in a local reduction of protein level and characteristic symptoms of DM1 [79]. Several compounds have been shown to bind $(CUG)_n$ RNA and release the splicing factors. PTM was selected, together with aminoglycoside antibiotic neomycin B, from a small library of RNA binding compounds using in vitro and in vivo studies. Results showed that PTM is capable of binding the minor groove of AT-rich DNA and of preventing the formation of CUG – MBNL aggregates [80]. Additionally, PTM has recently been indicated as a therapeutic candidate for cardiac defects in DM1 and *Dystrophia myotonica* type 2 using fly heart models (*Drosophila*). Unfortunately, its high toxicity at therapeutic dose in vivo prevented its clinical use [81].

Administration, fate, and clinical trials of PTM

Because of its toxicity, the pharmacokinetics of PTM has only been studied in patients and has best been described by open, two- or three-compartment models [82, 83]. After the i.v. and i.m. administration of 4 mg/kg, the mean peak serum concentrations were found to be 0.6 mg/L and 0.2 mg/L, respectively, with large volumes of distribution at steady-state of 821 L and 2724 L, respectively. Multiple dosing results in progressive drug accumulation, and the steady-state was achieved after 8 days of i.v. therapy [83]. Mean plasma levels after 21 days of inhaled PTM isethionate at 600 mg/day via a nebulizer averaged 11.8 ± 10 ng/mL in patients with acute PCP [19]. PTM is approximately 70% protein bound and accumulates especially in the liver, spleen, kidneys, and adrenal glands [84]. Biliary excretion is the major elimination pathway for PTM, but release from the liver is slow (99% of the absorbed PTM in the liver is still present 24 h after i.v. infusion), whereas renal elimination only accounted for 4 to 7% of the administered dose [85].

The following clinical trials have been carried out, or are currently ongoing, to investigate the use of PTM for the treatment of a range of diseases.

I.v. administration

An i.v. formulation of PTM isethionate, OCZ 103 OS, has been tested as a potential therapy for cancer, including colorectal, pancreatic, and non-small cell lung cancers. However, the development of this formulation appears to have been discontinued after some phase I/II trials were completed (NCT00809796 [86], NCT01378143 [87], NCT00810953 [88], and NCT01844791[89]) (source US National Library of Medicine clinicaltrials.gov).

Oral administration

An oral formulation of PTM isethionate is being developed for the treatment of liver diseases, including hepatocellular carcinoma, non-alcoholic steatohepatitis, alcoholic steatohepatitis, non-alcoholic fatty liver disease, and liver metastasis. To date, as far as we know, the oral formulation has only been tested in a phase I study in adult cirrhotic patients with early-stage hepatocellular carcinoma, and safety, pharmacodynamics, and pharmacokinetics data were presented at the 67th Annual Meeting of the American Association for the Study of Liver Diseases [90, 91].

Local administration

The topical administration of PTM in a silicone-based gel is currently being tested for the treatment of hypertrophic scars in a phase I clinical trial that is still recruiting (NCT03403621) [92].

Intralesional injections of PTM for the treatment of cutaneous leishmaniasis have been tested in phase II/III studies in combination with topical miltefosine or paromomycin (NCT03445897 and NCT03096457) [93, 94].

PTM delivery approaches

PTM for parasitic diseases

The formulation of antiprotozoal drugs with nanocarriers is currently highly regarded as a promising approach in the treatment of leishmaniasis and trypanosomiasis [95–97], for which nanocarriers of different matrixes have been demonstrated to be effective [98–100]. The strategies that have been used to encapsulate PTM with drug delivery systems for the treatment of parasitic diseases are discussed below, and the characteristics of the PTM-based formulations are summarized in Table 2 and Fig. 3.

Liposomes

Liposomes, as drug delivery systems, are vesicles composed of phospholipids organized in concentric bilayers that enclose one or more aqueous spaces. A description of the preparation methods and their characteristics can be found elsewhere [101, 102]. The advantage of using liposomes as vehicles is their rapid accumulation in phagocytic cells as they are recognized as foreign particles, allowing liposomes to enhance the non-specific host defense [103]. However, there are only a few studies on the encapsulation of PTM in liposomes for use against *Leishmania* and human African trypanosomiasis. Nevertheless, after several different in vitro tests, researchers have found that glycoside-bearing liposomes can be used as systems to deliver drugs to macrophages in vivo [104]. On this basis, Banerjee et al. have described how sugar-grafted liposomes were prepared and tested against leishmaniasis in hamsters. Golden hamsters were infected via the intracardial passage of strain AG 83 from an Indian kala-azar patient. Different types of sugars, including mannose, galactose, and glucose, were tested. These formulations were injected subcutaneously (s.c.) into each animal every 3 days for a total of four doses over 10 days. Mannose-grafted liposomes that encapsulated PTM isethionate reduced the parasite load of the spleen by 85.1%, whereas liposomes without sugar lowered it by only 46.6%. Consequently, mannose-grafted liposomes were found to be the most efficient PTM delivery system, compared to other sugar-grafted carriers and sugar-free vesicles [105].

In another study, PTM isethionate was loaded into liposomes and tested against *Acanthamoeba*, which is an opportunistic protozoan pathogen that can cause blinding keratitis and fatal granulomatous encephalitis. Liposomes were prepared via the dehydration-rehydration method using L-α-phosphatidylcholine and either cholesterol or ergosterol. The results showed that both liposomal cholesterol-PTM and ergosterol-PTM were about 10 times more effective than the free drug at preventing the binding of *Acanthamoeba* to human brain microvascular endothelial cells. Moreover, loaded liposomes were more effective at reducing parasite-mediated human cell cytopathogenicity than free PTM [106].

Polymeric nanoparticles

The use of polymers has been widely investigated as they offer several advantages, such as controlled drug release, the protection of drugs against premature degradation, and surface engineering [107, 108]. Studies on PTM delivery have reported the applicability of polymeric nanoparticles as potential tools for the improvement of the drug's pharmacokinetics and pharmacodynamics drawbacks [109]. In one of the first studies on the encapsulation of anti-*Leishmania* therapeutic agents into polymeric nanoparticles, Gaspar et al. described the ability of polyalkylcyanoacrylate nanoparticles to reduce the effective dose (ED_{50}) of primaquine. Increased effectiveness was demonstrated in vitro in macrophages infected with the *Leishmania* parasite, compared to free primaquine [110]. The emerging knowledge of nanomedicine and the potential applicability of PTM have led to the same technological approach being studied and activity investigations being performed on the formulation of PTM with different acrylate nanoparticles. Optimized formulations of PTM-loaded methacrylate nanoparticles (mean size: 350 nm) were firstly tested in vitro using a strand of *Leishmania major* MON 25 and monocytes U 937, with increased drug efficacy being reported, compared to the free drug [111]. These interesting results led to Fusai et al. describing PTM-loaded polymethacrylate nanoparticles and their efficacy in vivo. The nanoparticles were first prepared via the emulsion polymerization technique using PTM isethionate, based on electrostatic interactions between drug and polymer [112]. Subsequently, in vivo studies on BALB/c inbred mice were performed to confirm the superior effectiveness of the PTM-loaded nanoparticles. The mice that were administered the free drug by i.v immediately showed side effects, while in the group that received drug-loaded nanoparticles there was no evidence of shock after the injection. The state of infection was evaluated after

Table 2 Recapitulative table of the described nanosystems that encapsulate PTM

Class of nanocarrier	Nanocarrier composition	PTM form	Preparation technique	Development phase	Admin. route	Pathology	Ref
Lipidic	Mannose-grafted liposomes	Isethionate salt	Thin lipid evaporation and hydration method	In vivo leishmaniasis hamster model	s.c	Leishmaniasis	Banerjee et al. [105]
	PEG-coated liposomes	Free base or isethionate salt	Thin lipid evaporation and hydration method or transmembrane gradient	In vitro test on a cancer cell line	/	Cancer	Stella et al. [148]
	PEG-coated liposomes	Isethionate salt	Thin lipid evaporation and hydration method	In vivo cancer mouse models	i.v	Cancer	Merian et al. [149]
Polymeric	Polymethacrylate	Isethionate salt	Emulsion polymerization	In vivo BALB/c	i.v	Leishmaniasis	Paul et al. [112]
	Methacrylate	Methane sulfonate solution	Emulsion polymerization	In vivo BALB/c	i.v	Leishmaniasis	Durand et al. [115]
	PCL	Isethionate salt	Double solvent evaporation	In vitro brain endothelial cells	/	Leishmaniasis	Omarch et al. [116]
	PEG-chitosan	Isethionate salt	Coacervation method	In vivo *T. brucei* mouse model	i.p	Trypanosomiasis	Unciti-Broceta et al. [119]
	PLA	Free base	Nanoprecipitation	In vivo BALB/c	i.v	Leishmaniasis	Paul et al. [112, 123] and Durand et al. [125]
	PEG-PLGA-PTM bioconjugate	Isethionate salt	Water/oil emulsion method	In vitro *L. infantum* amastigote-infected macrophages	/	Leishmaniasis	Scala et al. [127]
	PEG-PLGA	Not specified	Water-in-oil-in-water double emulsion/ solvent evaporation	In vivo African trypanosomiasis mouse model	i.p	Trypanosomiasis	Arias et al. [128]
	PLGA	Free base	Water-in-oil-in-water double emulsion/ solvent evaporation	In vivo leishmaniasis mouse model	s.c./os	Leishmaniasis	Valle et al. [129]
	Cyclodextrins	Isethionate salt	/	In vivo leishmaniasis mouse model	i.v./os	Leishmaniasis	De Paula et al. [134]
	Hyaluronic acid and polyarginine	Isethionate salt	Polyelectrolyte complexation	In vitro tests on cancer cell lines	/	Cancer	Carton et al. [147]
	PLGA and PEG-PLGA	Free base	Nanoprecipitation	In vitro test on a cancer cell line	/	Cancer	Stella et al. [148]

Table 2 (continued)

Class of nanocarrier	Nanocarrier composition	PTM form	Preparation technique	Development phase	Admin. route	Pathology	Ref
	Polysorbate 20, cholesterol, dicetyl phosphate, chitosan (niosomes)	Isethionate salt	Thin film hydration method	Physico-chemical characterization	/	Alzheimer's disease	Rinaldi et al. [141]
	Polysorbate 20, cholesterol, dicetyl phosphate, chitosan (niosomes)	Isethionate salt	Thin film hydration method	In vivo Parkinson's disease mouse model	Nasal	Parkinson's disease	Rinaldi et a. [143]
	Polysorbate 20, cholesterol, dicetyl phosphate, chitosan (niosomes)	Isethionate salt	Thin film hydration method	In vitro tests on human biopsies	/	Cancer	Seguella et al. [145]
Inorganic	Functionalized mesoporous silica	Free base or isethionate salt	Sol–gel method and functionalization	Physico-chemical characterization	/	/	Peretti et al. [151]
	PEG-gold	Not specified	Seed-mediated growth and PEGylation	In vitro tests on cancer cell lines	/	Cancer	Her at al. [153]

21 days by counting the number of amastigotes in the liver. Seventy-seven percent parasite suppression was reported in the group treated with loaded nanoparticles relative to the control group [113, 114]. Due to the increased interest in polyacrylate nanoparticles, Durand et al. have tested the activity of PTM-loaded methacrylate nanoparticles on a *Leishmania infantum* mouse model. The efficacy of encapsulated PTM against a different form of *Leishmania* was confirmed by the low value of ED_{50} obtained, demonstrating the ability of methacrylate nanoparticles to increase the efficacy of PTM and reduce side effects [115]. Nevertheless, the main problem of acrylate nanoparticles is their low biodegradability, which can be inconvenient for in vivo administration.

Moving on to other polymers, recent studies have involved the use of polycaprolactone polymer (PCL) loaded with PTM to enhance permeation through the BBB. PTM-loaded PCL nanoparticles were obtained using the double solvent evaporation method and their physiochemical characteristics were evaluated. Their spherical shape decreased from 345 to 270 nm after complexation with PTM, with a negative zeta potential value of around −30 mV and 12% drug release over a period of 24 h. The integrity of the BBB was evaluated in vitro on brain endothelial cells after loaded and unloaded nanoparticles were added; no significant tight junction alterations were observed, while loaded nanoparticles were shown to transport 66% of the PTM across the BBB [116].

Drug resistance, which complicates the management of *Leishmania* and African trypanosomiasis, is an important issue in the treatment of parasitic diseases [117, 118]. African trypanosome is generally covered by a single variant surface glycoprotein, termed VSG [42]. Combining PTM with targeted drug delivery systems overcomes possible drug resistance by taking advantage of the delivery systems' enhanced absorption into target cells, which is caused by surface engineering. Based on the chemical and biological structure of the infective parasite, Unciti-Broceta et al. have developed PEGylated chitosan nanoparticles that are surface-targeted with nanobodies that are able to specifically recognize specific VSG regions on a parasitic surface [119]. Indeed, these nanobodies are small enough to be able to infiltrate the dense parasite VSG coat and specifically recognize conserved epitopes common to the majority of the VSG molecules [120]. To this aim, nanobodies were coupled to the PEGylated PLGA nanoparticles via the EDC/NHS chemistry. Nanoparticles were obtained using coacervation methods and by selecting the right PEG chain length to allow the nanobodies to bind onto the parasitic membrane. Spherical-shape nanoparticles had a size of around 135 nm and a negative zeta potential value for both loaded and blank nanoparticles, meaning that PTM was completely loaded inside chitosan nanoparticles. In vitro drug release

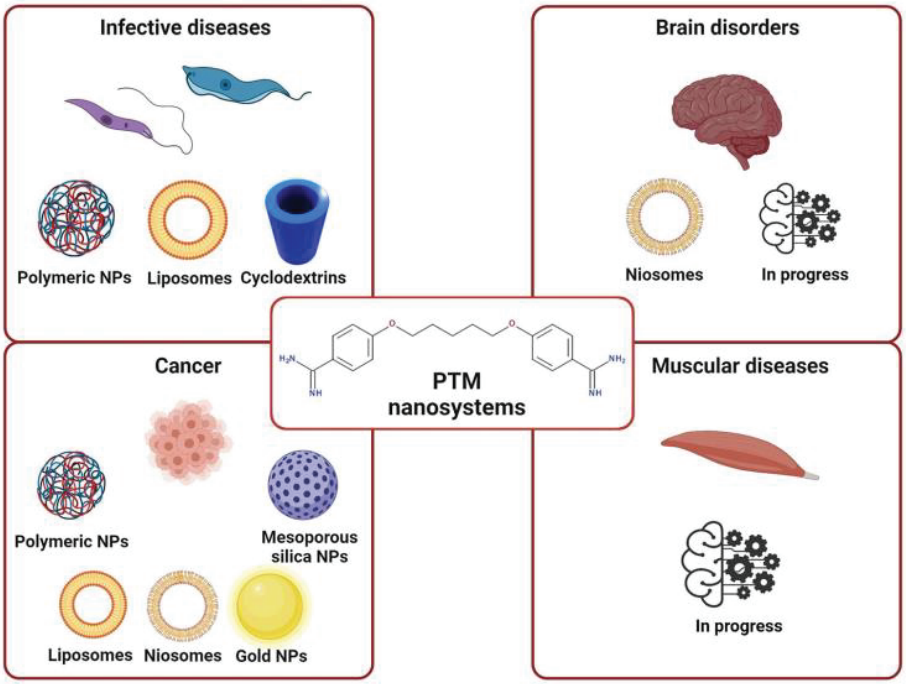

Fig. 3 Nanocarriers proposed for the delivery of PTM in different therapeutic approaches (created with BioRender.com)

had a pH-depend profile that increased in an acidic environment due to the chemical properties of PTM, which is advantageous for delivery to the parasitophorous vacuole of parasites (pH 5). The in vitro tests on the PTM-loaded nanoparticles showed a reduction in inhibitory concentration, compared to the unloaded and untargeted formulations. The in vivo therapeutic efficacy was evaluated in a mouse model infected by *Trypanosomiasis brucei* in order to provide further confirmation of the in vitro results. Mice were treated by intraperitoneal injection (i.p.) with PTM-loaded targeted nanoparticles, and the complete resolution of infection was observed, unlike the group receiving the same nanoparticle without the nanobody surface functionalization. The possibility of the alternative internalization of an active agent may decrease spontaneous drug resistance that can limit or reduce the applicability of some antiprotozoal drugs [119].

Other nanomedicine approaches have focused on poly(D,L-lactide) (PLA) and PLGA polyesters as they are known to be biodegradable and biocompatible [121, 122]. Paul et al. have described the preparation, the physiochemical properties and the stability of PTM-loaded PLA nanoparticles. Loaded nanocarriers were obtained via the nanoprecipitation technique using a combination of phospholipids and a poloxamer, which influences the physiochemical characteristics of the nanosuspension. PTM loading improved when the lipid content was directly increased: indeed, varying the phospholipid concentration from 0.6 to 1.25% (w:v), the highest drug loading (75.8%) was obtained with the highest concentration of phospholipids (1.25%). The formulation was stable over 9 months, in terms of its size and morphology [123, 124]. The biological evaluation of PTM-loaded PLA nanoparticles was performed by determining the ED_{50} against *Leishmania infantum* in male adult BALB/c mice by i.v. injection. A comparison between free PTM and loaded PTM showed the ability of PLA nanoparticles to induce a threefold increase in PTM activity (ED_{50}: 1.05 mg/kg for PTM vs. 0.32 mg/kg for loaded nanoparticles) [125].

Due to the growing interest in polymeric nanoparticles for antiprotozoal drug delivery, PLGA nanocarriers have been widely described. In particular, investigations into PLGA nanoparticles as a potential tool to deliver PTM have been reported. Starting from the formulation of PLGA microparticles to improve the pharmacokinetics and pharmacodynamics drawbacks of PTM [126], several research groups have focused their attention on nano-structured PLGA drug delivery systems. Recently, Scala et al. have proposed the covalent linkage of PTM with a PEG-PLGA block copolymer and a hyaluronic acid backbone by click chemistry. They aimed to evaluate the activity of free PTM and PTM bioconjugates. Moreover, they compared the therapeutic effects of PTM-loaded PEG-PLGA-PTM nanoparticles. The anti-leishmanial activity of PTM bioconjugates and PTM nanoparticles was assessed in vitro against infected macrophages. PTM bioconjugate and PTM nanoparticles displayed an IC_{50} 3.6 and 3.4 times lower than free PTM, respectively. In particular, the bioconjugate with hyaluronic acid was found to be the most active derivate, characterized by an IC_{50} value of 1.7 μM compared

to 7.5 μM of free PTM, confirming the effectiveness of the hyaluronic acid targeting scaffold [127].

As has already been reported for polyacrylates, PLGA nanoparticles were loaded with PTM and surface-engineered to efficiently recognize the surface of the protozoan pathogen *Trypanosoma brucei*, in particular a hidden conserved epitope within the glycophosphatidylinositol (GPI) anchor of the VSG protein (Fig. 4). PEGylated PTM-loaded PLGA nanoparticles were prepared via the water-in-oil-in-water (w/o/w) double emulsion/solvent evaporation technique, followed by PLGA functionalization with PEG chains and NbAn33 nanobodies (both through the EDC/NHS approach) for protozoan-surface recognition. A monodispersed nanosuspension that was characterized by a 145 nm mean diameter and a negative zeta potential value, of around -20 mV, was produced. In vitro studies highlighted the threefold increased efficacy of PTM-loaded PLGA nanocarriers. Moreover, the efficacy of the polymeric formulation increased fourfold again after surface functionalization by nanobodies, which underlines the importance of active targeting in enhancing cellular uptake in parasitic diseases. In vivo tests in an acute mouse model of African trypanosomiasis confirmed the urgent need for surface-nanobody conjugation. The infections of mice injected i.p. with the nanobody-targeted formulation were completely resolved at a tenfold lower dose. In vivo PTM activity was significantly optimized by PLGA encapsulation and, most of all, by surface functionalization, demonstrating that the trypanosome surface was an excellent therapeutic target [128].

PTM-loaded PLGA nanoparticles were developed, using the same preparation technique, for oral delivery in the treatment of *Leishmania* [129]. For the first time, the application of nanoparticles was devoted to the oral delivery of an antiprotozoal drug. The formulation of PTM-loaded PLGA nanoparticles included polyvinyl alcohol (PVA) as a stabilizer, which reduced the zeta potential value to around neutrality and gave a size of around 250 nm. The in vitro release profile confirmed the data reported by Arias et al. which described an initial burst release followed by constant release over 25 days [128]. In this study, the evaluation of the possible oral delivery of PTM-loaded nanoparticles was innovative and highly interesting. In vivo tests performed in a murine visceral leishmaniasis model aimed to compare infection resolution via the oral and s.c. delivery of loaded nanoparticles. S.c. administration did not lead to significant reductions in spleen and liver weight, which is the major end point in infective-disease studies. Interestingly, a reduction in the parasite presence in the spleen occurred after oral administration, which demonstrated the enhanced PTM uptake that was achieved by the oral route [129].

An innovative approach has recently been proposed to understand the toxicity of PTM through the BBB in the treatment of African trypanosomiasis. Sanderson et al. have evaluated the complexation of PTM with Pluronic, a polymer that can act as a stabilizer to prevent aggregation, opsonization, and recognition by macrophages and thus increase drug half-life, but that can also assemble into micelles to encapsulate drugs. Although the study did not show the increased uptake of PTM by the brain, this is, nonetheless, a new formulation of PTM that has been proposed as an alternative approach to test the activity of PTM on an African trypanosomiasis model [54].

Inclusion complexes

Cyclodextrins (CD) are composed of 6, 7, or 8 glucopyranose units (named α-, β-, and γ-CD, respectively) linked by a glycosidic bond and organized in a truncated cone. Polar hydroxyl groups on the molecule's border confer water solubility, while the inner hydrophobic cavity allows a variety of drugs to be hosted, forming inclusion complexes. β-CD are useful as they can improve the physico-chemical and biological properties of the included molecules, increasing tolerance and alleviating the drawbacks [130–133].

De Paula et al. have investigated the inclusion of PTM into the β-CD cavity, and then studied its activity when given via oral administration. First, β-CD that contained PTM (β-CD:PTM) were prepared using a freeze-drying method and tested in vivo

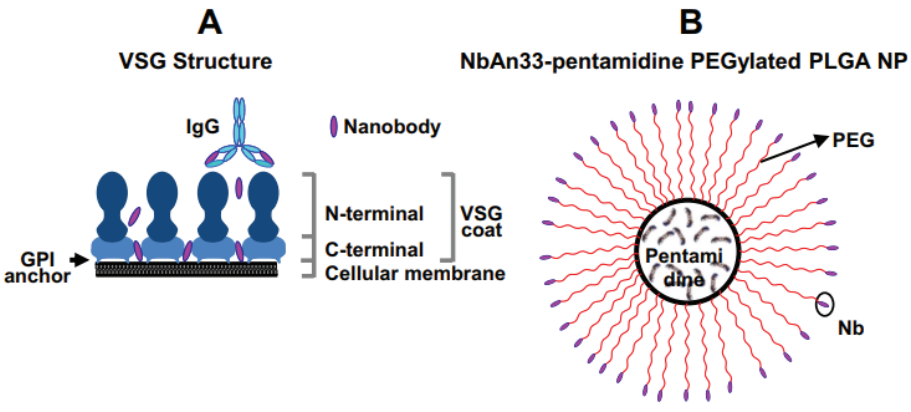

Fig. 4 **A** Schema of the VSG coat on trypanosome surface, in which the NbAn33 nanobody recognizes a hidden conserved epitope within the GPI anchor. **B** Schema of a NbAn33-PTM-PLGA nanoparticle. Reproduced with permission from [128]. Copyright Elsevier 2015

against *Leishmania infantum chagasi* parasites. Groups of mice were infected in the tail vein with promastigotes and treated with free PTM, β-CD:PTM (1:1), a saline solution, and Glucantime® (meglumine antimoniate, an approved antiprotozoal drug). No differences were found in the groups treated with free PTM and the control group, which was treated with the saline solution, in the liver and spleen. Orally administered β-CD:PTM and Glucantime® had similar efficacy, which was in contrast with the results obtained with orally administered PTM, which did not induce a significant reduction of the parasite burden. In addition, β-CD:PTM showed a greater reduction of parasitemia in the liver. The results demonstrated that β-CD:PTM are a promising alternative for the treatment of leishmaniasis [134].

PTM for other therapeutic purposes

As reported above, PTM has also been considered for possible clinical repositioning as an anti-Alzheimer's, anti-Parkinson's, and anticancer drug. PTM has been incorporated into different nanocarrier systems, whose composition and physico-chemical characteristics depend on both the administration route and physiopathological features, for each of these diseases (Table 2 and Fig. 3).

Niosomes

Besides liposomes, other nanoscale vesicles that contain aqueous cores have been used to deliver PTM, namely niosomes. Also known as non-ionic surfactant vesicles, niosomes are self-assembled vesicular nanocarriers formed of one or more layers of non-ionic surfactants and additives; niosomes can overcome some of the problems associated with liposomes, such as their low physical stability and high manufacturing costs [135].

PTM-loaded niosomes have been designed to reach the brain via intranasal administration, bypassing the BBB as a possible tool in brain disorders. Indeed, PTM inhibits S100 calcium-binding protein B (S100B) in glial cells through the blockage of the interaction between the S100B and p53 proteins [136]; PTM is able to exert anti-inflammatory and neuroprotective effects [137], as high expression levels of S100B have been shown to cause neuroinflammation and the progression of brain diseases [138, 139]. Nevertheless, PTM has a poor capacity to cross the BBB and reach the brain after intranasal administration [140]. In a first approach to the delivery of PTM to the brain, the drug was associated to niosomes for the treatment of Alzheimer's disease [141]. Commercial PTM isethionate was located in the bilayer, with an entrapment efficiency of about 10%, using the thin film hydration method. To overcome the low drug availability that is caused by rapid mucus clearance in the nasal cavity, mucoadhesive properties were provided to PTM-loaded niosomes by coating them with chitosan glutamate (CG) thanks to the electrostatic interactions between positively charged chitosan and the negatively charged dicetyl phosphate on the niosome surface. The interaction with mucin was confirmed using dynamic light scattering and fluorescence turbidity measurements for both uncoated and CG-coated niosomes, and is probably due to a non-specific mucin interaction. Nevertheless, CG can also act as a stabilizer and a penetration enhancer by widening the tight junctions between mucosal epithelial cells [142].

Further studies with PTM-niosomes were conducted in a Parkinson's disease murine model. In particular, chitosan-coated niosomes that contained PTM (entrapment efficiency of about 25%) were administered daily via the intranasal route in subchronic (1-methyl-4-phenyl-1,2,3,6-tetrahydropyridine) hydrochloride (MPTP)–intoxicated mice. The results showed that PTM-niosomes allowed 35–40% of the drug to be delivered into the brain. Moreover, the intranasal administration of PTM-loaded niosomes leads to an improvement of all the disease hallmarks and a significant reduction in neuroinflammation markers in mice, leading to a significant improvement in parkinsonian motor dysfunctions [143].

The S100B protein is also constitutionally expressed by enteric glial cells in the enteric nervous system; when it is overexpressed, it has a role in the perpetuation of a tumor-promoting microenvironment, driving the progression from chronic intestinal inflammation to colonic neoplastic lesions [144]. Thus, in order to evaluate PTM as a potential anticancer drug, the expression levels of the S100B and p53 proteins were quantified in human biopsies that were derived from controls, peritumoral tissues, ulcerative colitis, and colon cancer patients, at baseline and after the addition of PTM-loaded niosomes. The results showed that encapsulated PTM inhibits S100B activity and rescues p53 expression, leading to pro-apoptotic control in colon cancer. Moreover, the combination of PTM with gastro-resistant and bioadhesive niosomes will allow the drug to increase colonic bioavailability after oral administration [145].

Polymer nanoparticles and liposomes

In other approaches, the design of biocompatible PTM-loaded polymer nanocarriers has taken advantage of the drug's chemical structure, as PTM has two terminal amidine groups that are protonated in a wide pH range, including physiological/neutral conditions [146]. For example, PTM has been combined with nanocomplexes, made of the polymers hyaluronic acid and polyarginine, thanks to the electrostatic interactions between the anionic polysaccharide and the cationic drug (Fig. 5) [147]. In these structures, polyarginine was used to crosslink hyaluronic acid and form nanoparticles.

The measurements of the counterion isethionate released from the drug during nanoparticle formation, using ion

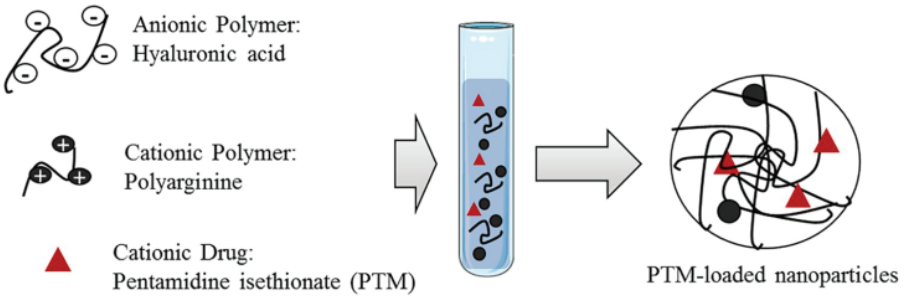

Fig. 5 Formation of PTM-loaded nanoparticles by polyelectrolyte association. Reproduced with permission from [147]. Copyright Elsevier 2019

exchange chromatography, showed a high drug encapsulation efficiency (80%). A comparison of the in vitro anticancer activity of free and encapsulated PTM in human lung (A549) and breast (MDA-MB-231) cancer cell lines suggested that the polyelectrolyte complexes allow enhanced cell internalization of the cationic drug to occur, with this probably being due to its more hydrophobic character after complexation, and increased cytotoxicity was thus observed. Moreover, both cell lines express CD44 receptors that specifically recognize hyaluronic acid. The polyelectrolyte complexes can therefore be selectively targeted towards these cancer cells through the interaction with these receptors [147].

Other biocompatible polymers have been used to deliver PTM to cancer cells via electrostatic interactions. In particular, negatively charged PLGA (with and without PEG) has been used to load the PTM free base (obtained from the commercial PTM isethionate to increase the drug lipophilicity) via the nanoprecipitation technique. In the same study, PTM was encapsulated into liposomes, as the free base or with different counterions, namely PTM citrate and PTM sulfate, for comparison. PTM base–containing liposomes were prepared using the thin lipid film hydration method by mixing phospholipids, cholesterol, and the PTM base in the organic phase, while PTM citrate and PTM sulfate were encapsulated into liposomes with a transmembrane citrate or sulfate gradient, starting from PTM isethionate in the external liposomal phase. This approach increased the encapsulation efficiency from 20% for the PTM base to 30% for PTM citrate and 45% for PTM sulfate. In PLGA nanoparticles, the PTM free base was almost totally incorporated (about 90%) thanks to the lipophilic and ionic interactions between PLGA and PTM. Drug release was faster for polymer nanoparticles than liposomes and, as a consequence, the cytotoxicity (evaluated in the A2780 human ovarian carcinoma cell line) was different and tunable according to the nanocarrier and the PTM form [148].

Moving on to liposomes in the anticancer field, other liposomal PTM formulations have been prepared using saturated/unsaturated phospholipids of different chain lengths and cholesterol content, with or without PEG on the outer surface. In this study, PTM isethionate was incorporated, using the thin lipid film hydration method, via its addition to the aqueous phase in the hydration procedure. The liposome composition greatly influenced the particle mean size, zeta potential, and encapsulation efficiency, which was in the 1–13% range. The pharmacokinetics profile of PTM, in five liposome formulations administered in non-tumor-bearing mice, showed that both the clearance and volume of distribution of PTM were significantly lower when administered in liposomes, compared to the free drug. PTM biodistribution and tumor accumulation after i.v. administration were evaluated in tumor-bearing mice (colorectal, lung, ovarian, and breast cancer). The results showed that liposomal PTM increased tumor drug accumulation and lowered drug exposure to vulnerable tissues, such as the kidneys, compared to the free drug [149].

Inorganic nanoparticles

Inorganic nanocarriers have also been used, with functionalized mesoporous silica nanoparticles (MSN) having been proposed for PTM delivery. MSN are versatile and stable materials with a mesoporous structure, a high specific surface area, and a huge, tunable pore volume that can accommodate large amounts of bioactive compounds. Both the external and inner surfaces can be functionalized with linkers, and this functionalization can affect therapeutic agent loading and release profiles and greatly influence MSN fate in biological fluids [150]. In particular, the encapsulation of PTM isethionate and the PTM free base into bare (MSN-OH), aminopropyl (MSN-NH_2), cyanopropyl (MSN-CN), and carboxypropyl (MSN-COOH)–functionalized MSN has been investigated. PTM isethionate was not incorporated into any MSN, while the PTM free base displayed significant drug loading with MSN-OH and MSN-COOH thanks to the electrostatic interactions. MSN-CN showed slower drug loading, while the adsorption capacity of MSN-NH_2 was found to be negligible. The presence of different functional groups also influenced the release of the drug: MSN-COOH showed higher retention than MSN-OH, indicating that the hydrophobic interactions of the drug with the grafted propyl chains had a significant impact on the stabilization of the host–guest complex [151]. This work allowed the authors to select MSN-COOH as the most promising functionalized MSN to be further used as

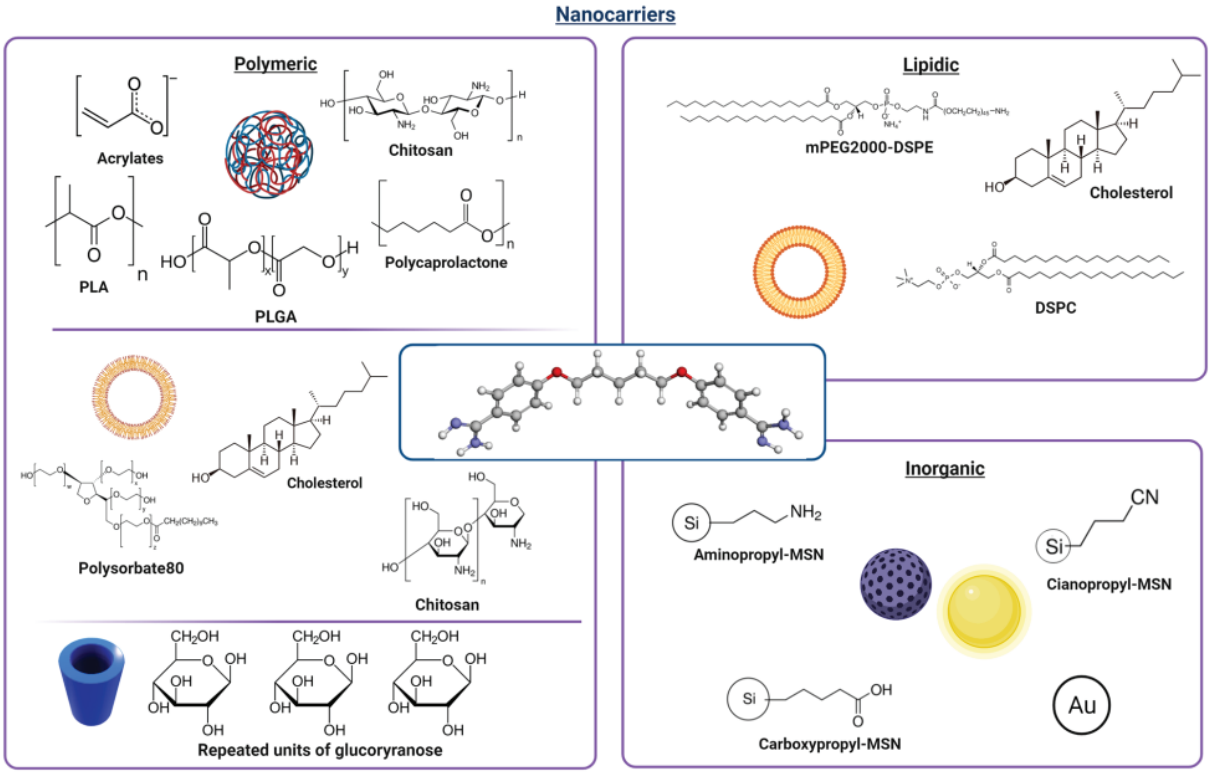

Fig. 6 Summary of PTM-loaded nanocarriers as a function of their chemical composition (created with BioRender.com)

drug delivery system that could be proposed for PTM delivery towards either cancer or muscle cells [152].

PTM has also been considered for use in combination with PEG-stabilized gold nanoparticles (AuNP) to enhance the effect of radiotherapy, in two triple-negative breast cancer cell lines, by targeting multiple pathways of radiosensitization. Although the loading of PTM onto AuNP was not the goal of the study, the authors evaluated the effect of AuNP as a single agent, in combination with PTM and after the pre-adsorption of the drug onto the nanoparticle surface to elucidate the underlying mechanisms of radiosensitization by the AuNP-PTM combination. The results showed that PTM enhances the radiosensitization effect of PEG-AuNP by exerting a dual action: by inhibiting radiation-induced DNA repair and increasing the cellular uptake of PEG-AuNP after surface adsorption, causing a change in the particle surface charge [153].

Conclusion

PTM is an old, FDA- and EMA-approved drug whose repurposing and delivery via nanocarriers of different composition have been extensively investigated (Fig. 6). Indeed, the interest in PTM is due to its well-known toxicology profile and multifactorial mechanism of action, although the latter has not yet been fully understood. PTM is appealing in terms of the design of nano-sized carriers as it is a small molecule whose physico-chemical characteristics (e.g., solubility in water and organic solvents) can be changed according to the PTM form (salt or free base) and the counterion in the salts. Moreover, PTM is positively charged at physiological pH, thus allowing both electrostatic and lipophilic interactions with nanocarrier components that can, in this way, reduce the positive charge of the drug and increase its passage through the cell membrane. The incorporation into nanocarriers may also modify the toxicological profile of PTM and/or allow the drug to be actively targeted towards the target site, lowering the administered dose. Finally, the reported variety of nanocarriers that are suitable for PTM delivery facilitate the tuning of drug encapsulation efficiency and release rate as a function of the disease and patient features. This aspect is of a crucial importance, as it has been demonstrated that PTM could be repurposed for pathologies other than infectious ones, especially rare muscular diseases, and this aspect justifies a renewed interest in PTM and further multidisciplinary efforts for investigations in this field.

However, several papers on PTM-loaded nanocarriers reported in the present review describe only preliminary in vitro results or even just formulative studies. Therefore,

a deeper analysis on the in vivo behavior of PTM-loaded nanocarriers is needed, particularly using models with animals infected with parasites or affected by the diseases for which PTM has been repurposed.

In conlusion, it is worth adding that the combination of PTM and nanocarriers implies also well-known critical features, especially in terms of industrial feasibility, as the system complexity increases. Indeed, the encapsulation of PTM would involve higher costs if compared to the production of the free drug. Furthermore, problems concerning the scalability, reproducibility (in terms of physico-chemical characteristics, such as mean size, zeta potential, drug loading), and compliance to regulatory standards can hamper its use in the clinic. All these issues have to be taken into account and evaluated as a function of the repurposed application.

Acknowledgements The authors thank Dr. Dale James Matthew Lawson for language editing.

Author contribution All authors contributed to the writing of this manuscript.

Availability of data and materials Not applicable.

Declarations

Ethics approval and consent to participate Not applicable.

Consent for publication All authors approved the version to be published.

Competing interests The authors declare no competing interests.

References

1. Shi J, Votruba AR, Farokhzad OC, Langer R. Nanotechnology in drug delivery and tissue engineering: from discovery to applications. Nano Lett. 2010;10:3223–30.
2. Nicolas J, Mura S, Brambilla D, Mackiewicz N, Couvreur P. Design, functionalization strategies and biomedical applications of targeted biodegradable/biocompatible polymer-based nanocarriers for drug delivery. Chem Soc Rev. 2013;42:1147–235.
3. Kim KS, Suzuki K, Cho H, Youn YS, Bae YH. Oral nanoparticles exhibit specific high-efficiency intestinal uptake and lymphatic transport. ACS Nano. 2018;12:8893–900.
4. van der Meel R, Sulheim E, Shi Y, Kiessling F, Mulder WJM, Lammers T. Smart cancer nanomedicine. Nat Nanotechnol. 2019;14:1007–17.
5. Babazadeh A, Mohammadi Vahed F, Jafari SM. Nanocarrier-mediated brain delivery of bioactives for treatment/prevention of neurodegenerative diseases. J Control Release. 2020;321:211–221.
6. Hanif S, Muhammad P, Chesworth R, Rehman FU, Qian RJ, Zheng M, Shi BY. Nanomedicine-based immunotherapy for central nervous system disorders. Acta Pharmacol Sin. 2020;41:936–53.
7. Tavakol S, Zahmatkeshan M, Mohammadinejad R, Mehrzadi S, Joghataei MT, Alavijeh MS, Seifalian A. The role of nanotechnology in current COVID-19 outbreak. Heliyon. 2021;7:e06841.
8. Tan YF, Lao LL, Xiong GM, Venkatraman S. Controlled-release nanotherapeutics: state of translation. J Control Release. 2018;284:39–48.
9. Arpicco S, Battaglia L, Brusa P, Cavalli R, Chirio D, Dosio F, Gallarate M, Milla P, Peira E, Rocco F, Sapino S, Stella B, Ugazio E, Ceruti M. Recent studies on the delivery of hydrophilic drugs in nanoparticulate systems. Journal of Drug Delivery Science and Technology. 2016;32:298–312.
10. FDA Abbreviated New Drug Application: 206666 pentamidine isethionate.
11. List of EU nationally authorized medicinal products with active substance pentamidine. Procedure No.: PSUSA/00002338/201706.
12. Sands M, Michael AK, Brown RB. Pentamidine: a review. Rev Infect Dis. 1985;7:625–34.
13. Burri C. Chemotherapy against human African trypanosomiasis: is there a road to success? Parasitology. 2010;137:1987–94.
14. Wishart DS, Feunang YD, Guo AC, Lo EJ, Marcu A, Grant JR, Sajed T, Johnson D, Li C, Sayeeda Z, Assempour N, Iynkkaran I, Liu Y, MacIejewski A, Gale N, Wilson A, Chin L, Cummings R, Le D, Pon A, Knox C, Wilson M. DrugBank 5.0: A major update to the DrugBank database for 2018. Nucleic Acids Res. 2018;46:D1074–D1082.
15. Fairlamb AH. Chemotherapy of human African trypanosomiasis: current and future prospects. Trends Parasitol. 2003;19:488–94.
16. Clement B, Burenheide A, Rieckert W, Schwarz J. Diacetyldiamidoximeester of pentamidine, a prodrug for treatment of protozoal diseases: synthesis, in vitro and in vivo biotransformation. ChemMedChem. 2006;1:1260–7.
17. Girard PM, Brun-Pascaud M, Farinotti R, Tamisier L, Kernbaum S. Pentamidine aerosol in prophylaxis and treatment of murine Pneumocystis carinii pneumonia. Antimicrob Agents Chemother. 1987;31:978–81.
18. Pentam (pentamidine isethionate i.v., i.m. injection) [Product Information]. APP Pharmaceuticals, LLC, Schaumburg, IL, 2008.
19. NebuPent (pentamidine isethionate oral inhalation) [Product Information]. APP Pharmaceuticals, LLC, Schaumburg, IL, 2011.
20. Jamshaid H, Din FU, Khan GM. Nanotechnology based solutions for anti-leishmanial impediments: a detailed insight. J Nanobiotechnology. 2021;19:106.
21. Porcheddu A, Giacomelli G, De Luca L. New pentamidine analogues in medicinal chemistry. Curr Med Chem. 2012;19:5819–36.
22. Soeiro MN, Werbovetz K, Boykin DW, Wilson WD, Wang MZ, Hemphill A. Novel amidines and analogues as promising agents against intracellular parasites: a systematic review. Parasitology. 2013;140:929–51.

23. Mandal TK. Evaluation of a novel phase separation technique for the encapsulation of water-soluble drugs in biodegradable polymer. Drug Dev Ind Pharm. 1998;24:623–9.
24. Mandal TK. Effect of solvent on the characteristics of pentamidine loaded microcapsule. J Biomater Sci Polym Ed. 1999;10:1–17.
25. Mandal TK, Bostanian LA, Graves RA, Chapman SR, Idodo TU. Porous biodegradable microparticles for delivery of pentamidine. Eur J Pharm Biopharm. 2001;52:91–6.
26. Mandal TK, Bostanian LA, Graves RA, Chapman SR. Poly(D, L-lactide-co-glycolide) encapsulated poly(vinyl alcohol) hydrogel as a drug delivery system. Pharm Res. 2002;19:1713–9.
27. Bray PG, Barrett MP, Ward SA, de Koning HP. Pentamidine uptake and resistance in pathogenic protozoa: past, present and future. Trends Parasitol. 2003;19:232–9.
28. Huang YS, Yang JJ, Lee NY, Chen GJ, Ko WC, Sun HY, Hung CC. Treatment of Pneumocystis jirovecii pneumonia in HIV-infected patients: a review. Expert Rev Anti Infect Ther. 2017;15:873–92.
29. Soeiro MN, De Souza EM, Stephens CE, Boykin DW. Aromatic diamidines as antiparasitic agents. Expert Opin Investig Drugs. 2005;14:957–72.
30. Werbovetz K. Diamidines as antitrypanosomal, antileishmanial and antimalarial agents. Curr Opin Investig Drugs. 2006;7:147–57.
31. Alvar J, Velez ID, Bern C, Herrero M, Desjeux P, Cano J, Jannin J, den Boer M, W.H.O.L.C. Team. Leishmaniasis worldwide and global estimates of its incidence. PLoS One. 2012;7:e35671.
32. World Health Organization, Health Topics, Leishmaniasis. https://www.who.int/westernpacific/health-topics/leishmaniasis. Accessed 15 Mar 2021.
33. Burza S, Croft SL, Boelaert M. Leishmaniasis. Lancet. 2018;392:951–70.
34. Reithinger R, Dujardin JC, Louzir H, Pirmez C, Alexander B, Brooker S. Cutaneous leishmaniasis. Lancet Infect Dis. 2007;7:581–96.
35. Mann S, Frasca K, Scherrer S, Henao-Martinez AF, Newman S, Ramanan P, Suarez JA. A review of leishmaniasis: current knowledge and future directions. Curr Trop Med Rep. 2021;1–12.
36. Chawla B, Madhubala R. Drug targets in Leishmania. J Parasit Dis. 2010;34:1–13.
37. Stone NR, Bicanic T, Salim R, Hope W. Liposomal amphotericin B (AmBisome(®)): a review of the pharmacokinetics, pharmacodynamics, clinical experience and future directions. Drugs. 2016;76:485–500.
38. Sundar S, Jha TK, Thakur CP, Sinha PK, Bhattacharya SK. Injectable paromomycin for visceral leishmaniasis in India. N Engl J Med. 2007;356:2571–81.
39. Ponte-Sucre A, Gamarro F, Dujardin JC, Barrett MP, Lopez-Velez R, Garcia-Hernandez R, Pountain AW, Mwenechanya R, Papadopoulou B. Drug resistance and treatment failure in leishmaniasis: a 21st century challenge. PLoS Negl Trop Dis. 2017;11:e0006052.
40. Bansal R, Sen SS, Muthuswami R, Madhubala R. Stigmasterol as a potential biomarker for amphotericin B resistance in Leishmania donovani. J Antimicrob Chemother. 2020;75:942–50.
41. Kennedy PG. Clinical features, diagnosis, and treatment of human African trypanosomiasis (sleeping sickness). Lancet Neurol. 2013;12:186–94.
42. Kennedy PGE, Rodgers J. Clinical and neuropathogenetic aspects of human African trypanosomiasis. Front Immunol. 2019;10:39.
43. World Health Organization, Fact sheets, Trypanosomiasis, human African (sleeping sickness). https://www.who.int/news-room/fact-sheets/detail/trypanosomiasis-human-african-(sleeping-sickness). Accessed 15 Mar 2021.
44. Dubois ME, Demick KP, Mansfield JM. Trypanosomes expressing a mosaic variant surface glycoprotein coat escape early detection by the immune system. Infect Immun. 2005;73:2690–7.
45. Brun R, Blum J, Chappuis F, Burri C. Human African trypanosomiasis. Lancet. 2010;375:148–59.
46. Bottieau E, Clerinx J. Human African trypanosomiasis: progress and stagnation. Infect Dis Clin North Am. 2019;33:61–77.
47. Buscher P, Cecchi G, Jamonneau V, Priotto G. Human African trypanosomiasis. Lancet. 2017;390:2397–409.
48. Arino T, Karakawa S, Ishiwata Y, Nagata M, Yasuhara M. Effect of cimetidine on pentamidine induced hyperglycemia in rats. Eur J Pharmacol. 2012;693:72–9.
49. Coyle P, Carr AD, Depczynski BB, Chisholm DJ. Diabetes mellitus associated with pentamidine use in HIV-infected patients. Med J Aust. 1996;165:587–8.
50. Kuryshev YA, Ficker E, Wang L, Hawryluk P, Dennis AT, Wible BA, Brown AM, Kang J, Chen XL, Sawamura K, Reynolds W, Rampe D. Pentamidine-induced long QT syndrome and block of hERG trafficking. J Pharmacol Exp Ther. 2005;312:316–23.
51. Antoniou T, Gough KA. Early-onset pentamidine-associated second-degree heart block and sinus bradycardia: case report and review of the literature. Pharmacotherapy. 2005;25:899–903.
52. Glikson M, Dresner-Feigin R, Pollack A, Wolf D, Galun E, Tur-Kaspa R. Pentamidine-induced cardiotoxicity. Isr J Med Sci. 1990;26:588–9.
53. de Menezes JP, Guedes CE, Petersen AL, Fraga DB, Veras PS. Advances in development of new treatment for leishmaniasis. Biomed Res Int. 2015;2015:815023.
54. Sanderson L, da Silva M, Sekhar GN, Brown RC, Burrell-Saward H, Fidanboylu M, Liu B, Dailey LA, Dreiss CA, Lorenz C, Christie M, Persaud SJ, Yardley V, Croft SL, Valero M, Thomas SA. Drug reformulation for a neglected disease. The NANOHAT project to develop a safer more effective sleeping sickness drug. PLoS Negl Trop Dis. 2021;15:e0009276.
55. Pelucio MT, Rothenhaus T, Smith M, Ward DJ. Fatal pancreatitis as a complication of therapy for HIV infection. J Emerg Med. 1995;13:633–7.
56. Prabhavalkar S, Masengu A, O'Rourke D, Shields J, Courtney A. Nebulized pentamidine-induced acute renal allograft dysfunction. Case Rep Transplant. 2013;2013:907593.
57. Huang TL, Mayence A, Vanden Eynde JJ. Some non-conventional biomolecular targets for diamidines. A short survey. Bioorg Med Chem. 2014;22:1983–1992.
58. Ortiz SC, Huang M, Hull CM. Spore germination as a target for antifungal therapeutics. Antimicrob Agents Chemother. 2019.
59. Vallieres C, Singh N, Alexander C, Avery SV. Repurposing nonantifungal approved drugs for synergistic targeting of fungal pathogens. ACS Infect Dis. 2020;6:2950–8.
60. Wu C, Xia L, Huang W, Xu Y, Gu Y, Liu C, Ji L, Li W, Wu Y, Zhou K, Feng X. Pentamidine sensitizes FDA-approved non-antibiotics for the inhibition of multidrug-resistant Gram-negative pathogens. Eur J Clin Microbiol Infect Dis. 2020;39:1771–9.
61. Nixon SA, Saez NJ, Herzig V, King GF, Kotze AC. The antitrypanosomal diarylamidines, diminazene and pentamidine, show anthelmintic activity against Haemonchus contortus in vitro. Vet Parasitol. 2019;270:40–6.
62. Walhart T, Isaacson-Wechsler E, Ang KH, Arkin M, Tugizov S, Palefsky JM. A cell-based Renilla luminescence reporter plasmid assay for high-throughput screening to identify novel FDA-approved drug inhibitors of HPV-16 infection. SLAS Discov. 2020;25:79–86.
63. Stead AM, Bray PG, Edwards IG, DeKoning HP, Elford BC, Stocks PA, Ward SA. Diamidine compounds: selective uptake and targeting in Plasmodium falciparum. Mol Pharmacol. 2001;59:1298–306.

64. Tomar PPS, Krugliak M, Arkin IT. Blockers of the SARS-CoV-2 3a channel identified by targeted drug repurposing. Viruses. 2021;13.
65. Franco J, Scarone L, Comini MA. Chapter Three - Drugs and drug resistance in African and American trypanosomiasis. In: Botta M editor. Annual reports in medicinal chemistry. Academic Press; 2018. p. 97–133.
66. Reynolds IJ, Aizenman E. Pentamidine is an N-methyl-D-aspartate receptor antagonist and is neuroprotective in vitro. J Neurosci. 1992;12:970–5.
67. Block F, Schmitt T, Schwarz M. Pentamidine, an inhibitor of spinal flexor reflexes in rats, is a potent N-methyl-D-aspartate (NMDA) antagonist in vivo. Neurosci Lett. 1993;155:208–11.
68. Kitamura Y, Arima T, Imaizumi R, Sato T, Nomura Y. Inhibition of constitutive nitric oxide synthase in the brain by pentamidine, a calmodulin antagonist. Eur J Pharmacol. 1995;289:299–304.
69. Sun T, Zhang Y. Pentamidine binds to tRNA through non-specific hydrophobic interactions and inhibits aminoacylation and translation. Nucleic Acids Res. 2008;36:1654–64.
70. Pathak MK, Dhawan D, Lindner DJ, Borden EC, Farver C, Yi T. Pentamidine is an inhibitor of PRL phosphatases with anticancer activity. Mol Cancer Ther. 2002;1:1255–64.
71. Chow TY, Alaoui-Jamali MA, Yeh C, Yuen L, Griller D. The DNA double-stranded break repair protein endo-exonuclease as a therapeutic target for cancer. Mol Cancer Ther. 2004;3:911–9.
72. Lee MS, Johansen L, Zhang Y, Wilson A, Keegan M, Avery W, Elliott P, Borisy AA, Keith CT. The novel combination of chlorpromazine and pentamidine exerts synergistic antiproliferative effects through dual mitotic action. Cancer Res. 2007;67:11359–67.
73. Smith J, Stewart BJ, Glaysher S, Peregrin K, Knight LA, Weber DJ, Cree IA. The effect of pentamidine on melanoma ex vivo. Anticancer Drugs. 2010;21:181–5.
74. Jung HJ, Suh SI, Suh MH, Baek WK, Park JW. Pentamidine reduces expression of hypoxia-inducible factor-1alpha in DU145 and MDA-MB-231 cancer cells. Cancer Lett. 2011;303:39–46.
75. Qiu G, Jiang J, Liu XS. Pentamidine sensitizes chronic myelogenous leukemia K562 cells to TRAIL-induced apoptosis. Leuk Res. 2012;36:1417–21.
76. Zerbini LF, Bhasin MK, de Vasconcellos JF, Paccez JD, Gu X, Kung AL, Libermann TA. Computational repositioning and preclinical validation of pentamidine for renal cell cancer. Mol Cancer Ther. 2014;13:1929–41.
77. Rahman A, O'Sullivan P, Rozas I. Recent developments in compounds acting in the DNA minor groove. Medchemcomm. 2019;10:26–40.
78. Liu L, Wang F, Tong Y, Li LF, Liu Y, Gao WQ. Pentamidine inhibits prostate cancer progression via selectively inducing mitochondrial DNA depletion and dysfunction. Cell Prolif. 2020:53;e12718.
79. Andreana I, Repellin M, Carton F, Kryza D, Briancon S, Chazaud B, Mounier R, Arpicco S, Malatesta M, Stella B, Lollo G. Nanomedicine for gene delivery and drug repurposing in the treatment of muscular dystrophies. Pharmaceutics. 2021;13.
80. Warf MB, Nakamori M, Matthys CM, Thornton CA, Berglund JA. Pentamidine reverses the splicing defects associated with myotonic dystrophy. Proc Natl Acad Sci U S A. 2009;106:18551–6.
81. Chakraborty M, Llamusi B, Artero R. Modeling of myotonic dystrophy cardiac phenotypes in Drosophila. Front Neurol. 2018;9:473.
82. Conte JE Jr, Upton RA, Phelps RT, Wofsy CB, Zurlinden E, Lin ET. Use of a specific and sensitive assay to determine pentamidine pharmacokinetics in patients with AIDS. J Infect Dis. 1986;154:923–9.
83. Conte JE Jr. Pharmacokinetics of intravenous pentamidine in patients with normal renal function or receiving hemodialysis. J Infect Dis. 1991;163:169–75.
84. Donnelly H, Bernard EM, Rothkotter H, Gold JW, Armstrong D. Distribution of pentamidine in patients with AIDS. J Infect Dis. 1988;157:985–9.
85. Thomas SH, Page CJ, Blower PJ, Chowienczyk P, Ward A, Kamali F, Bradbeer CS, Bateman NT, O'Doherty MJ. Disposition of intravenous 123iodopentamidine in man. Nucl Med Biol. 1997;24:327–32.
86. A safety study of pentamidine in patients with metastatic colon cancer undergoing standard chemotherapy as second-line and/or third-line treatment. https://ClinicalTrials.gov/show/NCT00809796. Accessed 6 Jun 2021.
87. Using OCZ103-OS in patients with unresectable and locally recurrent or metastatic colorectal cancer undergoing standard chemotherapy. https://ClinicalTrials.gov/show/NCT01378143. Accessed 06 Jun 2021.
88. A safety study using pentamidine in patients with pancreatic cancer undergoing standard therapy, https://ClinicalTrials.gov/show/NCT00810953. Accessed 6 Jun 2021.
89. An exploratory study of OCZ103-OS in combination with standard of care in stage IV non-small cell lung cancer (NSCLC) patients. https://ClinicalTrials.gov/show/NCT01844791. Accessed 6 Jun 2021.
90. M.S. Bilodeau M, Burak KW, Duan J, Ravenelle F, Colin P. Clinical evidence of hepatoselectivity of oral pentamidine (VLX103) in cirrhotic patients with early stage hepatocellular carcinoma. Hepatology. 2016;64:136–361.
91. M.S. Bilodeau M, Burak KW, Duan J, Ravenelle F, Colin P. Clinical safety and pharmacodynamics of VLX103, a new orally administered pentamidine formulation, in cirrhotic patients with early stage hepatocellular carcinoma. Hepatology. 2016;64:136–361.
92. Hypertrophic scar prevention by novel topical gel application. https://ClinicalTrials.gov/show/NCT03403621. Accessed 6 Jun 2021.
93. Miltefosine plus IL pentamidine for Bolivian CL. https://ClinicalTrials.gov/show/NCT03445897. Accessed 6 Jun 2021.
94. Topical paromomycin for cutaneous leishmaniasis in Bolivia. https://ClinicalTrials.gov/show/NCT03096457. Accessed 6 Jun 2021.
95. Nafari A, Cheraghipour K, Sepahvand M, Shahrokhi G, Gabal E, Mahmoudvand H. Nanoparticles: new agents toward treatment of leishmaniasis, Parasite Epidemiol. Control. 2020;10:e00156–e00156.
96. Ortega V, Giorgio S, de Paula E. Liposomal formulations in the pharmacological treatment of leishmaniasis: a review. J Liposome Res. 2017;27:234–48.
97. de Almeida L, Terumi Fujimura A, Del Cistia ML, Fonseca-Santos B, Braga Imamura K, Michels PAM, Chorilli M, Graminha MAS. Nanotechnological strategies for treatment of leishmaniasis--a review. J Biomed Nanotechnol. 2017;13:117–133.
98. Tosyali OA, Allahverdiyev A, Bagirova M, Abamor ES, Aydogdu M, Dinparvar S, Acar T, Mustafaeva Z, Derman S. Nano-co-delivery of lipophosphoglycan with soluble and autoclaved leishmania antigens into PLGA nanoparticles: evaluation of in vitro and in vivo immunostimulatory effects against visceral leishmaniasis. Mater Sci Eng C Mater Biol Appl. 2021;120:111684.
99. Borborema SET, Osso Jr JA, Tempone AG, de Andrade Jr HF, do Nascimento N. Pharmacokinetic of meglumine antimoniate encapsulated in phosphatidylserine-liposomes in mice model: a candidate formulation for visceral leishmaniasis. Biomed Pharmacother. 2018;103:1609–1616.
100. Kimani NM, Backhaus S, Matasyoh JC, Kaiser M, Herrmann FC, Schmidt TJ, Langer K. Preparation of sesquiterpene

lactone-loaded PLA nanoparticles and evaluation of their antitrypanosomal activity. Molecules. 2019;24.
101. Pattni BS, Chupin VV, Torchilin VP. New developments in liposomal drug delivery. Chem Rev. 2015;115:10938–66.
102. Allen TM, Cullis PR. Liposomal drug delivery systems: from concept to clinical applications. Adv Drug Deliv Rev. 2013;65:36–48.
103. Jain K, Jain NK. Novel therapeutic strategies for treatment of visceral leishmaniasis. Drug Discov Today. 2013;18:1272–81.
104. Das N, Mahato SB, Naskar K, Ghosh DK, Basu MK. Targeting of urea stibamine encapsulated in liposomes to reticuloendothelial system for the treatment of experimental leishmaniasis. Biochem Med Metab Biol. 1990;43:133–9.
105. Banerjee G, Nandi G, Mahato SB, Pakrashi A, Basu MK. Drug delivery system: targeting of pentamidines to specific sites using sugar grafted liposomes. J Antimicrob Chemother. 1996;38:145–50.
106. Siddiqui R, Syed A, Tomas S, Prieto-Garcia J, Khan NA. Effect of free versus liposomal-complexed pentamidine isethionate on biological characteristics of Acanthamoeba castellanii in vitro. J Med Microbiol. 2009;58:327–30.
107. Nguyen NB, Chen CH, Zhang Y, Zhao P, Wu BM, Ardehali R. Harnessing the versatility of PLGA nanoparticles for targeted Cre-mediated recombination. Nanomedicine. 2019;19:106–14.
108. Kefayat A, Vaezifar S. Biodegradable PLGA implants containing doxorubicin-loaded chitosan nanoparticles for treatment of breast tumor-bearing mice. Int J Biol Macromol. 2019;136:48–56.
109. Bruni N, Stella B, Giraudo L, Della Pepa C, Gastaldi D, Dosio F. Nanostructured delivery systems with improved leishmanicidal activity: a critical revie. Int J Nanomedicine. 2017;12:5289–5311.
110. Gaspar R, Opperdoes FR, Preat V, Roland M. Drug targeting with polyalkylcyanoacrylate nanoparticles: in vitro activity of primaquine-loaded nanoparticles against intracellular Leishmania donovani. Ann Trop Med Parasitol. 1992;86:41–9.
111. Deniau M, Durand R, Bories C, Paul M, Astier A, Couvreur P, Houin R. In vitro study of leishmanicidal agents with drug carriers. Ann Parasitol Hum Comp. 1993;68:34–7.
112. Paul M, Durand R, Boulard Y, Fusai T, Fernandez C, Rivollet D, Deniau M, Astier A. Physicochemical characteristics of pentamidine-loaded polymethacrylate nanoparticles: implication in the intracellular drug release in Leishmania major infected mice. J Drug Target. 1998;5:481–90.
113. Fusai T, Deniau M, Durand R, Bories C, Paul M, Rivollet D, Astier A, Houin R. Action of pentamidine-bound nanoparticles against Leishmania on an in vivo model. Parasite. 1994;1:319–24.
114. Fusai T, Boulard Y, Durand R, Paul M, Bories C, Rivollet D, Astier A, Houin R, Deniau M. Ultrastructural changes in parasites induced by nanoparticle-bound pentamidine in a Leishmania major/mouse model. Parasite. 1997;4:133–9.
115. Durand R, Paul M, Rivollet D, Houin R, Astier A, Deniau M. Activity of pentamidine-loaded methacrylate nanoparticles against Leishmania infantum in a mouse model. Int J Parasitol. 1997;27:1361–7.
116. Omarch G, Kippie Y, Mentor S, Ebrahim N, Fisher D, Murilla G, Swai H, Dube A. Comparative in vitro transportation of pentamidine across the blood-brain barrier using polycaprolactone nanoparticles and phosphatidylcholine liposomes, Artif Cells Nanomed. Biotechnol. 2019;47:1428–36.
117. Maran N, Gomes PS, Freire-de-Lima L, Freitas EO, Freire-de-Lima CG, Morrot A. Host resistance to visceral leishmaniasis: prevalence and prevention. Expert Rev Anti Infect Ther. 2016;14:435–42.
118. Onyilagha C, Uzonna JE. Host immune responses and immune evasion strategies in African trypanosomiasis. Front Immunol. 2019;10:2738.
119. Unciti-Broceta JD, Arias JL, Maceira J, Soriano M, Ortiz-Gonzalez M, Hernandez-Quero J, Munoz-Torres M, de Koning HP, Magez S, Garcia-Salcedo JA. Specific cell targeting therapy bypasses drug resistance mechanisms in African trypanosomiasis. PLoS Pathog. 2015;11:e1004942.
120. Stijlemans B, Conrath K, Cortez-Retamozo V, Van Xong H, Wyns L, Senter P, Revets H, De Baetselier P, Muyldermans S, Magez S. Efficient targeting of conserved cryptic epitopes of infectious agents by single domain antibodies. African trypanosomes as paradigm, J Biol Chem. 2004;279:1256–61.
121. Makadia HK, Siegel SJ. Poly Lactic-co-glycolic acid (PLGA) as biodegradable controlled drug delivery carrier. Polymers (Basel). 2011;3:1377–97.
122. Danhier F, Ansorena E, Silva JM, Coco R, Le Breton A, Preat V. PLGA-based nanoparticles: an overview of biomedical applications. J Control Release. 2012;161:505–22.
123. Paul M, Fessi H, Laatiris A, Boulard Y, Durand R, Deniau M, Astier A. Pentamidine-loaded poly(d, l-lactide) nanoparticles: physicochemical properties and stability work. Int J Pharm. 1997;159:223–32.
124. Paul M, Laatiris A, Fessi H, Dufeu B, Durand R, Deniau M, Astier A. Pentamidine-loaded poly(D, L-lactide) nanoparticles: adsorption and drug release. Drug Dev Res. 1998;43:98–104.
125. Durand R, Paul M, Rivollet D, Fessi H, Houin R, Astier A, Deniau M. Activity of pentamidine-loaded poly (D, L-lactide) nanoparticles against Leishmania infantum in a murine model. Parasite. 1997;4:331–6.
126. Graves RA, Pamujula S, Moiseyev R, Freeman T, Bostanian LA, Mandal TK. Effect of different ratios of high and low molecular weight PLGA blend on the characteristics of pentamidine microcapsules. Int J Pharm. 2004;270:251–62.
127. Scala A, Piperno A, Micale N, Mineo PG, Abbadessa A, Risoluti R, Castelli G, Bruno F, Vitale F, Cascio A, Grassi G. "Click" on PLGA-PEG and hyaluronic acid: gaining access to anti-leishmanial pentamidine bioconjugates. J Biomed Mater Res B Appl Biomater. 2018;106:2778–85.
128. Arias JL, Unciti-Broceta JD, Maceira J, Del Castillo T, Hernández-Quero J, Magez S, Soriano M, García-Salcedo JA. Nanobody conjugated PLGA nanoparticles for active targeting of African Trypanosomiasis. J Control Release. 2015;197:190–8.
129. Valle IV, Machado ME, Araujo C, da Cunha-Junior EF, da Silva Pacheco J, Torres-Santos EC, da Silva L, Cabral LM, do Carmo FA, Sathler PC. Oral pentamidine-loaded poly(d,l-lactic-co-glycolic) acid nanoparticles: an alternative approach for leishmaniasis treatment. Nanotechnology 2019:30;455102.
130. Brewster ME, Loftsson T. Cyclodextrins as pharmaceutical solubilizers. Adv Drug Deliv Rev. 2007;59:645–66.
131. Loftsson T, Hreinsdottir D, Masson M. Evaluation of cyclodextrin solubilization of drugs. Int J Pharm. 2005;302:18–28.
132. Carrier RL, Miller LA, Ahmed I. The utility of cyclodextrins for enhancing oral bioavailability. J Control Release. 2007;123:78–99.
133. De Sousa FB, Lima AC, Denadai AM, Anconi CP, De Almeida WB, Novato WT, Dos Santos HF, Drum CL, Langer R, Sinisterra RD. Superstructure based on beta-CD self-assembly induced by a small guest molecule. Phys Chem Chem Phys. 2012;14:1934–44.
134. De Paula EE, De Sousa FB, Da Silva JC, Fernandes FR, Melo MN, Frezard F, Grazul RM, Sinisterra RD, Machado FC. Insights into the multi-equilibrium, superstructure system based on beta-cyclodextrin and a highly water soluble guest. Int J Pharm. 2012;439:207–15.

135. Chen S, Hanning S, Falconer J, Locke M, Wen J. Recent advances in non-ionic surfactant vesicles (niosomes): fabrication, characterization, pharmaceutical and cosmetic applications. Eur J Pharm Biopharm. 2019;144:18–39.
136. Markowitz J, Chen I, Gitti R, Baldisseri DM, Pan Y, Udan R, Carrier F, MacKerell AD Jr, Weber DJ. Identification and characterization of small molecule inhibitors of the calcium-dependent S100B–p53 tumor suppressor interaction. J Med Chem. 2004;47:5085–93.
137. Cirillo C, Capoccia E, Iuvone T, Cuomo R, Sarnelli G, Steardo L, Esposito G. S100B unhibitor pentamidine attenuates reactive gliosis and reduces neuronal loss in a mouse model of Alzheimer's disease. Biomed Res Int. 2015;2015:508342.
138. Cristovao JS, Gomes CM. S100 proteins in Alzheimer's disease. Front Neurosci. 2019;13:463.
139. Liu J, Wang H, Zhang L, Xu Y, Deng W, Zhu H, Qin C. S100B transgenic mice develop features of Parkinson's disease. Arch Med Res. 2011;42:1–7.
140. Sekhar GN, Georgian AR, Sanderson L, Vizcay-Barrena G, Brown RC, Muresan P, Fleck RA, Thomas SA. Organic cation transporter 1 (OCT1) is involved in pentamidine transport at the human and mouse blood-brain barrier (BBB). PLoS One. 2017;12:e0173474.
141. Rinaldi F, Hanieh PN, Chan LKN, Angeloni L, Passeri D, Rossi M, Wang JT, Imbriano A, Carafa M, Marianecci C. Chitosan glutamate-coated niosomes: a proposal for nose-to-brain delivery. Pharmaceutics. 2018;10.
142. Kean T, Thanou M. Biodegradation, biodistribution and toxicity of chitosan. Adv Drug Deliv Rev. 2010;62:3–11.
143. Rinaldi F, Seguella L, Gigli S, Hanieh PN, Del Favero E, Cantu L, Pesce M, Sarnelli G, Marianecci C, Esposito G, Carafa M. inPentasomes: an innovative nose-to-brain pentamidine delivery blunts MPTP parkinsonism in mice. J Control Release. 2019;294:17–26.
144. Cirillo C, Sarnelli G, Esposito G, Turco F, Steardo L, Cuomo R. S100B protein in the gut: the evidence for enteroglial-sustained intestinal inflammation. World J Gastroenterol. 2011;17:1261–6.
145. Seguella L, Rinaldi F, Marianecci C, Capuano R, Pesce M, Annunziata G, Casano F, Bassotti G, Sidoni A, Milone M, Aprea G, de Palma GD, Carafa M, Pesce M, Esposito G, Sarnelli G. Pentamidine niosomes thwart S100B effects in human colon carcinoma biopsies favouring wtp53 rescue. J Cell Mol Med. 2020;24:3053–63.
146. Lourie EM, Yorke W. Studies in chemotherapy. Ann Trop Med Parasitol. 1939;33:289–304.
147. Carton F, Chevalier Y, Nicoletti L, Tarnowska M, Stella B, Arpicco S, Malatesta M, Jordheim LP, Briancon S, Lollo G. Rationally designed hyaluronic acid-based nano-complexes for pentamidine delivery. Int J Pharm. 2019;568:118526.
148. Stella B, Andreana I, Zonari D, Arpicco S. Pentamidine-loaded lipid and polymer nanocarriers as tunable anticancer drug delivery systems. J Pharm Sci. 2020;109:1297–302.
149. Merian J, De Souza R, Dou Y, Ekdawi SN, Ravenelle F, Allen C. Development of a liposome formulation for improved biodistribution and tumor accumulation of pentamidine for oncology applications. Int J Pharm. 2015;488:154–64.
150. Stephen S, Gorain B, Choudhury H, Chatterjee B. Exploring the role of mesoporous silica nanoparticle in the development of novel drug delivery systems. Drug Deliv Transl Res. 2021.
151. Peretti E, Miletto I, Stella B, Rocco F, Berlier G, Arpicco S. Strategies to obtain encapsulation and controlled release of pentamidine in mesoporous silica nanoparticles. Pharmaceutics. 2018;10.
152. Costanzo M, Vurro F, Cisterna B, Boschi F, Marengo A, Montanari E, Meo CD, Matricardi P, Berlier G, Stella B, Arpicco S, Malatesta M. Uptake and intracellular fate of biocompatible nanocarriers in cycling and noncycling cells. Nanomedicine (Lond). 2019;14:301–16.
153. Her S, Cui L, Bristow RG, Allen C. Dual action enhancement of gold nanoparticle radiosensitization by pentamidine in triple negative breast cancer. Radiat Res. 2016;185:549–62.

Review

Nanomedicine for gene delivery and drug repurposing in the treatment of muscular dystrophies

I. Andreana, M. Repellin, F. Carton, D. Kryza, S. Briançon, B. Chazaud, R. Mounier, S. Arpicco, M. Malatesta, B. Stella, G. Lollo

(Published in 2021)

pharmaceutics

MDPI

Review

Nanomedicine for Gene Delivery and Drug Repurposing in the Treatment of Muscular Dystrophies

Ilaria Andreana [1,2,†], Mathieu Repellin [1,3,†], Flavia Carton [3,4,†], David Kryza [1,5], Stéphanie Briançon [1], Bénédicte Chazaud [6], Rémi Mounier [6], Silvia Arpicco [2], Manuela Malatesta [3], Barbara Stella [2,*] and Giovanna Lollo [1,*]

1 Laboratoire d'Automatique, de Génie des Procédés et de Génie Pharmaceutique, Université Claude Bernard Lyon 1, CNRS UMR 5007, 43 bd 11 Novembre 1918, 69622 Villeurbanne, France; ilaria.andreana@unito.it (I.A.); mathieu.repellin@univr.it (M.R.); david.kryza@univ-lyon1.fr (D.K.); stephanie.briancon@univ-lyon1.fr (S.B.)
2 Department of Drug Science and Technology, University of Turin, Via P. Giuria 9, 10125 Torino, Italy; silvia.arpicco@unito.it
3 Department of Neurosciences, Biomedicine and Movement Sciences, Anatomy and Histology Section, University of Verona, Strada Le Grazie 8, 37134 Verona, Italy; flavia.carton@uniupo.it (F.C.); manuela.malatesta@univr.it (M.M.)
4 Department of Health Sciences, University of Eastern Piedmont, Via Solaroli 17, 28100 Novara, Italy
5 Hospices Civils de Lyon, 69437 Lyon, France
6 Institut NeuroMyoGène, University of Lyon, INSERM U1217, CNRS UMR 5310, 8 Avenue Rockefeller, 69008 Lyon, France; benedicte.chazaud@inserm.fr (B.C.); remi.mounier@inserm.fr (R.M.)
* Correspondence: barbara.stella@unito.it (B.S.); giovanna.lollo@univ-lyon1.fr (G.L.); Tel.: +39-011-670-66-60 (B.S.); +33-0-4-72-44-85-84 (G.L.)
† These authors contributed equally to this work.

Abstract: Muscular Dystrophies (MDs) are a group of rare inherited genetic muscular pathologies encompassing a variety of clinical phenotypes, gene mutations and mechanisms of disease. MDs undergo progressive skeletal muscle degeneration causing severe health problems that lead to poor life quality, disability and premature death. There are no available therapies to counteract the causes of these diseases and conventional treatments are administered only to mitigate symptoms. Recent understanding on the pathogenetic mechanisms allowed the development of novel therapeutic strategies based on gene therapy, genome editing CRISPR/Cas9 and drug repurposing approaches. Despite the therapeutic potential of these treatments, once the actives are administered, their instability, susceptibility to degradation and toxicity limit their applications. In this frame, the design of delivery strategies based on nanomedicines holds great promise for MD treatments. This review focuses on nanomedicine approaches able to encapsulate therapeutic agents such as small chemical molecules and oligonucleotides to target the most common MDs such as Duchenne Muscular Dystrophy and the Myotonic Dystrophies. The challenge related to in vitro and in vivo testing of nanosystems in appropriate animal models is also addressed. Finally, the most promising nanomedicine-based strategies are highlighted and a critical view in future developments of nanomedicine for neuromuscular diseases is provided.

Keywords: nanoparticles; Duchenne Muscular Dystrophy; myotonic dystrophy; antisense oligonucleotides; small molecules; CRISPR/Cas9

check for updates

Citation: Andreana, I.; Repellin, M.; Carton, F.; Kryza, D.; Briançon, S.; Chazaud, B.; Mounier, R.; Arpicco, S.; Malatesta, M.; Stella, B.; et al. Nanomedicine for Gene Delivery and Drug Repurposing in the Treatment of Muscular Dystrophies. *Pharmaceutics* **2021**, *13*, 278. https://doi.org/10.3390/pharmaceutics13020278

Academic Editor: Avi Domb

Received: 29 December 2020
Accepted: 14 February 2021
Published: 19 February 2021

Publisher's Note: MDPI stays neutral with regard to jurisdictional claims in published maps and institutional affiliations.

1. Introduction

Muscular dystrophies (MDs) are a group of chronic inherited genetic diseases, with a worldwide estimated prevalence of 19.8–25.1 per 100,000 persons [1,2]. These multi-organ diseases mainly affect muscles, especially skeletal muscles, which undergo a progressive degeneration causing severe health problems that lead to poor life quality, loss of independence, disability and premature death [3,4]. Among the various types of MDs described

so far, the most commons are the Duchenne Muscular Dystrophy (DMD) and Myotonic Dystrophies (DMs) [2,3,5].

Currently, no therapies are available to counteract the pathogenic causes of these diseases, and conventional treatments based on immunosuppressants such as corticosteroids or anti-inflammatory treatments are aimed to only mitigate symptoms [6–10]. Although corticosteroids are considered as the "gold standard" to preserve muscle strength in MDs, especially in DMD, their long-term administration is associated with serious adverse effects such as leg oedema, glaucoma, depression, hypertension, hyperglycaemia, osteoporosis, osteonecrosis and fractures [11–13]. Medical devices such as pacemaker, respiratory assistance or wheelchairs, rehabilitative therapy and as a last resort surgery are also widely used in the management of MDs patients [14–16]. Altogether, these approaches represent the current restricted therapies and methods approved to reduce pain and improve the quality of life. Recently, a variety of possible therapeutic strategies have been proposed such as repurposing US Food and Drug Administration (FDA)-approved molecules for the treatment of other diseases or developing novel gene therapy for exon-skipping strategy or genome editing [17–22]. However, due to their rapid clearance or associated adverse effects, further refinements are required to enter clinics.

Over the last several years, drug delivery nanosystems, referred to as nanomedicine, have been extensively explored for the development of more effective and safer treatments with main applications in cancers [23–26], central nervous system-related disorders [27–29] and immune diseases [30–32]. More recently, nanomedicine has also been investigated for the treatment of viral infections [33] such as the lately approved Moderna's and Pfizer's Covid-19 nanoparticle-based vaccines [34–37]. In cancer therapy, nanomedicine holds potential to improve current treatments by reducing side effects of chemotherapeutic agents. Moreover, combination approaches and immunomodulation strategies have been successfully developed to boost their performances [38–40]. Nevertheless, only 15 nanoparticle-based cancer therapies have received clinical approval and entered the market, such as the recent liposomal Onivyde® and Vyxeos® formulations [41,42].

Currently, novel nanomedicines are optimized for the treatment of skeletal muscle pathologies like MDs. However, multiple biological and pharmaceutical barriers challenge nanomedicine delivery to skeletal muscles. Biological barriers are embodied by the complex architecture of the skeletal muscle, which encompasses the skeletal muscle parenchyma itself, connective tissue, blood vessels and nerves. One of the main hurdles for delivery to skeletal muscles lies in the presence of the dense extracellular matrix (ECM), which accounts for 1 to 10% of the muscle mass [43–45]. Mostly made of fibrous-forming proteins (collagens, glycoproteins, proteoglycans and glycosaminoglycans) it hampers nanoparticles (NPs) penetration by retaining them in the ECM via electrostatic and mechanical interactions [46,47].

Pharmaceutical barriers encompass formulation and associated aspects related to scaling up of nanomedicine products. Recently, formulation techniques based on scalable processes have been developed to allow transposition of nanomedicine to industrial settings [48–50].

In addition to these barriers, an important requirement is that NPs have to be biocompatible to prevent additional muscle degeneration of severely injured skeletal muscles. For instance, sarcolemma membrane of DMD patients is severely affected and therefore more susceptible to damage by any treatment [51].

The present review aims at highlighting the major advances in the nanomedicine-based strategies for treating MDs. We reviewed the most recent approaches to treat MDs focused on oligonucleotides or antisense oligonucleotides, and small molecules and how nanocarriers have been designed to deliver them to muscle cells. In addition, the genome editing CRISPR/Cas9 system is also described. Finally, future perspectives for nanomedicine optimisation are presented.

2. Muscular Dystrophies Characterised by Gene Alteration

Most common MDs are represented by the two well-known DMD and DMs [1,3,4]. These two types of dystrophies are caused by diverse gene mutations and lead to different molecular pathogenesis, as illustrated in Figure 1.

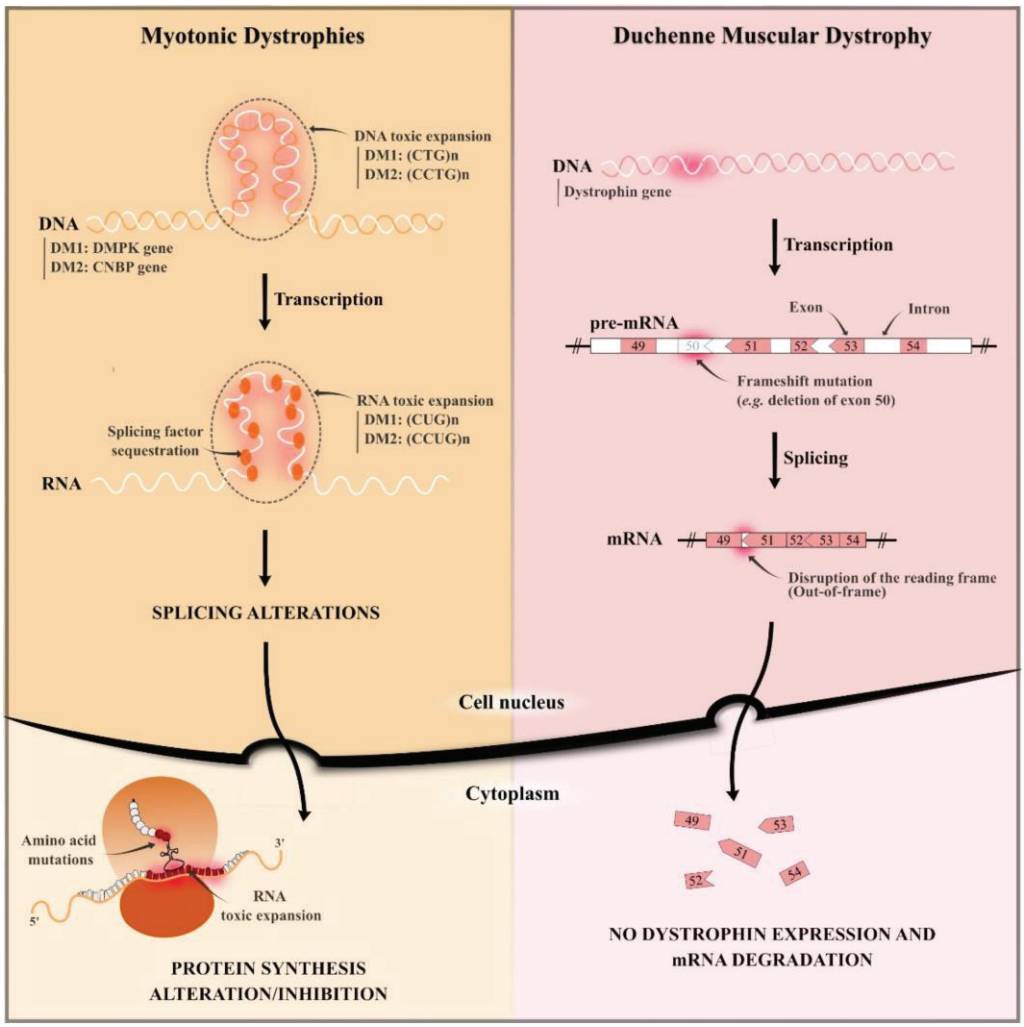

Figure 1. Schematic representation of the pathogenesis of both Myotonic Dystrophies and Duchenne Muscular Dystrophy. (DM1: Myotonic Dystrophy type 1; DM2: Myotonic Dystrophy type 2.)

2.1. Duchenne Muscular Dystrophy

DMD is the most common form of MD characterised by progressive muscle degeneration and weakness, firstly affecting proximal muscles. This X-linked recessive rare disorder appears essentially in males with a worldwide prevalence of one in 5000 boys in early childhood and the clinical signs are not revealed at birth [52]. In most cases, the diagnosis is established around four years old, when the first symptoms start to appear. The disease progression is fast and the patients completely lose their motor functions around 10 years old. DMD patients develop also important cardiac and respiratory complications that generally manifest around 10 years old and are prevalent in most patients by 20 years old [53].

DMD is caused by mutations in the dystrophin gene (DMD gene) located on chromosome Xp21.2 that codes for the dystrophin protein through its 79 exons [54]. Dystrophin protein is essential for muscle homeostasis: it is localised on the plasma membrane of cardiac and skeletal muscles (sarcolemma), connecting the cytoskeleton to the ECM through the dystroglycan complex (DGC) and stabilising the muscle fibre during contraction. Lack of dystrophin induces severe muscle weakness, inflammation and wasting, described as cardinal signs of DMD. Diverse mutations on DMD gene have been reported worldwide [55]. Over the years, DMD gene has been characterised, identifying which mutations lead to a severe DMD phenotype [56,57]. Of DMD cases, 60–70% are caused by large deletions of one or more exons. Point mutations affect 15–30% of DMD patients, and there are smaller changes that do not involve an entire exon. Among them, nonsense mutations cause a premature stop in the gene which results in reduced dystrophin production or no production at all. Duplications affect only 10% of DMD patients and can occur throughout all 79 exons of the dystrophin gene. Understanding the nature of mutations improves the identification of therapeutic approaches able to rescue genetic mutations [58,59].

2.2. Myotonic Dystrophies (Type 1 and 2)

Myotonic dystrophies (DMs) are genetic disorders of autosomal dominance inheritance and represent the second most common form of MDs in adulthood [60,61]. These multisystemic diseases cause progressive dysfunctions of multiple organs and tissues (e.g., muscle tissues, skin, endocrine system, ocular system, central nervous system) among which skeletal muscle is the most severely affected tissue [5]. Muscle damages are characterised by progressive myopathy, muscle weakness, and progressive myotonia which is defined as a slow-down of muscle relaxation after a normal contraction. Most serious features concern the cardiopulmonary system and can lead to premature death, amounting to 70% of deaths [62].

Two distinct forms of DM caused by similar mutations are identified: i) DM1, also named Steinert disease (OMIM 160900), which is the most common and severe form; and ii) DM2, termed proximal myotonic myopathy (OMIM 602668). These DMs are caused by pathological expansions of small DNA sequences regarding two different genes [63]. DM1 is due to a (CTG)n expansion in the 3′ UTR region of the DMPK gene, while DM2 is caused by a (CCTG)n expansion in the first intron of the ZNF9/CNBP gene. Mutant (CTG)n and (CCTG)n expansions are highly unstable, leading to different repeat sizes constantly generated and increasing when transmitted from one generation to the next [64]. These mutant DNA expansions are transcribed into (CUG)n and (CCUG)n mutant RNA expansions for DM1 and DM2, respectively, aggregated in the nucleus in specific hairpin structures that are called nuclear foci [65].

The most accepted pathogenic hypothesis for DMs is an RNA-gain-of-function due to mutant RNA expansions that alter RNA-binding splicing regulators [66]. As illustrated in Figure 1, the main molecular hallmark of DMs is the sequestration of Muscleblind protein (MBNL), resulting in a local reduction of these protein levels [67]. It is responsible for several symptoms depending on the DM type and repeat size range, such as myotonia, muscle weakness, cardiac arrhythmia, diabetes, cataracts, male hypogonadism, cognitive disorders and hypersomnia [68]. Other splicing factors are mis-regulated in DMs, such as the up-regulation of CUGBP1 [63] and hnRNP H protein [69,70]. Understanding the molecular pathogenic mechanism helped the development and identification of diverse therapeutic approaches such as the reduction of toxic RNA levels [71,72], the prevention of the MBNL protein sequestration, or the inhibition of the signalling pathway that leads to CUGBP1 up-regulation [73–75].

3. Targets and How to Reach Them: DNA and RNA

MDs are genetic disorders caused by localised mutations of DNA. Such DNA mutations result in a lack of dystrophin protein in DMD and an alteration of the protein production in DMs (Figure 1) [57,76]. No curative therapies are available to treat the

pathogenic causes, and the identification of new therapeutic approaches to target genetic mutations is urgently needed [10]. The most recent strategies to counteract MDs concern gene therapy and repurposing of drugs, as summarised in Table 1. In order to reach the target and achieve therapeutic effect, active agents must attain skeletal muscle tissue. A representation of their localisation is reported in Figure 2.

Table 1. Therapeutic strategies for the treatment of MDs (DMD, Duchenne Muscular Dystrophy; DM, Myotonic Dystrophy; ASO, antisense oligonucleotide; CRISPR, clustered regularly interspaced short palindromic repeats).

Approach	Active Agent	Target	Pathology	Limitations	Development Phase	Reference
Antisense oligonucleotides	Etelprisen	mRNA	DMD	Rapid degradation by exonuclease Low cellular uptake Activation of immune systemInflammatory effects	FDA approved (Clin. Trial NCT02255552)	[77]
	Drisapersen				Phase III (Clin. Trial NCT01254019)	[78,79]
	cEt ASO	CUG/CCUG^{exp}	DM		Preclinical studies	[80,81]
CRISPR/Cas9	Not approved	DNA	DMD	Higher accumulation in proliferating cells than in fully differentiated cells Rapid degradation	Preclinical studies	[82–85]
	Not approved	CTG^{exp} DNA	DM	Uncompleted repair of protein expression Low transfection efficiency	Preclinical studies	[86]
Small molecules	Aminoglycoside antibiotics	Non-sense mutations on mRNA	DMD	Ototoxicity Nephrotoxicity	Preclinical studies	[87–89]
	Ataluren	Non-sense mutations on mRNA	DMD	High dosage required	EMA approved (Clin. Trial NCT01826487)	[90,91]
	Pentamidine	CUG^{exp} RNA	DM	Nephrotoxicity Off-label use	Preclinical studies	[18,92]
	Furamidine and erytromicin	CTG^{exp} DNA	DM	Off-label use	Preclinical studies	[93–95]
	ISOX and vorinostat	MBNL1-splicing factors	DM1	Off-label use	Preclinical studies	[96]

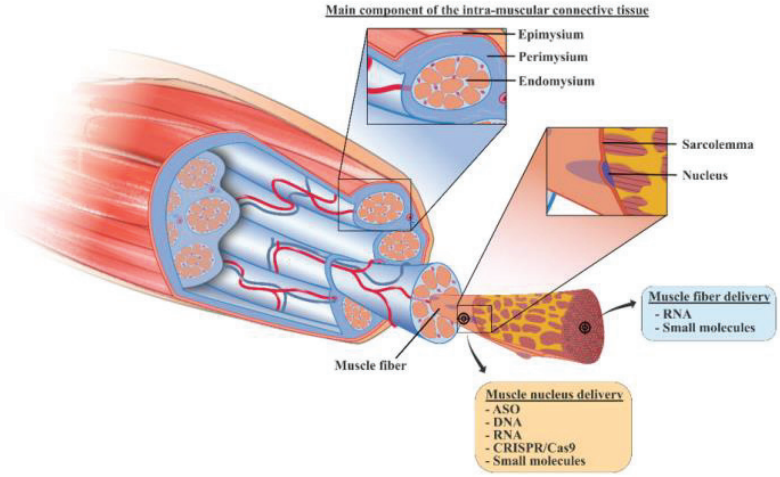

Figure 2. Organization of the skeletal muscle tissue and the target-tissue related to the class of experimental molecules (ASO, antisense oligonucleotide; CRISPR, clustered regularly interspaced short palindromic repeats).

3.1. Gene Therapy and Genome Editing for MDs

Gene therapy aims at targeting gene mutations. Genetic strategy and genome editing offer the advantage of a durable and possibly curative approach. They aimed at improving patient's quality of life by i) reducing the administration frequency, thus increasing their compliance to the treatment [97,98], and ii) providing a personalised therapy for the correction of genetic mutations [99].

Application of gene therapy in muscle pathologies is performed by exon-skipping [58] and CRISPR/Cas9 system [59] Exon-skipping is based on the use small of pieces of modified oligonucleotides, termed antisense oligonucleotides (ASOs), which recognise and bind specific sequences of mRNA [58,100]. ASOs exert their activity in the nucleus by: (i) blocking protein maturation and splicing alteration of pre-mRNA, (ii) degrading targeted RNA by RNase H-enzyme and reducing mRNA level [101]. Despite their promising features, drawbacks related to ASO's instability, limited distribution to all diseased tissues, rapid body clearance and difficulties of cellular internalisation have been described [102]. To overcome these issues, chemical modifications on ASO chemical structure have been studied. Several ASO drugs were modified using the phosphorothioate backbone modification where one of the non-bridging oxygen atoms of the phosphodiester linkage was replaced with sulphur. This modification increased the half-life of ASOs [103] and reduced their degradation by exonucleases [104]. However, ASO-based therapies present potential toxicities such as the off-target RNA hybridisation and the possibility to alter protein expression [105]. In addition, they can be recognised by the immune system, inducing proinflammatory effects [106].

In DMD patients affected by an out-of-frame mutation of DMD gene, ASO therapy can restore the reading frame of mRNA leading to the expression of a partially functional dystrophin protein [107]. Eteplirsen was approved in 2016 by the FDA as the first antisense therapy for DMD. Eteplirsen is a 30-nucleotide phosphorodiamidate morpholino (PMO) ASO that resulted in an increased dystrophin production in all patients treated by weekly intravenous (I.V.) infusion for at least 24 weeks [77]. Drisapersen, a 2′-O-methyl-phosphorothioate ASO, is another exon-skipping therapy for DMD in clinical development. Phase 3 study (DMD114044; NCT01254019) evaluated the efficacy of drisapersen after subcutaneous (S.C.) injection. The six-minute walk distance (6MWD) was the primary endpoint considered, and no differences were reported between placebo and treated patients. Data analysis considering secondary endpoints such as the North Star Ambulatory Assessment (NSAA), 4-stair climb ascent velocity and 10-metre walk/run velocity, showed lack of statistical significance due to the greater data variability and subgroup heterogeneity. However, statistically significant results were obtained in the young patients treated in the early stage of the pathology [78]. Further studies were focused on the preclinical optimisation of drisapersen, testing its efficacy on young and older DMD mouse model, *mdx*. This mouse model is characterised by an induced nonsense point mutation in the dystrophin gene, which leads to a loss of functional protein expression [108]. Preclinical investigation showed a comparable efficiency of exon-skipping mechanism in young and older mice, but functional and physical improvement was only reported for treated young mice, meaning that the stage of pathology is relevant for treatment efficacy. In vivo studies highlighted that an early intervention with drisapersen led to functional benefits despite the low level of dystrophin restoration. In addition, the application of drisapersen was also limited by the reported side effects at the injection site and mostly proteinuria, which increased α1-microglobulin levels [79]. Although ASO therapy and exon-skipping reached important outcomes, their applicability is limited to patients affected by out-of-frame mutation and requires continuous administrations throughout the lifetime of the patients [109,110].

ASO therapy is also reported for the treatment of DM where it targets and neutralises toxic CUG/CCUG^{exp} RNAs which sequestrate splicing factors [111]. Although there is no approved ASO therapy for DM1, in vitro and in vivo results are promising [112–114]. It has been reported that ASOs containing 2′- 4′- constrained ethyl (cEt) modifications can be employed to target DMPK genes and substantially reduce CUG^{exp} RNA nuclear

foci in patient-derived DM1 myoblasts [80]. Klein et al. developed an arginine rich Pip6a cell-penetrating peptide-conjugated PMO ASO to overcome the poor distribution of ASOs in skeletal muscle. Pipa6-conjugated ASO directed against CUG^{exp} allowed an effective concentration of ASOs in muscle fibres recovering MBNL1-dependent splicing defects [81].

In contrast to ASO therapy, genome editing induces a permanent correction of gene mutation [115]. Initially, engineered zinc finger nucleases (ZFNs) and transcription activator-like effector (TALENs) have been used to permanently remove splicing sequences in DMD gene and to restore dystrophin expression [116,117]. Recently, Clustered Regularly Interspaced Short Palindromic Repeats (CRISPR) in association with specific DNA endonuclease protein called Cas9, targeting DNA sequencing, has been investigated to restore the genetic mutation [118–120]. Cas9 nuclease requires a single guide RNA (sgRNA) to form a complex with DNA by recognition with a defined 20 bp DNA sequence, known as protospacer. The protospacer sequence is immediately followed by a short sequence called protospacer-adjacent motif (PAM), needed by Cas9 for DNA cleavage and for genome editing to start [121].

Promising results of CRISPR/Cas9 in MD treatment were reported. Dystrophin recovery by CRISPR/Cas9 system was observed in a new DMD mouse model characterised by a lacking exon 44 of the dystrophin gene, one of the hotspot regions for DMD gene mutation. In this study, Cas9 and sgRNA, the main gene editing components, were encoded by adeno-associated viruses serotype 9 (AAVs). The ratio between AAVs encoding for Cas9 and for sgRNA had an important effect on gene correction. Higher level of sgRNA ensured higher Cas9 activity, which increased dystrophin restoration due to long-lasting presence of sgRNA that allows continuous editing in myofibers. Combination of optimized sgRNA and AAV vectors for delivery increased long-term correction of dystrophin mutation in mice [82]. AAV9 have been already associated to CRISPR/Cas9 system for dystrophin recovery in a deltaE50-MD canine model of DMD, which leads to loss of exon 50. An sgRNA was optimised to target a region adjacent to the exon 51 splice acceptor site, and it resulted in high frequency of reframing events. Dystrophin protein expression was restored to 60% by intramuscular (I.M.) injection of AAV9-Cas9 and AAVs-sgRNA-51 [83]. Besides, CRISPR/Cas9 ability to target repeated DNA sequences also provides a possible strategy in DM therapy [122]. Dastidar et al. evaluated CRISPR/Cas9 activity, delivered through viral vector to excise CTG repeats in DM1 patient-derived cells, leading to the normalisation of DMPK gene expression and the degradation of toxic RNAs. The study demonstrated the potential application of CRISPR/Cas9 excision in trinucleotides repeat expansion up to 1200 repeats [88].

Genome editing by CRISPR/Cas9 strategy requires an efficient delivery system. AAV are used most often and have a low cargo capacity as compared with other viral vectors, requiring a high AAV dose to deliver sgRNA for gene reprogramming in vivo [21], increasing the risk of immunogenicity [123]. Traditional genome editing based on CRISPR/Cas9 technologies introduces double-stranded (ds) DNA breaks at a target locus as the first step to gene correction. However, the potential applications of Cas9 nucleases are limited in part by their reliance on DNA breaks, which could cause deletions, insertions or chromosomal rearrangements. Due to recent advances, CRISPR/Cas9-associated base editing (BE) approaches have emerged. These strategies do not require a dsDNA backbone but mediate the direct conversion of base pairs, advancing the treatment of genetic disorders associated with single nucleotide mutations [124,125]. Cytosine and adenine base-editors are the most used tools to exert mutation transition (Cytosine (C) > Thymine (T) and Adenine (A) > Guanine (G)), guided by a new CRISPR/Cas9 system which targets the non-edited DNA strand [126]. Ryu et al. demonstrated the application of BE in DMD treatment, using a dual trans-splicing AAV to deliver adenine base editors (ABE). ABE treatments achieve a precise A-to-G base mutation, restoring dystrophin expression in 17% of myofibers, following I.M. into tibialis anterior in *mdx* mice [127]. Moreover, due to increased interest in BE, non-viral vectors are under investigation to replace viral constructs as delivery systems [21]. Jiang et al. demonstrated a successful delivery of ABE using lipid nanoparticles in Tyrosinemia

I mice, correcting the gene mutation and showing the promise of the BE approach [128]. Despite the far-reaching capabilities of the BE strategy, a major limitation of this technique has been the ability to generate precise edits beyond the allowed transition mutations. Anzalone et al. described a new genome editing strategy called prime editing. This search-and-replace technology directly writes new genetic information into targeted DNA using a catalytically impaired Cas fused to an engineered reverse transcriptase enzyme, and a prime editing guide RNA (pegRNA) able to recognise and bind the target site [129]. This technology with its simplicity and precision holds great promise for the correction of point mutation in human genetic disorders.

3.2. Drug Repurposing

Another current approach in MD treatment is drug repurposing, a strategy for identifying new applications for approved or investigational drugs that are outside the scope of the original medical indication. Drug repurposing has promising expectations regarding efficacy, safety, cost and translation to the clinical setting. This is because repurposed drugs have been already studied in preclinical models and humans for safety assessments. Moreover, in many cases the formulation aspects are already developed [130].

In order to select the right candidate in a repurposing strategy, a systematic approach that combines computational techniques and experimental studies is required. Computational approaches are based on data-analysis (gene expression, chemical structure, genotype or proteomic data, or electronic health records (EHRs)), to validate the repurposing hypothesis. Experimental approaches are also required to identify target interactions and efficacy in appropriate models [131]. Table 1 lists the most common drugs used for repurposing strategies in DMD and DM.

About 10% of DMD patients present a nonsense mutation, which induces a premature stop codon in dystrophin mRNA leading to non-functional protein [132–134]. Some compounds are able to bind the stop codon, forcing the translational machinery to incorporate amino acids into the assembling protein, overcoming the stop signal and obtaining a functional protein [87]. Restoration of dystrophin protein was studied using gentamicin, an aminoglycoside antibiotic made of a mixture of major and minor aminoglycoside components [88]. Barton-Davis et al. demonstrated the possibility of treating DMD nonsense mutation using gentamicin. The drug was administered by S.C. injection to *mdx* mice at different dosages to identify the optimal dose to restore the full-length dystrophin [87,89]. To determine the efficacy on the suppression of premature stop codon in *mdx* mice, evaluation of dystrophin protection against contraction-induced damage was examined. The number of damaged fibres was reduced in treated *mdx* mice, as compared with wild type mice. Prolonged use of gentamicin implicates nephrotoxicity, limiting the long-term administration required for genetic diseases [135]. To address toxicity issues, new aminoglycosides and non-aminoglycosides were explored. Friesen et al. demonstrated the efficacy and greater read through-safety window than other compounds, of a minor gentamicin component called gentamicin X2, which shows a lower toxicity than gentamicin [136]. From the evaluation of neuromast toxicity (cytotoxic concentration, CC50), as a substitute for ototoxicity, CC50 of gentamicin X2 was significantly reduced compared to gentamicin. Minor component X2 has great potential for clinical utility in treating genetic diseases caused by nonsense mutations. Among non-aminoglycoside compounds, ataluren is a novel, orally administered, synthetic molecule that suppresses nonsense mutation in a way similar to aminoglycosides and increases dystrophin production [90]. Data from a phase III trial did not show improvement in 6MWD of treated patients, but less physical deterioration was demonstrated for patients receiving ataluren than for those receiving placebo. Results reported in this trial confirmed the clinical benefit of ataluren in terms of preservation of muscle function in DMD patients [91]. Further studies should evaluate the long-term benefits the drug.

In DM, the toxic foci made of CUG/CCUG^{exp} RNA aggregates are able to sequestrate MBNL1 splicing factor, thus altering the protein expression [61]. As an example, pentamidine, furamidine and erythromycin can inhibit the sequestration of splicing factors such as MBNL1 by CUG^{exp} RNA sequence. Docking analyses are useful to predict the binding conformation of small molecules to appropriate binding sites. They have been reported for rational screens of molecules that might selectively bind CUG structures and consequently improve biological activity in DM1 models [137].

Recently, pentamidine, a diamine compound that FDA approved for the treatment of trypanosomiasis and leishmaniasis infections [138], has been proposed for MD treatment and its efficacy was evaluated in vitro and in vivo. Pentamidine treatment reduced CUG^{exp} RNA level and rescued mis-splicing events in HeLa DM1 transfected cells, which expressed 960 interrupted CUG repeats. The number of nuclear foci was reduced by 21% [139]. The efficacy of pentamidine treatment was evaluated on DM1 mouse model HSA^{LR} (human skeletal actin long repeat length) that expresses ~250 CUG repeats into the final exon of human skeletal actin [18]. Pentamidine was administered by intraperitoneal (I.P.) injection and the correction of chloride-1 and Serca1 mRNA mis-splicing was essayed. The treatment partially reversed mis-splicing events. In vivo studies highlighted a narrow dosage window for pentamidine which cannot be used over 30 mg/kg twice a day. To overcome dosage toxicity, chemical modifications were performed to enhance the specificity to CUG^{exp} RNA and to reduce the dosage. Based on the chemical backbone of pentamidine, other drugs showing chemical similarities were selected. Furamidine is a diamine compound that rescues the mis-splicing events in vitro and in vivo models [92]. In HSA^{LR} mice, furamidine increased MNBL1 functional expression by inhibiting transcription of CTG^{exp} DNA and by disrupting the MNBL-CUG^{exp} complex [93]. Compared to pentamidine, furamidine presented the lowest number of off-target gene expression changes [94]. In combination with erythromycin, furamidine enhanced the effects on MNBL-CUG^{exp} complex disruption, reducing nuclear foci presence in patient-derived DM1 cells, without specific toxic effects [95]. Considering the reduction of MBNL1 in DM1 affected cells, small molecules improve the pathological condition by overexpression of splicing factors. For example, ISOX and vorinostat were tested in normal and DM1 fibroblasts, increasing MBNL1 expression and revealing positive effects on DM1 models [96].

Globally, repurposing of small molecules for the treatment of DM requires extensive investigation concerning their off-label use and the need of novel approaches to define their therapeutic potential for a different disease.

4. New Treatments based on Nanocarriers as Alternative Strategies to Facilitate Skeletal Muscle Targeting

Over the last years, the application of nanomedicine as a promising innovative approach to treat different pathologies such as MDs has been investigated. The architectural and structural complexities of skeletal muscles challenge nanomedicine delivery, especially due to the important presence of ECM [45,140]. To restrict interactions with ECM, administration of NPs by I.V. appears as a potential strategy for targeting skeletal muscle. The dense blood capillary network of skeletal muscles increases NPs access to muscle fibres [141,142]. However, once in the blood circulation, NPs can be rapidly cleared through the mononuclear phagocyte system via opsonisation or complexation with plasma proteins [143–146]. Physical and chemical instability [147,148], immunogenicity [149,150] or premature degradation [151] are other limiting factors that might interfere with NPs delivery.

In addition, long-term administration is required to cure chronic disorders such as MDs, which makes biocompatibility and biodegradability of the nanosystems important requirements [152]. NPs should persist long enough to reverse muscle damages without involving any additional muscle degeneration, before undergoing gradual degradation [51,153]. Therefore, their design has to be optimised to associate or encapsulate active compounds and to deliver them to skeletal muscles. As illustrated in Figure 3, various NPs structures have been described [154]. RNA- and DNA-based nanocarriers are obtained via electrostatic and hydrophobic-hydrophobic interactions with polymers or

lipids [155–157]. In the case of delivery of the small molecules, their chemical properties, such as their molecular size, structure and n-octanol-water partition coefficient have an impact on the selection criteria for nanocarrier strategy [158,159]. Interestingly, synthetic nanocarriers interacting by electrostatic and hydrophobic-hydrophobic interactions have been demonstrated to deliver complex CRISPR/Cas9 systems under various forms such as DNA, mRNA or ribonucleoproteins [160–162].

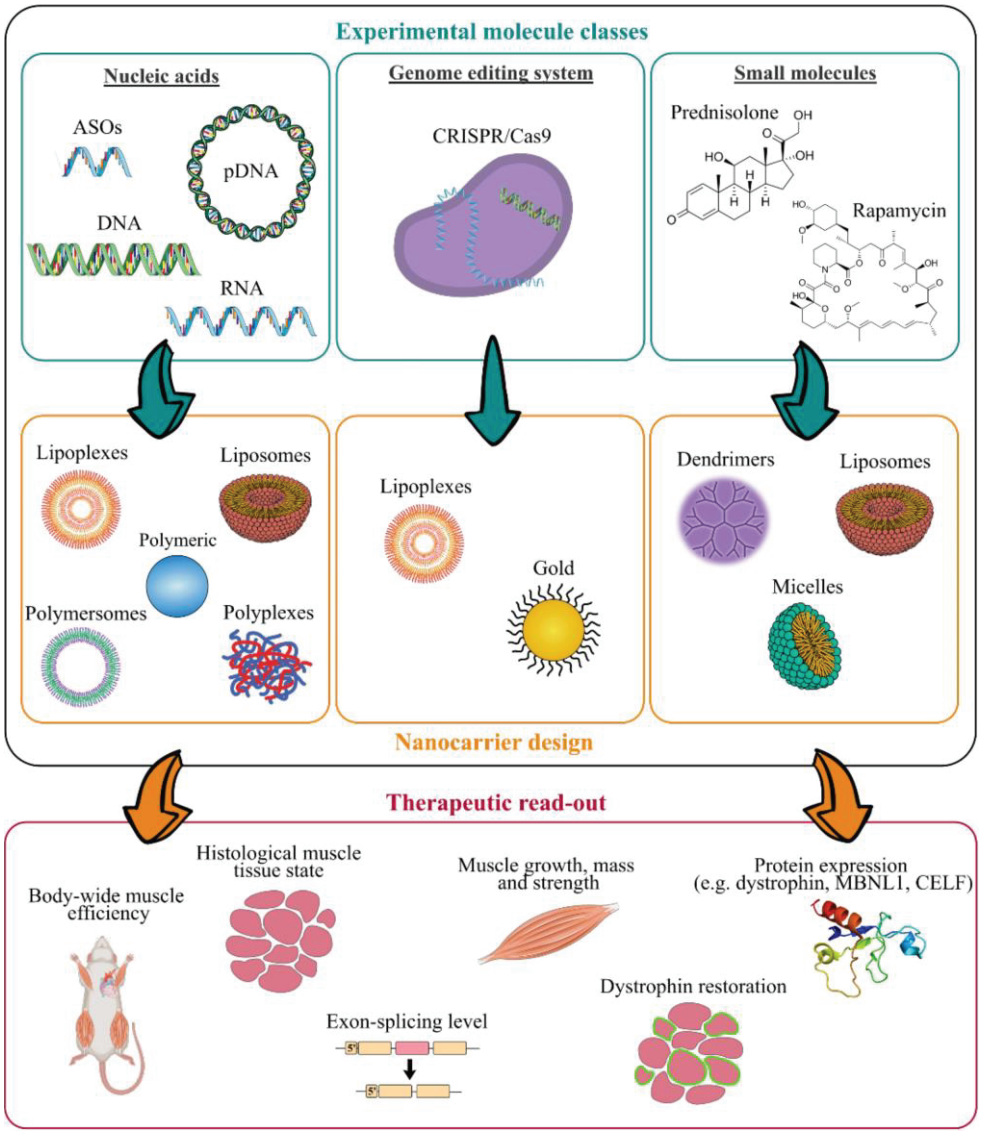

Figure 3. Work flow for the design of innovative nanomedicine and therapeutic readout. (ASOs, antisense oligonucleotides; CRISPR, clustered regularly interspaced short palindromic repeats).

As illustrated in Figure 3, many experimental molecules and macromolecules have been selected as candidates for MD therapies, and a wide range of nanocarriers has allowed their delivery to skeletal muscles, promoting in most of the cases their therapeutic potential.

The present section aims at highlighting nanosystems used for DMD and DM applications that reached preclinical studies. An overview of the various described nanosystems is reported in Table 2.

Table 2. Recapitulative table of the diverse described nanosystems tested in vivo for treating MDs (PEI, polyethylenimine; PEG, polyethylene glycol; PLGA, poly(lactic-*co*-glycolic acid); PMMA, poly(methyl methacrylate); NIPAM, N-isopropylacrylamide; PEA, poly(ethylene adipate); PLys, poly(l-lysine); PPE-EA, poly(2-aminoethyl propylene phosphate); PAMAM-OH, hydroxyl-terminated poly(amidoamine); DMPC, L-a-dimyristoylphosphatidylcholine; (C12(EO)23), polyoxyethylene(23) lauryl ether; NPs, nanoparticles; ASO, antisense oligonucleotide; PMO, phosphorodiamidate morpholino oligomer; GA, glatiramer acetate; CRISPR, clustered regularly interspaced short palindromic repeats; I.M., intramuscular injection; I.V., intravenous injection; I.P., intraperitoneal).

Class of Nanocarriers	Nanocarrier Composition	Muscle Pathology	Loaded Molecules	Therapeutic Target	Mouse Model	Advantages and Limitations	Admin. Route	Ref.
Polymeric	PEI-PEG	DMD	2′-OMe ASO	Dystrophin pre-mRNA	mdx	(+) high dystrophin-positive fibers increased (+) long term residual efficacy over 6 weeks (-) low general transfection efficiency	I.M.	[163]
	PEI-PEG/PLGA	DMD	2′-OMe ASO	Dystrophin pre-mRNA	mdx	(-) no improvement compared to PEI-PEG-ASO	I.M.	[164]
	PEI-Pluronic®	DMD	PMO ASO	Dystrophin pre-mRNA	mdx	(+) dystrophin-positive fibers increased up to 4-fold after I.M. (+) dystrophin-positive fibers increased up to 3-fold in all skeletal muscles after I.V. (+) dystrophin-positive fibers increased up to 5-fold in heart after I.V. (+) low muscle tissue, liver and kidney toxicity (-) mild general transfection efficiency	I.M./I.V.	[165]
		DMD	2′-OMe ASO	Dystrophin pre-mRNA	mdx	(+) dystrophin-positive fibers increased up to 10-fold	I.M.	[166]
	PEG-polycaprolactone PEG-(polylactic acid)	DMD	PMO ASO	Dystrophin pre-mRNA	mdx	(+) dystrophin-positive fibers increased up to 3-fold (+) low muscle tissue toxicity (-) mild general transfection efficiency	I.M.	[167]
	PMMA	DMD	2′-OMe ASO	Dystrophin pre-mRNA	mdx	(+) dystrophin-positive fibers increased up to 7-fold (-) slow biodegradability	I.P.	[168]
	PMMA/NIPAM	DMD	2′-OMe ASO	Dystrophin pre-mRNA	mdx	(+) dystrophin-positive fibers increased up to 4-fold (+) body-wide dystrophin restoration after I.V. (+) exon-skipping level enhanced up to 20-fold (+) long term residual efficacy over 90 days	I.P./I.V.	[169, 170]
	PEA	DMD	2′-OMe ASO	Dystrophin pre-mRNA	mdx	(+) dystrophin-positive fibers increased up to 3–10-fold	I.M.	[171]
		DMD	PMO ASO	Dystrophin pre-mRNA	mdx	(+) dystrophin-positive fibers increased up to 3-fold after I.M. (+) body-wide dystrophin-positive fibers increased up to 3-fold after I.V.	I.M./I.V.	[171]
		Muscle atrophy/ DMD	pDNA	Cell nucleus	mdx	(+) transfection efficiency enhanced up to 6-fold	I.M.	[172]
	PLys-PEG	Muscle atrophy	pDNA	Cell nucleus	Balb/c	(+) transfection efficiency enhanced up to 10-fold	I.V.	[173]

Table 2. *Cont.*

Class of Nanocarriers	Nanocarrier Composition	Muscle Pathology	Loaded Molecules	Therapeutic Target	Mouse Model	Advantages and Limitations	Admin. Route	Ref.
	PPE-EA	Muscle atrophy	pDNA	Cell nucleus	Balb/c	(+) transfection efficiency enhanced up to 13-fold (+) long term residual efficacy over 14 days	I.M.	[174]
	Atelocollagen	Muscle atrophy/ DMD	siRNA	Cytoplasm	mdx	(+) higher mass muscle increase	I.M./I.V.	[175]
	PAMAM-OH	Muscle atrophy	Angiotensin (1–7)	Cytoplasm	Balb/c	(+) higher anti-atrophic effects	I.P.	[176]
Lipidic	PEG-bubble liposomes	DMD	PMO ASO	Dystrophin pre-mRNA	mdx	(+) dystrophin-positive fibers increased up to 1.5-fold (+) exon-skipping level enhanced up to 5-fold	I.M.	[177]
		DM1	PMO ASO	Clcn1 pre-mRNA	HSA^{LR}	(+) increased expression of Clcn1 protein up to 1.4-fold	I.M.	[178]
	Nanolipoden-drosomes	DMD	MyoD and GA	Cytoplasm	SW-1	(+) slight mass muscle increase	I.M.	[179]
	Nanoliposomes	DMD	Glucocorticoide	Cell nucleus	mdx	(+) lower inflammatory induced response (+) lower bone catabolic effects	I.V.	[180]
	Hybrid liposomes DMPC and $(C_{12}(EO)_{23})$	DMD	Gentamicin	Ribosomes	mdx	(+) dystrophin-positive fibers increased up to 4-fold (+) lower ototoxicity and nephrotoxicity	I.P.	[181]
	Perfluorocarbon	DMD	Rapamycin	mTORC1 complex	mdx	(+) high muscle strength increase (+) high cardiac contractile performance increase	I.V.	[182]
	Lipid NPs	DMD	CRISPR/Cas9	Dystrophin DNA sequence	ΔEx44	(+) dystrophin expression restored up to 5%	I.M.	[183]
Inorganic	Gold	DMD	CRISPR/Cas9	Dystrophin DNA sequence	mdx	(+) HDR in the dystrophin gene enhanced up to 18-fold	I.M.	[184]

4.1. Antisense Oligonucleotides

ASO-based therapy is a powerful tool for inducing post-transcriptional modifications and thereby regulating target genes. There are several classes of ASOs for therapeutic purposes which differ from their phosphate backbone and ribose sugar group modifications [185]. Most ASOs used for DMD and DM are 2′O-methyl (2′O-Me), phosphorothioate (PS) ASO and PMO oligomer modified ASOs. Depending on their chemistry, different strategies can be obtained to modulate gene expression.

The phosphodiester and phosphorothioate internucleotide linkages confer a highly negative charge to PS or 2′O-Me ASOs. Hence, the most common approach to incorporate such ASOs into NPs remains to form stable complexes with cationic polymers or lipids. Polyplexes have been currently used for this purpose [186]. Poly(ethylene imine) (PEI) was one of the first cationic polymers explored for gene therapy because of its efficient binding association to nucleic acids and good transfection efficiency [187]. Nonetheless, the high positive surface potential results in significant toxicity, especially for in vivo skeletal muscle delivery, due to interactions with many biological components. To reduce the surface potential, poly(ethylene glycol) (PEG) has been added to the formulation [188,189]. Lutz's group developed PEI-PEG NPs obtained by the complexation of 2′O-Me ASOs with a cationic copolymer of PEI and PEG, to restore dystrophin expression in *mdx* mice [163,190,191]. PEI was conjugated to nonionic linear PEG to provide NPs with a steric shield, greatly

improving their biocompatibility. PEI-PEG-ASOs were shown to locally improve the levels of dystrophin expression up to 20% of normal dystrophin expression in WT animals after I.M. injection without eliciting toxicity. However, cationic PEI-PEG showed poor muscle distribution, evidenced by large untransfected areas in muscles, due to the nanoparticle entrapment into the ECM by non-specific binding [163].

In line with Lutz's group, Sirsi et al. proposed a strategy to shield the positive charges of PEI-PEG-ASO polyplexes by encapsulating them into PLGA nanospheres [164]. In vitro release studies in physiological medium showed a low PEI-PEG-ASO release from PLGA nanospheres. Such slow release was correlated to the Mw of PLGA; high PLGA Mw (72 kDa) impaired complex release, while lower PLGA Mw (17 kDa) reached 66.5% release over 26 days. This different release span could be ascribed to the kinetic rate of hydrolysis of PLGA. However, in vivo studies in *mdx* mouse following I.M. injection of free or PLGA (17 kDa) encapsulated PEI-PEG-ASOs showed that dystrophin expression was not improved, probably related to an incomplete ASO release of PEI-PEG-ASOs from PLGA. Despite this lack of dystrophin expression, polyplexes encapsulation through PLGA nanospheres appears to be an efficient sustained delivery strategy of interest for treating chronic diseases.

Wang et al. designed PEI conjugated with Pluronic® polycarbamates (PCM) to deliver 2′O-Me ASOs in *mdx* mice [166]. After I.M. administration, PEI-PCM NPs showed a local increased number of dystrophin-positive fibres up to three-eight fold, superior to ASO alone or unmodified ASO-PEI NPs. The addition of the carbamate hydrophobic groups contributed to ASO complexation to the NPs and enhanced transfection efficiency. 2′O-Me ASOs were also complexed using poly(ester-amine) (PEA), a constructed polymer obtained from PEI conjugated with Pluronic®. This polyplex demonstrated an efficacy similar to that of PCM with a number of dystrophin-positive fibres up to 3–10 fold higher than ASO alone [171].

Cationic polymethylmethacrylate (PMMA) NPs are other promising systems intended for nucleic acids delivery [192]. Rimessi et al. proved that cationic PMMA (named T1 NPs) complexed with 2′O-Me PS ASOs, administered by I.P. injection, restored dystrophin expression in body-wide striated muscles of *mdx* mice [168]. Dystrophin appeared expressed at moderate levels on the membrane of myofibers of the diaphragm, gastrocnemius and quadriceps and was restored at lower levels on the membrane of cardiomyocytes, showing the wide muscle distribution of T1 NPs. However, PMMA NPs are slowly degradable and might form small aggregates at high concentration in blood circulation, limiting their clinical use [192]. Based on these results, Ferlini et al. designed PMMA/N-isopropilacrylamide+ (NIPAM) NPs (ZM2 NPs) to improve the potential of PMMA-based NPs [169]. PMMA core was shielded with NIPAM cationic copolymer and used to bind and convey 2′O-Me PS ASOs to *mdx* mice following I.P. administration. ZM2-ASOs NPs induced efficient and widespread dystrophin restoration at low dose of ASOs in both striated and smooth muscles, with a dystrophin expression up to 40% of muscle fibres and an exon-skipping level up to 20% after seven days. Moreover, these nanocarriers showed long-term residual efficacy over 90 days, demonstrating their potential as gene delivery systems for ASO delivery [170].

Other non-ribose modified ASOs less frequently used for MDs applications are PMO. These ASO modifications are aimed at increasing their nuclease resistance and mRNA binding efficacy, but provide poor cellular uptake and rapid blood clearance related to the uncharged nature conferred by the morpholino rings [193,194]. In contrast to negatively charged ASOs, the use of cationic entities as a delivery vehicle is not suitable with this well-established ASO delivery strategy. For efficient delivery of these neutral oligonucleotide analogues, lipophilic interactions through PMO and hydrophobic carriers are privileged [195]. Kim et al. showed, as proof of concept, the potential of non-ionic PEG-polycaprolactone and PEG-(polylactic acid) polymersomes for the I.M. administration of PMO for DMD application into *mdx* mice [167]. The polymersomes successfully enhanced dystrophin expression in the entire muscle length increasing three-fold the number of

dystrophin-positive fibres as compared with free-PMO. Furthermore, these degradable carriers were biocompatible upon injection in the muscle, showing long-circulating properties with an improvement of dystrophin expression over three weeks after a single injection.

Wang et al. proved previously described PCM NPs for PMO delivery in *mdx* mice to be a strategy for DMD therapy [165]. Hydrophobic region of the carbamate groups enabled the formation of ASO-PCM carriers. These NPs dramatically improved dystrophin expression in muscles after I.M. injections with up to 57% of dystrophin-positive fibres, four-fold superior to ASO alone. After I.V. administration, up to 15% of myofibers were dystrophin-positive, resulting in a transfection efficiency 3-fold superior to ASO alone. In heart muscle, PCMs demonstrated an improvement of dystrophin-positive cardiomyocytes up to 5-fold superior, nevertheless leading to only 5% of dystrophin-positive cells. Hydrophobic PCM NPs showed high toxicity, whereas more hydrophilic PCM NPs were found ineffective to deliver PMO, emphasising the importance of a polymer's hydrophobic and hydrophilic balance to improve charge-neutral PMO delivery.

Amphiphilic PEA NPs previously described for 2′-OMe ASO complexation, also proved to be efficient in delivering PMOs for DMD application in *mdx* mice [171]. PEA-PMOs induced three-fold more dystrophin positive myofibers than PMOs alone after both I.M. and I.V. injection, with the widespread presence of dystrophin-positive fibres in diaphragm, biceps and heart after systemic delivery.

Other works demonstrated that bubble liposomes combined with ultrasound exposure are an effective tool to enhance the delivery of PMOs in both HSA^{LR} and *mdx* mice for DM and DMD applications, respectively. The interesting transfection efficiency properties of these liposomes containing ultrasound imaging gas rely on their ability to cavitate under ultrasound exposure. This combination produces transient pores in cell membranes, enabling the direct entry of the therapeutic compounds into the cytoplasm without involvement of the endosomal pathway [196,197]. Koebis et al., demonstrated that bubble liposomes-PMO I.M. delivered in HSA^{LR} mice locally improved the alternative splicing of the chloride channel 1 (Clcn1) gene, downregulating the high Clcn1 protein level in DM muscles and thereby enhancing one of the multiple DM features [178]. To our knowledge, this is the only study on ASO delivery using nanomedicine for DM applications that has been tested in vivo. Negishi et al. showed the potency of identical bubble liposomes to deliver PMO for DMD application [177]. This combination of bubble liposomes and PMOs, followed by ultrasound exposure, locally restored dystrophin expression in *mdx* mice muscles with an exon 23-skipping improvement to less than two times and a number of dystrophin positive fibres ~five-fold superior as compared with PMO alone. Thus, the co-administration of bubble liposomes combined with ultrasound exposure may provide an effective non-invasive method for PMO therapy.

Overall, to effectively deliver ASOs in skeletal muscle, nanomedicine is a fundamental tool to ensure protection from degradation while improving both tissue and intracellular uptake. The equilibrium of the degree of hydrophobicity, Mw and charge potential is the key to ensure an optimum compromise between stable complex formation, efficiency and tissue compatibility. With regard to all studies presented above, nanomedicine has achieved encouraging improvement of ASO's efficiency with special attention to skeletal muscles. Furthermore, systemic administration has showed promising results on the body-wide carrier distribution into skeletal, smooth and also cardiac muscles.

4.2. Oligonucleotides

RNA and DNA-based therapeutics are efficient and versatile strategies to regulate gene expression, making this class of drugs attractive for a variety of applications. Similar to negatively charged ASOs, strategies for oligonucleotides delivery are mainly based on electrostatic interactions [198–201].

Kinouchi et al. used atelocollagen (ATCOL) to condense a siRNA downregulating myostatin, a negative regulator of skeletal muscle growth [175]. ATCOL is a highly purified collagen chosen for its biocompatibility with skeletal muscle, as collagen occurs naturally

as one of its principal components [43]. Moreover, it has been reported that ATCOL displays low in vivo immunogenicity and toxicity [202,203]. ATCOL-siRNA NPs markedly decreased the protein levels of myostatin and thereby increased muscle mass within two weeks after a single I.M. injection in *mdx* mice. The authors also demonstrated the potential of systemic ATCOL-siRNA delivery to repress myostatin expression, inducing muscle hypertrophy in normal mice.

Poly(2-aminoethyl propylene phosphate) (PPE-EA) polymer has also demonstrated good potential for pDNA delivery to the muscle tissue in healthy Balb/c mice [204]. The high PPE-EA molecular weight ensures suitable hydrolytic stability of the PPE-EA/pDNA complexes. Furthermore, the cleavage of the PPE-EA phosphoester bond in physiological conditions gives this polymer interesting biodegradability properties. In vivo gene transfer efficiency was evaluated using LacZ, coding for β-galactosidase, as a model gene. After I.M. injection, PPE-EA/pDNA demonstrated a significantly higher and delayed β-galactosidase expression in muscles, up to 17-fold superior to DNA alone, highlighting the great potential of PPE-EA polymer as muscle gene delivery [174].

Itaka et al. designed PEG-poly(L-lysine) (PEG-PLys)/pDNA NPs-mediated gene delivery systems for skeletal muscle in order to find novel strategies to inhibit tumour growth through the extensive capillary network wrapped around the muscle fibres [173]. The authors designed PEG-PLys to reconcile DNA binding affinity within cationic PLys core, and tolerance under physiologic conditions through the electrically neutral shell of PEG [205]. The transgene expression efficacy in the skeletal muscle of healthy Balb/c mice was evaluated using pDNA encoding luciferase and GFP, as a model gene. After injection into the blood stream of murine muscle limbs, PEG-PLys/pDNA induced a luciferase expression up to 10-fold higher than pDNA alone in the injected muscle over 25 days. Moreover, PEG-PLys/pDNA promoted an increased number of fluorescent-positive muscle fibres compared to pDNA alone, a better time-dependent profile of transgene expression without any overt signs of toxicity. Thus, PEG-PLys NPs provide prolonged transgene expression in skeletal muscle, which is promising for the field of muscle pathologies.

Hyperbranched poly(ester amine)s (demonstrated an efficient PEAs) obtained from chemical modifications of PEI also demonstrated interesting properties as pDNA delivery carriers in C2C12 murine muscle cells and *mdx* mice [172]. The authors cross-linked low-molecular-weight PEI polymers to raise a dispersed positive charge density into the core and enhanced gene transfection efficiency while reducing PEI associated cytotoxicity. These biodegradable NPs effectively condensed a pDNA coding for GFP and showed a low in vitro cytotoxicity on muscle cells. PEAs/pDNA complexes in vitro transfection with up to 87% of fluorescent-positive C2C12 muscle cells, suggesting a transfection efficiency 2–3-fold higher than that of cells transfected with PEI/pDNA. Finally, these nanosystems also proved to have good potential for muscle gene delivery, showing a substantial increase in fluorescent-positive muscle fibres after I.M. administration.

In a way similar to ASOs, the main strategies adopted to deliver oligonucleotides into skeletal muscle rely on the use of materials ensuring electrostatic and hydrophobic interactions. Finding a compromise between hydrophobic and charge degree is crucial in gene delivery to ensure carriers stability and great transfection efficiency while sustaining high tissue integrity. Although these studies have been presented as promising proof-of-concept for skeletal muscle delivery, further investigations using oligonucleotides designed for treating MDs could warrant the use of such nanocarriers to critically cure affected muscles.

4.3. Small Molecules

Drug repurposing is an effective strategy to reuse existing licensed drugs for novel medical indication while reducing development time, costs and minimising risk of failure [112,206]. In addition, nanomedicine has been used to enhance therapeutic potential of drugs with restricted pharmacological profile and encompass toxicity limitations and poor availability [207–210].

One of the first small molecules encapsulated for MD applications was gentamicin, to enhance its poor delivery profile to the muscle tissue and to decrease its toxicity [120,181]. In order to overcome these drawbacks, Yukihara et al. encapsulated gentamicin into liposomes made of phosphatidylcholine or phosphocholine and PEG. Efficient accumulation of these nanosystems in the cytoplasm and cytoplasmic membranes of myofibers after I.P. injection was observed. Gentamicin-loaded liposomes increased the percentage of dystrophin positive myofibers up to 7.7% compared to 2.4% for gentamicin alone and were able to suppress the drug related ototoxicity and nephrotoxicity. However, despite the positive features of liposomes, which led to an enhanced pharmacological profile of gentamicin, this small molecule is candidate for only nonsense DMD mutations, thus restricting its clinical potential only to a narrow population of DMD patients [211].

Regulating downregulated myogenic recovery factors such as Myogenic differentiation 1 (MyoD) appears to be a good strategy to restore muscle differentiation and regeneration [212]. For this purpose, Afzal et al. designed nanolipodendrosomes loaded with synthetised MyoD and glatiramer acetate (GA), a synthetic drug that increases the level of anti-inflammatory cytokines [179]. The results demonstrated that these loaded nanosystems significantly improved muscle mass of lower-limbs in healthy SW-1 mice after I.M. injection, while no improvement was observed in the other muscles. Authors suggested that further research would warrant the use of nanolipodendrosomes loaded with these two candidate drugs to ameliorate muscle regeneration.

Bibee et al. developed lipid NPs of perfluorocarbon (PFC) to deliver rapamycin [182], an immunosuppressant and anti-inflammatory agent that proved to restore defective autophagy mechanism in *mdx* mice, associated with many side effects [213]. The main advantage of PFC NPs is their exceedingly good stability in blood, as they were originally developed as a blood substitute [214,215]. After systemic injection, nanocarriers were able to rescue a correct autophagy flux in *mdx* mice, thus improving both skeletal muscle strength and cardiac contractile performance. On the other hand, no equivalent improvement was achieved with conventional oral rapamycin administration delivered at a concentration even 10-fold superior, corresponding to the pharmacological doses. Furthermore, these muscle performance improvements were observed in young or adult wild-type mice as well as in aged mice, demonstrating the broad efficiency of this therapy. Clinically, potential deleterious consequences of rapamycin could be mitigated by the lower required dose administration of rapamycin once loaded into PFC NPs.

Lowering the severe side effects associated with chronic glucocorticosteroid administration has been investigated by Turjeman et al., encapsulating methylprednisolone hemisuccinate (MPS) into PEGylated nanoliposomes (NSSL) [180]. These smaller liposomes (80 nm) benefit from the inflamed tissues' unique vascular abnormality, achieving muscle passive targeting and accumulation into the inflamed tissue [216,217]. NSSL/MPS were mostly internalised into the diaphragm of young *mdx* mice after I.V. injection, due to the multiple tissue damages occurring in this organ at this stage, resulting in NPs leakage from capillaries. A significant decrease of TGF-β1 protein level was observed in serum, as a result of protective effects against inflammation. NSSL/MPS significantly ameliorated osteoporosis in elderly *mdx* mice, whereas MPS alone further increased bone catabolic effects, increasing DMD phenotype. Finally, differences in NSSL/MPS treatment doses showed diverse muscle benefits: lower doses demonstrating advantages in terms of muscle strength, whereas higher doses showing benefits in terms of mobility.

Márquez-Miranda et al. developed hydroxyl-terminated poly(amidoamine) (PAMAM-OH) dendrimer as a carrier for angiotensin (1–7), an anti-atrophic bioactive heptapeptide highly beneficial in the treatment of skeletal muscle pathologies [176]. PAMAM-OH dendrimers were used to increase angiotensin (1–7) short half-life, hydrolytic stability and poor systemic distribution. To observe the anti-atrophic effect of angiotensin (1–7), the authors unilaterally immobilised lower hind limbs of normal mice for 14 days. Loaded nanosystems demonstrated the ability to restore muscle strength and recover fibres diameter of immobilised limbs to levels similar to non-immobilised limbs after I.P. administration,

whereas angiotensin (1–7) alone did not induce any recovery. Moreover, bone micro-architectural structure in elderly *mdx* mice was less damaged over 58 weeks of NSSL-MPS administration compared to mice treated with MPS. Altogether, these findings highlight the potency of PAMAM-OH/angiotensin (1–7) nanocarriers as an efficient general treatment of dystrophies for mitigating muscle atrophy.

Many therapeutic approaches have been explored through the screening of small molecules to reverse pathological consequences of MDs. Despite several advantages including lower costs, ease of therapy management and faster development process, small molecules are intended only to target downstream effects at the splicing or protein level and not to correct mutations at the DNA or RNA levels. In the studies presented above, nanomedicine has allowed for an increase in the therapeutic impact of experimental small molecules or well-known effective molecules, while significantly decreasing potential deleterious side effects.

4.4. CRISPR/Cas9 System

CRISPR/Cas9 system is a recent and powerful genome editing tool of great interest to treat genetic disorders such as DMD and DM [100,218]. The delivery of Cas9/sgRNA ribonucleoprotein complexes via non-viral delivery systems has been investigated to boost its clinical applications [219,220]. Challenges rely principally on the large size of Cas9 protein and the difficulty to prevent ribonucleoprotein complexes from degrading during the entire formulation and delivery process [183]. Lee et al. used gold NPs (GNP) to develop innovative carriers for the delivery of the entire CRISPR/Cas9 system (named CRISPR-Gold) to restore dystrophin expression by inducing in vivo homologous directed repair (HDR) in *mdx* mice [184]. Authors selected GNP as they can be easily coated with a densely packed layer of DNA and can be internalised by a variety of cell types [221,222]. To obtain complex CRISPR-Gold, the authors coated GNP with a thiol-terminated DNA to efficiently hybridize thiol-terminated donor DNA and trigger its rapid release once into the cytoplasm by disulfide-bond cleavage. Cas9 protein/sgRNA was then adsorbed onto the NPs, then finally covered with PAsp(DET) endosomal disruptive polymer. CRISPR-Gold demonstrated the ability to efficiently deliver in vitro and in vivo both the protein and the nucleic acid of the CRISPR/Cas9 system, through their affinity with the GNP coating of packed layer DNA. Injected simultaneously with cardiotoxin to induce further muscle damage, CRISPR-Gold revealed in *mdx* mice an HDR efficiency up to 18 times higher than CRISPR/Cas9 system itself with 5.4% restoration of the dystrophin gene. Moreover, cryosections of CRISPR-Gold-injected muscles showed a robust dystrophin expression nearly similar to that of wild-type mice muscle and reduced levels of muscle fibrosis, a sign of better tissue health. CRISPR-Gold delivered under clinically relevant conditions (without cardiotoxin) were shown to enhance animal strength and agility in *mdx* mice with HDR efficiency of 1% in the dystrophin gene and minimal off-target genomic damage. Finally, this work evidenced the absence of a broad immune response that could be potentially induced by the Cas9 bacterial protein, suggesting the possible safety of multiple injections of CRISPR-Gold. In conclusion, the authors designed NPs able to bind all CRISPR/Cas9 components but also to intracellularly deliver them through endosomal disruptive and disulphide reduction mechanisms. Complex and innovative CRISPR-Gold has the potential to regenerate wild-type dystrophin to a fully functional level, appearing as a promising treatment for genetic diseases such as DMD.

Recently, Wei et al. efficiently delivered Cas9/sgRNA ribonucleoprotein complexes to muscle, brain, liver and lungs using lipid NPs [183]. By adjusting the molecular components and ratios of lipids, the authors achieved tissue-specific gene editing in liver and lungs of healthy mice C57BL/6J after systemic injection. More interestingly, these nanosystems were evaluated in ΔEx44 DMD mice and were proven to restore dystrophin expression up to ~5% after I.M. administration.

To our knowledge, NPs here presented are the only CRISPR/Cas9 delivery systems using non-viral NPs that have been described for MD applications. Although CRISPR/Cas9

is currently one of the most efficient tools for genome editing, non-viral delivery strategies are needed to improve precise gene correction.

5. Limitations In In Vitro and In Vivo Testing of Novel Treatments

The evaluation of nanomedicine behaviour in appropriate in vitro and in vivo models able to mimic physiology and phenotypes of MDs is an important requirement for their clinical translation. For preliminary studies and screening of different drugs, in vitro and ex vivo models based on immortalised or mutant human and animal cells, muscle preservation systems or tissue engineered constructs have been set-up as alternatives to rare patient cells. In addition, different animal models have been also set up to provide accurate in vivo MD models. An overview of the common used in vitro, ex vivo or in vivo models for testing novel MD treatments is provided in Figure 4.

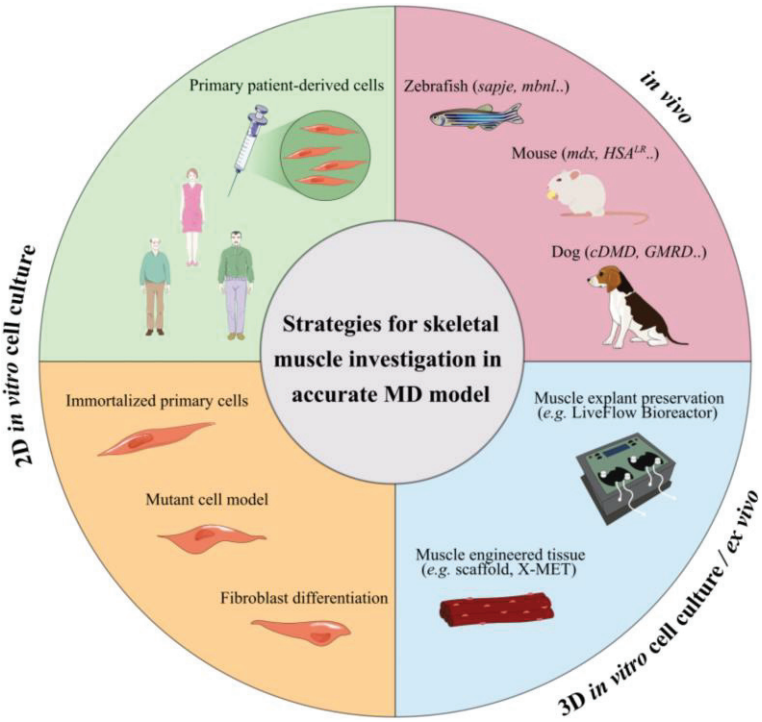

Figure 4. Strategies and accurate models to explore MD treatments. Broad in vitro, ex vivo and in vivo MD models to promote the translation of nanomedicine-based therapies (MD, muscular dystrophies; X-MET, ex vivo-vascularized muscle engineered tissue).

In vitro studies provide a unique preliminary resource to clarify the potential risk of NPs administration [223]. Primary cells are the most representative cell model for studying the molecular hallmarks of these pathologies as they are directly isolated from the patient's tissue [224]. However, their use is limited by the poor availability of muscle tissue due to the small samples collected by biopsy and the limited proliferative capacity of the satellite cells isolated from the explanted tissue [225–229]. To overcome these limitations, different strategies have been proposed. Genetic mutation characteristics of the pathology can be exogenously introduced into immortalised cell lines such as HeLa, C2C12 myoblasts or induced pluripotent stem cells (iPS). Even if these experimental models do not reproduce the entire genomic context, these transfected cells express the main features of the pathogenic mechanism, providing a cell-based model for studying the splicing defects of MDs [18,86,230]. Another approach consists in the immortalisation of primary muscle cells by reducing their replicative senescence with the use of telomere shortening, inhibiting the dominant p16 pathway [223,231–233]. Skin fibroblasts from patient skin biopsies can

also differentiate into multinucleated myotubes by inducing the myogenic regulator factor MyoD [223,224,234,235]. However, these 2D monolayer cultures inaccurately representing in vitro tissue cells and cellular response to therapeutic treatments might be erroneous due to the unnatural microenvironment [236,237]. In this context, 3D culture systems have gained increasing interest as they are able to provide accurate models of organs or tissue physiology and associated disorders. However, they are not exempt from limitations, such as lack of nutrients and oxygen distribution, and accumulation of wastes into the core of 3D culture [236,238,239]. Diverse biomimetic engineered muscle constructs, such as scaffold or organoid cell culture, have demonstrated structural and functional characteristics similar to native muscle, mimicking the tissue complexity [240–242]. These skeletal muscle organoids offer an attractive alternative to preliminary in vivo studies for disease modelling and in vitro drug screening.

Ex-vivo models have also reproduced accurate natural environment models for broad applications, overcoming 3D cell culture challenges related to heterogeneous oxygen, nutrient and metabolic waste distribution [237,243–245]. One possible approach for muscle investigations is culturing skeletal muscle explants as intact muscle fibres (myofibers) or intact muscles, preserving cell/tissue architecture and its relationship with the surrounding anatomical structures [246]. Moreover, fluid dynamic systems may improve the organ preservation, overcoming the loss of vasculature function by mimicking the physiological flow for nutrient supply and catabolite withdrawal, thus supporting the metabolic activity of the explanted tissues [243,247]. Recently, Carton et al. demonstrated the great benefit in terms of structural preservation obtained by maintaining explanted soleus murine muscle in a bioreactor under dynamic conditions [248]. The progressive structural deterioration of the muscle tissue was markedly slowed, prolonging its preservation up to two days. This innovative system allows experimental testing on the living organism with positive ethical impact, overcoming animal injuries related to therapeutic trial. Bioengineered three-dimensional vascularised skeletal muscle tissue (named X-MET) has also been developed by Carosio et al., using heterogeneous primary cell populations such as myoblasts, fibroblasts and endothelial cells [249]. This vascularised ex-vivo system closely mimicking the cellular complexity of the muscle tissue showed biomechanical properties and activity similar to adult skeletal muscles. Furthermore, X-MET transplanted into damaged muscle has demonstrated interesting properties to restore muscle functionality.

To further investigate therapeutic efficacy, in vivo testing remains the most representative means of study for understanding the complex cellular and tissue mechanisms' interactions [250,251]. Over the last years, various animal models of MDs have contributed to clarifying the molecular phenotypes involved in these pathologies and investigating drug screening [252–254]. Several DMD animal models have been developed by reproducing the deficient dystrophin expression. As previously reported, the *mdx* mouse (BL10-*mdx*) is the most commonly used DMD animal model and is characterised by the presence of a stop codon located in exon 23 that leads to loss of full-length dystrophin whereas smaller isoforms are still expressed [89,255]. Recently, D2-*mdx* mouse models issued from a different genetic background (DBA2/J) have demonstrated a more pronounced phenotype closer to patients [256]. Furthermore, Desguerre et al. described a model of chronic mechanical muscle injury to trigger muscle fibrosis at the same time of dystrophin-deficiency expression in *mdx* hindlimb muscle [257]. DMD canine model (cDMD, GRMD) also carries dystrophin deficit and expresses clinical phenotypes more severely than *mdx* mouse, better aligning with the progressive course of DMD and thereby better translating to humans [252,258,259]. Two zebrafish dystrophin mutants, sapje and sapje-like (sapc/100), carry a mutation in the dystrophin gene, which results in a premature stop codon, thus mimicking muscle dysfunction with a severe phenotype [260,261]. Other less common DMD animal models include *Caenorhabditis elegans*, *Drosophila melanogaster*, feline, rat and pig models [252].

Regarding DM, animal models have been developed by reproducing CUG expansion, MBNL-deficient or CELF-overexpressing phenotypes. Two main mouse models are com-

monly used for the study of DM1 and DM2: DMSXL mice, carrying ~ 1000–1800 CTG repeats with multisystemic transgene expression, and HSA^{LR} mice that express human skeletal actin (HSA) transcripts containing ~ 250 trinucleotide repeats within the 3′ DMPK UTR with skeletal muscle transgene expression [262,263]. These murine models reproduce the DM1 and DM2 pathogenesis similarly to the human phenotype [264–268]. Two zebrafish models of MBNL loss of function, typical of DM1, have been generated to study the pathological aspects that characterise skeletal and heart muscles in DM [269,270]. Other transgenic animals, such as *Caenorhabditis elegans* and *Drosophila melanogaster* have also been engineered to mimic some characteristics of DM phenotypes [252,262].

Although no animal model is able to completely recapitulate the aspects of the multisystemic phenotypes typical of MDs, their use is required to provide critical in-depth assessment of proof-of-principle concept studies and preclinical experiments. The actual growing interest and knowledge for development of in vitro and ex vivo alternatives to reduce clinical animal experimentation could warrant novel and better methods for assisting in assessment of MDs therapy.

6. Future Perspectives

The recent understanding of the pathogenic mechanisms of MDs highlights the urgent need of new and more effective treatments [20,100]. Nanomedicine demonstrated to enhance the therapeutic potential of gene therapy and drug repurposing approaches. As an example, pentamidine-loaded nanomedicines were used to explore the activity of the drug, not only as an anti-leishmaniasis agent but also as an anticancer agent to reduce drug associated toxicity, such as its severe nephrotoxicity [271,272]. Ongoing investigations are aimed at demonstrating the efficacy of this novel formulation to treat DM1 (study in progress).

New therapeutic approaches needed a continuous administration throughout patient's life, making the biocompatibility and biodegradability of delivery systems a crucial feature to preserve skeletal muscle from additional alterations. As presented in this review, the main advantages of nanosystems rely on their physico-chemical properties, namely composition, size and surface potential that can be modulated to avoid nanocarrier toxicity, and to load specific actives and deliver them in a target site.

To disclose the potential of nanomedicine application to MDs treatment, the gap between in vitro and in vivo testing has to be filled. In addition, to understand the fate of nanosystems once administered to MDs mice, biodistribution studies need to be addressed. To date, only a few investigations reported NPs biodistribution into skeletal muscles through different administration routes as I.V., I.P. and I.M. (tibialis anterior and gastrocnemius muscles) [173,273,274]. After systemic administration, NPs spread into tissues through blood systemic circulation, then, extravasate into the ECM before reaching muscle fibres. It has been suggested that the dense blood capillary network wrapping skeletal myofibers could be favourable to NPs accumulation and distribution following I.V. injection [196]. Hydrodynamic injection is also known to facilitate gene delivery by transient enhancement of the plasma membrane's permeability [142,275,276]. However, the applied pressure due to the hindrance of the blood flow might cause oedema and inflammation, restricting the translation of this technique to clinic [277].

Overcoming the ECM barrier remains another important goal to improve NPs distribution in skeletal muscle fibres. Surface engineered nanosystems have been designed to actively promote the interaction between nanosystems and cells [278]. The high specificity of antibodies for their corresponding antigen provides a selective and potent approach for therapeutic NPs targeting [279]. As an example, the murine monoclonal antibody (3E10), capable of binding the surface of muscle cells, has been reported to improve active targeting [280,281]. However, no scientific studies on antibody-functionalised NPs have been conducted for skeletal muscle targeting so far. More commonly used, short peptides sequences (*e.g.*, ASSLNIA or SKTFNTHPQSTP) have proved promising as NPs functionalization for specific tissue-targeting [282–284]. Several examples of peptides

targeting muscle cells have been reported [285–287] and association to nanosystems may lead to improved selectivity of NPs for skeletal muscle. Polymeric nanosystems have been functionalised with active targeting agents that preferentially bind active molecules or receptors expressed on the surface of muscle cells. Active targeting-dependent uptake has been demonstrated using PLGA nanocarriers functionalised with a muscle-homing peptide M12 [288]. Biodistribution studies revealed a preferential accumulation of targeted NPs in skeletal muscle cells in *mdx* mice, compared to untargeted nanocarriers, increasing the accumulation of polymeric NPs and enhancing therapeutic efficacy [274].

As presented in this review, nanomedicine holds promise for the development of efficient and safe MD treatments. With the rise in biologic products development, there is an increasing interest for effective biocompatible delivery systems that can be better suited for biologics leading to more effective therapeutic strategies. Further development of nanomedicine in this area is expected to result from complementary expertise in different research fields. Indeed, a multi-disciplinary study in drug discovery, nanomedicine, biotechnology, biology and medicine is key to providing valid and reliable strategies that can offer unprecedented opportunities to MD patients.

Author Contributions: I.A., M.R. and F.C. wrote the first draft of the review. G.L., B.S., S.A., M.M., S.B. and D.K. reviewed the manuscript and contributed to the critical analysis and the future perspectives of the work. R.M. and B.C. helped with the description of the disease. G.L., B.S., S.A. and M.M. conceptualised the work. All authors have read and agreed to the published version of the manuscript.

Funding: I.A. has a fellowship from the Italian Ministry of University and Research. M.R. has a fellowship from the INVITE project of the University of Verona (PhD Programme in Nanoscience and Advanced Technologies). INVITE is an initiative funded by European Union's Horizon 2020 Research and Innovation Programme under the Marie Skłodowska-Curie grant agreement No. 754345.

Institutional Review Board Statement: Not applicable.
Informed Consent Statement: Not applicable.

Data Availability Statement: Not applicable.

Acknowledgments: Euronanomed III (Joint Translational Call 2017, Project RESOLVE), the Italian Ministry of University and Research–University of Turin "Fondi Ricerca Locale (ex-60%)". Figures have been designed using Inkscape v.0.92.2 software. Some scientific illustrations were used from Servier Medical Art templates, which are licensed under a Creative Commons Attribution 3.0 Unported License; https://smart.servier.com.

Conflicts of Interest: The authors declare no conflict of interest.

References

1. Shieh, P.B. Muscular dystrophies and other genetic myopathies. *Neurol. Clin.* **2013**, *31*, 1009–1029. [CrossRef] [PubMed]
2. Theadom, A.; Rodrigues, M.; Roxburgh, R.; Balalla, S.; Higgins, C.; Bhattacharjee, R.; Jones, K.; Krishnamurthi, R.; Feigin, V. Prevalence of muscular dystrophies: A systematic literature review. *Neuroepidemiology* **2014**, *43*, 259–268. [CrossRef] [PubMed]
3. Mercuri, E.; Bönnemann, C.G.; Muntoni, F. Muscular dystrophies. *Lancet Lond. Engl.* **2019**, *394*, 2025–2038. [CrossRef]
4. Carter, J.C.; Sheehan, D.W.; Prochoroff, A.; Birnkrant, D.J. Muscular Dystrophies. *Clin. Chest Med.* **2018**, *39*, 377–389. [CrossRef]
5. Johnson, N.E. Myotonic Dystrophies. *Continuum* **2019**, *25*, 1682–1695. [CrossRef] [PubMed]
6. Meola, G. Clinical aspects, molecular pathomechanisms and management of myotonic dystrophies. *Acta Myol.* **2013**, *32*, 154–165.
7. Messina, S.; Vita, G.L. Clinical management of Duchenne muscular dystrophy: The state of the art. *Neurol. Sci.* **2018**, *39*, 1837–1845. [CrossRef] [PubMed]
8. Nio, Y.; Tanaka, M.; Hirozane, Y.; Muraki, Y.; Okawara, M.; Hazama, M.; Matsuo, T. Phosphodiesterase 4 inhibitor and phosphodiesterase 5 inhibitor combination therapy has antifibrotic and anti-inflammatory effects in *mdx* mice with Duchenne muscular dystrophy. *FASEB J.* **2017**, *31*, 5307–5320. [CrossRef] [PubMed]
9. Zanotti, S.; Bragato, C.; Zucchella, A.; Maggi, L.; Mantegazza, R.; Morandi, L.; Mora, M. Anti-fibrotic effect of pirfenidone in muscle derived-fibroblasts from Duchenne muscular dystrophy patients. *Life Sci.* **2016**, *145*, 127–136. [CrossRef]
10. McDonald, C.M.; Henricson, E.K.; Abresch, R.T.; Duong, T.; Joyce, N.C.; Hu, F.; Clemens, P.R.; Hoffman, E.P.; Cnaan, A.; Gordish-Dressman, H.; et al. Long-term effects of glucocorticoids on function, quality of life, and survival in patients with Duchenne Muscular Dystrophy: A prospective cohort study. *Lancet* **2018**, *391*, 451–461. [CrossRef]

11. Kao, K.-T.; Joseph, S.; Capaldi, N.; Brown, S.; Di Marco, M.; Dunne, J.; Horrocks, I.; Shepherd, S.; Ahmed, S.F.; Wong, S.C. Skeletal disproportion in glucocorticoid-treated boys with Duchenne muscular dystrophy. *Eur. J. Pediatr.* **2019**, *178*, 633–640. [CrossRef] [PubMed]
12. Mayo, A.L.; Craven, B.C.; McAdam, L.C.; Biggar, W.D. Bone health in boys with Duchenne muscular dystrophy on long-term daily deflazacort therapy. *Neuromuscul. Disord.* **2012**, *22*, 1040–1045. [CrossRef]
13. Ward, L.M.; Weber, D.R. Growth, pubertal development, and skeletal health in boys with Duchenne muscular dystrophy. *Curr. Opin. Endocrinol. Diabetes Obes.* **2019**, *26*, 39–48. [CrossRef]
14. Birnkrant, D.J.; Bushby, K.; Bann, C.M.; Apkon, S.D.; Blackwell, A.; Brumbaugh, D.; Case, L.E.; Clemens, P.R.; Hadjiyannakis, S.; Pandya, S.; et al. Diagnosis and management of Duchenne muscular dystrophy, part 1: Diagnosis, and neuromuscular, rehabilitation, endocrine, and gastrointestinal and nutritional management. *Lancet Neurol.* **2018**, *17*, 251–267. [CrossRef]
15. Fayssoil, A.; Lazarus, A.; Wahbi, K.; Ogna, A.; Nardi, O.; Lofaso, F.; Clair, B.; Orlikowski, D.; Annane, D. Cardiac implantable electronic devices in tracheotomized muscular dystrophy patients: Safety and risks. *Int. J. Cardiol.* **2016**, *222*, 975–977. [CrossRef] [PubMed]
16. Bach, J.R.; Saporito, L.R.; Shah, H.R.; Sinquee, D. Decanulation of patients with severe respiratory muscle insufficiency: Efficacy of mechanical insufflation-exsufflation. *J. Rehabil. Med.* **2014**, *46*, 1037–1041. [CrossRef]
17. Warf, M.B.; Nakamori, M.; Matthys, C.M.; Thornton, C.A.; Berglund, J.A. Pentamidine reverses the splicing defects associated with myotonic dystrophy. *Proc. Natl. Acad. Sci. USA* **2009**, *106*, 18551–18556. [CrossRef]
18. Konieczny, P.; Selma-Soriano, E.; Rapisarda, A.S.; Fernandez-Costa, J.M.; Perez-Alonso, M.; Artero, R. Myotonic dystrophy: Candidate small molecule therapeutics. *Drug Discov. Today* **2017**, *22*, 1740–1748. [CrossRef] [PubMed]
19. Lee, J.E.; Bennett, C.F.; Cooper, T.A. RNase H-mediated degradation of toxic RNA in myotonic dystrophy type 1. *Proc. Natl. Acad. Sci. USA* **2012**, *109*, 4221–4226. [CrossRef]
20. Verhaart, I.E.C.; Aartsma-Rus, A. Therapeutic developments for Duchenne muscular dystrophy. *Nat. Rev. Neurol.* **2019**, *15*, 373–386. [CrossRef]
21. Zhang, Y.; Li, H.; Min, Y.L.; Sanchez-Ortiz, E.; Huang, J.; Mireault, A.A.; Shelton, J.M.; Kim, J.; Mammen, P.P.A.; Bassel-Duby, R.; et al. Enhanced CRISPR-Cas9 correction of Duchenne muscular dystrophy in mice by a self-complementary AAV delivery system. *Sci. Adv.* **2020**, *6*, eaay6812. [CrossRef]
22. Lo Scrudato, M.; Poulard, K.; Sourd, C.; Tomé, S.; Klein, A.F.; Corre, G.; Huguet, A.; Furling, D.; Gourdon, G.; Buj-Bello, A. Genome editing of expanded CTG repeats within the human DMPK gene reduces nuclear RNA foci in the muscle of DM1 mice. *Mol. Ther.* **2019**, *27*, 1372–1388. [CrossRef]
23. Pedrini, I.; Gazzano, E.; Chegaev, K.; Rolando, B.; Marengo, A.; Kopecka, J.; Fruttero, R.; Ghigo, D.; Arpicco, S.; Riganti, C. Liposomal nitrooxy-doxorubicin: One step over caelyx in drug-resistant human cancer cells. *Mol. Pharm.* **2014**, *11*, 3068–3079. [CrossRef] [PubMed]
24. Autio, K.A.; Dreicer, R.; Anderson, J.; Garcia, J.A.; Alva, A.; Hart, L.L.; Milowsky, M.I.; Posadas, E.M.; Ryan, C.J.; Graf, R.P.; et al. Safety and efficacy of BIND-014, a docetaxel nanoparticle targeting prostate-specific membrane antigen for patients with metastatic castration-resistant prostate cancer: A phase 2 clinical trial. *JAMA Oncol.* **2018**, *4*, 1344–1351. [CrossRef]
25. Van der Meel, R.; Sulheim, E.; Shi, Y.; Kiessling, F.; Mulder, W.J.M.; Lammers, T. Smart cancer nanomedicine. *Nat. Nanotechnol.* **2019**, *14*, 1007–1017. [CrossRef]
26. Wang-Gillam, A.; Hubner, R.A.; Siveke, J.T.; Von Hoff, D.D.; Belanger, B.; de Jong, F.A.; Mirakhur, B.; Chen, L.-T. NAPOLI-1 phase 3 study of liposomal irinotecan in metastatic pancreatic cancer: Final overall survival analysis and characteristics of long-term survivors. *Eur. J. Cancer* **2019**, *108*, 78–87. [CrossRef] [PubMed]
27. Hanif, S.; Muhammad, P.; Chesworth, R.; Rehman, F.U.; Qian, R.; Zheng, M.; Shi, B. Nanomedicine-Based Immunotherapy for Central Nervous System Disorders. *Acta Pharmacol. Sin.* **2020**, *41*, 936–953. [CrossRef] [PubMed]
28. You, L.; Wang, J.; Liu, T.; Zhang, Y.; Han, X.; Wang, T.; Guo, S.; Dong, T.; Xu, J.; Anderson, G.J.; et al. Targeted brain delivery of rabies virus glycoprotein 29-modified deferoxamine-loaded nanoparticles reverses functional deficits in Parkinsonian mice. *ACS Nano* **2018**, *12*, 4123–4139. [CrossRef]
29. Dos Santos Tramontin, N.; da Silva, S.; Arruda, R.; Ugioni, K.S.; Canteiro, P.B.; de Bem Silveira, G.; Mendes, C.; Silveira, P.C.L.; Muller, A.P. Gold nanoparticles treatment reverses brain damage in Alzheimer's disease model. *Mol. Neurobiol.* **2020**, *57*, 926–936. [CrossRef] [PubMed]
30. Pearson, R.M.; Podojil, J.R.; Shea, L.D.; King, N.J.C.; Miller, S.D.; Getts, D.R. Overcoming challenges in treating autoimmuntity: Development of tolerogenic immune-modifying nanoparticles. *Nanomedicine* **2019**, *18*, 282–291. [CrossRef]
31. Zhao, G.; Liu, A.; Zhang, Y.; Zuo, Z.-Q.; Cao, Z.-T.; Zhang, H.-B.; Xu, C.-F.; Wang, J. Nanoparticle-delivered siRNA targeting Bruton's tyrosine kinase for rheumatoid arthritis therapy. *Biomater. Sci.* **2019**, *7*, 4698–4707. [CrossRef] [PubMed]
32. Horwitz, D.A.; Bickerton, S.; Koss, M.; Fahmy, T.M.; La Cava, A. Suppression of murine Lupus by CD4+ and CD8+ treg cells induced by T cell-targeted nanoparticles loaded with interleukin-2 and transforming growth factor β. *Arthritis Rheumatol.* **2019**, *71*, 632–640. [CrossRef]
33. Fries, C.N.; Curvino, E.J.; Chen, J.-L.; Permar, S.R.; Fouda, G.G.; Collier, J.H. Advances in nanomaterial vaccine strategies to address infectious diseases impacting global health. *Nat. Nanotechnol.* **2020**, 1–14. [CrossRef] [PubMed]
34. Nanomedicine and the COVID-19 vaccines. *Nat. Nanotechnol.* **2020**, *1*. [CrossRef]

35. Sahin, U.; Muik, A.; Derhovanessian, E.; Vogler, I.; Kranz, L.M.; Vormehr, M.; Baum, A.; Pascal, K.; Quandt, J.; Maurus, D.; et al. COVID-19 vaccine BNT162b1 elicits human antibody and TH1 T cell responses. *Nature* **2020**, *586*, 594–599. [CrossRef] [PubMed]
36. Baden, L.R.; El Sahly, H.M.; Essink, B.; Kotloff, K.; Frey, S.; Novak, R.; Diemert, D.; Spector, S.A.; Rouphael, N.; Creech, C.B.; et al. Efficacy and safety of the MRNA-1273 SARS-CoV-2 vaccine. *N. Engl. J. Med.* **2020**, *384*, 403–416. [CrossRef] [PubMed]
37. Chung, Y.H.; Beiss, V.; Fiering, S.N.; Steinmetz, N.F. COVID-19 vaccine frontrunners and their nanotechnology design. *ACS Nano* **2020**, *14*, 12522–12537. [CrossRef]
38. Kranz, L.M.; Diken, M.; Haas, H.; Kreiter, S.; Loquai, C.; Reuter, K.C.; Meng, M.; Fritz, D.; Vascotto, F.; Hefesha, H.; et al. Systemic RNA delivery to dendritic cells exploits antiviral defence for cancer immunotherapy. *Nature* **2016**, *534*, 396–401. [CrossRef] [PubMed]
39. Xin, X.; Kumar, V.; Lin, F.; Kumar, V.; Bhattarai, R.; Bhatt, V.R.; Tan, C.; Mahato, R.I. Redox-responsive nanoplatform for codelivery of miR-519c and gemcitabine for pancreatic cancer therapy. *Sci. Adv.* **2020**, eabd6764. [CrossRef] [PubMed]
40. Sasso, M.S.; Lollo, G.; Pitorre, M.; Solito, S.; Pinton, L.; Valpione, S.; Bastiat, G.; Mandruzzato, S.; Bronte, V.; Marigo, I.; et al. Low dose gemcitabine-loaded lipid nanocapsules target monocytic myeloid-derived suppressor cells and potentiate cancer immunotherapy. *Biomaterials* **2016**, *96*, 47–62. [CrossRef] [PubMed]
41. Lancet, J.E.; Uy, G.L.; Cortes, J.E.; Newell, L.F.; Lin, T.L.; Ritchie, E.K.; Stuart, R.K.; Strickland, S.A.; Hogge, D.; Solomon, S.R.; et al. CPX-351 (cytarabine and daunorubicin) liposome for injection versus conventional cytarabine plus daunorubicin in older patients with newly diagnosed secondary acute myeloid leukemia. *J. Clin. Oncol.* **2018**, *36*, 2684–2692. [CrossRef]
42. Salvioni, L.; Rizzuto, M.A.; Bertolini, J.A.; Pandolfi, L.; Colombo, M.; Prosperi, D. Thirty years of cancer nanomedicine: Success, frustration, and hope. *Cancers* **2019**, *11*, 1855. [CrossRef]
43. Gillies, A.R.; Lieber, R.L. Structure and function of the skeletal muscle extracellular matrix. *Muscle Nerve* **2011**, *44*, 318–331. [CrossRef]
44. Yhee, J.Y.; Yoon, H.Y.; Kim, H.; Jeon, S.; Hergert, P.; Im, J.; Panyam, J.; Kim, K.; Nho, R.S. The effects of collagen-rich extracellular matrix on the intracellular delivery of glycol chitosan nanoparticles in human lung fibroblasts. *Int. J. Nanomed.* **2017**, *12*, 6089–6105. [CrossRef] [PubMed]
45. Sleboda, D.A.; Stover, K.K.; Roberts, T.J. Diversity of extracellular matrix morphology in vertebrate skeletal muscle. *J. Morphol.* **2020**, *281*, 160–169. [CrossRef] [PubMed]
46. Engin, A.B.; Nikitovic, D.; Neagu, M.; Henrich-Noack, P.; Docea, A.O.; Shtilman, M.I.; Golokhvast, K.; Tsatsakis, A.M. Mechanistic understanding of nanoparticles' interactions with extracellular matrix: The cell and immune system. *Part. Fibre Toxicol.* **2017**, *14*, 22. [CrossRef] [PubMed]
47. Stylianopoulos, T.; Poh, M.Z.; Insin, N.; Bawendi, M.G.; Fukumura, D.; Munn, L.L.; Jain, R.K. Diffusion of particles in the extracellular matrix: The effect of repulsive electrostatic interactions. *Biophys. J.* **2010**, *99*, 1342–1349. [CrossRef] [PubMed]
48. Zhigaltsev, I.V.; Belliveau, N.; Hafez, I.; Leung, A.K.K.; Huft, J.; Hansen, C.; Cullis, P.R. Bottom-up design and synthesis of limit size lipid nanoparticle systems with aqueous and triglyceride cores using millisecond microfluidic mixing. *Langmuir* **2012**, *28*, 3633–3640. [CrossRef]
49. Evers, M.J.W.; Kulkarni, J.A.; van der Meel, R.; Cullis, P.R.; Vader, P.; Schiffelers, R.M. State-of-the-art design and rapid-mixing production techniques of lipid nanoparticles for nucleic acid delivery. *Small Methods* **2018**, *2*, 1700375. [CrossRef]
50. Feng, J.; Markwalter, C.E.; Tian, C.; Armstrong, M.; Prud'homme, R.K. Translational formulation of nanoparticle therapeutics from laboratory discovery to clinical scale. *J. Transl. Med.* **2019**, *17*, 200. [CrossRef] [PubMed]
51. Ebner, D.C.; Bialek, P.; El-Kattan, A.F.; Ambler, C.M.; Tu, M. Strategies for skeletal muscle targeting in drug discovery. *Curr. Pharm. Des.* **2015**, *21*, 1327–1336. [CrossRef] [PubMed]
52. Mah, J.K.; Korngut, L.; Fiest, K.M.; Dykeman, J.; Day, L.J.; Pringsheim, T.; Jette, N. A Systematic review and meta-analysis on the epidemiology of the muscular dystrophies. *Can. J. Neurol. Sci.* **2015**, *43*, 163–177. [CrossRef]
53. Nascimento Osorio, A.; Medina Cantillo, J.; Camacho Salas, A.; Madruga Garrido, M.; Vilchez Padilla, J.J. Consensus on the diagnosis, treatment and follow-up of patients with Duchenne muscular dystrophy. *Neurologia* **2019**, *34*, 469–481. [CrossRef]
54. Koenig, M.; Hoffman, E.P.; Bertelson, C.J.; Monaco, A.P.; Feener, C.; Kunkel, L.M. Complete cloning of the Duchenne muscular dystrophy (DMD) cDNA and preliminary genomic organization of the DMD gene in normal and affected individuals. *Cell* **1987**, *50*, 509–517. [CrossRef]
55. Zhu, J.F.; Liu, H.H.; Zhou, T.; Tian, L. Novel mutation in exon 56 of the dystrophin gene in a child with Duchenne muscular dystrophy. *Int. J. Mol. Med.* **2013**, *32*, 1166–1170. [CrossRef] [PubMed]
56. Muntoni, F.; Torelli, S.; Ferlini, A. Dystrophin and mutations: One gene, several proteins, multiple phenotypes. *Lancet Neurol.* **2003**, *2*, 731–740. [CrossRef]
57. Koenig, M.; Beggs, A.H.; Moyer, M.; Scherpf, S.; Heindrich, K.; Bettecken, T.; Meng, G.; Müller, C.R.; Lindlöf, M.; Kaariainen, H.; et al. The molecular basis for Duchenne versus Becker muscular dystrophy: Correlation of severity with type of deletion. *Am. J. Hum. Genet.* **1989**, *45*, 498–506. [PubMed]
58. Miyatake, S.; Mizobe, Y.; Takizawa, H.; Hara, Y.; Yokota, T.; Takeda, S.; Aoki, Y. Exon skipping therapy using phosphorodiamidate morpholino oligomers in the *mdx*52 mouse model of Duchenne muscular dystrophy. *Methods Mol. Biol.* **2018**, *1687*, 123–141. [CrossRef]
59. Zhu, P.; Wu, F.; Mosenson, J.; Zhang, H.; He, T.-C.; Wu, W.-S. CRISPR/Cas9-mediated genome editing corrects dystrophin mutation in skeletal muscle stem cells in a mouse model of muscle dystrophy. *Mol. Ther. Nucleic Acids* **2017**, *7*, 31–41. [CrossRef]

60. Bird, T.D. Myotonic Dystrophy Type 1. In *GeneReviews®*; Adam, M.P., Ardinger, H.H., Pagon, R.A., Wallace, S.E., Bean, L.J., Stephens, K., Amemiya, A., Eds.; University of Washington: Seattle, WA, USA, 1993–2020.
61. Thornton, C.A. Myotonic dystrophy. *Neurol. Clin.* **2014**, *32*, 705–719. [CrossRef] [PubMed]
62. Turner, C.; Hilton-Jones, D. The myotonic dystrophies: Diagnosis and management. *J. Neurol. Neurosurg. Psychiatry* **2010**, *81*, 358–367. [CrossRef]
63. Lee, J.E.; Cooper, T.A. Pathogenic mechanisms of myotonic dystrophy. *Biochem. Soc. Trans.* **2009**, *37*, 1281–1286. [CrossRef]
64. De Temmerman, N.; Sermon, K.; Seneca, S.; De Rycke, M.; Hilven, P.; Lissens, W.; Van Steirteghem, A.; Liebaers, I. Intergenerational instability of the expanded CTG repeat in the DMPK gene: Studies in human gametes and preimplantation embryos. *Am. J. Hum. Genet.* **2004**, *75*, 325–329. [CrossRef]
65. Malatesta, M.; Cardani, R.; Pellicciari, C.; Meola, G. RNA transcription and maturation in skeletal muscle cells are similarly impaired in myotonic dystrophy and sarcopenia: The ultrastructural evidence. *Front. Aging Neurosci.* **2014**, *6*, 196. [CrossRef]
66. Nakamori, M.; Sobczak, K.; Puwanant, A.; Welle, S.; Eichinger, K.; Pandya, S.; Dekdebrun, J.; Heatwole, C.R.; McDermott, M.P.; Chen, T.; et al. Splicing biomarkers of disease severity in myotonic dystrophy. *Ann. Neurol.* **2013**, *74*, 862–872. [CrossRef] [PubMed]
67. Miller, J.W.; Urbinati, C.R.; Teng-Umnuay, P.; Stenberg, M.G.; Byrne, B.J.; Thornton, C.A.; Swanson, M.S. Recruitment of human muscleblind proteins to (CUG)(n) expansions associated with myotonic dystrophy. *EMBO J.* **2000**, *19*, 4439–4448. [CrossRef] [PubMed]
68. Meola, G.; Cardani, R. Myotonic dystrophies: An update on clinical aspects, genetic, pathology, and molecular pathomechanisms. *Biochim. Biophys. Acta* **2015**, *1852*, 594–606. [CrossRef] [PubMed]
69. Paul, S.; Dansithong, W.; Kim, D.; Rossi, J.; Webster, N.J.; Comai, L.; Reddy, S. Interaction of muscleblind, CUG-BP1 and hnRNP H proteins in DM1-associated aberrant IR splicing. *EMBO J.* **2006**, *25*, 4271–4283. [CrossRef]
70. Perdoni, F.; Malatesta, M.; Cardani, R.; Giagnacovo, M.; Mancinelli, E.; Meola, G.; Pellicciari, C. RNA/MBNL1-containing foci in myoblast nuclei from patients affected by myotonic dystrophy type 2: An immunocytochemical study. *Eur. J. Histochem.* **2009**, *53*, e18. [CrossRef]
71. Mulders, S.A.M.; van den Broek, W.J.A.A.; Wheeler, T.M.; Croes, H.J.E.; van Kuik-Romeijn, P.; de Kimpe, S.J.; Furling, D.; Platenburg, G.J.; Gourdon, G.; Thornton, C.A.; et al. Triplet-repeat oligonucleotide-mediated reversal of RNA toxicity in myotonic dystrophy. *Proc. Natl. Acad. Sci. USA* **2009**, *106*, 13915–13920. [CrossRef]
72. Sardone, V.; Zhou, H.; Muntoni, F.; Ferlini, A.; Falzarano, M.S. Antisense oligonucleotide-based therapy for neuromuscular disease. *Molecules* **2017**, *22*, 563. [CrossRef] [PubMed]
73. Kanadia, R.N.; Shin, J.; Yuan, Y.; Beattie, S.G.; Wheeler, T.M.; Thornton, C.A.; Swanson, M.S. Reversal of RNA missplicing and myotonia after muscleblind overexpression in a mouse poly(CUG) model for myotonic dystrophy. *Proc. Natl. Acad. Sci. USA* **2006**, *103*, 11748–11753. [CrossRef]
74. Arambula, J.F.; Ramisetty, S.R.; Baranger, A.M.; Zimmerman, S.C. A simple ligand that selectively targets CUG trinucleotide repeats and inhibits MBNL protein binding. *Proc. Natl. Acad. Sci. USA* **2009**, *106*, 16068–16073. [CrossRef]
75. Childs-Disney, J.L.; Hoskins, J.; Rzuczek, S.G.; Thornton, C.A.; Disney, M.D. Rationally designed small molecules targeting the RNA that causes myotonic dystrophy type 1 are potently bioactive. *ACS Chem. Biol.* **2012**, *7*, 856–862. [CrossRef]
76. Udd, B.; Krahe, R. The myotonic dystrophies: Molecular, clinical, and therapeutic challenges. *Lancet Neurol.* **2012**, *11*, 891–905. [CrossRef]
77. Mendell, J.R.; Rodino-Klapac, L.R.; Sahenk, Z.; Roush, K.; Bird, L.; Lowes, L.P.; Alfano, L.; Gomez, A.M.; Lewis, S.; Kota, J.; et al. Eteplirsen for the treatment of Duchenne muscular dystrophy. *Ann. Neurol.* **2013**, *74*, 637–647. [CrossRef]
78. Goemans, N.; Mercuri, E.; Belousova, E.; Komaki, H.; Dubrovsky, A.; Mcdonald, C.M.; Kraus, J.E.; Lourbakos, A.; Lin, Z.; Campion, G.; et al. A randomized placebo-controlled phase 3 trial of an antisense oligonucleotide, drisapersen, in Duchenne muscular dystrophy. *Neuromuscul. Disord.* **2018**, *28*, 4–15. [CrossRef]
79. Goemans, N.M.; Tulinius, M.; van den Akker, J.T.; Burm, B.E.; Ekhart, P.F.; Heuvelmans, N.; Holling, T.; Janson, A.A.; Platenburg, G.J.; Sipkens, J.A.; et al. Systemic administration of PRO051 in Duchenne's muscular dystrophy. *N. Engl. J. Med.* **2011**, *365*, 1513–1522. [CrossRef]
80. Pandey, S.K.; Wheeler, T.M.; Justice, S.L.; Kim, A.; Younis, H.S.; Gattis, D.; Jauvin, D.; Puymirat, J.; Swayze, E.E.; Freier, S.M.; et al. Identification and characterization of modified antisense oligonucleotides targeting DMPK in mice and nonhuman primates for the treatment of myotonic dystrophy type 1s. *J. Pharmacol. Exp. Ther.* **2015**, *355*, 329–340. [CrossRef] [PubMed]
81. Klein, A.F.; Varela, M.A.; Arandel, L.; Holland, A.; Naouar, N.; Arzumanov, A.; Seoane, D.; Revillod, L.; Bassez, G.; Ferry, A.; et al. Peptide-conjugated oligonucleotides evoke long-lasting myotonic dystrophy correction in patient-derived cells and mice. *J. Clin. Investig.* **2019**, *129*, 4739–4744. [CrossRef]
82. Min, Y.L.; Li, H.; Rodriguez-Caycedo, C.; Mireault, A.A.; Huang, J.; Shelton, J.M.; McAnally, J.R.; Amoasii, L.; Mammen, P.P.A.; Bassel-Duby, R.; et al. CRISPR-Cas9 corrects Duchenne muscular dystrophy exon 44 deletion mutations in mice and human cells. *Sci. Adv.* **2019**, *5*, eaav4324. [CrossRef]
83. Amoasii, L.; Hildyard, J.C.W.; Li, H.; Sanchez-Ortiz, E.; Mireault, A.; Caballero, D.; Harron, R.; Stathopoulou, T.-R.; Massey, C.; Shelton, J.M.; et al. Gene editing restores dystrophin expression in a canine model of Duchenne muscular dystrophy. *Science* **2018**, *362*, 86–91. [CrossRef] [PubMed]
84. Hotta, A. Genome editing gene therapy for Duchenne muscular dystrophy. *J. Neuromuscul. Dis.* **2015**, *2*, 343–355. [CrossRef]

85. Amoasii, L.; Long, C.; Li, H.; Mireault, A.A.; Shelton, J.M.; Sanchez-Ortiz, E.; Mcanally, J.R.; Bhattacharyya, S.; Schmidt, F.; Grimm, D.; et al. Single-cut genome editing restores dystrophin expression in a new mouse model of muscular dystrophy. *Sci. Transl. Med.* **2017**, *29*, eaan8081. [CrossRef]
86. Dastidar, S.; Ardui, S.; Singh, K.; Majumdar, D.; Nair, N.; Fu, Y.; Reyon, D.; Samara, E.; Gerli, M.F.M.; Klein, A.F.; et al. Efficient CRISPR/Cas9-mediated editing of trinucleotide repeat expansion in myotonic dystrophy patient-derived iPS and myogenic cells. *Nucleic Acids Res.* **2018**, *46*, 8275–8298. [CrossRef]
87. Wagner, K.R.; Hamed, S.; Hadley, D.W.; Gropman, A.L.; Burstein, A.H.; Escolar, D.M.; Hoffman, E.P.; Fischbeck, K.H. Gentamicin treatment of Duchenne and Becker muscular dystrophy due to nonsense mutations. *Ann. Neurol.* **2001**, *49*, 706–711. [CrossRef]
88. Barton-Davis, E.R.; Cordier, L.; Shoturma, D.I.; Leland, S.E.; Sweeney, H.L. Aminoglycoside antibiotics restore dystrophin function to skeletal muscles of *mdx* mice. *J. Clin. Investig.* **1999**, *104*, 375–381. [CrossRef] [PubMed]
89. Vitiello, L.; Tibaudo, L.; Pegoraro, E.; Bello, L.; Canton, M. Teaching an old molecule new tricks: Drug repositioning for Duchenne muscular dystrophy. *Int. J. Mol. Sci.* **2019**, *20*, 6053. [CrossRef] [PubMed]
90. Welch, E.M.; Barton, E.R.; Zhuo, J.; Tomizawa, Y.; Friesen, W.J.; Trifillis, P.; Paushkin, S.; Patel, M.; Trotta, C.R.; Hwang, S.; et al. PTC124 targets genetic disorders caused by nonsense mutations. *Nature* **2007**, *447*, 87–91. [CrossRef] [PubMed]
91. McDonald, C.M.; Campbell, C.; Torricelli, R.E.; Finkel, R.S.; Flanigan, K.M.; Goemans, N.; Heydemann, P.; Kaminska, A.; Kirschner, J.; Muntoni, F.; et al. Ataluren in patients with nonsense mutation Duchenne muscular dystrophy (ACT DMD): A multicentre, randomised, double-blind, placebo-controlled, phase 3 trial. *Lancet* **2017**, *390*, 1489–1498. [CrossRef]
92. Siboni, R.B.; Bodner, M.J.; Khalifa, M.M.; Docter, A.G.; Choi, J.Y.; Nakamori, M.; Haley, M.M.; Berglund, J.A. Biological efficacy and toxicity of diamidines in myotonic dystrophy type 1 models. *J. Med. Chem.* **2015**, *58*, 5770–5780. [CrossRef]
93. Jenquin, J.R.; Coonrod, L.A.; Silverglate, Q.A.; Pellitier, N.A.; Hale, M.A.; Xia, G.; Nakamori, M.; Berglund, J.A. Furamidine rescues myotonic dystrophy type I associated mis-splicing through multiple mechanisms. *ACS Chem. Biol.* **2018**, *13*, 2708–2718. [CrossRef]
94. Reddy, K.; Jenquin, J.R.; Cleary, J.D.; Berglund, J.A. Mitigating RNA toxicity in myotonic dystrophy using small molecules. *Int. J. Mol. Sci.* **2019**, *20*, 4017. [CrossRef] [PubMed]
95. Jenquin, J.R.; Yang, H.; Huigens III, R.W.; Nakamori, M.; Berglund, J.A. Combination treatment of erythromycin and furamidine provides additive and synergistic rescue of mis-splicing in myotonic dystrophy type 1 models. *ACS Pharmacol. Transl. Sci.* **2019**, *2*, 247–263. [CrossRef] [PubMed]
96. Zhang, F.; Bodycombe, N.E.; Haskell, K.M.; Sun, Y.L.; Wang, E.T.; Morris, C.A.; Jones, L.H.; Wood, L.D.; Pletcher, M.T. A flow cytometry-based screen identifies MBNL1 modulators that rescue splicing defects in myotonic dystrophy type I. *Hum. Mol. Genet.* **2017**, *26*, 3056–3068. [CrossRef]
97. Naldini, L. Gene therapy returns to centre stage. *Nature* **2015**, *526*, 351–360. [CrossRef]
98. Fischer, A.; Hacein-Bey-Abina, S.; Cavazzana-Calvo, M. 20 years of gene therapy for SCID. *Nat. Immunol.* **2010**, *11*, 457–460. [CrossRef] [PubMed]
99. Dunbar, C.E.; High, K.A.; Joung, J.K.; Kohn, D.B.; Ozawa, K.; Sadelain, M. Gene therapy comes of age. *Science* **2018**, *359*, eaan4672. [CrossRef] [PubMed]
100. Smith, R.A.; Miller, T.M.; Yamanaka, K.; Monia, B.P.; Condon, T.P.; Hung, G.; Lobsiger, C.S.; Ward, C.M.; McAlonis-Downes, M.; Wei, H.; et al. Antisense oligonucleotide therapy for neurodegenerative disease. *J. Clin. Investig.* **2006**, *116*, 2290–2296. [CrossRef]
101. Liang, X.H.; Sun, H.; Nichols, J.G.; Crooke, S.T. RNase H1-dependent antisense oligonucleotides are robustly active in directing RNA cleavage in both the cytoplasm and the nucleus. *Mol. Ther.* **2017**, *25*, 2075–2092. [CrossRef]
102. Geary, R.S.; Norris, D.; Yu, R.; Bennett, C.F. Pharmacokinetics, biodistribution and cell uptake of antisense oligonucleotides. *Adv. Drug Deliv. Rev.* **2015**, *87*, 46–51. [CrossRef]
103. Liang, X.-H.; Shen, W.; Sun, H.; Kinberger, G.A.; Prakash, T.P.; Nichols, J.G.; Crooke, S.T. Hsp90 protein interacts with phosphorothioate oligonucleotides containing hydrophobic 2′-modifications and enhances antisense activity. *Nucleic Acids Res.* **2016**, *44*, 3892–3907. [CrossRef]
104. He, X.-Y.; Wang, J.; Lu, D.-D.; Wang, S.-Q. Synthesis and antisense properties of 2′β-F-arabinouridine modified oligonucleotides with 4′-C-OMe substituent. *Molecules* **2018**, *23*, 2374. [CrossRef]
105. Hagedorn, P.H.; Pontoppidan, M.; Bisgaard, T.S.; Berrera, M.; Dieckmann, A.; Ebeling, M.; Møller, M.R.; Hudlebusch, H.; Jensen, M.L.; Hansen, H.F.; et al. Identifying and avoiding off-target effects of RNase H-dependent antisense oligonucleotides in mice. *Nucleic Acids Res.* **2018**, *46*, 5366–5380. [CrossRef]
106. Bosgra, S.; Sipkens, J.; De Kimpe, S.; Den Besten, C.; Datson, N.; Van Deutekom, J. The pharmacokinetics of 2′-O-methyl phosphorothioate antisense oligonucleotides: Experiences from developing exon skipping therapies for Duchenne muscular dystrophy. *Nucleic Acid Ther.* **2019**, *29*, 305–322. [CrossRef] [PubMed]
107. Hara, Y.; Mizobe, Y.; Miyatake, S.; Takizawa, H.; Nagata, T.; Yokota, T.; Takeda, S.I.; Aoki, Y. Exon skipping using antisense oligonucleotides for laminin-alpha2-deficient muscular dystrophy. *Methods Mol. Biol.* **2018**, *1828*, 553–564. [CrossRef] [PubMed]
108. Sicinski, P.; Geng, Y.; Ryder-Cook, A.S.; Barnard, E.A.; Darlison, M.G.; Barnard, P.J. The molecular basis of muscular dystrophy in the *mdx* mouse: A point mutation. *Science* **1989**, *244*, 1578–1580. [CrossRef]
109. Kinali, M.; Arechavala-Gomeza, V.; Feng, L.; Cirak, S.; Hunt, D.; Adkin, C.; Guglieri, M.; Ashton, E.; Abbs, S.; Nihoyannopoulos, P.; et al. Local restoration of dystrophin expression with the morpholino oligomer AVI-4658 in Duchenne muscular dystrophy: A single-blind, placebo-controlled, dose-escalation, proof-of-concept study. *Lancet Neurol.* **2009**, *8*, 918–928. [CrossRef]

110. Watanabe, N.; Nagata, T.; Satou, Y.; Masuda, S.; Saito, T.; Kitagawa, H.; Komaki, H.; Takagaki, K.; Takeda, S. NS-065/NCNP-01: An antisense oligonucleotide for potential treatment of exon 53 skipping in Duchenne muscular dystrophy. *Mol. Ther. Nucleic Acids* **2018**, *13*, 442–449. [CrossRef]
111. Gao, Z.; Cooper, T.A. Antisense oligonucleotides: Rising stars in eliminating RNA toxicity in myotonic dystrophy. *Hum. Gene Ther.* **2013**, *24*, 499–507. [CrossRef] [PubMed]
112. Huguet, A.; Medja, F.; Nicole, A.; Vignaud, A.; Guiraud-Dogan, C.; Ferry, A.; Decostre, V.; Hogrel, J.Y.; Metzger, F.; Hoeflich, A.; et al. Molecular, physiological, and motor performance defects in DMSXL mice carrying >1,000 CTG repeats from the human DM1 locus. *PLoS Genet.* **2012**, *8*, e1003043. [CrossRef] [PubMed]
113. Wheeler, T.M.; Leger, A.J.; Pandey, S.K.; MacLeod, A.R.; Nakamori, M.; Cheng, S.H.; Wentworth, B.M.; Bennett, C.F.; Thornton, C.A. Targeting nuclear RNA for in vivo correction of myotonic dystrophy. *Nature* **2012**, *488*, 111–115. [CrossRef]
114. Jauvin, D.; Chrétien, J.; Pandey, S.K.; Martineau, L.; Revillod, L.; Bassez, G.; Lachon, A.; McLeod, A.R.; Gourdon, G.; Wheeler, T.M.; et al. Targeting DMPK with antisense oligonucleotide improves muscle strength in myotonic dystrophy type 1 mice. *Mol. Ther. Nucleic Acids* **2017**, *7*, 465–474. [CrossRef]
115. Ousterout, D.G.; Kabadi, A.M.; Thakore, P.I.; Majoros, W.H.; Reddy, T.E.; Gersbach, C.A. Multiplex CRISPR/Cas9-based genome editing for correction of dystrophin mutations that cause Duchenne muscular dystrophy. *Nat. Commun.* **2015**, *6*, 6244. [CrossRef]
116. Ousterout, D.G.; Kabadi, A.M.; Thakore, P.I.; Perez-Pinera, P.; Brown, M.T.; Majoros, W.H.; Reddy, T.E.; Gersbach, C.A. Correction of dystrophin expression in cells from Duchenne Muscular Dystrophy patients through genomic excision of exon 51 by Zinc Finger Nucleases. *Mol. Ther.* **2015**, *23*, 523–532. [CrossRef] [PubMed]
117. Ousterout, D.G.; Perez-Pinera, P.; Thakore, P.I.; Kabadi, A.M.; Brown, M.T.; Qin, X.; Fedrigo, O.; Mouly, V.; Tremblay, J.P.; Gersbach, C.A. Reading frame correction by targeted genome editing restores dystrophin expression in cells from Duchenne Muscular Dystrophy patients. *Mol. Ther.* **2013**, *21*, 1718–1726. [CrossRef]
118. Doudna, J.A.; Charpentier, E. Genome editing. The new frontier of genome engineering with CRISPR-Cas9. *Science* **2014**, *346*, 1258096. [CrossRef]
119. Nance, M.E.; Hakim, C.H.; Yang, N.N.; Duan, D. Nanotherapy for Duchenne muscular dystrophy. *Wiley Interdiscip. Rev. Nanomed. Nanobiotechnol.* **2018**, *10*, e1472. [CrossRef] [PubMed]
120. Amitai, G.; Sorek, R. CRISPR-Cas adaptation: Insights into the mechanism of action. *Nat. Rev. Microbiol.* **2016**, *14*, 67–76. [CrossRef]
121. Kleinstiver, B.P.; Prew, M.S.; Tsai, S.Q.; Topkar, V.V.; Nguyen, N.T.; Zheng, Z.; Gonzales, A.P.W.; Li, Z.; Peterson, R.T.; Yeh, J.-R.J.; et al. Engineered CRISPR-Cas9 nucleases with altered PAM specificities. *Nature* **2015**, *523*, 481–485. [CrossRef] [PubMed]
122. Wang, Y.; Hao, L.; Wang, H.; Santostefano, K.; Thapa, A.; Cleary, J.; Li, H.; Guo, X.; Terada, N.; Ashizawa, T.; et al. Therapeutic genome editing for myotonic dystrophy type 1 using CRISPR/Cas9. *Mol. Ther.* **2018**, *26*, 2617–2630. [CrossRef]
123. Naso, M.F.; Tomkowicz, B.; Perry, W.L.; Strohl, W.R. Adeno-associated virus (AAV) as a vector for gene therapy. *BioDrugs* **2017**, *31*, 317–334. [CrossRef] [PubMed]
124. Komor, A.C.; Kim, Y.B.; Packer, M.S.; Zuris, J.A.; Liu, D.R. Programmable editing of a target base in genomic DNA without double-stranded DNA cleavage. *Nature* **2016**, *533*, 420–424. [CrossRef] [PubMed]
125. Gaudelli, N.M.; Komor, A.C.; Rees, H.A.; Packer, M.S.; Badran, A.H.; Bryson, D.I.; Liu, D.R. Programmable base editing of A•T to G•C in genomic DNA without DNA cleavage. *Nature* **2017**, *551*, 464–471. [CrossRef]
126. Abudayyeh, O.O.; Gootenberg, J.S.; Franklin, B.; Koob, J.; Kellner, M.J.; Ladha, A.; Joung, J.; Kirchgatterer, P.; Cox, D.B.T.; Zhang, F. A Cytosine deaminase for programmable single-base RNA editing. *Science* **2019**, *365*, 382–386. [CrossRef] [PubMed]
127. Ryu, S.-M.; Koo, T.; Kim, K.; Lim, K.; Baek, G.; Kim, S.-T.; Kim, H.S.; Kim, D.-E.; Lee, H.; Chung, E.; et al. Adenine base editing in mouse embryos and an adult mouse model of Duchenne Muscular Dystrophy. *Nat Biotechnol* **2018**, *36*, 536–539. [CrossRef]
128. Jiang, T.; Henderson, J.M.; Coote, K.; Cheng, Y.; Valley, H.C.; Zhang, X.-O.; Wang, Q.; Rhym, L.H.; Cao, Y.; Newby, G.A.; et al. Chemical modifications of adenine base editor mRNA and guide RNA expand its application scope. *Nat Commun* **2020**, *11*, 1979. [CrossRef]
129. Anzalone, A.V.; Randolph, P.B.; Davis, J.R.; Sousa, A.A.; Koblan, L.W.; Levy, J.M.; Chen, P.J.; Wilson, C.; Newby, G.A.; Raguram, A.; et al. Search-and-replace genome editing without double-strand breaks or donor DNA. *Nature* **2019**, *576*, 149–157. [CrossRef]
130. Pushpakom, S.; Iorio, F.; Eyers, P.A.; Escott, K.J.; Hopper, S.; Wells, A.; Doig, A.; Guilliams, T.; Latimer, J.; McNamee, C.; et al. Drug repurposing: Progress, challenges and recommendations. *Nat. Rev. Drug Discov.* **2019**, *18*, 41–58. [CrossRef]
131. Knapp, S. New opportunities for kinase drug repurposing and target discovery. *Br. J. Cancer* **2018**, *118*, 936–937. [CrossRef]
132. Wittenstein, A.; Caspi, M.; David, Y.; Shorer, Y.; Nadar-Ponniah, P.T.; Rosin-Arbesfeld, R. Serum starvation enhances nonsense mutation readthrough. *J. Mol. Med.* **2019**, *97*, 1695–1710. [CrossRef] [PubMed]
133. Chowdhury, H.M.; Siddiqui, M.A.; Kanneganti, S.; Sharmin, N.; Chowdhury, M.W.; Nasim, M.T. Aminoglycoside-mediated promotion of translation readthrough occurs through a non-stochastic mechanism that competes with translation termination. *Hum. Mol. Genet.* **2018**, *27*, 373–384. [CrossRef]
134. Shimizu-Motohashi, Y.; Komaki, H.; Motohashi, N.; Takeda, S.; Yokota, T.; Aoki, Y. Restoring dystrophin expression in Duchenne muscular dystrophy: Current status of therapeutic approaches. *J. Pers. Med.* **2019**, *9*, 1. [CrossRef]
135. Hayward, R.S.; Harding, J.; Molloy, R.; Land, L.; Longcroft-Neal, K.; Moore, D.; Ross, J.D.C. Adverse effects of a single dose of gentamicin in adults: A systematic review. *Br. J. Clin. Pharmacol.* **2018**, *84*, 223–238. [CrossRef] [PubMed]

136. Friesen, W.J.; Johnson, B.; Sierra, J.; Zhuo, J.; Vazirani, P.; Xue, X.; Tomizawa, Y.; Baiazitov, R.; Morrill, C.; Ren, H.; et al. The minor gentamicin complex component, X2, is a potent premature stop codon readthrough molecule with therapeutic potential. *PLoS ONE* **2018**, *13*, e0206158. [CrossRef]
137. Gonzalez, À.L.; Konieczny, P.; Llamusi, B.; Delgado-Pinar, E.; Borrell, J.I.; Teixidó, J.; García-España, E.; Pérez-Alonso, M.; Estrada-Tejedor, R.; Artero, R. In silico discovery of substituted pyrido[2,3-d] pyrimidines and pentamidine-like compounds with biological activity in myotonic dystrophy models. *PLoS ONE* **2017**, *12*, e0178931. [CrossRef]
138. Díaz, M.V.; Miranda, M.R.; Campos-Estrada, C.; Reigada, C.; Maya, J.D.; Pereira, C.A.; López-Muñoz, R. Pentamidine exerts in vitro and in vivo anti Trypanosoma cruzi activity and inhibits the polyamine transport in Trypanosoma cruzi. *Acta Trop.* **2014**, *134*, 1–9. [CrossRef] [PubMed]
139. Coonrod, L.A.; Nakamori, M.; Wang, W.; Carrell, S.; Cameron, L.; Bodner, M.J.; Siboni, R.B.; Docter, A.G.; Haley, M.M.; Charles, A.; et al. Reducing levels of toxic RNA with small molecules. *ACS Chem. Biol.* **2013**, *8*, 2528–2537. [CrossRef] [PubMed]
140. Theocharis, A.D.; Skandalis, S.S.; Gialeli, C.; Karamanos, N.K. Extracellular matrix structure. *Adv. Drug Deliv. Rev.* **2016**, *97*, 4–27. [CrossRef]
141. Zhang, G.; Budker, V.; Williams, P.; Subbotin, V.; Wolff, J.A. Efficient expression of naked DNA delivered intraarterially to limb muscles of nonhuman primates. *Hum. Gene Ther.* **2001**, *12*, 427–438. [CrossRef]
142. Hagstrom, J.E.; Hegge, J.; Zhang, G.; Noble, M.; Budker, V.; Lewis, D.L.; Herweijer, H.; Wolff, J.A. A facile nonviral method for delivering genes and siRNAs to skeletal muscle of mammalian limbs. *Mol. Ther.* **2004**, *10*, 386–398. [CrossRef] [PubMed]
143. Gref, R.; Minamitake, Y.; Peracchia, M.T.; Trubetskoy, V.; Torchilin, V.; Langer, R. Biodegradable long-circulating polymeric nanospheres. *Science* **1994**, *263*, 1600–1603. [CrossRef] [PubMed]
144. Longmire, M.; Choyke, P.L.; Kobayashi, H. Clearance properties of nano-sized particles and molecules as imaging agents: Considerations and caveats. *Nanomedicine* **2008**, *3*, 703–717. [CrossRef] [PubMed]
145. Gustafson, H.H.; Holt-Casper, D.; Grainger, D.W.; Ghandehari, H. Nanoparticle uptake: The phagocyte problem. *Nano Today* **2015**, *10*, 487–510. [CrossRef] [PubMed]
146. Blanco, E.; Shen, H.; Ferrari, M. Principles of nanoparticle design for overcoming biological barriers to drug delivery. *Nat. Biotechnol.* **2015**, *33*, 941–951. [CrossRef] [PubMed]
147. Nguyen, V.H.; Lee, B.-J. Protein corona: A new approach for nanomedicine design. *Int. J. Nanomed.* **2017**, *12*, 3137–3151. [CrossRef]
148. Tenzer, S.; Docter, D.; Kuharev, J.; Musyanovych, A.; Fetz, V.; Hecht, R.; Schlenk, F.; Fischer, D.; Kiouptsi, K.; Reinhardt, C.; et al. Rapid formation of plasma protein corona critically affects nanoparticle pathophysiology. *Nat. Nanotechnol.* **2013**, *8*, 772–781. [CrossRef]
149. Stano, A.; Nembrini, C.; Swartz, M.A.; Hubbell, J.A.; Simeoni, E. Nanoparticle size influences the magnitude and quality of mucosal immune responses after intranasal immunization. *Vaccine* **2012**, *30*, 7541–7546. [CrossRef] [PubMed]
150. Hoshyar, N.; Gray, S.; Han, H.; Bao, G. The effect of nanoparticle size on in vivo pharmacokinetics and cellular interaction. *Nanomedicine* **2016**, *11*, 673–692. [CrossRef] [PubMed]
151. Vlasova, I.I.; Kapralov, A.A.; Michael, Z.P.; Burkert, S.C.; Shurin, M.R.; Star, A.; Shvedova, A.A.; Kagan, V.E. Enzymatic oxidative biodegradation of nanoparticles: Mechanisms, significance and applications. *Toxicol. Appl. Pharmacol.* **2016**, *299*, 58–69. [CrossRef] [PubMed]
152. Tidball, J.G.; Welc, S.S.; Wehling-Henricks, M. Immunobiology of inherited muscular dystrophies. *Compr. Physiol.* **2018**, *8*, 1313–1356. [CrossRef]
153. Smoak, M.M.; Mikos, A.G. Advances in biomaterials for skeletal muscle engineering and obstacles still to overcome. *Mater. Today Bio* **2020**, *7*, 100069. [CrossRef] [PubMed]
154. Evers, M.M.; Toonen, L.J.A.; van Roon-Mom, W.M.C. Antisense oligonucleotides in therapy for neurodegenerative disorders. *Adv. Drug Deliv. Rev.* **2015**, *87*, 90–103. [CrossRef]
155. Kauffman, K.J.; Webber, M.J.; Anderson, D.G. Materials for non-viral intracellular delivery of messenger RNA therapeutics. *J. Control. Release* **2016**, *240*, 227–234. [CrossRef]
156. Parlea, L.; Puri, A.; Kasprzak, W.; Bindewald, E.; Zakrevsky, P.; Satterwhite, E.; Joseph, K.; Afonin, K.A.; Shapiro, B.A. Cellular delivery of RNA nanoparticles. *ACS Comb. Sci.* **2016**, *18*, 527–547. [CrossRef] [PubMed]
157. Wahane, A.; Waghmode, A.; Kapphahn, A.; Dhuri, K.; Gupta, A.; Bahal, R. Role of lipid-based and polymer-based non-viral vectors in nucleic acid delivery for next-generation gene therapy. *Molecules* **2020**, *25*, 2866. [CrossRef] [PubMed]
158. Mastria, E.M.; Cai, L.Y.; Kan, M.J.; Li, X.; Schaal, J.L.; Fiering, S.; Gunn, M.D.; Dewhirst, M.W.; Nair, S.K.; Chilkoti, A. Nanoparticle formulation improves doxorubicin efficacy by enhancing host antitumor immunity. *J. Control. Release* **2018**, *269*, 364–373. [CrossRef] [PubMed]
159. Yu, A.-M.; Choi, Y.H.; Tu, M.-J. RNA drugs and RNA targets for small molecules: Principles, progress, and challenges. *Pharmacol. Rev.* **2020**, *72*, 862–898. [CrossRef]
160. Givens, B.E.; Naguib, Y.W.; Geary, S.M.; Devor, E.J.; Salem, A.K. Nanoparticle based delivery of CRISPR/Cas9 genome editing therapeutics. *AAPS J.* **2018**, *20*, 108. [CrossRef]
161. Liu, C.; Zhang, L.; Liu, H.; Cheng, K. Delivery strategies of the CRISPR-Cas9 gene-editing system for therapeutic applications. *J. Control. Release* **2017**, *266*, 17–26. [CrossRef]
162. Min, Y.-L.; Bassel-Duby, R.; Olson, E.N. CRISPR correction of Duchenne muscular dystrophy. *Annu. Rev. Med.* **2019**, *27*, 239–255. [CrossRef] [PubMed]

163. Williams, J.H.; Schray, R.C.; Sirsi, S.R.; Lutz, G.J. Nanopolymers improve delivery of exon skipping oligonucleotides and concomitant dystrophin expression in skeletal muscle of *mdx* mice. *BMC Biotechnol.* **2008**, *8*, 35. [CrossRef] [PubMed]
164. Sirsi, S.R.; Schray, R.C.; Wheatley, M.A.; Lutz, G.J. Formulation of polylactide-co-glycolic acid nanospheres for encapsulation and sustained release of poly(ethylene imine)-poly(ethylene glycol) copolymers complexed to oligonucleotides. *J. Nanobiotechnol.* **2009**, *7*, 1. [CrossRef] [PubMed]
165. Wang, M.; Wu, B.; Lu, P.; Cloer, C.; Tucker, J.D.; Lu, Q. Polyethylenimine-modified Pluronics (PCMs) improve morpholino oligomer delivery in cell culture and dystrophic *mdx* mice. *Mol. Ther.* **2013**, *21*, 210–216. [CrossRef]
166. Wang, M.; Wu, B.; Lu, P.; Tucker, J.D.; Milazi, S.; Shah, S.N.; Lu, Q.L. Pluronic–PEI copolymers enhance exon-skipping of 2′-O-methyl phosphorothioate oligonucleotide in cell culture and dystrophic *mdx* mice. *Gene Ther.* **2014**, *21*, 52–59. [CrossRef] [PubMed]
167. Kim, Y.; Tewari, M.; Pajerowski, J.D.; Cai, S.; Sen, S.; Williams, J.; Sirsi, S.; Lutz, G.; Discher, D.E. Polymersome delivery of siRNA and antisense oligonucleotides. *J. Control. Release* **2009**, *134*, 132–140. [CrossRef]
168. Rimessi, P.; Sabatelli, P.; Fabris, M.; Braghetta, P.; Bassi, E.; Spitali, P.; Vattemi, G.; Tomelleri, G.; Mari, L.; Perrone, D.; et al. Cationic PMMA nanoparticles bind and deliver antisense oligoribonucleotides allowing restoration of dystrophin expression in the *mdx* mouse. *Mol. Ther.* **2009**, *17*, 820–827. [CrossRef] [PubMed]
169. Ferlini, A.; Sabatelli, P.; Fabris, M.; Bassi, E.; Falzarano, S.; Vattemi, G.; Perrone, D.; Gualandi, F.; Maraldi, N.M.; Merlini, L.; et al. Dystrophin restoration in skeletal, heart and skin arrector pili smooth muscle of *mdx* mice by ZM2 NP–AON complexes. *Gene Ther.* **2010**, *17*, 432–438. [CrossRef]
170. Bassi, E.; Falzarano, S.; Fabris, M.; Gualandi, F.; Merlini, L.; Vattemi, G.; Perrone, D.; Marchesi, E.; Sabatelli, P.; Sparnacci, K.; et al. Persistent dystrophin protein restoration 90 days after a course of intraperitoneally administered naked 2′OMePS AON and ZM2 NP-AON complexes in *mdx* Mice. *J. Biomed. Biotechnol.* **2012**, *2012*, 1–8. [CrossRef]
171. Wang, M.; Wu, B.; Tucker, J.D.; Bollinger, L.E.; Lu, P.; Lu, Q. Poly(ester amine) composed of polyethylenimine and Pluronic enhance delivery of antisense oligonucleotides in vitro and in dystrophic *mdx* mice. *Mol. Ther. Nucleic Acids* **2016**, *5*, e341. [CrossRef]
172. Wang, M.; Tucker, J.D.; Lu, P.; Wu, B.; Cloer, C.; Lu, Q. Tris[2-(acryloyloxy)ethyl]isocyanurate cross-linked low-molecular-weight polyethylenimine as gene delivery carriers in cell culture and dystrophic *mdx* mice. *Bioconjug. Chem.* **2012**, *23*, 837–845. [CrossRef] [PubMed]
173. Itaka, K.; Osada, K.; Morii, K.; Kim, P.; Yun, S.-H.; Kataoka, K. Polyplex nanomicelle promotes hydrodynamic gene introduction to skeletal muscle. *J. Control. Release* **2010**, *143*, 112–119. [CrossRef]
174. Wang, J.; Zhang, P.-C.; Mao, H.-Q.; Leong, K.W. Enhanced gene expression in mouse muscle by sustained release of plasmid DNA using PPE-EA as a carrier. *Gene Ther.* **2002**, *9*, 1254–1261. [CrossRef]
175. Kinouchi, N.; Ohsawa, Y.; Ishimaru, N.; Ohuchi, H.; Sunada, Y.; Hayashi, Y.; Tanimoto, Y.; Moriyama, K.; Noji, S. Atelocollagen-mediated local and systemic applications of myostatin-targeting siRNA increase skeletal muscle mass. *Gene Ther.* **2008**, *15*, 1126–1130. [CrossRef]
176. Márquez-Miranda, V.; Abrigo, J.; Rivera, J.C.; Araya-Duran, I.; Aravena, J.; Simon, F.; Pacheco, N.; Gonzalez-Nilo, F.D.; Cabello-Verrugio, C. The complex of PAMAM-OH dendrimer with angiotensin (1-7) prevented the disuse-induced skeletal muscle atrophy in mice. *Int. J. Nanomed.* **2017**, *12*, 1985–1999. [CrossRef]
177. Negishi, Y.; Ishii, Y.; Shiono, H.; Akiyama, S.; Sekine, S.; Kojima, T.; Mayama, S.; Kikuchi, T.; Hamano, N.; Endo-Takahashi, Y.; et al. Bubble liposomes and ultrasound exposure improve localized morpholino oligomer delivery into the skeletal muscles of dystrophic *mdx* mice. *Mol. Pharm.* **2014**, *11*, 1053–1061. [CrossRef] [PubMed]
178. Koebis, M.; Kiyatake, T.; Yamaura, H.; Nagano, K.; Higashihara, M.; Sonoo, M.; Hayashi, Y.; Negishi, Y.; Endo-Takahashi, Y.; Yanagihara, D.; et al. Ultrasound-enhanced delivery of morpholino with bubble liposomes ameliorates the myotonia of myotonic dystrophy model mice. *Sci. Rep.* **2013**, *3*, 2242. [CrossRef] [PubMed]
179. Afzal, E.; Zakeri, S.; Keyhanvar, P.; Bagheri, M.; Mahjoubi, P.; Asadian, M.; Omoomi, N.; Dehqanian, M.; Ghalandarlaki, N.; Darvishmohammadi, T.; et al. Nanolipodendrosome-loaded glatiramer acetate and myogenic differentiation 1 as augmentation therapeutic strategy approaches in muscular dystrophy. *Int. J. Nanomed.* **2013**, *8*, 2943–2960. [CrossRef]
180. Turjeman, K.; Yanay, N.; Elbaz, M.; Bavli, Y.; Gross, M.; Rabie, M.; Barenholz, Y.; Nevo, Y. Liposomal steroid nano-drug is superior to steroids as-is in *mdx* mouse model of Duchenne muscular mystrophy. *Nanomedicine* **2019**, *16*, 34–44. [CrossRef] [PubMed]
181. Yukihara, M.; Ito, K.; Tanoue, O.; Goto, K.; Matsushita, T.; Matsumoto, Y.; Masuda, M.; Kimura, S.; Ueoka, R. Effective drug delivery system for Duchenne muscular dystrophy using hybrid liposomes including gentamicin along with reduced toxicity. *Biol. Pharm. Bull.* **2011**, *34*, 712–716. [CrossRef] [PubMed]
182. Bibee, K.P.; Cheng, Y.; Ching, J.K.; Marsh, J.N.; Li, A.J.; Keeling, R.M.; Connolly, A.M.; Golumbek, P.T.; Myerson, J.W.; Hu, G.; et al. Rapamycin nanoparticles target defective autophagy in muscular dystrophy to enhance both strength and cardiac function. *FASEB J.* **2014**, *28*, 2047–2061. [CrossRef] [PubMed]
183. Wei, T.; Cheng, Q.; Min, Y.-L.; Olson, E.N.; Siegwart, D.J. Systemic nanoparticle delivery of CRISPR-Cas9 ribonucleoproteins for effective tissue specific genome editing. *Nat. Commun.* **2020**, *11*, 3232. [CrossRef]
184. Lee, K.; Conboy, M.; Park, H.M.; Jiang, F.; Kim, H.J.; Dewitt, M.A.; Mackley, V.A.; Chang, K.; Rao, A.; Skinner, C.; et al. Nanoparticle delivery of Cas9 ribonucleoprotein and donor DNA in vivo induces homology-directed DNA repair. *Nat. Biomed. Eng.* **2017**, *1*, 889–901. [CrossRef]

185. Järver, P.; O'Donovan, L.; Gait, M.J. A chemical view of oligonucleotides for exon skipping and related drug applications. *Nucleic Acid Ther.* **2014**, *24*, 37–47. [CrossRef] [PubMed]
186. Zhang, P.; Wagner, E. History of polymeric gene delivery systems. *Top. Curr. Chem.* **2017**, *375*, 26. [CrossRef] [PubMed]
187. Boussif, O.; Lezoualc'h, F.; Zanta, M.A.; Mergny, M.D.; Scherman, D.; Demeneix, B.; Behr, J.P. A versatile vector for gene and oligonucleotide transfer into cells in culture and *in vivo*: Polyethylenimine. *Proc. Natl. Acad. Sci. USA* **1995**, *92*, 7297–7301. [CrossRef]
188. Lu, Q.L.; Mann, C.J.; Lou, F.; Bou-Gharios, G.; Morris, G.E.; Xue, S.; Fletcher, S.; Partridge, T.A.; Wilton, S.D. Functional amounts of dystrophin produced by skipping the mutated exon in the *mdx* dystrophic mouse. *Nat. Med.* **2003**, *9*, 1009–1014. [CrossRef] [PubMed]
189. Lu, Q.L.; Bou-Gharios, G.; Partridge, T.A. Non-viral gene delivery in skeletal muscle: A protein factory. *Gene Ther.* **2003**, *10*, 131–142. [CrossRef] [PubMed]
190. Williams, J.H.; Sirsi, S.R.; Latta, D.R.; Lutz, G.J. Induction of dystrophin expression by exon skipping in *mdx* mice following intramuscular injection of antisense oligonucleotides complexed with PEG–PEI copolymers. *Mol. Ther.* **2006**, *14*, 88–96. [CrossRef]
191. Lutz, G.J.; Sirsi, S.R.; Williams, J.H. PEG-PEI copolymers for oligonucleotide delivery to Cells and tissues. *Methods Mol. Biol.* **2008**, *433*, 141–158. [CrossRef] [PubMed]
192. Castaldello, A.; Brocca-Cofano, E.; Voltan, R.; Triulzi, C.; Altavilla, G.; Laus, M.; Sparnacci, K.; Ballestri, M.; Tondelli, L.; Fortini, C.; et al. DNA prime and protein boost immunization with innovative polymeric cationic core-shell nanoparticles elicits broad immune responses and strongly enhance cellular responses of HIV-1 tat DNA vaccination. *Vaccine* **2006**, *24*, 5655–5669. [CrossRef]
193. Summerton, J.; Weller, D. Morpholino antisense oligomers: Design, preparation, and properties. *Antisense Nucleic Acid Drug Dev.* **1997**, *7*, 187–195. [CrossRef] [PubMed]
194. Miller, C.M.; Harris, E.N. Antisense oligonucleotides: Treatment strategies and cellular internalization. *RNA Dis.* **2016**, *3*, e1393. [CrossRef]
195. Järver, P.; Zaghloul, E.M.; Arzumanov, A.A.; Saleh, A.F.; McClorey, G.; Hammond, S.M.; Hällbrink, M.; Langel, Ü.; Smith, C.I.E.; Wood, M.J.A.; et al. Peptide nanoparticle delivery of charge-neutral splice-switching morpholino oligonucleotides. *Nucleic Acid Ther.* **2015**, *25*, 65–77. [CrossRef] [PubMed]
196. Suzuki, R.; Takizawa, T.; Negishi, Y.; Hagisawa, K.; Tanaka, K.; Sawamura, K.; Utoguchi, N.; Nishioka, T.; Maruyama, K. Gene delivery by combination of novel liposomal bubbles with perfluoropropane and ultrasound. *J. Control. Release* **2007**, *117*, 130–136. [CrossRef]
197. Negishi, Y.; Endo, Y.; Fukuyama, T.; Suzuki, R.; Takizawa, T.; Omata, D.; Maruyama, K.; Aramaki, Y. Delivery of siRNA into the cytoplasm by liposomal bubbles and ultrasound. *J. Control. Release* **2008**, *132*, 124–130. [CrossRef] [PubMed]
198. Tros de Ilarduya, C.; Sun, Y.; Düzgüneş, N. Gene delivery by lipoplexes and polyplexes. *Eur. J. Pharm. Sci.* **2010**, *40*, 159–170. [CrossRef]
199. Kulkarni, J.A.; Cullis, P.R.; van der Meel, R. Lipid nanoparticles enabling gene therapies: From concepts to clinical utility. *Nucleic Acid Ther.* **2018**, *28*, 146–157. [CrossRef]
200. Li, D.; Sharili, A.S.; Connelly, J.; Gautrot, J.E. Highly stable RNA capture by dense cationic polymer brushes for the design of cytocompatible, serum-stable siRNA delivery vectors. *Biomacromolecules* **2018**, *19*, 606–615. [CrossRef]
201. Kulkarni, J.A.; Myhre, J.L.; Chen, S.; Tam, Y.Y.C.; Danescu, A.; Richman, J.M.; Cullis, P.R. Design of lipid nanoparticles for in vitro and in vivo delivery of plasmid DNA. *Nanomedicine* **2017**, *13*, 1377–1387. [CrossRef]
202. Sano, A.; Maeda, M.; Nagahara, S.; Ochiya, T.; Honma, K.; Itoh, H.; Miyata, T.; Fujioka, K. Atelocollagen for protein and gene delivery. *Adv. Drug Deliv. Rev.* **2003**, *55*, 1651–1677. [CrossRef] [PubMed]
203. Ochiya, T.; Nagahara, S.; Sano, A.; Itoh, H.; Terada, M. Biomaterials for gene delivery: Atelocollagen-mediated controlled release of molecular medicines. *Curr. Gene Ther.* **2001**, *1*, 31–52. [CrossRef]
204. Wang, J.; Mao, H.-Q.; Leong, K.W. A novel biodegradable gene carrier based on polyphosphoester. *J. Am. Chem. Soc.* **2001**, *123*, 9480–9481. [CrossRef]
205. Itaka, K.; Yamauchi, K.; Harada, A.; Nakamura, K.; Kawaguchi, H.; Kataoka, K. Polyion complex micelles from plasmid DNA and poly(ethylene glycol)-poly(L-lysine) block copolymer as serum-tolerable polyplex system: Physicochemical properties of micelles relevant to gene transfection efficiency. *Biomaterials* **2003**, *24*, 4495–4506. [CrossRef]
206. Parvathaneni, V.; Kulkarni, N.S.; Muth, A.; Gupta, V. Drug repurposing: A promising tool to accelerate the drug discovery process. *Drug Discov. Today* **2019**, *24*, 2076–2085. [CrossRef] [PubMed]
207. He, H.; Markoutsa, E.; Li, J.; Xu, P. Repurposing disulfiram for cancer therapy via targeted nanotechnology through enhanced tumor mass penetration and disassembly. *Acta Biomater.* **2018**, *68*, 113–124. [CrossRef] [PubMed]
208. Amini, M.A.; Abbasi, A.Z.; Cai, P.; Lip, H.; Gordijo, C.R.; Li, J.; Chen, B.; Zhang, L.; Rauth, A.M.; Wu, X.Y. Combining tumor microenvironment modulating nanoparticles with doxorubicin to enhance chemotherapeutic efficacy and boost antitumor immunity. *J. Natl. Cancer Inst.* **2019**, *111*, 399–408. [CrossRef] [PubMed]
209. Lim, S.; Park, J.; Shim, M.K.; Um, W.; Yoon, H.Y.; Ryu, J.H.; Lim, D.-K.; Kim, K. Recent advances and challenges of repurposing nanoparticle-based drug delivery systems to enhance cancer immunotherapy. *Theranostics* **2019**, *9*, 7906–7923. [CrossRef] [PubMed]

210. Gregoriou, Y.; Gregoriou, G.; Yilmaz, V.; Kapnisis, K.; Prokopi, M.; Anayiotos, A.; Strati, K.; Dietis, N.; Constantinou, A.I.; Andreou, C. Resveratrol loaded polymeric micelles for theranostic targeting of breast cancer cells. *Nanotheranostics* **2021**, *5*, 113–124. [CrossRef]
211. Dunant, P.; Walter, M.C.; Karpati, G.; Lochmüller, H. Gentamicin fails to increase dystrophin expression in dystrophin-deficient muscle. *Muscle Nerve* **2003**, *27*, 624–627. [CrossRef] [PubMed]
212. Zammit, P.S. Function of the myogenic regulatory factors Myf5, MyoD, Myogenin and MRF4 in skeletal muscle, satellite cells and regenerative myogenesis. *Semin. Cell Dev. Biol.* **2017**, *72*, 19–32. [CrossRef] [PubMed]
213. Sehgal, S.N. Sirolimus: Its discovery, biological properties, and mechanism of action. *Transplant. Proc.* **2003**, *35*, 7S–14S. [CrossRef]
214. Flaim, S.F. Pharmacokinetics and side effects of perfluorocarbon-based blood substitutes. *Artif. Cells. Blood Substit. Immobil. Biotechnol.* **1994**, *22*, 1043–1054. [CrossRef]
215. Spahn, D.R. Blood substitutes. Artificial oxygen carriers: Perfluorocarbon emulsions. *Crit. Care* **1999**, *3*, R93–R97. [CrossRef] [PubMed]
216. Watanabe, A.; Tanaka, H.; Sakurai, Y.; Tange, K.; Nakai, Y.; Ohkawara, T.; Takeda, H.; Harashima, H.; Akita, H. Effect of particle size on their accumulation in an inflammatory lesion in a dextran sulfate sodium (DSS)-induced colitis model. *Int. J. Pharm.* **2016**, *509*, 118–122. [CrossRef]
217. Chen, K.-H.; Lundy, D.J.; Toh, E.K.-W.; Chen, C.-H.; Shih, C.; Chen, P.; Chang, H.-C.; Lai, J.J.; Stayton, P.S.; Hoffman, A.S.; et al. Nanoparticle distribution during systemic inflammation is size-dependent and organ-specific. *Nanoscale* **2015**, *7*, 15863–15872. [CrossRef]
218. Jinek, M.; Chylinski, K.; Fonfara, I.; Hauer, M.; Doudna, J.A.; Charpentier, E. A programmable dual-RNA-guided DNA endonuclease in adaptive bacterial immunity. *Science* **2012**, *337*, 816–821. [CrossRef]
219. Luther, D.C.; Lee, Y.W.; Nagaraj, H.; Scaletti, F.; Rotello, V.M. Delivery approaches for CRISPR/Cas9 therapeutics *in vivo*: Advances and challenges. *Expert Opin. Drug Deliv.* **2018**, *15*, 905–913. [CrossRef] [PubMed]
220. Lino, C.A.; Harper, J.C.; Carney, J.P.; Timlin, J.A. Delivering CRISPR: A review of the challenges and approaches. *Drug Deliv.* **2018**, *25*, 1234–1257. [CrossRef]
221. Ding, Y.; Jiang, Z.; Saha, K.; Kim, C.S.; Kim, S.T.; Landis, R.F.; Rotello, V.M. Gold nanoparticles for nucleic acid delivery. *Mol. Ther.* **2014**, *22*, 1075–1083. [CrossRef] [PubMed]
222. Chithrani, B.D.; Ghazani, A.A.; Chan, W.C.W. Determining the size and shape dependence of gold nanoparticle uptake into mammalian cells. *Nano Lett.* **2006**, *6*, 662–668. [CrossRef]
223. Arandel, L.; Polay Espinoza, M.; Matloka, M.; Bazinet, A.; De Dea Diniz, D.; Naouar, N.; Rau, F.; Jollet, A.; Edom-Vovard, F.; Mamchaoui, K.; et al. Immortalized human myotonic dystrophy muscle cell lines to assess therapeutic compounds. *Dis. Model. Mech.* **2017**, *10*, 487–497. [CrossRef]
224. Matloka, M.; Klein, A.F.; Rau, F.; Furling, D. Cells of matter—*in vitro* models for myotonic dystrophy. *Front. Neurol.* **2018**, *9*, 361. [CrossRef] [PubMed]
225. Bigot, A.; Klein, A.F.; Gasnier, E.; Jacquemin, V.; Ravassard, P.; Butler-Browne, G.; Mouly, V.; Furling, D. Large CTG repeats trigger P16-dependent premature senescence in myotonic dystrophy type 1 muscle precursor cells. *Am. J. Pathol.* **2009**, *174*, 1435–1442. [CrossRef]
226. Hayflick, L. The limited in vitro lifetime of human diploid cell strains. *Exp. Cell Res.* **1965**, *37*, 614–636. [CrossRef]
227. Renault, V.; Piron-Hamelin, G.; Forestier, C.; DiDonna, S.; Decary, S.; Hentati, F.; Saillant, G.; Butler-Browne, G.S.; Mouly, V. Skeletal muscle regeneration and the mitotic clock. *Exp. Gerontol.* **2000**, *35*, 711–719. [CrossRef]
228. Renna, L.V.; Cardani, R.; Botta, A.; Rossi, G.; Fossati, B.; Costa, E.; Meola, G. Premature senescence in primary muscle cultures of myotonic dystrophy type 2 is not associated with P16 induction. *Eur. J. Histochem.* **2014**, *58*, 2444. [CrossRef] [PubMed]
229. Thornell, L.-E.; Lindström, M.; Renault, V.; Klein, A.; Mouly, V.; Ansved, T.; Butler-Browne, G.; Furling, D. Satellite cell dysfunction contributes to the progressive muscle atrophy in myotonic dystrophy type 1. *Neuropathol. Appl. Neurobiol.* **2009**, *35*, 603–613. [CrossRef]
230. Liang, R.; Dong, W.; Shen, X.; Peng, X.; Aceves, A.G.; Liu, Y. Modeling myotonic dystrophy 1 in C2C12 myoblast cells. *J. Vis. Exp.* **2016**, *113*, 54078. [CrossRef]
231. Mamchaoui, K.; Trollet, C.; Bigot, A.; Negroni, E.; Chaouch, S.; Wolff, A.; Kandalla, P.K.; Marie, S.; Di Santo, J.; St Guily, J.L.; et al. Immortalized pathological human myoblasts: Towards a universal tool for the study of neuromuscular disorders. *Skelet. Muscle* **2011**, *1*, 34. [CrossRef] [PubMed]
232. O'Connor, M.S.; Carlson, M.E.; Conboy, I.M. Differentiation rather than aging of muscle stem cells abolishes their telomerase activity. *Biotechnol. Prog.* **2009**, *25*, 1130–1137. [CrossRef] [PubMed]
233. Massenet, J.; Gitiaux, C.; Magnan, M.; Cuvellier, S.; Hubas, A.; Nusbaum, P.; Dilworth, F.J.; Desguerre, I.; Chazaud, B. Derivation and characterization of immortalized human muscle satellite cell clones from muscular dystrophy patients and healthy individuals. *Cells* **2020**, *9*, 1780. [CrossRef]
234. Chaouch, S.; Mouly, V.; Goyenvalle, A.; Vulin, A.; Mamchaoui, K.; Negroni, E.; Di Santo, J.; Butler-Browne, G.; Torrente, Y.; Garcia, L.; et al. Immortalized skin fibroblasts expressing conditional MyoD as a renewable and reliable source of converted human muscle cells to assess therapeutic strategies for muscular mystrophies: Validation of an exon-skipping approach to restore dystrophin in Duchenne muscular dystrophy Cells. *Hum. Gene Ther.* **2009**, *20*, 784–790. [CrossRef] [PubMed]

235. Cooper, S.T.; Kizana, E.; Yates, J.D.; Lo, H.P.; Yang, N.; Wu, Z.H.; Alexander, I.E.; North, K.N. Dystrophinopathy carrier determination and detection of protein deficiencies in muscular dystrophy using lentiviral MyoD-forced myogenesis. *Neuromuscul Disord.* **2007**, *17*, 276–284. [CrossRef]
236. Edmondson, R.; Broglie, J.J.; Adcock, A.F.; Yang, L. Three-dimensional cell culture systems and their applications in drug discovery and cell-based biosensors. *Assay Drug Dev. Technol.* **2014**, *12*, 207–218. [CrossRef] [PubMed]
237. Duval, K.; Grover, H.; Han, L.-H.; Mou, Y.; Pegoraro, A.F.; Fredberg, J.; Chen, Z. Modeling physiological events in 2D vs. 3D cell culture. *Physiology* **2017**, *32*, 266–277. [CrossRef]
238. Knight, E.; Przyborski, S. Advances in 3D cell culture technologies enabling tissue-like structures to be created *in vitro*. *J. Anat* **2015**, *227*, 746–756. [CrossRef]
239. Jeffries, G.D.M.; Xu, S.; Lobovkina, T.; Kirejev, V.; Tusseau, F.; Gyllensten, C.; Singh, A.K.; Karila, P.; Moll, L.; Orwar, O. 3D micro-organisation printing of mammalian cells to generate biological tissues. *Sci. Rep.* **2020**, *10*, 19529. [CrossRef]
240. Liu, Y.; Wu, B.; Gong, L.; An, C.; Lin, J.; Li, Q.; Jiang, D.; Jin, K.; Mechakra, A.; Bunpetch, V.; et al. Dissecting cell diversity and connectivity in skeletal muscle for myogenesis. *Cell Death Dis.* **2019**, *10*, 427. [CrossRef]
241. Juhas, M.; Engelmayr, G.C.; Fontanella, A.N.; Palmer, G.M.; Bursac, N. Biomimetic Engineered muscle with capacity for vascular integration and functional maturation *in vivo*. *Proc. Natl. Acad. Sci. USA* **2014**, *111*, 5508–5513. [CrossRef] [PubMed]
242. Borselli, C.; Cezar, C.A.; Shvartsman, D.; Vandenburgh, H.H.; Mooney, D.J. The role of multifunctional delivery scaffold in the ability of cultured myoblasts to promote muscle regeneration. *Biomaterials* **2011**, *32*, 8905–8914. [CrossRef]
243. McLean, I.C.; Schwerdtfeger, L.A.; Tobet, S.A.; Henry, C.S. Powering ex vivo tissue models in microfluidic systems. *Lab. Chip* **2018**, *18*, 1399–1410. [CrossRef]
244. Gowing, G.; Svendsen, S.; Svendsen, C.N. Ex vivo gene therapy for the treatment of neurological disorders. *Prog. Brain Res.* **2017** *230*, 99–132. [CrossRef] [PubMed]
245. Mobini, S.; Song, Y.H.; McCrary, M.W.; Schmidt, C.E. Advances in ex vivo models and lab-on-a-chip devices for neural tissue engineering. *Biomaterials* **2019**, *198*, 146–166. [CrossRef] [PubMed]
246. Smith, L.R.; Meyer, G.A. Skeletal muscle explants: *Ex-vivo* models to study cellular behavior in a complex tissue environment *Connect. Tissue Res.* **2020**, *61*, 248–261. [CrossRef] [PubMed]
247. Kim, D.; Wu, X.; Young, A.T.; Haynes, C.L. Microfluidics-based in vivo mimetic systems for the study of cellular biology. *Acc Chem. Res.* **2014**, *47*, 1165–1173. [CrossRef] [PubMed]
248. Carton, F.; Calderan, L.; Malatesta, M. Incubation under fluid dynamic conditions markedly improves the structural preservation in vitro of explanted skeletal muscles. *Eur. J. Histochem.* **2017**, *61*, 2862. [CrossRef]
249. Carosio, S.; Barberi, L.; Rizzuto, E.; Nicoletti, C.; Del Prete, Z.; Musarò, A. Generation of *ex vivo*-vascularized muscle engineered tissue (X-MET). *Sci. Rep.* **2013**, *3*, 1420. [CrossRef] [PubMed]
250. Fischer, H.C.; Chan, W.C. Nanotoxicity: The growing need for in vivo study. *Curr. Opin. Biotechnol.* **2007**, *18*, 565–571. [CrossRef]
251. Bostrom, M.; O'Keefe, R. What experimental approaches (eg, *in vivo*, *in vitro*, tissue retrieval) are effective in investigating the biologic effects of particles? *J. Am. Acad. Orthop. Surg.* **2008**, *16*, S63–S67. [CrossRef]
252. McGreevy, J.W.; Hakim, C.H.; McIntosh, M.A.; Duan, D. Animal models of Duchenne muscular dystrophy: From basic mechanisms to gene therapy. *Dis. Model. Mech.* **2015**, *8*, 195–213. [CrossRef]
253. Wells, D.J. Tracking progress: An update on animal models for Duchenne muscular dystrophy. *Dis. Model. Mech.* **2018**, *11*, dmm035774. [CrossRef]
254. Collins, C.A.; Morgan, J.E. Duchenne's muscular dystrophy: Animal models used to investigate pathogenesis and develop therapeutic strategies. *Int. J. Exp. Pathol.* **2003**, *84*, 165–172. [CrossRef]
255. Bulfield, G.; Siller, W.G.; Wight, P.A.; Moore, K.J. X Chromosome-linked muscular dystrophy (*mdx*) in the mouse. *Proc. Natl. Acad. Sci. USA* **1984**, *81*, 1189–1192. [CrossRef]
256. van Putten, M.; Putker, K.; Overzier, M.; Adamzek, W.A.; Pasteuning-Vuhman, S.; Plomp, J.J.; Aartsma-Rus, A. Natural disease history of the D2-*mdx* mouse model for Duchenne muscular dystrophy. *FASEB J.* **2019**, *33*, 8110–8124. [CrossRef]
257. Desguerre, I.; Arnold, L.; Vignaud, A.; Cuvellier, S.; Yacoub-Youssef, H.; Gherardi, R.K.; Chelly, J.; Chretien, F.; Mounier, R.; Ferry, A.; et al. A new model of experimental fibrosis in hindlimb skeletal muscle of adult *mdx* mouse mimicking muscular dystrophy. *Muscle Nerve* **2012**, *45*, 803–814. [CrossRef] [PubMed]
258. Ng, R.; Banks, G.B.; Hall, J.K.; Muir, L.A.; Ramos, J.N.; Wicki, J.; Odom, G.L.; Konieczny, P.; Seto, J.; Chamberlain, J.R.; et al. Animal models of muscular dystrophy. *Prog. Mol. Biol. Transl. Sci.* **2012**, *105*, 83–111. [CrossRef] [PubMed]
259. Kornegay, J.N. The golden retriever model of Duchenne muscular dystrophy. *Skelet. Muscle* **2017**, *7*, 9. [CrossRef]
260. Kawahara, G.; Karpf, J.A.; Myers, J.A.; Alexander, M.S.; Guyon, J.R.; Kunkel, L.M. Drug screening in a zebrafish model of Duchenne muscular dystrophy. *Proc. Natl. Acad. Sci. USA* **2011**, *108*, 5331–5336. [CrossRef] [PubMed]
261. Widrick, J.J.; Kawahara, G.; Alexander, M.S.; Beggs, A.H.; Kunkel, L.M. Discovery of novel therapeutics for muscular dystrophies using zebrafish phenotypic screens. *J. Neuromuscul. Dis.* **2019**, *6*, 271–287. [CrossRef]
262. Sicot, G.; Gomes-Pereira, M. RNA toxicity in human disease and animal models: From the uncovering of a new mechanism to the development of promising therapies. *Biochim. Biophys. Acta* **2013**, *1832*, 1390–1409. [CrossRef] [PubMed]
263. Gomes-Pereira, M.; Cooper, T.A.; Gourdon, G. Myotonic dystrophy mouse models: Towards rational therapy development. *Trends Mol. Med.* **2011**, *17*, 506–517. [CrossRef] [PubMed]

264. Guiraud-Dogan, C.; Huguet, A.; Gomes-Pereira, M.; Brisson, E.; Bassez, G.; Junien, C.; Gourdon, G. DM1 CTG expansions affect insulin receptor isoforms expression in various tissues of transgenic mice. *Biochim. Biophys. Acta* **2007**, *1772*, 1183–1191. [CrossRef]
265. Lin, X.; Miller, J.W.; Mankodi, A.; Kanadia, R.N.; Yuan, Y.; Moxley, R.T.; Swanson, M.S.; Thornton, C.A. Failure of MBNL1-dependent post-natal splicing transitions in myotonic dystrophy. *Hum. Mol. Genet.* **2006**, *15*, 2087–2097. [CrossRef] [PubMed]
266. Mankodi, A.; Logigian, E.; Callahan, L.; McClain, C.; White, R.; Henderson, D.; Krym, M.; Thornton, C.A. Myotonic dystrophy in transgenic mice expressing an expanded CUG repeat. *Science* **2000**, *289*, 1769–1773. [CrossRef]
267. Mankodi, A.; Takahashi, M.P.; Jiang, H.; Beck, C.L.; Bowers, W.J.; Moxley, R.T.; Cannon, S.C.; Thornton, C.A. Expanded CUG repeats trigger aberrant splicing of ClC-1 chloride channel pre-mRNA and hyperexcitability of skeletal muscle in myotonic dystrophy. *Mol. Cell* **2002**, *10*, 35–44. [CrossRef]
268. Seznec, H.; Agbulut, O.; Sergeant, N.; Savouret, C.; Ghestem, A.; Tabti, N.; Willer, J.C.; Ourth, L.; Duros, C.; Brisson, E.; et al. Mice transgenic for the human myotonic dystrophy region with expanded CTG repeats display muscular and brain abnormalities. *Hum. Mol. Genet.* **2001**, *10*, 2717–2726. [CrossRef]
269. Hinman, M.N.; Richardson, J.I.; Sockol, R.A.; Aronson, E.D.; Stednitz, S.J.; Murray, K.N.; Berglund, J.A.; Guillemin, K. Zebrafish mbnl mutants model physical and molecular phenotypes of myotonic dystrophy. *bioRxiv* **2020**, 665380. [CrossRef]
270. Machuca-Tzili, L.E.; Buxton, S.; Thorpe, A.; Timson, C.M.; Wigmore, P.; Luther, P.K.; Brook, J.D. Zebrafish deficient for Muscleblind-like 2 exhibit features of myotonic dystrophy. *Dis. Model. Mech.* **2011**, *4*, 381–392. [CrossRef]
271. Carton, F.; Chevalier, Y.; Nicoletti, L.; Tarnowska, M.; Stella, B.; Arpicco, S.; Malatesta, M.; Jordheim, L.P.; Briançon, S.; Lollo, G. Rationally designed hyaluronic acid-based nano-complexes for pentamidine delivery. *Int. J. Pharm.* **2019**, *568*, 118526. [CrossRef] [PubMed]
272. Stella, B.; Andreana, I.; Zonari, D.; Arpicco, S. Pentamidine-loaded lipid and polymer nanocarriers as tunable anticancer drug delivery systems. *J. Pharm. Sci.* **2020**, *109*, 1297–1302. [CrossRef]
273. Falzarano, M.S.; Bassi, E.; Passarelli, C.; Braghetta, P.; Ferlini, A. Biodistribution studies of polymeric nanoparticles for drug delivery in mice. *Hum Gene Ther.* **2014**, *25*, 927–928. [CrossRef]
274. Huang, D.; Yue, F.; Qiu, J.; Deng, M.; Kuang, S. Polymeric nanoparticles functionalized with muscle-homing peptides for targeted delivery of phosphatase and tensin homolog inhibitor to skeletal muscle. *Acta Biomater.* **2020**, *118*, 196–206. [CrossRef] [PubMed]
275. Herweijer, H.; Wolff, J.A. Gene therapy progress and prospects: Hydrodynamic gene delivery. *Gene Ther.* **2007**, *14*, 99–107. [CrossRef]
276. Kumbhari, V.; Li, L.; Piontek, K.; Ishida, M.; Fu, R.; Khalil, B.; Garrett, C.M.; Liapi, E.; Kalloo, A.N.; Selaru, F.M. Successful liver-directed gene delivery by ERCP-guided hydrodynamic injection (with Videos). *Gastrointest. Endosc.* **2018**, *88*, 755–763. [CrossRef] [PubMed]
277. Le Guen, Y.T.; Le Gall, T.; Midoux, P.; Guégan, P.; Braun, S.; Montier, T. Gene transfer to skeletal muscle using hydrodynamic limb vein injection: Current applications, hurdles and possible optimizations. *J. Gene Med.* **2020**, *22*, e3150. [CrossRef] [PubMed]
278. Ashfaq, U.A.; Riaz, M.; Yasmeen, E.; Yousaf, M. Recent advances in nanoparticle-based targeted drug-delivery systems against cancer and role of tumor microenvironment. *Crit. Rev. Ther. Drug Carrier Syst.* **2017**, *34*, 317–353. [CrossRef]
279. Pietersz, G.A.; Wang, X.; Yap, M.L.; Lim, B.; Peter, K. Therapeutic targeting in nanomedicine: The future lies in recombinant antibodies. *Nanomedicine* **2017**, *12*, 1873–1889. [CrossRef] [PubMed]
280. Arahata, K.; Ishiura, S.; Ishiguro, T.; Tsukahara, T.; Suhara, Y.; Eguchi, C.; Ishiharat, T.; Nonaka, I.; Ozawa, E.; Sugita, H. Immunostaining of skeletal and cardiac muscle surface membrane with antibody against Duchenne muscular dystrophy peptide. *Nature* **1988**, *333*, 861–863. [CrossRef]
281. Zhang, R.; Kim, A.S.; Fox, J.M.; Nair, S.; Basore, K.; Klimstra, W.B.; Rimkunas, R.; Fong, R.H.; Lin, H.; Poddar, S.; et al. Mxra8 is a receptor for multiple arthritogenic alphaviruses. *Nature* **2018**, *557*, 570–574. [CrossRef] [PubMed]
282. Poon, W.; Zhang, X.; Bekah, D.; Teodoro, J.G.; Nadeau, J.L. Targeting B16 tumors in vivo with peptide-conjugated gold nanoparticles. *Nanotechnology* **2015**, *26*, 285101. [CrossRef] [PubMed]
283. Yu-Wai-Man, C.; Tagalakis, A.D.; Manunta, M.D.; Hart, S.L.; Khaw, P.T. Receptor-targeted liposome-peptide-siRNA nanoparticles represent an efficient delivery system for MRTF silencing in conjunctival fibrosis. *Sci. Rep.* **2016**, *6*, 21881. [CrossRef] [PubMed]
284. Tajau, R.; Rohani, R.; Abdul Hamid, S.S.; Adam, Z.; Mohd Janib, S.N.; Salleh, M.Z. Surface functionalisation of poly-APO- b -polyol ester cross-linked copolymers as core–shell nanoparticles for targeted breast cancer therapy. *Sci. Rep.* **2020**, *10*, 21704. [CrossRef] [PubMed]
285. Yu, C.-Y.; Yuan, Z.; Cao, Z.; Wang, B.; Qiao, C.; Li, J.; Xiao, X. A muscle-targeting peptide displayed on AAV2 improves muscle tropism on systemic delivery. *Gene Ther.* **2009**, *16*, 953–962. [CrossRef]
286. Seow, Y.; Yin, H.; Wood, M.J.A. Identification of a novel muscle targeting peptide in *mdx* mice. *Peptides* **2010**, *31*, 1873–1877. [CrossRef]
287. Tsoumpra, M.K.; Fukumoto, S.; Matsumoto, T.; Takeda, S.; Wood, M.J.A.; Aoki, Y. Peptide-conjugate antisense based splice-correction for Duchenne muscular dystrophy and other neuromuscular diseases. *EBioMedicine* **2019**, *45*, 630–645. [CrossRef]
288. Gao, X.; Zhao, J.; Han, G.; Zhang, Y.; Dong, X.; Cao, L.; Wang, Q.; Moulton, H.M.; Yin, H. Effective dystrophin restoration by a novel muscle-homing peptide-morpholino conjugate in dystrophin-deficient *mdx* mice. *Mol. Ther.* **2014**, *22*, 1333–1341. [CrossRef]

Experimental section

Chapter I

Selective delivery of pentamidine by self-assembled nanoparticles

I. Andreana, E. Gazzano, E. Gianquinto, G. Piatti, V. Bincoletto, D. Kryza, G. Lollo, F. Spyrakis, C. Riganti, S. Arpicco, B. Stella

(Submitted to International Journal of Pharmaceutics)

Drug-squalene bioconjugates have been exploited for their ability to self-assemble into nanoparticles (NPs) in water. The possibility to synthesize an acid derivative of squalene, namely squalenic acid (SQ-COOH), opened the possibility to formulate NPs without any covalent linkage between the drug and the squalene moiety.

Main aim

The aim of this chapter was the design of squalene NPs based on electrostatic interactions between SQ-COOH and pentamidine free base (PTM-B). Moreover, SQ-COOH was exploited as an indirect targeting agent toward cancer cells for its ability to bind to low density lipoproteins (LDL).

Specific objectives

- Prepare PTM-B-loaded SQ-COOH NPs using the nanoprecipitation technique; optimize the formulation process; physico-chemically characterize the system; asses the SQ-COOH/PTM-B molar ratio to increase drug loading
- Study the interaction of SQ-COOH and PTM-B molecules and how they stabilize the nanosuspension
- Study the *in vitro* anticancer activity of PTM-B-loaded NPs in cancer cell lines with different expression of the receptor of LDL (LDLR)

Highlights of the chapter

- Squalene NPs were obtained without covalently linking the lipid to the drug. SQ-COOH/PTM-B molar ratio was analyzed to increase drug loading and system stability. Organic/aqueous phase volume ratio was studied to improve physico-chemical properties of NPs and maximize drug loading
- Molecular modelling analysis was performed to understand the molecules behavior at different molar ratios
- *In vitro* release was studied at physiological pH 7.4 and pH 5.0, to highlight how electrostatic interactions affect the release profile
- *In vitro* tests demonstrated the enhanced PTM-B anticancer activity in cell lines with higher expression of LDLR, due to the recognition of the squalene moiety by LDL and preferential uptake by LDLR

Selective delivery of pentamidine by self-assembled nanoparticles

Ilaria Andreana[a,b], Elena Gazzano[c,1], Eleonora Gianquinto[a], Giulia Piatti[a], Valeria Bincoletto[a], David Kryza[b,d], Giovanna Lollo[b], Francesca Spyrakis[a], Chiara Riganti[c], Silvia Arpicco[a], Barbara Stella[a,*]

[a] *Dipartimento di Scienza e Tecnologia del Farmaco, Università degli Studi di Torino, Via P. Giuria 9, 10125 Torino, Italy*

[b] *Laboratoire d'Automatique, de Génie des Procédés et de Génie Pharmaceutique, Université Claude Bernard Lyon 1, CNRS UMR 5007, 43 bd 11 Novembre 1918, 69622 Villeurbanne, France*

[c] *Dipartimento di Oncologia, Università degli Studi di Torino, Via Santena 5/bis, 10126 Torino, Italy*

[d] *Hospices Civils de Lyon, 69437 Lyon, France*

***** Corresponding author at: Dipartimento di Scienza e Tecnologia del Farmaco, Università degli Studi di Torino, Via P. Giuria 9, 10125 Torino, Italy. E-mail address: barbara.stella@unito.it. Phone: +39.011.670.66.60.

[1] Currently working at Dipartimento di Scienze della Vita e Biologia dei Sistemi, Università degli Studi di Torino, Via Accademia Albertina 13, 10123 Torino, Italy

Abstract

Pentamidine (PTM) is an aromatic diamidine approved for the treatment of parasitic infections that has been recently proposed for possible repositioning as an anticancer drug. To this aim, efforts have been made to improve its therapeutic efficacy and reduce associated adverse effects through both covalent derivatization and association with nanocarriers. In the attempt to encapsulate PTM into biocompatible nanoparticles with high drug loading while enhancing its selectivity toward cancer cells, we selected a squalene (SQ) derivative (1,1′,2-tris-norsqualenoic acid, SQ-COOH) to prepare PTM-loaded self-assembling nanocarriers. Indeed, SQ and its derivatives have been shown to self-assemble into nanoparticles in aqueous media. Furthermore, SQ-bioconjugates strongly interact with low-density lipoproteins (LDL), thus favoring preferential accumulation in cells overexpressing the LDL receptor (LDLR). Hence, we report here the preparation of nanocarriers by ion-pairing between the negatively charged SQ-COOH and the positively charged PTM free base (PTM-B), which allowed us to avoid the covalent grafting of SQ to PTM. The nanoparticles were characterized and a molecular modelling study of the interaction between SQ-COOH and PTM-B confirmed the nanocarrier stability. Finally, the ability to indirectly target LDLR-overexpressing cancer cells was evaluated by *in vitro* cell viability assays and confirmed by LDLR silencing, serum privation and simvastatin treatment.

Keywords: pentamidine; squalene; nanoparticles; molecular modelling; low-density lipoprotein receptor; cancer cells.

Graphical abstract

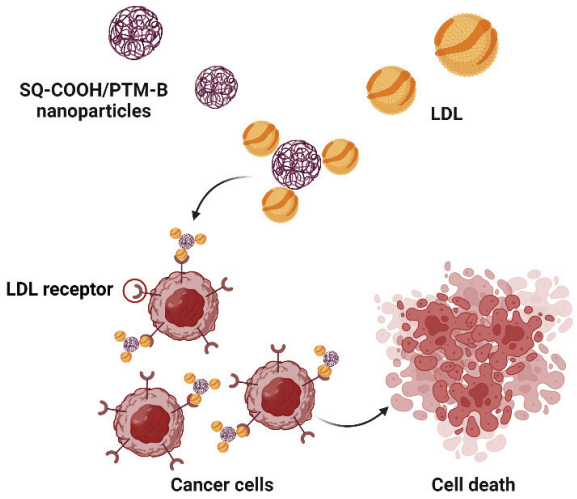

1. Introduction

Pentamidine (PTM) is a diamine composed of two phenyl amidines groups linked by a five-carbon methylene linker. Marketed in the form of two salts (isethionate and mesylate), it is administered *via* the intravenous and intramuscular routes, and *via* inhalation for treating systemic and cutaneous parasitic diseases, such as trypanosomiasis, leishmaniasis, *Pneumocystis* pneumonia (PCP) and to prevent PCP in high-risk, HIV-infected patients [1]. Thanks to its wide use in clinics, PTM is the most studied member of the diamidines to be repurposed for other therapeutic strategies, such as, among others, anticancer therapy [2]. Indeed, several studies have shown its *in vitro* and *in vivo* activity on a wide range of tumor types, including breast, melanoma, prostate, leukemia, and renal cancers, highlighting a multifactorial mechanism [3–11]. Although these studies open up interesting perspectives for the use of PTM as an antineoplastic drug, its assumption is accompanied by several side effects, such as hypo- and hyperglycemia [12–14], cardiotoxicity [15–17], pancreatic complications [18] and nephrotoxicity [19]. To overcome PTM therapy drawbacks while enhancing its bioavailability, different nanoformulations (polymeric, lipidic and inorganic) for anticancer therapy have been proposed [2]. In this context, to improve our previous approaches in terms of drug loading and nanocarrier biocompatibility [20–22], we associated PTM to a squalene (SQ) derivative to obtain biocompatible self-assembling nanoparticles. Indeed, SQ is a natural triterpene and a precursor of the synthesis of cholesterol that has been largely exploited to obtain SQ-drug conjugates able to self-assemble into nanoparticles in aqueous media without adding any surfactant [23–25]. This versatile approach has also been used without covalently linking the drug to the triterpene moiety: in this case, SQ derivatives have been physically associated to drugs through electrostatic interactions, thus avoiding drug derivatization [25,26]. Nanoencapsulation by ion-pairing is a widely used method based on the formation of hydrophobic complexes between charged hydrophilic drugs or dyes and a counterion; the complexes are then encapsulated into different lipophilic matrixes using techniques developed for poorly-water-soluble therapeutics [27,28]. In the case of SQ-based nanoparticles obtained by ion-pairing, the SQ moiety act as both the counterion and the nanocarrier matrix, thus avoiding complex composite formulations. Exploiting this strategy, in the present study we obtained SQ-based nanoparticles by ion-pairing PTM free base (PTM-B) to a negatively charged SQ derivative, namely 1,1′,2-tris-norsqualenoic acid (SQ-COOH) without any other excipient. Another advantage of this strategy consists in the ability of SQ to allow an indirect targeting to some type of cells. Indeed, previous studies demonstrated that SQ-based

nanoparticles strongly interact with low-density lipoproteins (LDL) in human blood thanks to the presence of the SQ moiety that is similar to cholesterol, the natural load of LDL; the nanoparticles are thus transported by LDL and indirectly targeted towards cells with high LDL receptor (LDLR) expression, which is not the case of free drugs [29,30]. The observed spontaneous interaction between drug-loaded SQ-nanoparticles and circulating LDL represents a promising approach in anticancer drug delivery, since fast proliferating tumor cells often overexpress LDLR [31,32]. As a further demonstration of the ability of SQ to act not only as the nanoparticle matrix, but also as an indirect targeting agent towards LDLR-overexpressing cancer cells, we prepared PTM-loaded SQ-based nanoparticles upon both electrostatic and hydrophobic interactions between the negatively charged SQ-COOH and the positively charged PTM-B. The nanoparticles have been physicochemically characterized and molecular dynamics simulations have been carried out to better explain the key role of the SQ-COOH/PTM-B molar ratio for the nanoparticle formation. Finally, the LDLR-mediated uptake of SQ-COOH/PTM nanoparticles was evaluated by studying the nanoparticle cytotoxicity on cancer cells lines with different LDL receptor levels in various conditions, *i.e.*, in the presence and absence of serum, simvastatin, and by silencing the LDLR.

2. Experimental Section

2.1. Materials

PTM isethionate (PTM-I) was purchased from Sigma-Aldrich (Milan, Italy). 1,1′,2-tris-norsqualenoic acid (SQ-COOH) was synthetized as already described [33]. All the solvents used were of analytical grade and purchased from Carlo Erba Reagenti (Milan, Italy). Filtered MilliQ water (Millipore®, Italy) was used. Solvent evaporation was carried out using a rotating evaporator (Heidolph Laborota 400, Heidolph Instruments, Schwabach, Germany) equipped with a vacuum pump (Diaphragm Vacuum Pump DC-4). Lyophilization was performed with a LyoQuest-85® freeze drier (Azbil Telstar Technologies, Barcelona, Spain).

2.2. Preparation and characterization of free base form of PTM

Free base form of PTM (PTM-B) was obtained by adding to PTM-I dissolved in distilled water a 25% w/w NH_4OH solution at 4 °C under magnetic stirring. The solution was then filtered. The white precipitate was washed three times with a diluted NH_4OH solution (5% w/w) and dried under vacuum. The conversion of PTM-I into PTM-B was confirmed by mass spectrometry analysis using electrospray ionization or by atmospheric pressure chemical

ionization, in positive ion mode, on a Micromass ZQ spectrometer (Waters, Milan, Italy), as previously reported [21].

2.3. Preparation of PTM-B-nanoparticles

PTM-B-loaded nanoparticles were prepared by the nanoprecipitation technique [34]. To this aim, SQ-COOH and PTM-B were dissolved in ethanol in different molar ratios (1:1, 2:1, 3:1, 4:1, 4.5:1, 5:1, 6:1). Then, each organic solution was added drop-wise under stirring to MilliQ® water (volume ratio ethanol/water (V_e/V_w) 1:2). Nanoparticle formation occurred spontaneously without using any surfactant. After stirring for 15 minutes, the organic solvent was eliminated using the rotating evaporator to obtain an aqueous suspension of nanoparticles (total SQ-COOH/PTM-B concentration: 2 mg/mL). To investigate the influence of the volume ratio V_e/V_w, further tests were performed with the formulation SQ-COOH/PTM-B molar ratio 3:1, for which SQ-COOH and PTM-B were dissolved in different volumes of ethanol (0.2, 0.3, 0.5, 0.7 or 1 mL) and then each of them was added to 1 mL of water. To purify the nanoparticles from non-incorporated drug, PTM-loaded nanoparticles were dialyzed against MilliQ® water at 4 °C (Spectra/Por® 3500 MWCO dialysis membrane, Spectrum, Huston, TX). Unloaded SQ-COOH nanoparticles (*i.e.*, without PTM-B) were prepared as well. The nanoparticle suspensions were then stored at 4 °C until further use.

2.4. Characterization of PTM-B-nanoparticles

The mean particle size and the polydispersity index (PDI) of the different nanoparticle samples were determined at 25 °C by quasi-elastic light scattering (QELS) using a nanosizer (Nanosizer Nano Z, Malvern Inst., Malvern, UK). The selected angle was 173° and the measurement was made after 1/10 dilution of the particulate suspensions in MilliQ® water. Each measurement was performed in triplicate.

The particle surface charge of the formulations was investigated by zeta potential measurements at 25 °C using the Smoluchowski equation and the Nanosizer Nano Z after 1/10 dilution of the suspensions in MilliQ® water. Each value reported is the average of three measurements.

The physical colloidal stability of the nanoparticles in storage conditions (4 °C) was monitored by measuring mean diameter, PDI and zeta potential by QELS at different time intervals for 28 days. For the SQ-COOH/PTM-B 3:1 (V_e/V_w 0.2:1) nanoparticles, the drug content stability was also tested in storage conditions.

The amount of incorporated PTM-B of the formulations was determined spectrophotometrically (DU 730 UV-vis spectrophotometer, Beckman Coulter, Brea, CA) at

264 nm using a calibration curve (Stella et al., 2020). To this aim, each suspension was lyophilized for 24 h; the product was then dissolved in methanol and the absorbance was measured at 264 nm. Each sample was analyzed in triplicate. The results were expressed as encapsulation efficiency (EE) (calculated as the ratio between the amount of entrapped drug and the initial amount used in the preparation of nanocarriers × 100) and drug loading (DL) (calculated as the ratio between the amount of entrapped PTM-B and the total nanocarrier weight × 100).

SQ-COOH/PTM-B 3:1 (V_e/V_w 0.2:1) nanoparticles have also been freeze-dried adding trehalose 5% (w/w) as cryoprotectant after nanoparticles formation; then, mean size, PDI, zeta potential and EE of the freeze-dried nanoparticles after rehydration were evaluated by QELS and compared to those of nanoparticles before freeze-drying.

2.5. Molecular modelling

SQ-COOH and PTM-B were simulated in different proportions, as reported in Table 1.

Table 1 Details of box settings for each simulated system.

SQ-COOH/PTM-B in MD simulations	N° SQ-COOH molecules	N° PTM-B molecules	N° water molecules	BOX size (Å^3)
1:1	6	6	193713	125
3:1	9	3	243963	135
4:1	12	3	249429	135
4.5:1	18	4	293790	140

All simulations were set up according to the following protocol.

System setup. SQ-COOH and PTM-B protonation state was calculated at pH 7, using the MoKa software [35]. The molecules were parametrized with the *ab initio* RESP charges fitting method implemented in the BiKi software suite [36,37]. SQ-COOH and PTM-B were randomly placed in a cubic box, which was then filled with TIP3P water molecules. Periodic boundary conditions (PBC) were set, and electrostatic and Van der Waals interactions were cut off at 11 Å. Long range electrostatic effects were treated with the Particle-Mesh Ewald (PME) method. The system was minimized with 5000 steepest descent steps and subsequently heated up from 0 to 300 K during three equilibration steps (0.1 ns each) in the NVT ensemble. The fourth equilibration step (1 ns) was performed in the NPT ensemble, coupling the system to the Parrinello-Rahman barostat and rescaling velocities for keeping the temperature at 300 K. The 100 ns-long production was carried out in the NVT ensemble at 300 K. When necessary (*i.e.*, the aggregates were still not stable), an extension of the simulation was performed. An additional replica was performed for systems 4:1 and 4.5:1.

2.6. Cryogenic transmission electron microscopy (cryo-TEM)

The morphology of SQ-COOH/PTM-B 3:1 (V_e/V_w 0.2:1) nanoparticles was visualized using cryo-TEM analysis. The diluted sample was dropped onto 300 Mesh holey carbon film (Quantifoil R2/1) and quench-frozen in liquid ethane using cryo-plunge workstation (made at LPS Orsay). The specimens were then mounted on a precooled Gatan 62 specimen holder, transferred in the microscope (Philips CM 120) and observed at an accelerating voltage of 120 kV (Centre Technologique des Microstructures (CTμ), platform of the Université Claude Bernard Lyon 1, Villeurbanne, France).

2.7. PTM-B release from nanoparticles

In order to evaluate PTM-B release from the nanoparticles, SQ-COOH/PTM-B 3:1 (V_e/V_w 0.2:1) suspension was incubated at 37 °C in 10 mM phosphate-buffered saline (PBS) buffer pH 7.4 or in 100 mM acetate buffer pH 5. Aliquots (1 mL) were withdrawn at predetermined time intervals (0, 2, 4, 8, 16, 24 and 48 h) and, after purification by dialysis, the drug content was measured as previously described and compared with the initial value.

2.8. Cell lines

Human breast cancer MCF7 and MDA-MD-231 cells, human prostate cancer LNCap and PC-3 cells, human hepatoma HepG2 cells were purchased from ATCC (Manassas, VA). All cell lines were authenticated by microsatellite analysis, using the PowerPlex kit (Promega Corporation, Madison, WI; last authentication: October 2022). Cells were maintained in the respective media containing 1% v/v penicillin-streptomycin, with or without 10% v/v fetal bovine serum (FBS), in a humidified atmosphere at 37 °C.

2.9. Cholesterol synthesis

Cells were labeled with 1 μCi/mL [^{3}H]-acetate (3600 mCi/mmol; Amersham Bioscience, Piscataway, NJ) for 24 h. The synthesis of the radiolabeled cholesterol was determined after lipid extraction, separation by thin layer chromatography (TLC) and liquid scintillation counting [38]. Results were expressed as pmoles/mg protein, according to the relative calibration curve.

2.10. LDLR expression

To measure the total amount of LDLR, cells were lysed in MLB buffer (Millipore, Burlington, MA), sonicated and centrifuged at 13,000×g for 10 min at 4 °C. Twenty μg cell lysates were subjected to 4-15% SDS-PAGE and probed with the following antibodies: anti-LDLR (clone EP1553Y, diluted 1:500; Abcam, Cambridge, CA); anti-β-tubulin (clone D10, diluted 1:1,000, Santa Cruz Biotechnology Inc., Santa Cruz, CA), followed by the secondary peroxidase-conjugated antibodies (Bio-Rad). Proteins were detected by enhanced chemiluminescence (Bio-Rad). To measure the amount of surface LDLR, plasma-membrane associated proteins were isolated by a biotinylation assay [39]. The extracts were resolved by SDS-PAGE and probed with an anti-LDLR or an anti-pancadherin (mouse, clone CH-19; Santa Cruz Biotechnology Inc.) antibody.

2.11. LDLR silencing

2×10^5 cells, seeded in 0.25 ml FBS/antibiotic-free medium, were transfected either with a non-targeting scrambled siRNA pool or with a siRNA pool targeting LDLR (target sequences: NM_000527.4; NM_001195798.1; NM_001195799.1; NM_001195800.1; ThermoScientific, Waltham, MA), as per manufacturer's protocol. The efficacy of silencing was verified by immunoblotting 48 h after the transfection.

2.12. Cell viability

Cell viability was measured by the ATPlite Luminescence Assay System (PerkinElmer, Waltham, MA), using the manufacturer's instructions. To this aim, a PTM solution and a SQ-COOH/PTM-B 3:1 (V_e/V_w 0.2:1) nanoparticle suspension, after a previous incubation in culture medium containing FBS for 30 min at 37 °C to allow the interaction with serum, were incubated with cells for 24, 48, 72 h. The test was performed with cells maintained in medium both with or without 10% FBS. Results were expressed as percentage of viable cells relative to untreated cells, considered 100% viable.

In a further experimental set, MCF-7, PC-3 and HepG2 cells were pre-treated with simvastatin to decrease the endogenous synthesis of cholesterol and increase the expression of LDLR for 18 h (successively removed by washing with PBS) and then incubated with the PTM solution and SQ-COOH/PTM-B 3:1 (V_e/V_w 0.2:1) nanoparticles.

2.13. Statistical analysis

All data in text and figures are presented as means ± SD. The results were analyzed by a one-way analysis of variance (ANOVA), using Statistical Package for Social Science (SPSS) software (IBM SPSS Statistics v. 19). $p < 0.05$ was considered statistically significant.

3. Results and discussion

3.1. Preparation and characterization of PTM-B-nanoparticles

In this work, the less water-soluble free base form of PTM (PTM-B) was obtained from the isethionate salt to promote the association of the drug to a synthetic derivative of SQ (SQ-COOH), forming biocompatible lipid nanocarriers in a single step by the nanoprecipitation technique. To this aim, since both the molecules are soluble in ethanol, they were pre-solubilized in the same organic solvent and then added to the aqueous phase under magnetic stirring. The spontaneous self-assembly in water was due to the peculiar characteristics of SQ-COOH, which is able to form nanoparticles in aqueous media, as many other SQ derivatives [24]. Moreover, in this case the association of PTM-B to SQ-COOH was ascribed to the formation of an ion-complex between the two compounds: indeed, at physiological pH (7.4) the two amidines residues of PTM-B (pKa=12) are positively charged, while SQ-COOH has a negatively charged carboxylic group (pKa=4.5) (Fig. 1). Thus, monodispersed PTM-B-loaded SQ-COOH nanoparticles were obtained by both ionic and hydrophobic interactions that together allowed the carrier stabilization without any surfactant. This approach has also been successfully used with a polyanionic drug, fondaparinux, which was formulated with two cationic squalenyl derivatives for oral administration in the anticoagulant therapy [26].

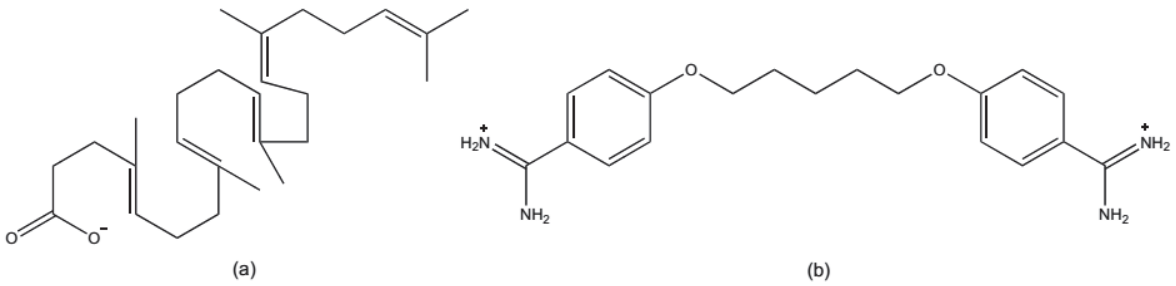

Fig. 1. Chemical structures of SQ-COOH (a) and PTM-B (b) at physiological pH

The nanoparticle preparation was performed tuning the different experimental parameters. In particular, in a first set of experiments we used different molar ratios between SQ-COOH and PTM-B (from 1:1 to 6:1) that correspond to different charge ratios (from 0.5:1 to 3:1), taking into account that SQ-COOH has one negative charge and PTM-B has two positively charged groups (Tab. 2). For all the formulations we kept the same total concentration to avoid the influence of this parameter on the physicochemical characteristics of the particles.

QELS analysis showed that, except for the molar ratios 1:1, corresponding to a positive global charge (for which the nanoparticles aggregated immediately after the mixing of ethanol and water) and 2:1, corresponding to a neutral global charge (for which the particle size was high and they were unstable during the first day of storage), the mean particle diameter for the different molar ratios was always lower than 200 nm (Tab. 2), suggesting that an excess of negative charges is necessary to stabilize the nanoparticles. Curiously, the nanocarriers with molar ratio 4:1 did not form and a precipitate was observed. Thus, we carried out a nanoprecipitation procedure with a 4.5:1 molar ratio; in this case nanoparticles were obtained. All the formulations were monodispersed (PDI<0.1) with a negative zeta potential, suggesting that part of the SQ-COOH carboxylic groups were disposed on the nanoparticle surface. Moreover, the zeta potential value slightly increased from -37 mV for unloaded carriers (molar ratio 1:0) to about -20 mV for PTM-B-containing nanoparticles (Tab. 2). Pure PTM-B (*i.e.*, drug nanoprecipitated without SQ-COOH) gave a limpid solution.

Over 4 weeks of storage at 4 °C, no precipitation and/or aggregation occurred for all the samples; nevertheless, the mean size, PDI and zeta potential were stable only for SQ-COOH/PTM-B 3:1 molar ratio (less than 10% of change), while for pure SQ-COOH nanoparticles and other SQ-COOH/PTM molar ratios the mean diameter increased of 30%-50% during the storage.

Table 2 Physicochemical characteristics (mean diameter, polydispersity index (PDI) and zeta potential) of the nanoparticles with different SQ-COOH/PTM-B molar ratios (*n*=3).

Molar ratio (SQ-COOH/PTM-B)	Charge ratio (SQ-COOH/PTM-B)	Mean diameter (nm ± SD)	PDI	Zeta potential (mV ± SD)
1:0	1:0	167 ± 10	0.057	-36.9 ± 3.8
1:1	0.5:1	---	---	---
2:1	1:1	373 ± 2	0.076	-22.2 ± 0.6
3:1	1.5:1	188 ± 2	0.099	-23.6 ± 0.5
4:1	2:1	---	---	---
4.5:1	2.25:1	189 ± 3	0.069	-26.5 ± 0.3
5:1	2.5:1	196 ± 1	0.083	-25.6 ± 0.2
6:1	3:1	200 ± 4	0.090	-18.2 ± 1.4

All the formulations allowed a high drug EE (>75%); nevertheless, the values were different in terms of calculated DL, since it diminished when the SQ-COOH/PTM-B molar ratio increased (see Table 3 for the samples with the highest DL).

Table 3 EE and DL of SQ-COOH/PTM-B 3:1 and 4.5:1 nanoparticles (*n*=3).

Molar ratio (SQ-COOH/PTM-B)	Charge ratio (SQ-COOH/PTM-B)	Mean diameter (nm ± SD)	EE (% ± SD)	DL (% ± SD)
3:1	1.5:1	188 ± 2	75 ± 12	17 ± 2
4.5:1	2.25:1	189 ± 3	86 ± 7	14 ± 3

It is noteworthy to mention that we previously encapsulated different forms of PTM into liposomes, inorganic and polymer nanoparticles for cancer treatment [20–22]; nevertheless, in the case of SQ-COOH/PTM-B nanoparticles, the low molecular weight of SQ-COOH and its low percentage in the formulations, in comparison to those of conventional particle constituents, allowed the DL to significantly increase. Furthermore, the ionic interactions between SQ-COOH and PTM-B enabled the nanoparticles to stably encapsulate the drug.

Thus, considering mean size, stability and DL, we selected the formulation SQ-COOH/PTM-B molar ratio 3:1 for further characterization tests. For this formulation, the variation of the volume ratio between the organic and aqueous phases was studied. As shown in Table 4, we

observed that increasing the V_e/V_w ratio, the nanoparticle mean diameter and PDI were higher, as reported for other SQ-based nanoparticles [26], while the zeta potential slightly diminished.

Table 4 Physicochemical characteristics (mean diameter, polydispersity index (PDI) and zeta potential) of SQ-COOH/PTM-B 3:1 nanoparticles as a function of the V_e/V_w ratio (n=3).

Volume ratio (V_e/V_w)	Mean diameter (nm ± SD)	PDI	Zeta potential (mV ± SD)
0.2	109 ± 1	0.063	-20.7 ± 1.080
0.3	132 ± 2	0.080	-22.8 ± 1.270
0.5	188 ± 2	0.099	-23.6 ± 0.493
0.7	289 ± 5	0.168	-26.2 ± 2.850
1	328 ± 12	0.221	-33.0 ± 1.190

The physical stability of the nanoparticles prepared with the different V_e/V_w ratios was evaluated: results showed that only 0.2, 0.3 and 0.5 ratios allowed the mean diameter and PDI to remain stable (mean variation <10%). Moreover, the evaluation of drug encapsulation showed that the 0.2 V_e/V_w ratio has the highest EE and DL (EE: 82%; DL: 19%) and that the drug content was stable during storage (83% of the initial content).

Taken together, these results justified our choice to use SQ-COOH/PTM-B 3:1 (V_e/V_w 0.2:1) nanoparticles, prepared with the lowest volume ratio, for further studies. In this case, the nanoparticle formation was obtained in the 'Ouzo' region at high water-to-ethanol volume ratio, leading to smaller and monodisperse nanocarriers [40]. This formulation was then tested *in vitro* and compared to the free drug.

3.2. Molecular modelling

To better explain why the SQ-COOH/PTM-B molar ratio was crucial for the formation of the nanoparticles, we performed plain molecular dynamics simulations with the aim of observing the behavior of SQ-COOH and PTM-B in solution, and the possible formation of nanoparticles, at 1:1, 3:1, 4:1 and 4.5:1 molar ratio (Table 1). Systems were built up as reported in the Experimental Section, placing in a water box the necessary number of molecules to maintain the aforementioned ratios, as indicated in the left labels of Figure 2.

The simulation of 1:1 ratio highlighted a clear excess of PTM-B that cannot be completely incorporated in the aggregates, which present an overall positive charge. In contrast, the 4:1

system showed, in both replicas, the formation of a SQ-COOH aggregate, possibly destabilizing the nanoparticle formation.

Lastly, the 3:1 and 4.5:1 ratio led to the formation of particle clusters in which no PTM-B excess and no SQ-COOH aggregates were recorded. In particular, stable aggregates emerging from 3:1 and 4.5:1 simulations contained a negatively charged, hydrophobic SQ-COOH core, partially shielded from the solvent by PTM-B molecules. These observations might support the previously reported experimental, according to which only 3:1 and 4.5:1 allowed the formation of stable nanoparticles among the molar ratios evaluated by molecular modelling.

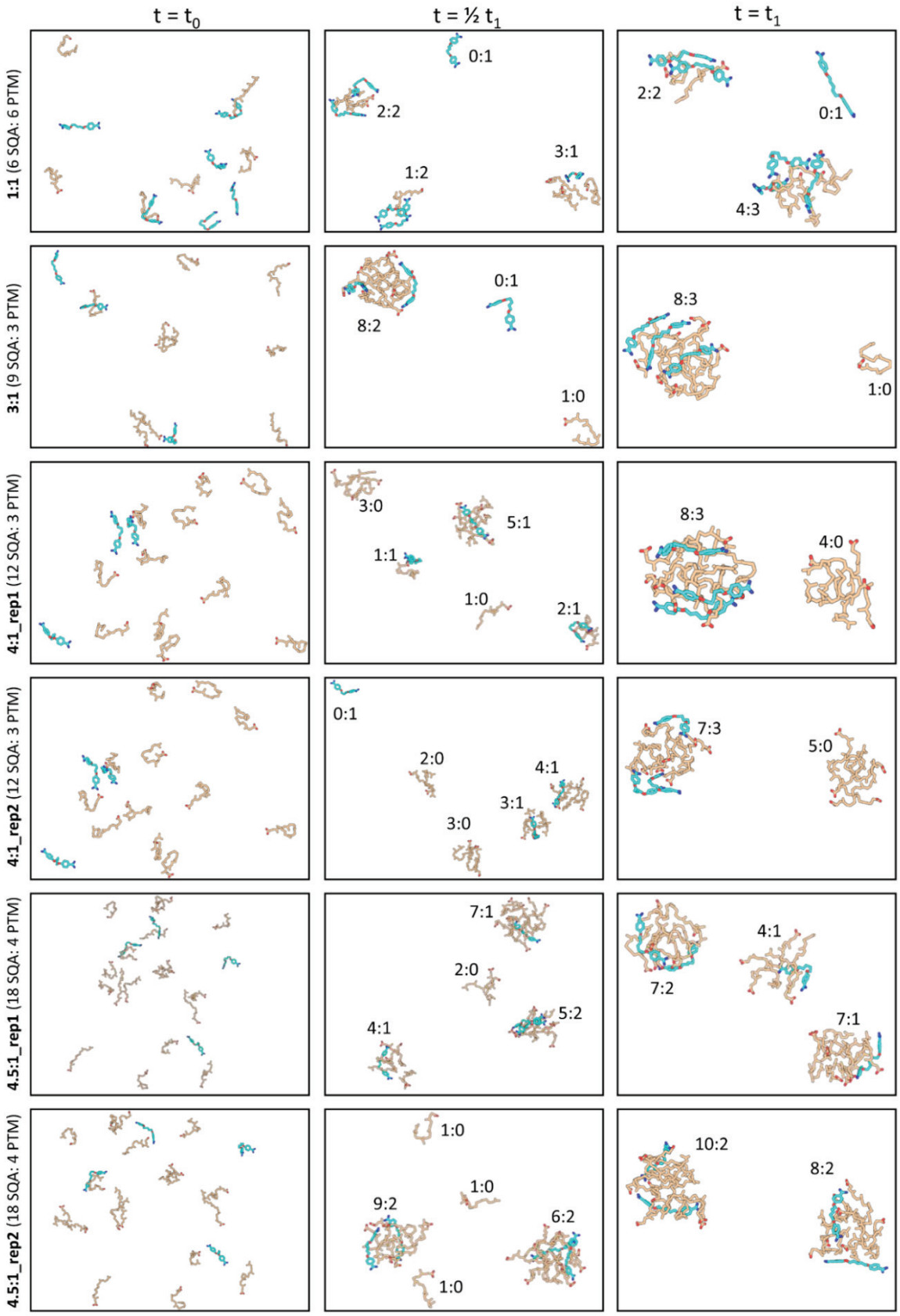

Fig. 2. Aggregation process of SQ-COOH (SQA) and PTM-B (PTM) molecules during MD simulations. Each row corresponds to a simulation, the number of SQ-COOH and PTM-B molecules is reported in brackets. Frames were extracted at the beginning ($t = t_0$), at half ($t = ½\ t_1$) and at the end ($t = t_1$) of the simulation time. Molecules are depicted as capped sticks, in cyan (PTM-B) and beige (SQ-COOH). Each aggregate is labelled according to the SQ-COOH/PTM-B ratio.

3.3. Cryogenic transmission electron microscopy (cryo-TEM)

The morphology of SQ-COOH/PTM-B 3:1 (V_e/V_w 0.2:1) nanoparticles was investigated by cryo-TEM microscopy. The nanoparticles showed a homogeneous core and a spherical shape, confirming the diameter found by QELS analysis (Fig. 3). The SQ-COOH/PTM-B 3:1 (V_e/V_w 0.2:1) nanoparticle morphology was found to be similar to the one of other SQ-based nanocarriers obtained without covalent binding between the drug and the lipid derivative [41].

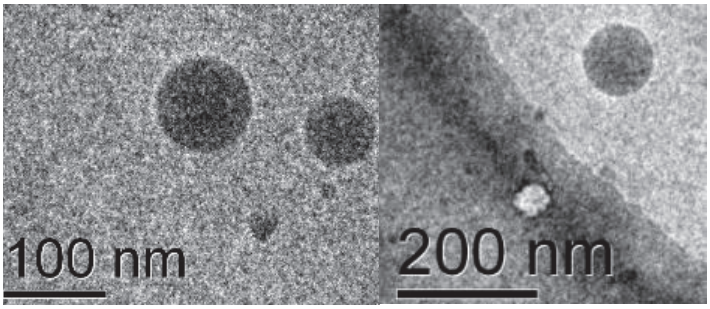

Fig. 3. Cryo-TEM images of SQ-COOH/PTM-B 3:1 (V_e/V_w 0.2:1) nanoparticles.

3.4. PTM-B release from nanoparticles

To evaluate the PTM-B release from the SQ-COOH/PTM-B 3:1 (V_e/V_w 0.2:1) nanoparticles, the suspension was incubated for 48 h at 37 °C in PBS pH 7.4 or in acetate buffer pH 5 (Fig. 4). At pH 7.4 the drug is stably associated to SQ-COOH and after 48 h only about 30% is released. Indeed, at this pH value, protonated amidine groups of PTM-B strongly interact with negatively charged SQ-COOH by ionic interaction. Since the endosomal and tumor environments are usually characterized by acidic pH [42], we evaluated the PTM-B release profile at pH 5.0. In these conditions, the formulation showed a pH-responsive behavior: after 4 h, a complete release of PTM-B occurred. Indeed, at pH 5.0, the carboxylic groups of SQ-COOH are partially protonated, disrupting their electrostatic interactions with amidine functions of PTM-B, thus enabling the drug release from nanoparticles.

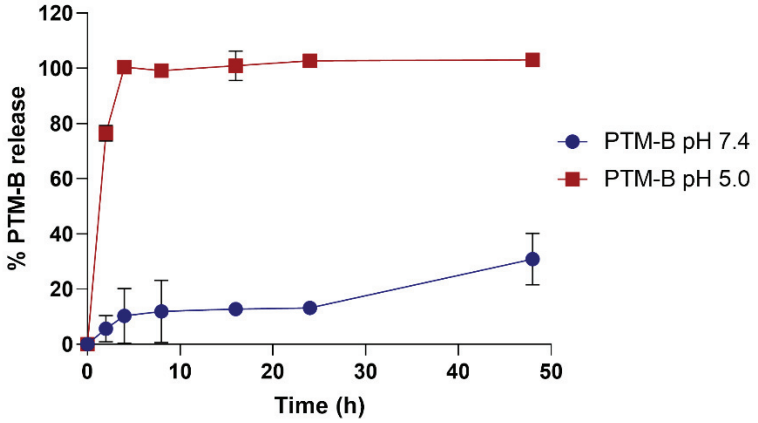

Fig. 4. PTM-B release from SQ-COOH/PTM-B 3:1 (V_e/V_w 0.2:1) nanoparticles as a function of time in PBS pH 7.4 or acetate buffer pH 5.0 at 37 °C.

The SQ-COOH/PTM-B 3:1 (V_e/V_w 0.2:1) formulation was also characterized after freeze-drying using trehalose (5% w/w) as cryoprotectant [43]: nanoparticles were easily resuspended, presenting a mean diameter around 150 nm, without important variation on zeta potential values and an encapsulation efficiency of 71%. The physiochemical characteristics were maintained in resuspended formulation stored over 28 days.

3.5. In vitro cellular efficacy

As a further step, we intended to test SQ-COOH/PTM-B 3:1 (V_e/V_w 0.2:1) nanocarriers activity on LDLR-expressing cancer cells. We screened the cytotoxic efficacy of nanoparticles in a panel of cell lines, characterized by undetectable (MCF7 cells), low (LNCap cells), medium (MDA-MB-231 and PC-3 cells) expression of LDLR, in whole cell lysate and on cell surface (Fig. 5), since SQ has been reported to bind to LDLR for its structural homology with cholesterol [44]. HepG2 cells were included as a cell line with high expression of LDLR (Fig. 5). Since FBS in cell culture medium contained cholesterol-LDL that is physiologically taken up by cells [45], we compared the expression of LDLR in cells cultured with or without FBS. As expected, in cells with detectable levels of LDLR (MDA-MB-231, PC-3 and HepG2 cell lines), FBS-deprived cells increased the expression of LDLR in whole extracts, *i.e.*, the amount of protein present within the cell lysate, and the LDLR associated with plasma-membrane, *i.e.*, the active receptor on cell surface (Fig. 5). This trend is consequent to the lower uptake of exogenous cholesterol that forces cells to increase the transcription of LDLR [45]. Similarly, simvastatin, a strong inhibitor of the 3-β-hydroxy-3-β-methylglutaryl coenzyme reductase A, the pacemaker enzyme of the synthesis of cholesterol, up-regulates the levels of LDLR as a

consequence of the reduced endogenous synthesis of cholesterol [46]. Accordingly, simvastatin-treated MDA-MB-231, PC-3 and HepG2 cells had increased levels of LDLR. Such increase was particularly pronounced in simvastatin-treated cells grown under FBS-deprivation (Fig. 5).

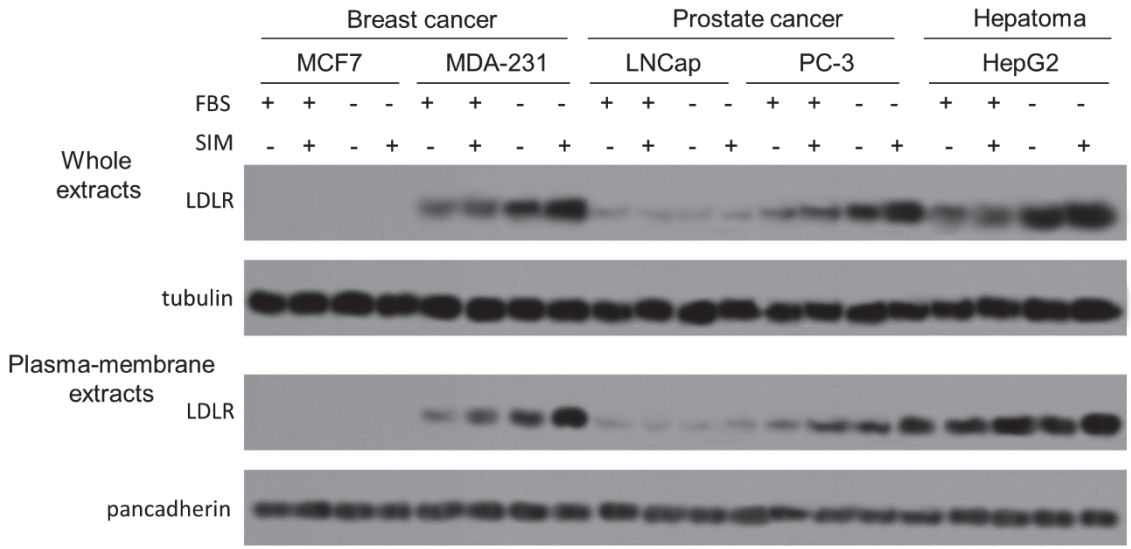

Fig. 5. Expression of LDLR in different cancer cell lines. Whole extracts and plasma-membrane associated extracts from breast cancer MCF7 and MDA-MB-231 cells, prostate cancer LNCap and PC-3 cells, hepatoma HepG2 cells, cultured 24 h in medium with (+) or without (-) 10% v/v FBS, with (+) or without (-) 10 μM simvastatin (SIM) were analyzed for the expression of LDLR. β-tubulin and pancadherin were used as control of equal protein loading. The figure is representative of 1 out of 3 experiments.

The FBS deprivation and simvastatin treatment, used in the same experimental conditions adopted for the measure of LDLR, increased and decreased the endogenous synthesis of cholesterol, respectively (Suppl. Fig. A.1). This experimental set suggests that the changes in LDLR were due to alterations of cholesterol homeostasis, as reported in most mammalian cells [45,46].

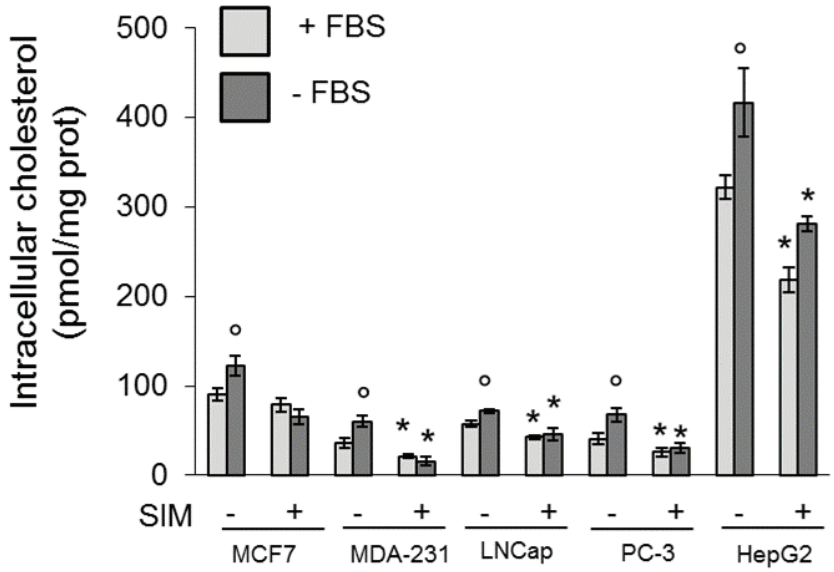

Fig. A.1. Intracellular cholesterol after FBS deprivation and simvastatin treatment. Breast cancer MCF7 and MDA-MB-231 cells, prostate cancer LNCap and PC-3 cells, hepatoma HepG2 cells, cultured 24 h in medium with (+) or without (-) 10% v/v FBS, with (+) or without (-) 10 µM simvastatin (SIM), were radiolabeled with 1 µCi/mL [^{3}H]-acetate for 24 h. Then, lipids were extracted, separated by TLC and the amount of synthesized cholesterol was measured by liquid scintillation. Data are presented as means ± SD. *p<0.05: SIM-treated *vs*. SIM-untreated cells; °p<0.05: FBS-deprived medium *vs.* FBS-containing medium.

To evaluate the cytotoxicity of SQ-COOH/PTM-B 3:1 (V_e/V_w 0.2:1) nanoparticles, samples containing different concentrations of PTM-B were incubated with FBS-containing medium for 30 minutes. Then, the suspensions were added to cell culture medium, with or without FBS. This pre-incubation has two aims: first, it favors the binding of nanoparticles to LDL present within FBS, increasing its potential to bind the LDLR. Second, it protects the nanocarriers that are unstable in the slightly acidic environment generated by cancer cells if unbound to lipoproteins. Indeed, SQ-COOH/PTM-B nanoparticles disaggregate and release PTM at pH 5.0 (Fig. 4) [47]. The viability assays demonstrated that both PTM-B and SQ-COOH/PTM-B nanoparticles exerted a time- and dose-dependent cytotoxicity, as indicated by the reduced viable cells (Fig. 6). The cytotoxicity induced by SQ-COOH/PTM-B nanocarriers was superior to free PTM-B - in particular after 48 and 72 h - in the LDLR-expressing cell lines with this rank order: MDA-MB-231 < PC-3 < HepG2 cells. By contrast, there were no significant differences between PTM-B and SQ-COOH/PTM-B nanoparticles in the cell lines with undetectable/low levels of LDLR, *i.e.* MCF7 and LNCap cells. These results suggest that SQ-COOH/PTM-B nanoparticles deliver a higher intracellular amount of PTM-B, with a LDLR-triggered mechanism, *e.g*. by inducing a receptor-mediated endocytosis. Such toxicity was not due to SQ-COOH, because it was not toxic in all the cell lines at 10^{-5} M, *i.e*. the highest concentration tested (data not shown). Comparing the cell cultures with or without FBS, we

observed that - using the same concentration of SQ-COOH/PTM-B nanoparticles - the cytotoxicity in LDLR-expressing cell lines was higher in FBS-deprived medium (Fig. 6). Indeed, the LDL present within the FBS may occupy part of LDLR, preventing the binding of SQ-COOH/PTM-B nanoparticles, thus reducing the PTM-B uptake. Moreover, FBS is a source of exogenous cholesterol, that - as reported in Fig. 5 - prevents any increase in LDLR. By contrast, in FBS-deprived medium, SQ-COOH/PTM-B nanoparticles resulted more cytotoxic for at least two reasons. First, in the absence of FBS, the only LDL present during the cytotoxicity assay are those associated with the nanoparticles during the 30 minutes pre-incubation. Second, cells are forced to increase LDLR on their surface and uptake SQ-COOH/PTM-B nanoparticles, which mimic LDL cholesterol and/or are associated with LDL cholesterol, since they did not receive exogenous cholesterol from the culture medium.

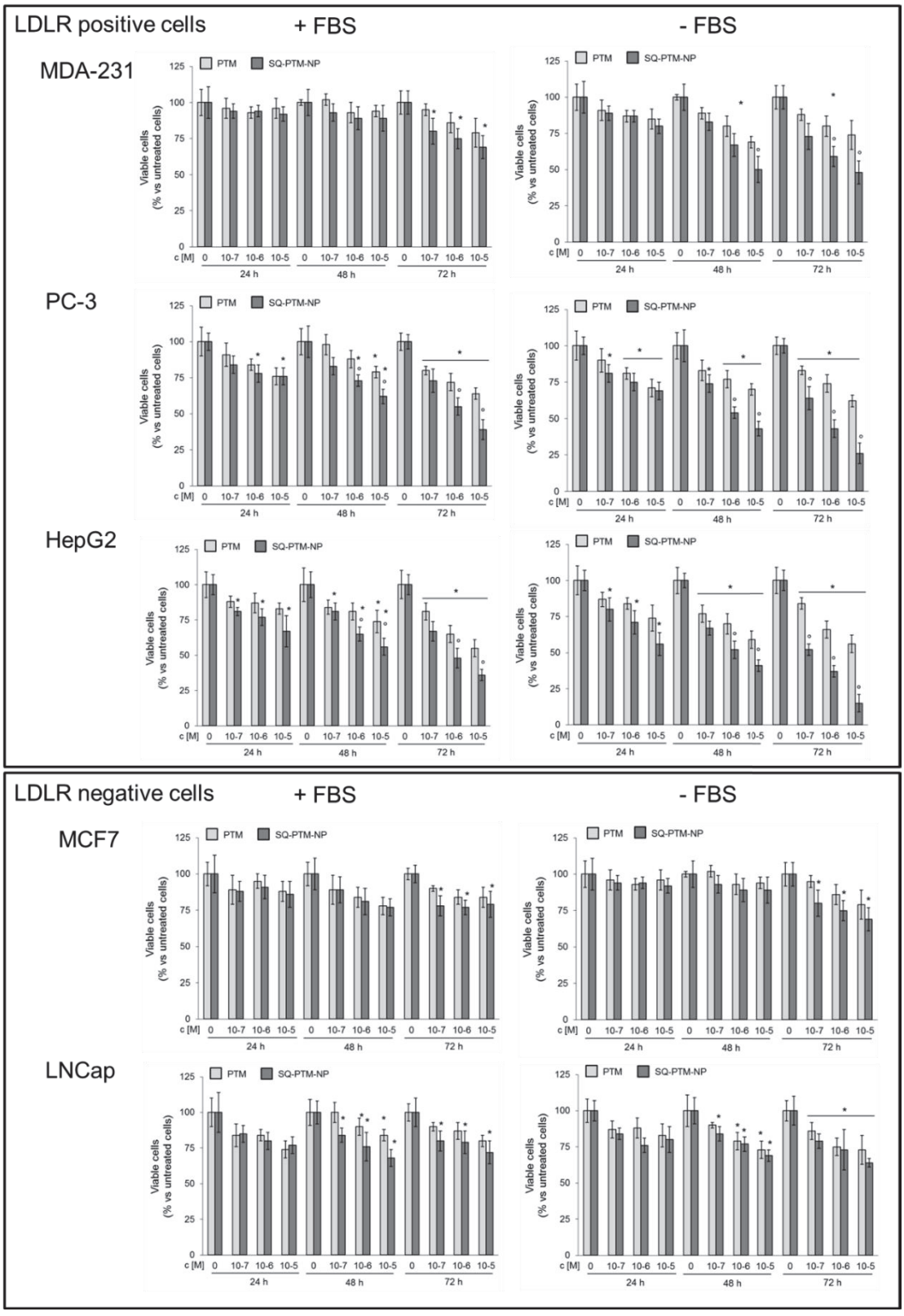

Fig. 6. Dose- and time-dependent cytotoxicity of SQ-COOH/PTM-B 3:1 (V_e/V_w 0.2:1) nanoparticles. LDLR-positive (MDA-MB-231, PC-3 and HepG2) and LDLR-negative (MCF7 and LNCap) cell lines were incubated for 24, 48 or 72 h, in the absence (0) or in the presence of free PTM-B (PTM) or SQ-COOH/PTM-B 3:1 (V_e/V_w 0.2:1) nanoparticles (SQ-PTM-NP) at 10^{-7}, 10^{-6}, 10^{-5} M, in a medium with (+) or without (-) 10% v/v FBS. Before the incubation, SQ-COOH/PTM-B 3:1 (V_e/V_w 0.2:1) nanoparticles were maintained 30 minutes in complete medium containing 10% v/v FBS. Cell viability was measured in triplicates using a chemiluminescence-based assay. Data are presented as means $\pm$ SD. *$p<0.05$: *vs*. the respective untreated (0) cells; °$p<0.05$: SQ-COOH/PTM-B 3:1 (V_e/V_w 0.2:1) nanoparticles *vs.* PTM-B.

Overall, we suggest that LDL are endogenous carriers of SQ-COOH/PTM-B nanoparticles in the systemic circulation, and the SQ moiety may be an indirect active targeting agent, able to increase the delivery of PTM-B toward LDLR-expressing cells compared to PTM-B alone, whose uptake is LDLR-independent.

In a second experimental set, we selected MCF7, PC-3 and HepG-2 cells, as example of with undetectable, medium and high levels of LDLR, respectively (Fig. 5). We pre-treated the cells with simvastatin for 24 h in order to increase – at least in PC-3 and HepG-2 cells - the expression of LDLR (Fig. 5); then, we added PTM-B or SQ-COOH/PTM-B 3:1 (V_e/V_w 0.2:1) nanoparticles for 72 h and we measured the cell viability. While we did not detect any differential toxicity between free PTM-B and SQ-COOH/PTM-B nanoparticles in MCF7, we observed that simvastatin significantly increased the cytotoxicity of SQ-COOH/PTM-B nanoparticles compared to free PTM-B in PC-3 and HepG-2 cells (Fig. 7). This can be due to the increase of LDLR expression induced by simvastatin that enhances the uptake of SQ-COOH/PTM-B nanoparticles. Again, in FBS-deprived cells - characterized by a basally higher LDLR expression (Fig. 5) - the toxicity induced by SQ-COOH/PTM-B nanoparticles was stronger than in cells grown in FBS-containing medium (Fig. 7).

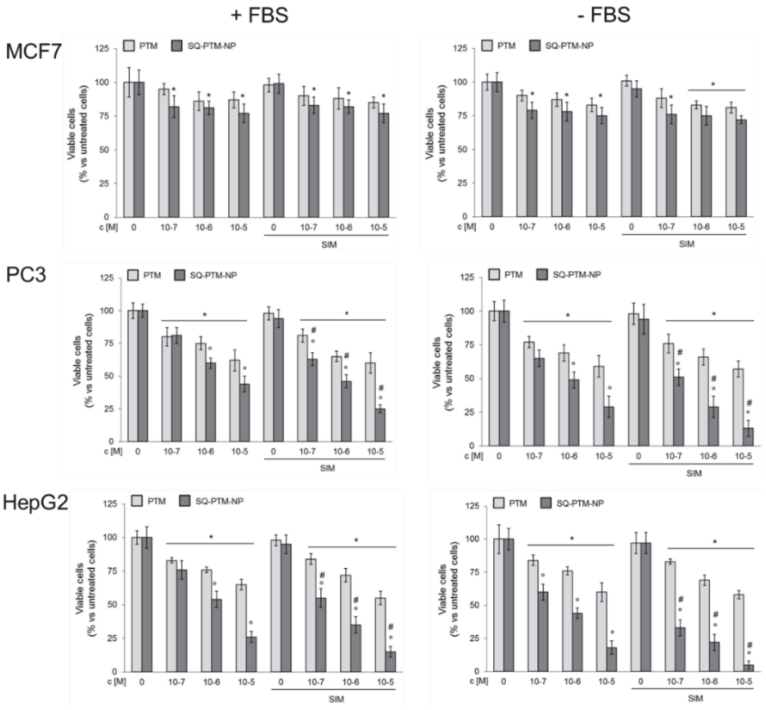

Fig. 7. Effects of simvastatin and FBS deprivation on the cytotoxicity of SQ-COOH/PTM-B 3:1 (V_e/V_w 0.2:1) nanoparticles. MCF7, PC-3 and HepG2 cell lines were incubated for 24 h in the absence or in the presence of 10 μM simvastatin (SIM), then washed and cultured for 72 h, in the absence (0) or in the presence of free PTM-B (PTM) or SQ-COOH/PTM-B 3:1 (V_e/V_w 0.2:1) nanoparticles (SQ-PTM-NP) at 10^{-7}, 10^{-6}, 10^{-5} M, in a medium with (+) or without (-) 10% v/v FBS. Before the incubation, SQ-COOH/PTM-B nanoparticles were maintained 30 minutes in complete medium containing 10% FBS. Cell viability was measured in triplicates using a chemiluminescence-based assay. Data are presented as means ± SD. *$p<0.05$: *vs*. the respective untreated (0) cells; °$p<0.05$: SQ-COOH/PTM-B nanoparticles *vs*. PTM-B; $^{\#}p<0.05$: SIM-treated cells *vs*. SIM-untreated cells.

As further confirmation of the role of LDLR in the delivery of PTM-B carried by SQ-based nanoparticles, we silenced the receptor in HepG2 cells. Our silencing conditions strongly reduced LDLR expression in whole extracts and on cell surface, both in the presence or absence of FBS and/or simvastatin (Fig. 8A). Notably, in all the silenced cells, the cytotoxicity induced by SQ-COOH/PTM-B nanoparticles was significantly lower (Fig. 8B). This experimental set indicates that SQ-COOH/PTM-B nanoparticle uptake was dependent on the presence of LDLR.

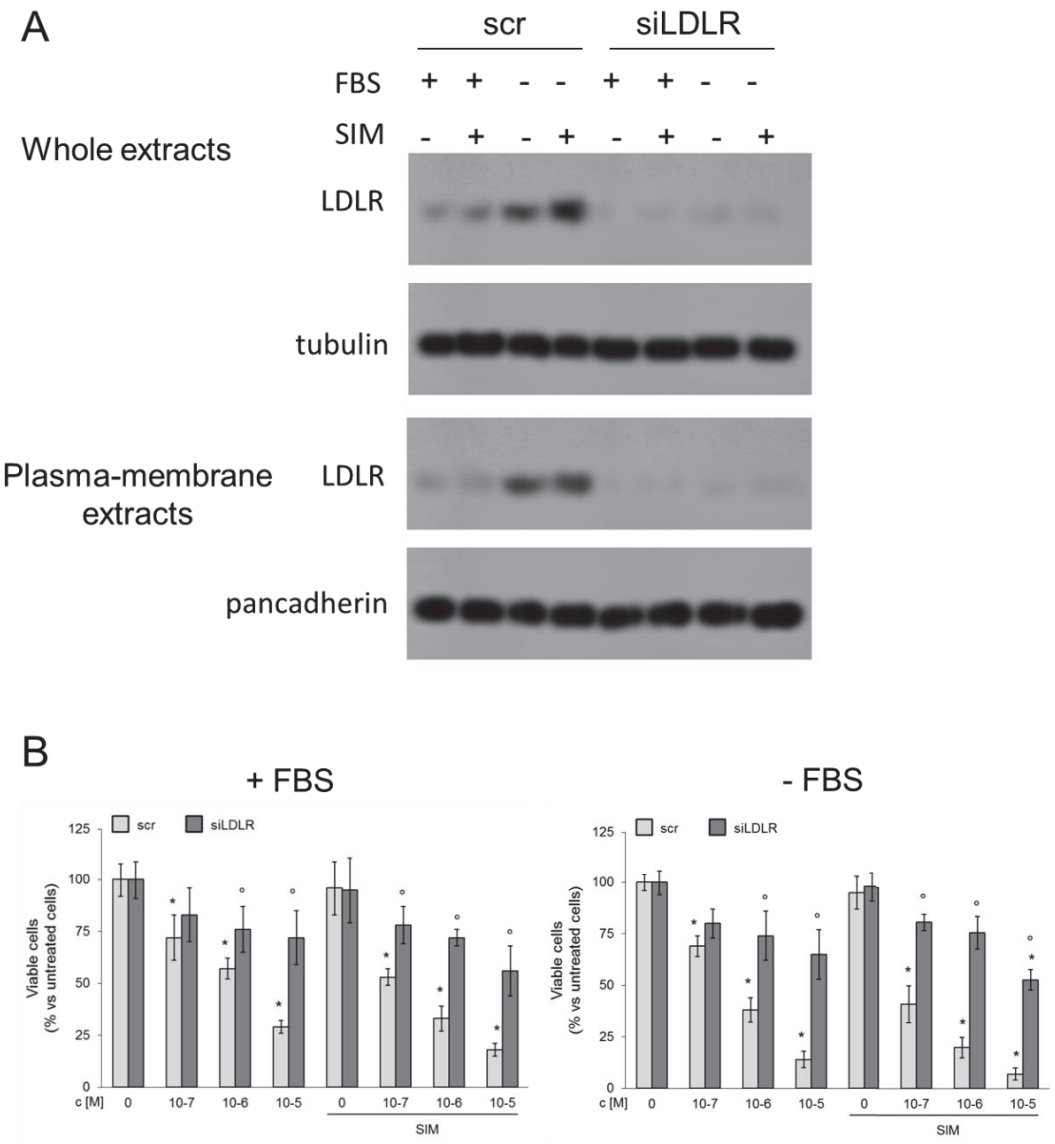

Fig. 8. Effect of LDLR silencing on the cytotoxicity of SQ-COOH/PTM-B 3:1 (V_e/V_w 0.2:1) nanoparticles. HepG2 cell line was treated with a non-targeting scrambled siRNA pool (scr) or with a siRNA pool targeting LDLR (siLDLR), in medium with (+) or without (-) 10% v/v FBS, in the absence or in the presence of 10 µM simvastatin (SIM) for the last 24 h. **A.** The expression of LDLR in whole extracts and plasma-membrane associated extracts was analyzed by immunoblotting 48 h after the transfection. β-tubulin and pancadherin were used as control of equal protein loading. The figure is representative of 1 out of 3 experiments. **B.** Cells treated as reported in A were cultured in the absence (0) or in the presence of SQ-COOH/PTM-B 3:1 (V_e/V_w 0.2:1) nanoparticles at 10^{-7}, 10^{-6}, 10^{-5} M. After 72 h, cell viability was measured in triplicates using a chemiluminescence-based assay. Data are presented as means ± SD. *p<0.05: *vs*. untreated (0) cells; °p<0.05: siLDR cells *vs*. scr cells.

4. Conclusions

Here we propose a new biocompatible nanoformulation of PTM-B based on the electrostatic interactions of the drug with a negatively charged SQ derivative, thus promoting a high DL and a pH-dependent drug release. Since the SQ moiety enables the association of the nanoparticles with LDL, PTM could be repurposed in this nanosystem as a drug that indirectly targets cancer cells overexpressing LDLR. To this aim, we have shown that pretreatment with simvastatin increases the exposure of LDLR, exploiting the physiological alterations in cholesterol homeostasis. Our work paves the way for an interesting new combinatorial treatment based on statin followed by SQ-COOH/PTM-B as promising strategies against those tumors, such as breast, prostate and liver cancers, with active cholesterol metabolism and high expression of LDLR.

CRediT authorship contribution statement

I. Andreana, E. Gazzano: investigation, data curation, writing - original draft. **E. Gianquinto:** investigation, formal analysis, writing - original draft. **G. Piatti:** investigation, validation, writing - original draft. **V. Bincoletto:** investigation, validation, writing - original draft. **D. Kryza, G. Lollo:** conceptualization, writing - review & editing. **F. Spyrakis, C. Riganti, S. Arpicco:** conceptualization, supervision, writing - review & editing. **B. Stella:** conceptualization, methodology, supervision, writing - review & editing. All authors have read and agreed to the published version of the manuscript.

Declaration of Competing Interest

The authors declare that they have no known competing financial interests or personal relationships that could have appeared to influence the work reported in this paper.

Acknowledgements

We thank Mr. Costanzo Costamagna for the technical assistance. The research was supported by the Italian Association for Cancer Research (AIRC; IG21408), Compagnia di San Paolo Funding 2021 and the Ministry of University and Research - University of Turin “Fondi Ricerca Locale (ex-60%)”.

Appendix A. Supplementary material

Supplementary data to this article can be found online at …

References

FDA Abbreviated New Drug Application: 206666 pentamidine isethionate

List of EU nationally authorized medicinal products with active substance pentamidine. Procedure No.: PSUSA/00002338/20170

1. Sands, M.; Kron, M.A.; Brown, R.B. Pentamidine: A Review. *Rev Infect Dis* **1985**, *7*, 625–634, doi:10.1093/clinids/7.5.625.
2. Andreana, I.; Bincoletto, V.; Milla, P.; Dosio, F.; Stella, B.; Arpicco, S. Nanotechnological Approaches for Pentamidine Delivery. *Drug Deliv Transl Res* **2022**, doi:10.1007/s13346-022-01127-4.
3. Chow, T.Y.-K.; Alaoui-Jamali, M.A.; Yeh, C.; Yuen, L.; Griller, D. The DNA Double-Stranded Break Repair Protein Endo-Exonuclease as a Therapeutic Target for Cancer. *Mol Cancer Ther* **2004**, *3*, 911–919.
4. Jung, H.-J.; Suh, S.-I.; Suh, M.-H.; Baek, W.-K.; Park, J.-W. Pentamidine Reduces Expression of Hypoxia-Inducible Factor-1α in DU145 and MDA-MB-231 Cancer Cells. *Cancer Lett* **2011**, *303*, 39–46, doi:10.1016/j.canlet.2011.01.008.
5. Lee, M.S.; Johansen, L.; Zhang, Y.; Wilson, A.; Keegan, M.; Avery, W.; Elliott, P.; Borisy, A.A.; Keith, C.T. The Novel Combination of Chlorpromazine and Pentamidine Exerts Synergistic Antiproliferative Effects through Dual Mitotic Action. *Cancer Res* **2007**, *67*, 11359–11367, doi:10.1158/0008-5472.CAN-07-2235.
6. Liu, L.; Wang, F.; Tong, Y.; Li, L.-F.; Liu, Y.; Gao, W.-Q. Pentamidine Inhibits Prostate Cancer Progression via Selectively Inducing Mitochondrial DNA Depletion and Dysfunction. *Cell Prolif* **2020**, *53*, e12718, doi:10.1111/cpr.12718.
7. Pathak, M.K.; Dhawan, D.; Lindner, D.J.; Borden, E.C.; Farver, C.; Yi, T. Pentamidine Is an Inhibitor of PRL Phosphatases with Anticancer Activity. *Mol Cancer Ther* **2002**, *1*, 1255–1264.
8. Qiu, G.; Jiang, J.; Liu, X. Pentamidine Sensitizes Chronic Myelogenous Leukemia K562 Cells to TRAIL-Induced Apoptosis. *Leuk Res* **2012**, *36*, 1417–1421, doi:10.1016/j.leukres.2012.07.017.
9. Rahman, A.; O'Sullivan, P.; Rozas, I. Recent Developments in Compounds Acting in the DNA Minor Groove. *Medchemcomm* **2019**, *10*, 26–40, doi:10.1039/c8md00425k.
10. Smith, J.; Stewart, B.J.; Glaysher, S.; Peregrin, K.; Knight, L.A.; Weber, D.J.; Cree, I.A. The Effect of Pentamidine on Melanoma Ex Vivo. *Anticancer Drugs* **2010**, *21*, 181–185, doi:10.1097/CAD.0b013e3283340cee.
11. Zerbini, L.F.; Bhasin, M.K.; de Vasconcellos, J.F.; Paccez, J.D.; Gu, X.; Kung, A.L.; Libermann, T.A. Computational Repositioning and Preclinical Validation of Pentamidine for Renal Cell Cancer. *Mol Cancer Ther* **2014**, *13*, 1929–1941, doi:10.1158/1535-7163.MCT-13-0750.
12. Arino, T.; Karakawa, S.; Ishiwata, Y.; Nagata, M.; Yasuhara, M. Effect of Cimetidine on Pentamidine Induced Hyperglycemia in Rats. *Eur J Pharmacol* **2012**, *693*, 72–79, doi:10.1016/j.ejphar.2012.07.043.
13. Coyle, P.; Carr, A.D.; Depczynski, B.B.; Chisholm, D.J. Diabetes Mellitus Associated with Pentamidine Use in HIV-Infected Patients. *Med J Aust* **1996**, *165*, 587–588, doi:10.5694/j.1326-5377.1996.tb138654.x.
14. Kennedy, P.G. Clinical Features, Diagnosis, and Treatment of Human African Trypanosomiasis (Sleeping Sickness). *Lancet Neurol* **2013**, *12*, 186–194, doi:10.1016/S1474-4422(12)70296-X.
15. Antoniou, T.; Gough, K.A. Early-Onset Pentamidine-Associated Second-Degree Heart Block and Sinus Bradycardia: Case Report and Review of the Literature. *Pharmacotherapy* **2005**, *25*, 899–903, doi:10.1592/phco.2005.25.6.899.

16. Glikson, M.; Dresner-Feigin, R.; Pollack, A.; Wolf, D.; Galun, E.; Tur-Kaspa, R. Pentamidine-Induced Cardiotoxicity. *Isr J Med Sci* **1990**, *26*, 588–589.
17. Kuryshev, Y.A.; Ficker, E.; Wang, L.; Hawryluk, P.; Dennis, A.T.; Wible, B.A.; Brown, A.M.; Kang, J.; Chen, X.-L.; Sawamura, K.; et al. Pentamidine-Induced Long QT Syndrome and Block of HERG Trafficking. *J Pharmacol Exp Ther* **2005**, *312*, 316–323, doi:10.1124/jpet.104.073692.
18. Pelucio, M.T.; Rothenhaus, T.; Smith, M.; Ward, D.J. Fatal Pancreatitis as a Complication of Therapy for HIV Infection. *J Emerg Med* **1995**, *13*, 633–637, doi:10.1016/0736-4679(95)00068-l.
19. Prabhavalkar, S.; Masengu, A.; O'Rourke, D.; Shields, J.; Courtney, A. Nebulized Pentamidine-Induced Acute Renal Allograft Dysfunction. *Case Reports in Transplantation* **2013**, *2013*, e907593, doi:10.1155/2013/907593.
20. Carton, F.; Chevalier, Y.; Nicoletti, L.; Tarnowska, M.; Stella, B.; Arpicco, S.; Malatesta, M.; Jordheim, L.P.; Briançon, S.; Lollo, G. Rationally Designed Hyaluronic Acid-Based Nano-Complexes for Pentamidine Delivery. *Int J Pharm* **2019**, *568*, 118526, doi:10.1016/j.ijpharm.2019.118526.
21. Peretti, E.; Miletto, I.; Stella, B.; Rocco, F.; Berlier, G.; Arpicco, S. Strategies to Obtain Encapsulation and Controlled Release of Pentamidine in Mesoporous Silica Nanoparticles. *Pharmaceutics* **2018**, *10*, E195, doi:10.3390/pharmaceutics10040195.
22. Stella, B.; Andreana, I.; Zonari, D.; Arpicco, S. Pentamidine-Loaded Lipid and Polymer Nanocarriers as Tunable Anticancer Drug Delivery Systems. *J Pharm Sci* **2020**, *109*, 1297–1302, doi:10.1016/j.xphs.2019.11.011.
23. Couvreur, P.; Stella, B.; Reddy, L.H.; Hillaireau, H.; Dubernet, C.; Desmaële, D.; Lepêtre-Mouelhi, S.; Rocco, F.; Dereuddre-Bosquet, N.; Clayette, P.; et al. Squalenoyl Nanomedicines as Potential Therapeutics. *Nano Lett* **2006**, *6*, 2544–2548, doi:10.1021/nl061942q.
24. Desmaële, D.; Gref, R.; Couvreur, P. Squalenoylation: A Generic Platform for Nanoparticular Drug Delivery. *J Control Release* **2012**, *161*, 609–618, doi:10.1016/j.jconrel.2011.07.038.
25. Ho, D.-K.; Christmann, R.; Murgia, X.; De Rossi, C.; Frisch, S.; Koch, M.; Schaefer, U.F.; Loretz, B.; Desmaele, D.; Couvreur, P.; et al. Synthesis and Biopharmaceutical Characterization of Amphiphilic Squalenyl Derivative Based Versatile Drug Delivery Platform. *Front Chem* **2020**, *8*, 584242, doi:10.3389/fchem.2020.584242.
26. Ralay-Ranaivo, B.; Desmaële, D.; Bianchini, E.P.; Lepeltier, E.; Bourgaux, C.; Borgel, D.; Pouget, T.; Tranchant, J.F.; Couvreur, P.; Gref, R. Novel Self Assembling Nanoparticles for the Oral Administration of Fondaparinux: Synthesis, Characterization and in Vivo Evaluation. *J Control Release* **2014**, *194*, 323–331, doi:10.1016/j.jconrel.2014.07.060.
27. Oliveira, M.S.; Goulart, G.C.A.; Ferreira, L.A.M.; Carneiro, G. Hydrophobic Ion Pairing as a Strategy to Improve Drug Encapsulation into Lipid Nanocarriers for the Cancer Treatment. *Expert Opin Drug Deliv* **2017**, *14*, 983–995, doi:10.1080/17425247.2017.1266329.
28. Ristroph, K.D.; Prud'homme, R.K. Hydrophobic Ion Pairing: Encapsulating Small Molecules, Peptides, and Proteins into Nanocarriers. *Nanoscale Adv* **2019**, *1*, 4207–4237, doi:10.1039/c9na00308h.
29. Sobot, D.; Mura, S.; Rouquette, M.; Vukosavljevic, B.; Cayre, F.; Buchy, E.; Pieters, G.; Garcia-Argote, S.; Windbergs, M.; Desmaële, D.; et al. Circulating Lipoproteins: A Trojan Horse Guiding Squalenoylated Drugs to LDL-Accumulating Cancer Cells. *Mol Ther* **2017**, *25*, 1596–1605, doi:10.1016/j.ymthe.2017.05.016.
30. Sobot, D.; Mura, S.; Yesylevskyy, S.O.; Dalbin, L.; Cayre, F.; Bort, G.; Mougin, J.; Desmaële, D.; Lepetre-Mouelhi, S.; Pieters, G.; et al. Conjugation of Squalene to

Gemcitabine as Unique Approach Exploiting Endogenous Lipoproteins for Drug Delivery. *Nat Commun* **2017**, *8*, 15678, doi:10.1038/ncomms15678.
31. Versluis, A.J.; van Geel, P.J.; Oppelaar, H.; van Berkel, T.J.; Bijsterbosch, M.K. Receptor-Mediated Uptake of Low-Density Lipoprotein by B16 Melanoma Cells in Vitro and in Vivo in Mice. *Br J Cancer* **1996**, *74*, 525–532, doi:10.1038/bjc.1996.396.
32. Vitols, S.; Angelin, B.; Ericsson, S.; Gahrton, G.; Juliusson, G.; Masquelier, M.; Paul, C.; Peterson, C.; Rudling, M.; Söderberg-Reid, K. Uptake of Low Density Lipoproteins by Human Leukemic Cells in Vivo: Relation to Plasma Lipoprotein Levels and Possible Relevance for Selective Chemotherapy. *Proc Natl Acad Sci U S A* **1990**, *87*, 2598–2602, doi:10.1073/pnas.87.7.2598.
33. Maksimenko, A.; Dosio, F.; Mougin, J.; Ferrero, A.; Wack, S.; Reddy, L.H.; Weyn, A.-A.; Lepeltier, E.; Bourgaux, C.; Stella, B.; et al. A Unique Squalenoylated and Nonpegylated Doxorubicin Nanomedicine with Systemic Long-Circulating Properties and Anticancer Activity. *Proc Natl Acad Sci U S A* **2014**, *111*, E217-226, doi:10.1073/pnas.1313459110.
34. Fessi, H.; Puisieux, F.; Devissaguet, J.Ph.; Ammoury, N.; Benita, S. Nanocapsule Formation by Interfacial Polymer Deposition Following Solvent Displacement. *International Journal of Pharmaceutics* **1989**, *55*, R1–R4, doi:10.1016/0378-5173(89)90281-0.
35. Milletti, F.; Storchi, L.; Sforna, G.; Cruciani, G. New and Original PKa Prediction Method Using Grid Molecular Interaction Fields. *J Chem Inf Model* **2007**, *47*, 2172–2181, doi:10.1021/ci700018y.
36. Decherchi, S.; Bottegoni, G.; Spitaleri, A.; Rocchia, W.; Cavalli, A. BiKi Life Sciences: A New Suite for Molecular Dynamics and Related Methods in Drug Discovery. *J Chem Inf Model* **2018**, *58*, 219–224, doi:10.1021/acs.jcim.7b00680.
37. Spyrakis, F.; Benedetti, P.; Decherchi, S.; Rocchia, W.; Cavalli, A.; Alcaro, S.; Ortuso, F.; Baroni, M.; Cruciani, G. A Pipeline To Enhance Ligand Virtual Screening: Integrating Molecular Dynamics and Fingerprints for Ligand and Proteins. *J Chem Inf Model* **2015**, *55*, 2256–2274, doi:10.1021/acs.jcim.5b00169.
38. Riganti, C.; Pinto, H.; Bolli, E.; Belisario, D.C.; Calogero, R.A.; Bosia, A.; Cavallo, F. Atorvastatin Modulates Anti-Proliferative and pro-Proliferative Signals in Her2/Neu-Positive Mammary Cancer. *Biochem Pharmacol* **2011**, *82*, 1079–1089, doi:10.1016/j.bcp.2011.07.079.
39. Kopecka, J.; Campia, I.; Jacobs, A.; Frei, A.P.; Ghigo, D.; Wollscheid, B.; Riganti, C. Carbonic Anhydrase XII Is a New Therapeutic Target to Overcome Chemoresistance in Cancer Cells. *Oncotarget* **2015**, *6*, 6776–6793, doi:10.18632/oncotarget.2882.
40. Lepeltier, E.; Bourgaux, C.; Amenitsch, H.; Rosilio, V.; Lepetre-Mouelhi, S.; Zouhiri, F.; Desmaële, D.; Couvreur, P. Influence of the Nanoprecipitation Conditions on the Supramolecular Structure of Squalenoyled Nanoparticles. *European Journal of Pharmaceutics and Biopharmaceutics* **2015**, *96*, 89–95, doi:10.1016/j.ejpb.2015.07.004.
41. Ho, D.-K.; Murgia, X.; De Rossi, C.; Christmann, R.; Hüfner de Mello Martins, A.G.; Koch, M.; Andreas, A.; Herrmann, J.; Müller, R.; Empting, M.; et al. Squalenyl Hydrogen Sulfate Nanoparticles for Simultaneous Delivery of Tobramycin and an Alkylquinolone Quorum Sensing Inhibitor Enable the Eradication of P. Aeruginosa Biofilm Infections. *Angew Chem Int Ed Engl* **2020**, *59*, 10292–10296, doi:10.1002/anie.202001407.
42. Ko, M.; Quiñones-Hinojosa, A.; Rao, R. Emerging Links between Endosomal PH and Cancer. *Cancer Metastasis Rev* **2020**, *39*, 519–534, doi:10.1007/s10555-020-09870-1.
43. Rouquette, M.; Ser-Le Roux, K.; Polrot, M.; Bourgaux, C.; Michel, J.-P.; Testard, F.; Gobeaux, F.; Lepetre-Mouelhi, S. Towards a Clinical Application of Freeze-Dried Squalene-Based Nanomedicines. *J Drug Target* **2019**, *27*, 699–708, doi:10.1080/1061186X.2019.1566340.

44. Yesylevskyy, S.O.; Ramseyer, C.; Savenko, M.; Mura, S.; Couvreur, P. Low-Density Lipoproteins and Human Serum Albumin as Carriers of Squalenoylated Drugs: Insights from Molecular Simulations. *Mol Pharm* **2018**, *15*, 585–591, doi:10.1021/acs.molpharmaceut.7b00952.
45. Goldstein, J.L.; Brown, M.S. The LDL Receptor. *Arterioscler Thromb Vasc Biol* **2009**, *29*, 431–438, doi:10.1161/ATVBAHA.108.179564.
46. Goldstein, J.L.; Brown, M.S. A Century of Cholesterol and Coronaries: From Plaques to Genes to Statins. *Cell* **2015**, *161*, 161–172, doi:10.1016/j.cell.2015.01.036.
47. Cunningham, A.J.; Robinson, M.; Banquy, X.; Leblond, J.; Zhu, X.X. Bile Acid-Based Drug Delivery Systems for Enhanced Doxorubicin Encapsulation: Comparing Hydrophobic and Ionic Interactions in Drug Loading and Release. *Mol Pharm* **2018**, *15*, 1266–1276, doi:10.1021/acs.molpharmaceut.7b01091.

Chapter II

Pentamidine-loaded lipid and polymer nanocarriers as tunable anticancer drug delivery systems

B. Stella, I. Andreana, D. Zonari, S. Arpicco

(Published in 2020)

Poly(lactic-*co*-glycolic) acid (PLGA) nanoparticles (NPs) are excellent candidates for drug encapsulation, owing to the easy preparation, biocompatibility, biodegradability and protection of drugs.

Main aim

The aim of this chapter was a proof of concept to develop lipid and polymer nanosystems to propose the clinical repositioning of an antiprotozoal drug molecule.

Specific objectives

- Formulate and optimize pentamidine free base (PTM-B)-loaded PLGA NPs
- Comparisons with lipid-based drug delivery systems
- Evaluation of the *in vitro* anticancer activity of PTM-B-loaded lipid and polymer nanocarries

Highlights of the chapter

- PLGA NPs are biocompatible and biodegradable carriers. Acid end-capped PLGA can interact with PTM-B exploiting its carboxylic groups, ionized at physiological pH
- PTM-B is an old drug approved for its antiprotozoal activity that has anticancer activity which could allow its repositioning for new therapeutical applications. However, PTM-B toxicity *in vivo* prevents its clinical applicability
- Formulation of liposomes and NPs by electrostatic interactions allowed us to tune the NP release profile
- *In vitro* tests showed an increased IC_{50} for encapsulated PTM-B compared to the free drug. This opened the way for designing electrostatically based nanosystems for PTM-B encapsulation.

The studies presented in this chapter have been published as a research article in the Journal of Pharmaceutical Sciences, doi: 10.1016/j.xphs.2019.11.011.
The text is reproduced below.

Journal of Pharmaceutical Sciences 109 (2020) 1297-1302

Contents lists available at ScienceDirect

Journal of Pharmaceutical Sciences

journal homepage: www.jpharmsci.org

Pharmaceutics, Drug Delivery and Pharmaceutical Technology

Pentamidine-Loaded Lipid and Polymer Nanocarriers as Tunable Anticancer Drug Delivery Systems

Barbara Stella*, Ilaria Andreana, Daniele Zonari, Silvia Arpicco*

Dipartimento di Scienza e Tecnologia del Farmaco, Università degli Studi di Torino, Via P. Giuria 9, 10125, Torino, Italy

ARTICLE INFO

Article history:
Received 8 August 2019
Revised 1 October 2019
Accepted 12 November 2019
Available online 18 November 2019

Keywords:
liposomes
nanoparticles
formulation
drug delivery systems
controlled release

ABSTRACT

Initially developed as a synthetic analogue of insulin, pentamidine (PTM) is an antimicrobial drug that has recently shown *in vitro* and *in vivo* anticancer activity. Nevertheless, systemic administration of PTM causes severe side effects, especially nephrotoxicity. Here we propose the association of PTM to different biocompatible nanosystems in order to compare the physicochemical characteristics of the loaded nanocarriers and their influence on the drug cytotoxicity toward cancer cells. In particular, PTM (as free base or with different counterions) was encapsulated into liposomes and poly(lactide-*co*-glycolide) (PLGA) nanoparticles and all the formulations have been deeply characterized concerning mean diameter, polydispersity index, zeta potential, stability, morphology, PTM loading, and drug release profile. The anticancer activity was evaluated on a human ovarian cancer cell line over 72 h. Results showed that PTM is efficiently loaded into liposomes with a transmembrane citrate or sulfate gradient; concerning PLGA nanoparticles, important association occurred, thanks to ionic interactions between the drug and the polymer. The *in vitro* studies confirmed the anticancer activity of PTM, which was gradually released with different profiles depending on the drug form and the nanocarrier structure.

Introduction

Pentamidine (PTM), a diamide composed of 2 phenyl amidine groups linked by a 5-carbon methylene linker, is a Food and Drug Administration–approved drug for the treatment of different parasitic infections, including leishmaniasis, *Pneumocystis carinii* pneumonia, and trypanosomiasis.[1,2] Although much is still elusive about its antiparasitic mechanism, some studies have demonstrated its efficacy in cancer. PTM has shown to be a DNA minor groove binder forming noncovalent complexes with DNA.[3] Pathak et al. demonstrated for the first time the *in vitro* anticancer potential of PTM showing its growth-inhibitory activity when it links to the phosphatase regenerating liver family, a group of oncogenic phosphatases overexpressed in tumor cells; these results were further confirmed in a study in which PTM was combined with chlorpromazine.[4,5] Moreover, PTM is an inhibitor of the DNA endo-exonuclease whose repair processes have a main role in tumor cells. A reduced capacity in DNA repair processes has been reported to take part in cancer cell viability. The action of PTM with the endo-exonuclease may be due to the similar structure of the active site between the endo-exonuclease and phosphatase regenerating liver family.[6] Other studies proved a different anticancer mechanism of PTM, in particular in melanoma, for which p53-binding site on overexpressed S100B protein has been investigated as a target: PTM inhibits the Ca(+)-binding protein S100B and disrupts the S100B-p53 protein-protein interaction, thus restoring wild-type p53 tumor suppressor function in melanoma.[7] Moreover, PTM was found to be active against other cancer models, such as prostate, breast, leukemia, and renal cancers.[8-10]

However, PTM has a poor oral bioavailability, and pharmacokinetic studies after PTM administration by the intravenous route showed interindividual differences in rates of metabolism; moreover, the renal drug clearance was associated with acute kidney injury.[11,12] Thus, several drug delivery strategies have been developed to overcome adverse PTM pharmacokinetics and toxicity, such as by synthesizing PTM bioconjugates[13] or through the association with nanocarriers, but mainly in the treatment of leishmaniasis. In this field, among the different drug delivery nanosystems, liposomes and nanoparticles have been proposed to carry PTM[14,15] and even a recent study using both polycaprolactone nanoparticles and phosphatidylcholine liposomes was performed to compare the *in vitro* transportation of PTM across the blood-brain barrier.[16] On

* *Correspondence to*: Barbara Stella (Telephone: +39-011-6706660) and Silvia Arpicco (Telephone: +39-011-6706668).
E-mail addresses: barbara.stella@unito.it (B. Stella), silvia.arpicco@unito.it (S. Arpicco).

https://doi.org/10.1016/j.xphs.2019.11.011
0022-3549/

the contrary, only a minor effort has been devoted to the use of nanocarriers to deliver PTM in anticancer therapy. Concerning liposomes in this field, Mérian et al. tested some liposomal PTM formulations in order to enhance tumor drug accumulation and lower drug exposure to other tissues. Liposomes were prepared with saturated/unsaturated phospholipids of different chain lengths, tuning cholesterol (CHOL) content, and with or without the presence of PEG on the outer surface in order to optimize the physicochemical characteristics of liposomes. In tumor-bearing mice, liposomal delivery decreased PTM kidney drug levels and increased tumor drug exposure compared to free drug.[17]

Regarding the use of nonliposomal nanocarriers with PTM in anticancer therapy, PTM was associated with PEG-stabilized gold nanoparticles in order to enhance the effect of radiotherapy on triple-negative breast cancer. The results showed that the adsorption of PTM onto the PEG-gold nanoparticle surface increased their cellular uptake. In addition, the combination resulted in a significantly greater number of residual DNA double-strand breaks compared to that of single agents.[18] Moreover, we have recently proposed functionalized mesoporous silica nanoparticles for PTM delivery. Results showed that the tuning of the nanocarrier characteristics may greatly affect the efficacy of PTM encapsulation.[19] Nevertheless, despite the growing interest in the applications of gold and silica nanoparticles in drug delivery technologies, the long-term effects of inorganic materials for nanoparticle preparation are still an open issue.[20]

Besides the reported studies, to the best of our knowledge, a comparative study between PTM-loaded liposomes and polymer nanoparticles for anticancer therapy has not been performed yet. To this aim, here we describe the preparation and the characterization of different PTM-loaded, nontoxic, biocompatible, and biodegradable nanocarriers (i.e., liposomes and poly(lactide-*co*-glycolide) [PLGA] nanoparticles). PLGA is an attractive material for biomedical uses because it is approved for medical application by both Food and Drug Administration and European Medicines Agency and is already widely employed in the biomedical field.[21,22] The cytotoxicity of PTM-loaded nanocarriers was evaluated on the A2780 human ovarian carcinoma cell line. Results showed that the encapsulation of different forms of PTM into lipid or polymer nanosystems allowed the drug release (and, thus, the cytotoxicity) to be tuned and controlled.

Materials and Methods

Materials

All the phospholipids, CHOL, Sepharose CL-4B, PLGA 50:50 (Resomer® RG 502 H), PLGA 75:25 (Resomer® RG 752 H), PEG_{2000}-PLGA 50:50, PTM isethionate, and solvents (analytical grade) were purchased from Sigma-Aldrich (Milan, Italy).

Methods

Preparation of Liposomes and Polymer Nanoparticles Containing PTM

Preparation of Different PTM Forms. Free base form of PTM (PTM-B) was obtained by precipitation of PTM isethionate (PTM-I) solution in alkaline medium and characterized as previously reported.[19] PTM citrate (PTM-C) and PTM sulfate (PTM-S) were obtained by adding dropwise a solution of citrate buffer (150 mM, pH 4.5) or of ammonium sulfate (150 mM, pH 4.0), respectively, to a MilliQ® water solution of PTM-I (100 mg/mL) until the formation of a precipitate. The solutions were then filtered and the resulting precipitates were washed 3 times with MilliQ® water and dried under vacuum. Melting points of PTM-C and PTM-S were determined using a BUCHI Melting Point B-450 (set point: 165°C, heating rate: 2°C/min) and were 207°C and more than 300°C, respectively. The conversion of PTM-I into the desired PTM forms was confirmed by mass spectrometry analysis using electrospray ionization or by atmospheric pressure chemical ionization, in positive ion mode, on a Micromass ZQ spectrometer (Waters, Milan, Italy).

PTM-B-Containing Liposomes

PTM-B-containing liposomes (Lipo PTM-B) were prepared using the thin lipid film-hydration method mixing together 1,2-distearoil-*sn*-glycero-3-phosphocoline (DSPC), CHOL, and 1,2-distearoyl-*sn*-glycero-3-phosphoethanolamine-N-[amino(polyethylene glycol)-2000] (mPEG2000-DSPE) in 82:12:6 molar ratio. PTM-B was added to the lipid mixture in 40% ratio (mol drug/mol lipid). Lipids were dissolved in chloroform and PTM-B in methanol and evaporated by rotary evaporator. The resulting lipid film was hydrated with 900 μL of 4-(2-hydroxyethyl)piperazine-1-ethanesulfonic acid (HEPES) buffer pH 7.4. The suspension was vortex mixed for 10 min and bath sonicated. The formulations were extruded (Extruder; Lipex, Vancouver, Canada) at 60°C under nitrogen through 200-nm polycarbonate membrane (Costar; Corning Incorporated, New York, NY) and then purified by gel filtration using Sepharose CL-4B columns, eluting with HEPES buffer. Liposomes were stored at 4°C.

PTM-C- and PTM-S-containing Liposomes

The liposomes (Lipo PTM-C and Lipo PTM-S) were composed of DSPC, CHOL, and mPEG2000-DSPE in 75:20:5 molar ratio. The lipid film was hydrated with 1 mL of citrate buffer for Lipo PTM-C or ammonium sulfate solution for Lipo PTM-S, vortex mixed, and incubated for 45 min at 60°C. Liposomes were then extruded as previously reported and passed through a Sepharose CL-4B column equilibrated with HEPES buffer to replace the extraliposomal solution. Subsequently, a solution of PTM-I in HEPES buffer (0.75 mg/50 μL for Lipo PTM-C and 0.5 mg/100 μL for Lipo PTM-S) was added to liposome suspension and incubated for 60 min at 60°C. Finally, liposomal preparations were purified by gel filtration as previously reported and stored at 4°C.

PTM-B-containing PLGA Nanoparticles

PTM-B-loaded PLGA nanoparticles were prepared by the nanoprecipitation technique.[23] Practically, for each preparation, to 12 mg of PLGA 50:50 or 75:25 dissolved in acetone, an aliquot of an ethanolic stock solution of PTM-B (5 mg/mL) was added until a total volume of 1 mL. This organic solution was then poured into 2 mL of MilliQ® water under magnetic stirring. Precipitation of nanoparticles occurred spontaneously. After solvent evaporation under reduced pressure, an aqueous suspension was obtained. Further nanoparticle batches were prepared by 1:1 or 1:0.5 (w:w) polymeric blends between PLGA (50:50 or 75:25) and PEG_{2000}-PLGA 50:50 or by PEG_{2000}-PLGA 50:50 alone. To purify the nanoparticles from nonincorporated drug, PTM-B-loaded nanoparticles were extensively dialyzed against MilliQ® water at 4°C (Spectra/Por® 3500 MWCO dialysis membrane; Spectrum, Houston, TX). Unloaded PLGA nanoparticles (i.e., without adding PTM-B) were prepared as well. The particles were then stored at 4°C.

Characterization of PTM-containing Liposomes and Nanoparticles

The mean particle size and the polydispersity index of liposomes and nanoparticles were determined at 25°C by quasi-elastic light scattering using a nanosizer (Nanosizer Nano Z; Malvern

Table 1
Physicochemical Characteristics of Liposomes and PLGA Nanoparticles (NPs) ($N = 3$)

Formulation	Mean Diameter (nm ± SD)	Polydispersity Index	Zeta Potential (mV ± SD)
Lipo PTM-B	125 ± 1.6	0.160	−2.6 ± 1.17
Lipo PTM-C	140 ± 1.4	0.154	−3.6 ± 0.97
Lipo PTM-S	148 ± 2.0	0.106	−3.8 ± 0.92
PLGA 50:50 NPs	134 ± 1.2	0.074	−33.1 ± 1.17
PLGA 75:25 NPs	138 ± 1.3	0.071	−25.3 ± 0.64
PLGA 50:50 NPs PTM-B	120 ± 0.5	0.102	−25.4 ± 0.45
PLGA 75:25 NPs PTM-B	117 ± 0.7	0.097	−22.5 ± 0.72
PEG_{2000}-PLGA NPs PTM-B	77 ± 0.6	0.147	−19.3 ± 0.26
PLGA 50:50/PEG_{2000}-PLGA 1:1 NPs PTM-B	99 ± 1.4	0.086	−14.2 ± 0.36
PLGA 50:50/PEG_{2000}-PLGA 1:0.5 NPs PTM-B	143 ± 1.6	0.158	−15.8 ± 0.86
PLGA 75:25/PEG_{2000}-PLGA 1:1 NPs PTM-B	90 ± 0.5	0.142	−13.9 ± 0.44
PLGA 75:25/PEG_{2000}-PLGA 1:0.5 NPs PTM-B	129 ± 1.2	0.147	−16.6 ± 0.60

Instruments, Malvern, UK). The selected angle was 90° and the measurement was made after dilution of the particulate suspensions in MilliQ® water. The surface charge of liposomes and nanoparticles was evaluated by zeta potential measurements after dilution of the suspensions in 10 mM KCl using the Nanosizer Nano Z. Each measurement was carried out in triplicate.

The nanocarrier morphology was determined by cryogenic-transmission electron microscopy (cryo-TEM) analysis. The diluted samples were dropped onto 300 Mesh holey carbon films (Quantifoil R2/1) and quench-frozen in liquid ethane using a cryo-plunge workstation (made at LPS Orsay). The specimens were then mounted on a precooled Gatan 62 specimen holder, transferred in the microscope (Philips CM120) and observed at an accelerating voltage of 120 kV (Centre Technologique des Microstructures [CTμ], platform of the Université Claude Bernard Lyon 1, Villeurbanne, France).

The amount of PTM incorporated into liposomes and nanoparticles was determined spectrophotometrically (DU 730 UV-vis spectrophotometer; Beckman Coulter, Brea, CA) at 264 nm (PTM-B) or 267 nm (PTM-C and PTM-S). Each sample was analyzed in triplicate. To this aim, 100 μL of liposomal suspensions was diluted in 400 μL of ethanol, vortexed, and centrifuged for 5 min at 6000 rpm and the supernatants were analyzed spectrophotometrically. Phospholipid phosphorous was assessed in each liposome preparation by phosphate assay after destruction with perchloric acid.[24] For PLGA nanoparticles, the formulations were lyophilized and then 4-mg samples were dissolved in 200 μL of dichloromethane. To the solution, methanol (2 mL) was added followed by centrifugation (6000 rpm for 15 min) to completely separate the precipitated polymer.[25] The supernatants were then measured at 264 nm. The concentration of the polymer in the suspension was based on dry weight analysis.

To evaluate the PTM release from the suspensions, the formulations were incubated at pH 7.4 and 37°C in buffer (HEPES 20 mM for liposomes and phosphate-buffered saline 10 mM for nanoparticles) for various periods of time; drug leakage was determined after purification of liposomes by chromatography on Sepharose CL-4B columns, eluting with HEPES buffer, or PLGA nanoparticles by dialysis against MilliQ® water. Then, the drug content was measured as previously described and compared with initial values.

The physical stability of liposome and nanoparticle suspensions in the storage conditions (at 4°C) was determined by evaluating at different interval times the mean diameter, the zeta potential, and the drug leakage.

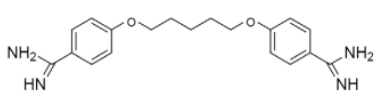

Figure 1. Chemical structure of PTM.

In Vitro *Cell Studies*

Tumor Cell Line Culture

A2780 (human ovarian carcinoma) cells were cultured in RPMI 1640 medium containing 10% fetal bovine serum, 0.03% of L-glutamine, 2% penicillin and streptomycin, and 25 μg/mL of gentamicin sulfate. Cells were maintained in a humidified incubator at 37°C in 5% CO_2.

Cytotoxicity

A2780 cells were seeded at 1×10^4 cells/well in 96-well microtiter plates and incubated overnight to allow cellular adhesion. Various dilutions of PTM-loaded liposomes and selected PLGA nanoparticles were added to the cells in the culture medium in triplicate and incubated for 24, 48, and 72 h. Empty liposomes and nanoparticles, as well as free PTM-B, PTM-C, and PTM-S, were also tested. Cell growth inhibition was evaluated by sulforhodamine B colorimetric proliferation assay, modified by Vichai and Kirtikara.[26]

Results and Discussion

Preparation and Characterization of PTM-containing Liposomes and Nanoparticles

Different forms of PTM (as free base and citrate and sulfate salts) were obtained and incorporated into lipid or polymer nanocarriers to obtain nontoxic, biocompatible, and biodegradable formulations of PTM with favorable characteristics if compared with previously reported nanosystems. In particular, the liposomal formulations described in the literature were obtained using PTM-I and were characterized by a quite low amount of encapsulated drug.[17,27] With the aim to improve the amount of entrapped drug, initially in this work the lipophilic derivative PTM-B was used and 9 different liposomal formulations were prepared changing the phospholipidic mixture composition and the amount of PTM-B added in the lipid film. A liposomal formulation (Lipo PTM-B) characterized by an encapsulation efficiency (EE%) value of 20%, higher than that found in the literature, was obtained; this result was achieved by reducing the CHOL content. However, to further improve the drug loading into the liposomes, the active drug encapsulation technique was exploited *via* citrate and ammonium sulfate method to prepare Lipo PTM-C and Lipo PTM-S, respectively.[28] PTM-C and PTM-S were also prepared to confirm their low water solubility (that was reported to be 0.6 and 1.4 mg/mL, respectively[29]) and to evaluate their UV spectra useful for the quantification of the drug loaded in liposomes. The EE% was around 30% for Lipo PTM-C and around 45% for Lipo PTM-S, confirming that this encapsulation method allows the amount of drug loaded into the liposomes to be increased.

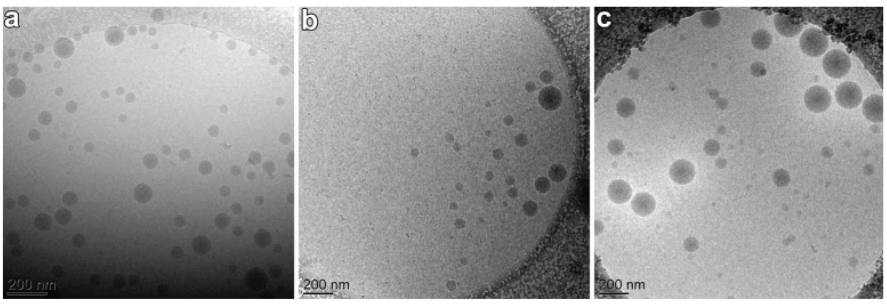

Figure 2. Representative cryo-TEM images of (a) unloaded PLGA 75:25 nanoparticles; (b) PTM-B-loaded PLGA 75:25 nanoparticles; and (c) PTM-B-loaded PLGA 75:25/PEG_{2000}-PLGA 1:0.5 nanoparticles. Bar, 200 nm.

These 2 formulations were then used for further *in vitro* tests and showed similar mean diameter and zeta potential values (Table 1).

PTM-B was also incorporated into PLGA nanoparticles, which were prepared in a single step by nanoprecipitation. Even if PTM was previously associated with poly(D,L-lactide) (PLA) nanoparticles[30] and polymethacrylate nanoparticles[31] for anti-*Leishmania* treatment, here we obtained monodispersed PTM-loaded PLGA nanoparticles without adding any surface-active agent and with high EE% values (95% and 83% for PLGA 50:50 and 75:25, respectively, for a maximum of 30 μg of drug/mg of polymer). These results can be ascribed to the molecular structure of PTM and PLGA: indeed, at physiological pH 7.4, PTM (Fig. 1) has 2 positively charged amidines (p*Ka* = 12), whereas PLGA has negatively charged carboxylic groups. Thus, PTM and PLGA in the nanoparticles interact and stabilize each other by ionic interactions; this phenomenon probably also leads to a decrease in the mean diameter of loaded PLGA nanoparticles if compared with empty carriers (Table 1). Moreover, as previously demonstrated,[31] in this condition PTM release is pH dependent: at acidic pH values, such as in lysosomes, PTM can be released from the polymer to reach its target.

As reported for PLGA nanoparticles prepared for active targeting of African trypanosomiasis,[32] we also obtained PEGylated PLGA nanoparticles; nevertheless, we did not covalently attach PEG to PLGA, but we co-nanoprecipitated 2 PLGA-based polymers (PLGA and PEG_{2000}-PLGA), as previously described.[33] When PEG_{2000}-PLGA was added to the formulations at 1:1 ratio, the mean diameter was lower than 100 nm, whereas it was higher at 1:0.5 ratio (Table 1). Concerning PTM content, while the EE% for PEG_{2000}-PLGA alone was very low (28%), for the polymeric blends PLGA/PEG_{2000}-PLGA it was only slightly lower (88% and 79% for 1:0.5 and 1:1 ratio, respectively) than that of non-PEGylated PLGA nanoparticles. The PLGA nanoparticle zeta potential was negative for all the formulations; however, the incorporation of PTM increased the values in all loaded nanoparticles (Table 1).

To further characterize the nanocarriers, a morphological study was performed by cryo-TEM microscopy. For PLGA nanoparticles, the analysis confirmed the diameter found with quasi-elastic light scattering (Fig. 2); moreover, the observed rounded shape was similar for both empty and PTM-loaded nanoparticles (PEGylated or uncoated). For liposomes, the analysis was applied to assess the physical state of PTM inside the vesicles; to this aim, empty and drug-loaded liposomes were analyzed and the resulting images have been summarized in Figure 3. PTM precipitation was observed inside the liposomes prepared *via* either citrate buffer method or sulfate gradient.

After 4-week storage at 4°C, all the formulations still conserved at least 90%-95% of the initial PTM content and over this period no appreciable size and zeta potential change and no precipitation or aggregation were observed, except for non-PEGylated PLGA nanoparticles, whose diameter showed a tendency to increase after 4 weeks until 200-230 nm.

The drug release profile of liposomes in HEPES buffer at 37°C showed the good stability of the formulations: it was observed that after 24 h only 7% of the less water-soluble PTM-C and 10% of PTM-S were released; after 72 h these values reached 14% for PTM-C and 30% for PTM-S. These results confirm that the precipitation of the drug in the aqueous core of liposomes allows to obtain an important controlled drug release, as previously observed for Doxil®, the commercial liposomal formulation of doxorubicin, in which the drug release was around 5% in buffer at 37°C after 24 h.[34] For PLGA nanoparticles, the PTM-B release was faster, as a consequence of the higher water solubility of PTM-B compared to that of PTM-C and PTM-S: after 24 h the 70% and 63% of the initial amount of PTM-B was released from PLGA 50:50 and PLGA 75:25 nanoparticles, respectively, until about 90% after 72 h. PEGylated PLGA

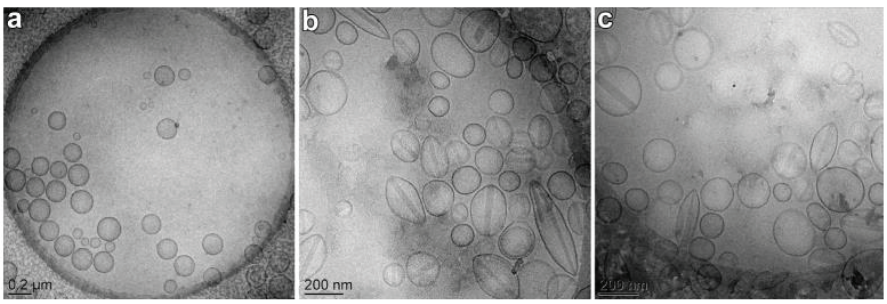

Figure 3. Representative cryo-TEM images of (a) unloaded liposomes; (b) Lipo PTM-C; and (c) Lipo PTM-S. Bar, 200 nm.

Table 2
Cytotoxic Activity (IC_{50}) on Human Tumor Cell Line A2780 at 24, 48, and 72 h. The Values are Arithmetic Means of 3 Determinations ($N = 3$; SD<10% for All Values)

Formulation	IC_{50} (μM) 24 h	IC_{50} (μM) 48 h	IC_{50} (μM) 72 h
PTM-B	8.0	0.5	0.3
PTM-C	6.3	1.1	0.4
PTM-S	6.4	1.2	0.5
Lipo PTM-C	15	4.5	2.1
Lipo PTM-S	45	30	7.3
PLGA 50:50 NPs PTM-B	12	0.8	0.3
PLGA 75:25 NPs PTM-B	14	0.9	0.5
PLGA 50:50/PEG_{2000}-PLGA 1:0.5 NPs PTM-B	11	1.1	0.5
PLGA 75:25/PEG_{2000}-PLGA 1:0.5 NPs PTM-B	8.4	0.9	0.5

nanoparticles showed a similar release profile, with about 75% after 24 h and 100% after 72 h.

Cytotoxicity

The cytotoxic activity of the different forms of PTM and the loaded nanocarriers was tested on A2780 (human ovarian carcinoma) cells at different incubation times (24, 48, and 72 h). Interestingly, to the best of our knowledge, this study reports for the first time an *in vitro* anticancer activity evaluation of PTM encapsulated in liposomes and polymer nanoparticles. Results reported in Table 2 show that the different forms of PTM (i.e., PTM-B, PTM-C, and PTM-S) have similar cytotoxicity profiles despite the different water solubility. Once encapsulated into the nanocarriers (both liposomes and nanoparticles), PTM maintains its anticancer activity, even if it is delayed due to the gradual release from the nanosystems, which show different cytotoxicity profiles. Interestingly, Lipo PTM-S are less cytotoxic than Lipo PTM-C, even if PTM-S presents a better water solubility. Loaded PLGA nanoparticle cytotoxicity is higher than that of liposomes; this can be due to the kinetics of matrix degradation that influences the drug release, but also to the higher water solubility of PTM-B (29.2 mg/L at 25°C) than that of PTM-C and PTM-S (49-fold and 21-fold higher, respectively). Moreover, in PLGA nanoparticles, PTM is dispersed within the polymer matrix, whereas in liposomes it is located in the central aqueous core. PLGA/PEG_{2000}-PLGA 1:1 blends were not tested because they displayed a lower EE% than that of 1:0.5 mixtures.

Unloaded liposomes and nanoparticles did not show any cytotoxic activity at the considered concentration range.

Conclusions

In conclusion, this study highlights the possibility to formulate PTM in liposomes and polymer nanoparticles for anticancer therapy. Moreover, it has been shown that the cytotoxic activity of PTM can be tuned depending on the type of nanocarriers considered and the form of PTM encapsulated. Thus, the nanocarriers here proposed could be considered as a platform for PTM delivery. Moreover, the encapsulation of PTM in lipid and polymer nanocarriers is also a proof of concept that could enlarge the field of application of these PTM drug delivery systems to other pathologies for which PTM has been shown to be active (other than *Leishmania*), such as myotonic dystrophy type 1, with different administration routes.

Funding

This work was supported by the Italian Ministry for University and Research (MIUR)—Università degli Studi di Torino, "Fondi Ricerca Locale (ex-60%)."

Declaration of Interest

None.

Acknowledgments

We would like to acknowledge the contribution of Pierre-Yves Dugas (University of Lyon 1, C2P2 UMR 5265) for cryo-TEM observations at the "Centre Technologique des Microstructures" (CTμ—University of Lyon 1).

References

1. Bray PG, Barrett MP, Ward SA, de Koning HP. Pentamidine uptake and resistance in pathogenic protozoa: past, present and future. *Trends Parasitol*. 2003;19(5):232-239.
2. Bruni N, Stella B, Giraudo L, Della Pepa C, Gastaldi D, Dosio F. Nanostructured delivery systems with improved leishmanicidal activity: a critical review. *Int J Nanomedicine*. 2017;12:5289-5311.
3. Baraldi PG, Bovero A, Fruttarolo F, et al. DNA minor groove binders as potential antitumor and antimicrobial agents. *Med Res Rev*. 2004;24(4):475-528.
4. Pathak MK, Dhawan D, Lindner DJ, Borden EC, Farver C, Yi T. Pentamidine is an inhibitor of PRL phosphatases with anticancer activity. *Mol Cancer Ther*. 2002;1(14):1255-1264.
5. Lee MS, Johansen L, Zhang Y, et al. The novel combination of chlorpromazine and pentamidine exerts synergistic antiproliferative effects through dual mitotic action. *Cancer Res*. 2007;67(23):11359-11367.
6. Chow TY, Alaoui-Jamali MA, Yeh C, Yuen L, Griller D. The DNA double-stranded break repair protein endo-exonuclease as a therapeutic target for cancer. *Mol Cancer Ther*. 2004;3(8):911-919.
7. Smith J, Stewart BJ, Glaysher S, et al. The effect of pentamidine on melanoma ex vivo. *Anticancer Drugs*. 2010;21(2):181-185.
8. Jung HJ, Suh SI, Suh MH, Baek WK, Park JW. Pentamidine reduces expression of hypoxia-inducible factor-1alpha in DU145 and MDA-MB-231 cancer cells. *Cancer Lett*. 2011;303(1):39-46.
9. Qiu G, Jiang J, Liu XS. Pentamidine sensitizes chronic myelogenous leukemia K562 cells to TRAIL-induced apoptosis. *Leuk Res*. 2012;36(11):1417-1421.
10. Zerbini LF, Bhasin MK, de Vasconcellos JF, et al. Computational repositioning and preclinical validation of pentamidine for renal cell cancer. *Mol Cancer Ther*. 2014;13(7):1929-1941.
11. Lidman C, Bronner U, Gustafsson LL, Rombo L. Plasma pentamidine concentrations vary between individuals with Pneumocystis carinii pneumonia and the drug is actively secreted by the kidney. *J Antimicrob Chemother*. 1994;33(4):803-810.
12. Prabhavalkar S, Masengu A, O'Rourke D, Shields J, Courtney A. Nebulized pentamidine-induced acute renal allograft dysfunction. *Case Rep Transpl*. 2013;2013:907593.
13. Scala A, Piperno A, Micale N, et al. "Click" on PLGA-PEG and hyaluronic acid: gaining access to anti-leishmanial pentamidine bioconjugates. *J Biomed Mater Res B Appl Biomater*. 2018;106(8):2778-2785.
14. Ortega V, Giorgio S, de Paula E. Liposomal formulations in the pharmacological treatment of leishmaniasis: a review. *J Liposome Res*. 2017;27(3):234-248.
15. de Almeida L, Terumi Fujimura A, Del Cistia ML, et al. Nanotechnological strategies for treatment of leishmaniasis–a review. *J Biomed Nanotechnol*. 2017;13(2):117-133.
16. Omarch G, Kippie Y, Mentor S, et al. Comparative in vitro transportation of pentamidine across the blood-brain barrier using polycaprolactone nanoparticles and phosphatidylcholine liposomes. *Artif Cells Nanomed Biotechnol*. 2019;47(1):1428-1436.
17. Merian J, De Souza R, Dou Y, Ekdawi SN, Ravenelle F, Allen C. Development of a liposome formulation for improved biodistribution and tumor accumulation of pentamidine for oncology applications. *Int J Pharm*. 2015;488(1-2):154-164.
18. Her S, Cui L, Bristow RG, Allen C. Dual action enhancement of gold nanoparticle radiosensitization by pentamidine in triple negative breast cancer. *Radiat Res*. 2016;185(5):549-562.
19. Peretti E, Miletto I, Stella B, Rocco F, Berlier G, Arpicco S. Strategies to obtain encapsulation and controlled release of pentamidine in mesoporous silica nanoparticles. *Pharmaceutics*. 2018;10(4).
20. De Matteis V. Exposure to inorganic nanoparticles: routes of entry, immune response, biodistribution and in vitro/in vivo toxicity evaluation. *Toxics*. 2017;5(4).
21. Ulery BD, Nair LS, Laurencin CT. Biomedical applications of biodegradable polymers. *J Polym Sci B Polym Phys*. 2011;49(12):832-864.
22. Danhier F, Ansorena E, Silva JM, Coco R, Le Breton A, Preat V. PLGA-based nanoparticles: an overview of biomedical applications. *J Control Release*. 2012;161(2):505-522.
23. Fessi H, Puisieux F, Devissaguet JP, Ammoury N, Benita S. Nanocapsule formation by interfacial polymer deposition following solvent displacement. *Int J Pharm*. 1989;55(1):R1-R4.
24. Bartlett GR. Phosphorus assay in column chromatography. *J Biol Chem*. 1959;234(3):466-468.

25. Mandal TK, Bostanian LA, Graves RA, Chapman SR. Poly(D,L-lactide-co-glycolide) encapsulated poly(vinyl alcohol) hydrogel as a drug delivery system. *Pharm Res*. 2002;19(11):1713-1719.
26. Vichai V, Kirtikara K. Sulforhodamine B colorimetric assay for cytotoxicity screening. *Nat Protoc*. 2006;1(3):1112-1116.
27. Banerjee G, Nandi G, Mahato SB, Pakrashi A, Basu MK. Drug delivery system: targeting of pentamidines to specific sites using sugar grafted liposomes. *J Antimicrob Chemother*. 1996;38(1):145-150.
28. Gubernator J. Active methods of drug loading into liposomes: recent strategies for stable drug entrapment and increased in vivo activity. *Expert Opin Drug Deliv*. 2011;8(5):565-580.
29. Pai S, Alam AS, Kapoor JN. *Pentamidine Salts Useful Treatment Prophylaxis Pneumocystis Carinii Pneumonia*. 1989. EP19880310395.
30. Paul M, Fessi H, Laatiris A, et al. Pentamidine-loaded poly(D,L-lactide) nanoparticles: physicochemical properties and stability work. *Int J Pharm*. 1997;159:223-232.
31. Paul M, Durand R, Boulard Y, et al. Physicochemical characteristics of pentamidine-loaded polymethacrylate nanoparticles: implication in the intracellular drug release in Leishmania major infected mice. *J Drug Target*. 1998;5(6):481-490.
32. Arias JL, Unciti-Broceta JD, Maceira J, et al. Nanobody conjugated PLGA nanoparticles for active targeting of African Trypanosomiasis. *J Control Release*. 2015;197:190-198.
33. Colzani B, Speranza G, Dorati R, et al. Design of smart GE11-PLGA/PEG-PLGA blend nanoparticulate platforms for parenteral administration of hydrophilic macromolecular drugs: synthesis, preparation and in vitro/ex vivo characterization. *Int J Pharm*. 2016;511(2):1112-1123.
34. Ohnishi N, Tomida H, Ito Y, Tahara K, Takeuchi H. Characterization of a doxorubicin liposome formulation by a novel in vitro release test methodology using column-switching high-performance liquid chromatography. *Chem Pharm Bull (Tokyo)*. 2014;62(6):538-544.

Chapter III

Role of stabilizers in pharmaceutical formulations

I. Andreana, B. Stella, D. Kryza, G. Lollo, Y. Chevalier

(In preparation)

Electrostatic stabilization is generally provided by particle surface charge and sufficiently high electrostatic repulsion prevents any kind of agglomeration**.** Formulation of PLGA NPs using acid end-capped PLGA leads to colloidal stability by the presence of dissociating carboxylic groups in water media.

Main aim

The aim of this chapter was to investigate the role of stabilizers in PLGA-based colloidal suspensions in water or complex media.

Specific objectives

- Formulation of PLGA NPs by nanoprecipitation and microfluidic technique
- Evaluation of critical coagulation concentration (*CCC*) in water media by increasing electrolytes concentrations
- Evaluation of colloidal stability in protein-containing media

Highlights of the chapter

- Influence of NPs size on colloidal stability. Acid-terminated PLGA NPs were prepared by nanoprecipitation and microfluidic technique to tune the particle size.
- Coagulation regime in presence of different electrolyte concentrations was related to NP mean diameter. A faster destabilization rate occurred for sub-100 nm NPs.
- The presence of albumin in complex media enhanced the stabilization of PLGA NPs. Stearic hindrance can be exploited by the adsorption of protein on particle surface.

Role of stabilizers in pharmaceutical formulations

Ilaria Andreana[a,b], Barbara Stella[a], David Kryza[b,c], Giovanna Lollo[b], Yves Chevalier[b,*]

[a] *Dipartimento di Scienza e Tecnologia del Farmaco, Università degli Studi di Torino, Via P. Giuria 9, 10125 Torino, Italy*

[b] *Laboratoire d'Automatique, de Génie des Procédés et de Génie Pharmaceutique, Université Claude Bernard Lyon 1, CNRS UMR 5007, 43 bd 11 Novembre 1918, 69622, Villeurbanne, France*

[c] *Hospices Civils de Lyon, 69437 Lyon, France*

***Correspondence to:**

Yves Chevalier. Postal address : Laboratoire d'Automatique, de Génie des Procédés et de Génie Pharmaceutique, Université Claude Bernard Lyon 1, CNRS UMR 5007, 43 bd 11 Novembre 1918, 69622, Villeurbanne, France. E-mail address: yves.chevalier@univ-lyon1.fr

Abstract

In nanoparticulate engineering for drug delivery systems, the addition of stabilizers represents the most used strategy to improve the stability of nanosuspensions. However, the real usefulness of stabilizers may be questioned in the case of nanoparticles made of acid-terminated PLGA. Indeed, the ionizable carboxylic acid groups bring negative charges at the surface of nanoparticles that stabilize them through electrostatic repulsions. The purpose of the present work is to investigate the efficiency of such stabilization and infer the usefulness of an extra stabilization by polymeric stabilizers. Nanoparticles were prepared by nanoprecipitation technique and microfluidic process to assess nanoparticles characterized by different mean diameters. Evaluation of the destabilization of acid-terminated PLGA nanoparticles upon addition of electrolytes highlighted a regime of slow destabilization rate at salt concentrations below the critical coagulation concentration (*CCC*) and a fast coagulation regime above the *CCC*. Addition of dispersants improves the stabilization, but it is actually not required because the *CCC* is found higher than the salt concentration in physiological conditions. Moreover, the presence of serum albumin improves the colloidal stability, even without surface absorption of stabilizers. Acid-terminated PLGA nanoparticles can reach stability due to their interaction with albumin that creates itself a steric hindrance to stabilize the nanosuspension, making nanoparticles suitable for parental administration. In conclusion, this study draws attention to the role of stabilizers in the field of nanomedicine.

Key words: PLGA, CCC, stabilizers, nanoparticles

1. Introduction

Generally, the colloidal stability of nanosuspensions is determined by the sum of interaction forces on nanoparticle surfaces, such as van der Waals electrostatic forces. The combination of these interactions forms the basis of DLVO theory of colloidal stability [1]. The perfect combination of repulsive and attractive forces avoids reversible or even irreversible coagulation of nanoparticles. Electrostatic stabilization is generally provided by particle surface charge and sufficiently high electrostatic repulsion prevents any kind of agglomeration [2]. Poly(lactic-*co*-glycolic) acid (PLGA) nanoparticles are commonly used as drug delivery systems due to their biodegradability and biocompatibility, drug protection, higher stability, tunable drug release, and higher drug safety that can be adjusted by controlling the characteristics of PLGA [3–6]. PLGA is usually commercialized with different end-capping. Formulation of PLGA nanoparticles using acid end-capped PLGA leads to colloidal stability by the presence of dissociating carboxylic groups in water media. Indeed, acid end-capped PLGA is electrically charged and used to obtain negatively charged nanoparticles for biomedical applications [7].
However, the colloidal stability of PLGA nanoparticles can be strongly affected by the composition of aqueous media. Destabilization of ester end-capped PLGA has been demonstrated in presence of high electrolyte solution concentrations in aqueous media [8]. The use of several molecules, called stabilizers, represents the main strategy to avoid nanoparticle aggregation. Thus, the ability of biocompatible macromolecules to adsorb on nanoparticle surface was studied to prevent flocculation or aggregation. It has been proved that the screen effect and surface hindrance properties of several macromolecules (*i.e.* poloxamer, poly(vinyl alcohol) (PVA)) can improve the stability of nanocarriers at storage conditions [9–11]. Santander-Ortega *et al*. demonstrated that Pluronic-coated PLGA nanoparticles have different stability patterns depending on the poloxamer coverage and the stability of nanosystems was governed by DLVO interactions at any stabilizer concentration [12]. However, the potential toxicity *in vitro* or *in vivo* of stabilizers is one of the main concerns in the nanomedicine field [13]. In this work, the influence of electrolyte concentration in aqueous media was assessed in presence or not of stabilizers for acid-terminated PLGA nanoparticles. Sodium chloride (NaCl) was used as a background electrolyte which adsorbed on nanoparticle surface, reducing negative surface charge and occurring in destabilization and consequently aggregation of nanosuspension. Turbidity study of coagulation kinetics was performed and the critical coagulation concentration (*CCC*) and stability factor *W* were specified. Moreover, we assessed the coagulation regime of PLGA nanoparticles prepared by classical nanoprecipitation

technique and microfluidic process, tuning the particle size [14]. In this way, we highlighted the correlation between nanoparticle size and coagulation regime. Indeed, sub-100 nm sized nanoparticles corresponded to a faster coagulation rate.

Furthermore, the behavior of stabilizer-free PLGA nanoparticles was assessed in bovine serum albumin (BSA)-containing media to investigate the role of blood protein in colloidal stability [15]. The adsorption of albumin on PLGA surface determined increased colloidal stability of the nanosystem. It is noteworthy, since, in the nanomedicine field, drug delivery systems are used for parental administration of active molecules. In complex media, the presence of serum proteins can enhance the stability of PLGA nanoparticles even without the use of stabilizers during the formulation process, which results useless in acid end-capped PLGA nanoparticles.

2. Materials and methods

2.1. Materials

PLGA 75:25 (Resomer® RG 752 H, M_w = 4-15 kDa, analytical grade), Pluronic F68, PVA (87-89% hydrolyzed, M_w 13-23 kDa), BSA (>96%) and solvents were purchased from Sigma-Aldrich® (St Quentin-Fallavier, France).

2.2. Preparation of PLGA nanoparticles by the nanoprecipitation technique

PLGA nanoparticles were prepared by nanoprecipitation technique [16]. Practically, 200 mg of PLGA were dissolved in 9.30 g of acetone. The organic solution was added to 100 mL of distilled water under magnetic stirring (600 rpm) and precipitation of nanoparticles occurred spontaneously. Then, the organic phase was evaporated by rotary evaporation under pressure at 40 °C. The complete evaporation was checked by measuring the mass loss. Nanoparticles were stored at 4 °C.

2.3. Preparation of PLGA nanoparticles by microfluidic technique

PLGA nanoparticles were produced using a benchtop NanoAssemblr™ (Precision NanoSystem, Inc., Vancouver, Canada). Disposable cartridges were employed together with the automated NanoAssemblr™. For each preparation, a solution of 55 mg of PLGA 75:25 in 5.5 mL acetonitrile was injected into the microfluidic device through one port of the NanoAssemblr™ instrument. The aqueous phase was simultaneously injected through the second port of the system so as to maintain a constant 1:2 organic:aqueous flow rate ratio and 12 mL/min total flow rate. Nanoparticle products were gathered in a 15 mL Falcon tube. After

evaporation of acetonitrile under reduced pressure, an aqueous suspension of nanoparticles was obtained. It was diluted with water to 2 mg/mL final concentration.

2.4. Physicochemical characterization of polymer nanoparticles

The hydrodynamic diameter and polydispersity index (PDI) of the prepared nanoparticles were measured by dynamic light scattering (DLS) using a Zetasizer Nano-ZS (Malvern Panalytical, Malvern, UK). The scattering angle was 173° and the measurement was carried out at 25 °C after dilution of the suspension in Milli Q water. The zeta potential (ζ) of nanoparticles was determined by electrophoretic mobility measurements using the Nanosizer Nano-ZS. U-shaped tubes equipped with electrodes (DTS 1070) were filled with the suspensions after appropriate dilution. The electrophoretic mobility was converted into ζ potential from the Henry equation under the Smoluchowski approximation.

2.5. Morphology of nanoparticles using transmission electron microscopy

The morphology of nanoparticles prepared by microfluidic technique was evaluated by transmission electron microscopy (TEM) analysis. TEM was performed with a Philips CM120 microscope at the Centre Technologique des Microstructures (CTμ) of the University Lyon 1 (http://microscopies.univ-lyon1.fr/). The diluted samples (10 µL at 0.01% concentration) were dropped onto a 200 mesh carbon/formvar microscope grid, stained with a sodium silicotungstate aqueous solution, and slowly dried in open air. The dry samples were observed by TEM under 120 kV acceleration voltage.

2.6. Colloidal stability assay

The colloidal stability of PLGA nanoparticles was studied by time-resolved turbidity measurements [17]. Turbidity measurements were carried out using a UV-vis absorption spectrometer (UV-1800 from Shimadzu) in quartz cuvettes of optical path l=1 cm at a wavelength of 600 nm. The absorbance (optical density, *OD*) was converted into turbidity (τ expressed in cm^{-1}) by $\tau = \ln(10)\frac{OD}{l}$. To study the influence of concentration of NaCl solutions (0.1-1 M) on the stability of PLGA nanoparticles with or without stabilizers, equal volumes (0.5 mL) of aqueous nanoparticles dispersions, and water or electrolyte solution of twice the target concentration were mixed in the measurement cuvette under fast magnetic stirring. The turbidity was recorded as a function of time, time of zero being the set as the moment when the salt solution was poured into the nanoparticle suspension. The effects of interparticle

interactions on the kinetics of aggregation of the colloidal suspension are expressed *via* the Fuchs stability ratio (*W*) [18], as presented in Section 2. The stability ratio, also namely Fuchs factor, defines the ratio of the total number of inter-particle collisions that results in the aggregating of colloidal dispersion. The rate of slow aggregation, which depends on the number of collisions, can be obtained by the following expression:

$$W = \frac{K_f}{K_s} = \frac{\left(\left(\frac{d\tau}{dt}\right)_{t\to 0}\right)_{fast}}{\left(\left({}^{d\tau}/_{dt}\right)_{t\to 0}\right)_{slow}} \quad (1)$$

where K_f and K_s are the fast and slow coagulation kinetic constants, respectively. $I(t)$ is the variation of the total light scattered intensity with time. According to the aggregation model of Lips *et al*. [19], the initial slope of $\tau(t)$ for two different colloidal dispersions is proportional to the aggregation rate constant at equal concentrations, *C*, of the two colloidal suspensions. The rate of coagulation in a colloidal dispersion depends on the concentration of the dispersions by the expression:

$$\left(\frac{dI}{dt}\right)_{t\to 0} = K_s FC \quad (2)$$

where *F* is an optical factor depending on the light scattering angle and the wavelength of the scattered light [20,21]. Information about the aggregation rate was obtained by plotting the turbidity *versus* time. To the slope of the curve, the critical coagulation concentration (*CCC*) was calculated.

3. Results

3.1. Characterization of nanoparticles

PLGA nanoparticles of different sizes were prepared by the conventional nanoprecipitation process and an innovative microfluidic technique. To this end, PLGA was dissolved in either acetone or acetonitrile and then added into the aqueous phase, by manual addition or mixed in the microfluidic device. The mean particle diameter of nanoprecipitation-prepared PLGA nanoparticles was around 150 nm and ζ was -35 mV, depending on carboxylic groups of PLGA. Microfluidic process was set up to tune nanoparticle size. Indeed, a high total flow rate of 12 mL/min yielded nanoparticles of sub-100 nm size, as already described in the literature [22]. Nanoparticles presented a smaller diameter around 90 nm, compared to the nanoprecipitated nanoparticles. The morphology of nanocarriers was investigated by TEM microscopy. The nanoparticles show a homogeneous core and a spherical shape, typical of PLGA nanoparticles

[23]. Moreover, TEM images showed nanoparticle mean diameter around 60 nm, confirming the sub-100 nm hydrodynamic diameter found by DLS analysis (Fig. 1). All information of sizes is given in Table 1.

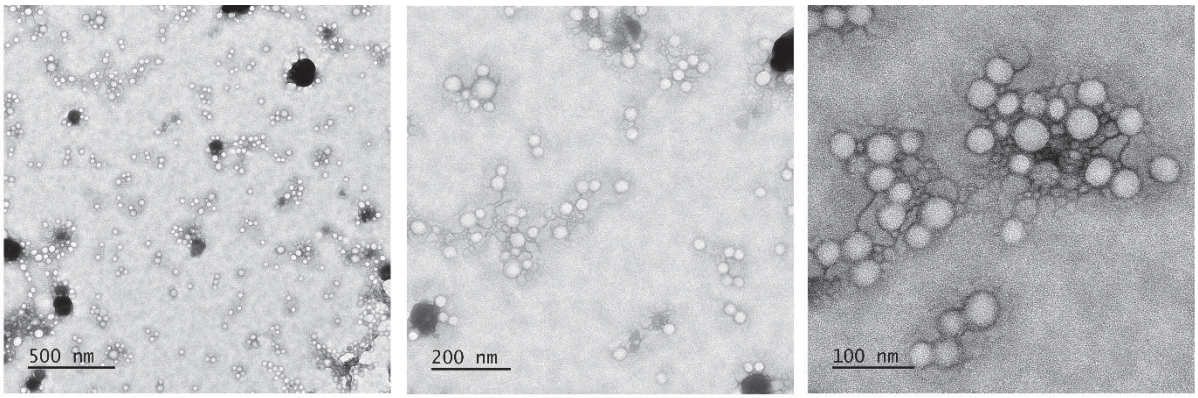

Fig. 1. TEM images of PLGA nanoparticles prepared by microfluidic procedure.

Table 1 Mean diameter, zeta potential (ζ) and critical coagulation concentration (*CCC*) of PLGA nanoparticles prepared by two different techniques.

Nanoprecipitation		**Microfluidic**	
Size (nm ± SEM)	ζ (mV ± SEM)	Size (nm ± SEM)	ζ (mV ± SEM)
150 ± 1	−35 ± 2	93 ± 1	−50 ± 2

3.2. Colloidal stability of bare particles

Sets of experiments were performed to determine different properties of PLGA nanoparticles prepared either by classical nanoprecipitation technique or microfluidic process. Colloidal stability as a function of the electrolyte concentration was assessed in the presence or not of stabilizers. For all the measurements, we kept the same concentration of 1 mg/mL PLGA to avoid the influence of this parameter on the colloidal behavior at measured pH of 6.56.

The colloidal stability of the complexes was analyzed by the turbidity variation as a function of increased ionic strength, using NaCl from 0.1 to 1 M concentrations. The stability of PLGA nanoparticles was evaluated by calculating the Fuchs stability ratio *W* [24,25] *versus* the salt concentration that induces the aggregation process. When 1 mL of salt solution was added into 1 mL of PLGA suspension, the turbidity varied because the concentration of nanoparticles (and salt) is reduced to its half during a very short mixing time (Fig. 2A,B). *W* is calculated from the

short time limiting slopes of the recorded curves of the turbidity against time $\lim_{t\to 0}\left[\frac{d\tau(t)}{dt}\right]$. As the NaCl concentration increases, this slope increases and finally assumes a constant maximum value at high NaCl concentration, which corresponds to the fast coagulation regime. The plots of Log(*W*) against Log[NaCl] (Fig. 2C,D) clearly show the two regimes of slow and fast coagulation. The salt concentration at the crossover is defined as the *CCC* [26]. The experimental *CCC* were around 0.390 M and 0.220 M for the nanoprecipitated and the microfluidic-based nanoparticles, respectively. The higher *CCC* of the nanoprecipitated particles indicate a higher stability coming from electrostatic repulsions. The coagulation of colloidal particles is affected by their mean diameter (150 nm for the nanoprecipitated against 90 nm for the microfluidic-based nanoparticles). Indeed, the surface charge density of nanoparticles is proportionally related to the volume-to-area ratio (*V*/*A*) of the nanoparticles. Each PLGA macromolecule has one negatively charged carboxylic group at one of its chain ends. Therefore, the charge of a PLGA particle is given by the number of contained PLGA macromolecules, that is, to the volume of the particle. The surface charge density is higher for larger particles (of radius *R*) because $V/A = R/3$ for spheres [27]. The higher *CCC* of larger nanoprecipitated nanoparticles is in accordance with their higher surface charge density. It is worth noticing that the *CCC* for both PLGA formulations were larger than that of physiological serum whose concentration of NaCl is 0.150 M. Therefore, electrostatic repulsions coming from the charged chain ends of PLGA are efficient enough for ensuring the colloidal stability in the framework of parenteral administration. The stability is good in pure water and it is in the slow coagulation regime in serum.

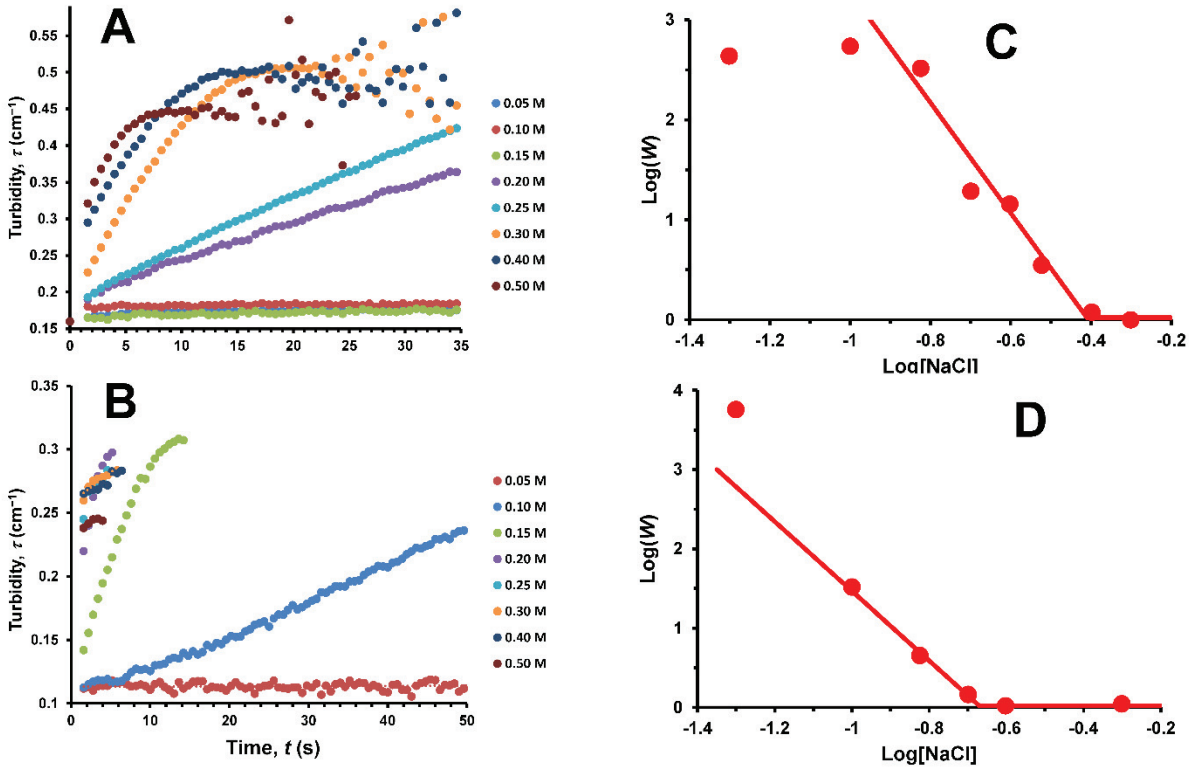

Fig. 2. Turbidity variation in function of salt additions at increasing concentrations of NaCl. (A) Nanoprecipitation and (B) microfluidic technique. (C-D) Stability ratio *versus* NaCl and *CCC* calculation. (C) Nanoprecipitation and (D) microfluidic technique.

3.3. Colloidal stability of nanoparticles coated by PVA and Pluronic F68

Coating the PLGA particle surface with a small amount of adsorbed polymeric stabilizer brings a supplementary steric stabilization [28]. PVA partially hydrolyzed and Pluronic F68 are two of the most commonly used dispersing agents for colloidal suspensions [29,30]. In this set of experiments, the colloidal stability in presence of stabilizers was evaluated in the way as for bare nanoparticles. For each preparation, PVA and Pluronic F68 were added after the preparation of PLGA nanoparticles at the commonly used 1% w/v concentration to improve the colloidal stability. No variation of turbidity was observed after the addition of NaCl at different concentrations (Fig. 3), confirming the stability of PLGA nanoparticles by steric hindrance of these dispersing agents. Moreover, DLS measurements did not detect any variation of the nanoparticle mean diameter after salt addition (data not shown), confirming the nanoparticle stability. Hence, a *CCC* could not be detected due to the absence of a clear slope in the plot of Log(*W*) against Log[NaCl]. Furthermore, the dense coating by adsorbed macromolecules led to a thicker layer on PLGA surface that decreased the ζ value from -35 mV for bare

nanoparticles to -20 mV for polymer-coated nanoparticles. This is due to the shift of the zero-shear plane beyond the polymer layer.

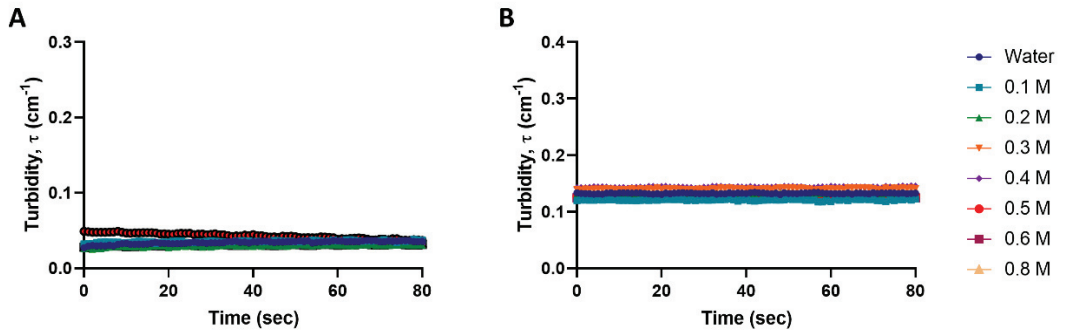

Fig. 3. Turbidity variation in function of salt addition in presence of Pluronic F68. Neither nanoparticles prepared by nanoprecipitation technique (A), nor nanoparticles prepared by microfluidic process (B) showed aggregation after salt addition.

3.4. Stabilization by bovine serum albumin

Upon parenteral administration *in vivo*, nanoparticles undergo interactions with serum proteins. The behavior of nanoparticles can be determined by the complex interplay between the charge state of nanoparticles and proteins [31]. In this context, colloidal stability tests were performed to assess the effect of serum proteins. Albumin is the most common protein found in human serum with a concentration ranging between 35 and 50 g/L. In the last set of experiments, we selected serum albumin at the maximum concentration of 50 g/L to evaluate colloidal stability after salt addition. The interactions between the carboxyl groups of PLGA and the protein amino acids caused adsorption of albumin to the nanoparticles, because albumin contains slightly positively charged amino acids that electrostatically interact with PLGA, stabilizing the nanosystem even by changing its conformation [32]. Although albumin undergoes conformational changes on PLGA surface, its adsorption led to a supplementary steric stabilization in the same way as the PVA or Pluronic F68 dispersing agents. Indeed, the salt-induced destabilization experiments gave the same results (data not shown) as those with PVA or Pluronic F68. Albumin acts as a steric stabilizer of PLGA nanoparticles in the serum after parenteral injection.

4. Conclusions

In this work, it has been demonstrated that the colloidal stability of acidic-terminated PLGA nanoparticles can be achieved without the addition of dispersing agents, even in the presence of moderately concentrated salt solutions, such as the blood serum. For pharmaceutical applications, PLGA nanoparticles can fit for parental administration with no need for supplementary stabilizer. Although the colloidal stability is influenced by the nanoparticles size, the two studied cases in the usual size range of PLGA nanoparticles were in the slow coagulation regime in salt solutions corresponding to physiological media. The presence of serum proteins leads to improved colloidal stability due to protein absorption on the particulate surface. To conclude, drug delivery systems based on negatively charged PLGA do not require the presence of exogenous stabilizers to improve the stability of the formulation. Indeed, PLGA suspensions are stable in pure water, once injected, the salt concentration in the blood shifts the suspension into the slow coagulation regime. At the same time, serum proteins (mainly albumin) adsorb at the surface of nanoparticles, thereby providing very efficient steric stabilization.

References

1. Derjaguin, B.; Landau, L. Theory of the Stability of Strongly Charged Lyophobic Sols and of the Adhesion of Strongly Charged Particles in Solutions of Electrolytes. *Progress in Surface Science* **1993**, *43*, 30–59, doi:10.1016/0079-6816(93)90013-L.
2. Tadros, T. General Principles of Colloid Stability and the Role of Surface Forces. In *Colloid Stability: The Role of Surface Forces - Part I*; 2011; Vol. 1, pp. 1–22 ISBN 978-3-527-31462-1.
3. Kim, S.M.; Patel, M.; Patel, R. PLGA Core-Shell Nano/Microparticle Delivery System for Biomedical Application. *Polymers* **2021**, *13*, doi:10.3390/polym13203471.
4. El-Hammadi, M.M.; Arias, J.L. Recent Advances in the Surface Functionalization of PLGA-Based Nanomedicines. *Nanomaterials (Basel)* **2022**, *12*, 354, doi:10.3390/nano12030354.
5. Huang, P.; Wang, X.; Liang, X.; Yang, J.; Zhang, C.; Kong, D.; Wang, W. Nano-, Micro-, and Macroscale Drug Delivery Systems for Cancer Immunotherapy. *Acta Biomater* **2019**, *85*, 1–26, doi:10.1016/j.actbio.2018.12.028.
6. Li, J.; Zhao, J.; Tan, T.; Liu, M.; Zeng, Z.; Zeng, Y.; Zhang, L.; Fu, C.; Chen, D.; Xie, T. Nanoparticle Drug Delivery System for Glioma and Its Efficacy Improvement Strategies: A Comprehensive Review. *Int J Nanomedicine* **2020**, *15*, 2563–2582, doi:10.2147/IJN.S243223.

7. Stella, B.; Andreana, I.; Zonari, D.; Arpicco, S. Pentamidine-Loaded Lipid and Polymer Nanocarriers as Tunable Anticancer Drug Delivery Systems. *J Pharm Sci* **2020**, *109*, 1297–1302, doi:10.1016/j.xphs.2019.11.011.
8. Saha, D.; Kumar, S.; Ray, D.; Mata, J.; Aswal, V.K. Structure and Stability of Biodegradable Polymer Nanoparticles in Electrolyte Solution. *Materials Letters: X* **2021**, *10*, 100066, doi:10.1016/j.mlblux.2021.100066.
9. Ramirez, J.C.; Flores-Villaseñor, S.E.; Vargas-Reyes, E.; Herrera-Ordonez, J.; Torres-Rincón, S.; Peralta-Rodríguez, R.D. Preparation of PDLLA and PLGA Nanoparticles Stabilized with PVA and a PVA-SDS Mixture: Studies on Particle Size, Degradation and Drug Release. *Journal of Drug Delivery Science and Technology* **2020**, *60*, doi:10.1016/j.jddst.2020.101907.
10. Shkodra-Pula, B.; Grune, C.; Traeger, A.; Vollrath, A.; Schubert, S.; Fischer, D.; Schubert, U.S. Effect of Surfactant on the Size and Stability of PLGA Nanoparticles Encapsulating a Protein Kinase C Inhibitor. *International Journal of Pharmaceutics* **2019**, *566*, 756–764, doi:10.1016/j.ijpharm.2019.05.072.
11. Uskoković, V. Factors Defining the Stability of Poly(Lactide-Co-Glycolide) Spheres for the Sustained Release of a Cysteine Protease Inhibitor. *International Journal of Pharmaceutics* **2020**, *583*, 119316, doi:10.1016/j.ijpharm.2020.119316.
12. Santander-Ortega, M.J.; Jódar-Reyes, A.B.; Csaba, N.; Bastos-González, D.; Ortega-Vinuesa, J.L. Colloidal Stability of Pluronic F68-Coated PLGA Nanoparticles: A Variety of Stabilisation Mechanisms. *J Colloid Interface Sci* **2006**, *302*, 522–529, doi:10.1016/j.jcis.2006.07.031.
13. Menon, J.U.; Kona, S.; Wadajkar, A.S.; Desai, F.; Vadla, A.; Nguyen, K.T. Effects of Surfactants on the Properties of PLGA Nanoparticles. *J Biomed Mater Res A* **2012**, *100*, 1998–2005, doi:10.1002/jbm.a.34040.
14. Operti, M.C.; Bernhardt, A.; Grimm, S.; Engel, A.; Figdor, C.G.; Tagit, O. PLGA-Based Nanomedicines Manufacturing: Technologies Overview and Challenges in Industrial Scale-Up. *International Journal of Pharmaceutics* **2021**, *605*, 120807, doi:10.1016/j.ijpharm.2021.120807.
15. Poller, B.; Painter, G.F.; Walker, G.F. Influence of Albumin in the Microfluidic Synthesis of PEG-PLGA Nanoparticles. *Pharm Nanotechnol* **2019**, *7*, 460–468, doi:10.2174/2211738507666191023091938.
16. Fessi, H.; Puisieux, F.; Devissaguet, J.Ph.; Ammoury, N.; Benita, S. Nanocapsule Formation by Interfacial Polymer Deposition Following Solvent Displacement. *International Journal of Pharmaceutics* **1989**, *55*, R1–R4, doi:10.1016/0378-5173(89)90281-0.
17. Timasheff, S.N. Turbidity as a Criterion of Coagulation. *Journal of Colloid And Interface Science* **1966**, *21*, 489–497, doi:10.1016/0095-8522(66)90047-X.
18. Vaccaro, A.; Sefcik, J.; Morbidelli, M. Characterization of Colloidal Polymer Particles through Stability Ratio Measurements. *Polymer* **2005**, *46*, 1157–1167, doi:10.1016/j.polymer.2004.11.058.
19. Lips, A.; Smart, C.; Willis, E. Light Scattering Studies on a Coagulating Polystyrene Latex. *Trans. Faraday Soc.* **1971**, *67*, 2979–2988, doi:10.1039/TF9716702979.
20. Einarson, M.B.; Berg, J.C. Electrosteric Stabilization of Colloidal Latex Dispersions. *Journal of Colloid and Interface Science* **1993**, *155*, 165–172, doi:10.1006/jcis.1993.1022.
21. Missana, T.; Adell, A. On the Applicability of DLVO Theory to the Prediction of Clay Colloids Stability. *Journal of Colloid and Interface Science* **2000**, *230*, 150–156, doi:10.1006/jcis.2000.7003.

22. Varani. M.; Campagna G.; Bentivoglio V.; Serafinelli M.; Martini M.L.; Galli F.; Signore A. Synthesis and Biodistribution of 99m Tc-Labeled PLGA Nanoparticles by Microfluidic Technique. *Pharmaceutics* **2021**, *13*, doi:10.3390/pharmaceutics13111769.
23. Shi, Y.; xue, J.; Jia, L.; Du, Q.; Niu, J.; Zhang, D. Surface-Modified PLGA Nanoparticles with Chitosan for Oral Delivery of Tolbutamide. *Colloids and Surfaces B: Biointerfaces* **2018**, *161*, 67–72, doi:10.1016/j.colsurfb.2017.10.037.
24. Jia, Z.; Wu, H.; Xie, J.; Morbidelli, M. Effect of Temperature and Surfactant Type on the Stability and Aggregation Behavior of Styrene-Acrylate Copolymer Colloids. *Langmuir* **2007**, *23*, 10323–10332, doi:10.1021/la7013013.
25. Mellema, M.; Van Opheusden, J.H.J.; Van Vliet, T. Relating Colloidal Particle Interactions to Gel Structure Using Brownian Dynamics Simulations and the Fuchs Stability Ratio. *Journal of Chemical Physics* **1999**, *111*, 6129–6135, doi:10.1063/1.479956.
26. Kobayashi, M.; Juillerat, F.; Galletto, P.; Bowen, P.; Borkovec, M. Aggregation and Charging of Colloidal Silica Particles: Effect of Particle Size. *Langmuir* **2005**, *21*, 5761–5769, doi:10.1021/la046829z.
27. Yuan, T.; Gao, L.; Zhan, W.; Dini, D. Effect of Particle Size and Surface Charge on Nanoparticles Diffusion in the Brain White Matter. *Pharm Res* **2022**, doi:10.1007/s11095-022-03222-0.
28. Zhang, F.; Wu, J.; Kang, D.; Zhang, H. Development of a Complex Hydrogel of Hyaluronan and PVA Embedded with Silver Nanoparticles and Its Facile Studies on Escherichia Coli. *Journal of Biomaterials Science, Polymer Edition* **2013**, *24*, 1410–1425, doi:10.1080/09205063.2012.763109.
29. Vallorz, E.L.; Encinas-Basurto, D.; Schnellmann, R.G.; Mansour, H.M. Design, Development, Physicochemical Characterization, and In Vitro Drug Release of Formoterol PEGylated PLGA Polymeric Nanoparticles. *Pharmaceutics* **2022**, *14*, 638, doi:10.3390/pharmaceutics14030638.
30. Hering, I.; Eilebrecht, E.; Parnham, M.J.; Günday-Türeli, N.; Türeli, A.E.; Weiler, M.; Schäfers, C.; Fenske, M.; Wacker, M.G. Evaluation of Potential Environmental Toxicity of Polymeric Nanomaterials and Surfactants. *Environ Toxicol Pharmacol* **2020**, *76*, 103353, doi:10.1016/j.etap.2020.103353.
31. Bolaños, K.; Kogan, M.J.; Araya, E. Capping Gold Nanoparticles with Albumin to Improve Their Biomedical Properties. *Int J Nanomedicine* **2019**, *14*, 6387–6406, doi:10.2147/IJN.S210992.
32. Ali, M.S.; Uttinger, M.J.; Romeis, S.; Schmidt, J.; Peukert, W. Effect of Protein Adsorption on the Dissolution Kinetics of Silica Nanoparticles. *Colloids and Surfaces B: Biointerfaces* **2022**, *214*, doi:10.1016/j.colsurfb.2022.112466.

Chapter IV

Manufacturing translation of polymer nanoparticles: from conventional batch to microfluidic process

I. Andreana, B. Stella, S. Arpicco, C. Bordes, Y. Chevalier, R. Mounier, G. Juban, D. Kryza, G. Lollo

(In preparation)

Polymer nanoparticles (NPs) have been widely studied for the delivery of several molecules (*e.g.* small molecules, proteins, antibodies). However, for their potential application as nanotechnological tools, preparation methods need to be improved.

Main aim

The aim of this chapter was the translation of PLGA NPs production from a classical method (nanoprecipitation) to the microfluidic technique. A complete characterization of PLGA formulations was carried out to study the process translation.

Specific objectives

- Prepare drug-loaded PLGA NPs using classical nanoprecipitation and microfluidic technique; physicochemically characterize the two systems
- Asses formulation and process variables on transposed formulation
- Study the influence of flow rate ratio (FRR), drug and polymer concentration to increase encapsulation efficiency and drug loading in microfluidic-prepared formulation

Highlights of the chapter

- Microfluidic technique is a promising tool to overcome the manufacturing limitations of classical preparation methods. It showed high reproducibility, controlled physicochemical properties of NPs and easy scale-up.
- Microfluidic process can modulate the physicochemical characteristic of drug-loaded PLGA NPs
- The elimination of organic solvent residual is a key point to increase drug encapsulation and release profile. Dialysis method allowed a complete elimination of unencapsulated drug, leading to a complete encapsulation of active molecule
- A Design of Experiments (DoE) evaluated how FRR and polymer and drug concentration affect the encapsulation efficiency and drug loading of a hydrophobic model drug

Manufacturing translation of polymer nanoparticles: from conventional batch to microfluidic process

Ilaria Andreana[a,b], Barbara Stella[a], Silvia Arpicco[a], Claire Bordes[b], Yves Chevalier[b], Rémi Mounier[c], Gaëtan Juban[c], David Kryza[b,d], Giovanna Lollo[b,*]

[a] *Dipartimento di Scienza e Tecnologia del Farmaco, Università degli Studi di Torino, Via P. Giuria 9, 10125 Torino, Italy*

[b] *Laboratoire d'Automatique, de Génie des Procédés et de Génie Pharmaceutique, Université Claude Bernard Lyon 1, CNRS UMR 5007, 43 bd 11 Novembre 1918, 69622, Villeurbanne, France*

[c] *Institut NeuroMyoGène, Laboratoire de Physiopathologie et Génétique du Neurone et du Muscle, University of Lyon, INSERM U1315, CNRS UMR 5261, Lyon, France*

[d] *Hospices Civils de Lyon, 69437 Lyon, France*

*** Correspondance to:**

Giovanna Lollo. Postal address : Laboratoire d'Automatique, de Génie des Procédés et de Génie Pharmaceutique, Université Claude Bernard Lyon 1, CNRS UMR 5007, 43 bd 11 Novembre 1918, 69622, Villeurbanne, France. E-mail address: giovanna.lollo@univ-lyon1.fr

Abstract

The possibility to control nanoparticle physicochemical properties, scale up the manufacturing process and reduce the batch-to-batch variability are important challenges for the development of nanoparticles. To address these issues, microfluidic has been recently proposed as an advanced production method that precisely controls nanoparticle properties by monitoring the diffusion/emulsification mechanism. Herein, poly(lactic-*co*-glycolic acid) copolymer (PLGA) nanoparticles have been used to study the manufacturing translation process from bulk mixing nanoprecipitation to the microfluidic method. As a model drug, a benzimidazole derivative was chosen and encapsulated into PLGA nanoparticles. Microfluidic-based manufacturing procedure yielded nanoparticles with a smaller size of 80 nm compared to 170 nm of batch production, and a polydispersity index below 0.2. Focus is given to the setting up of the microfluidic system and the conditions required to manufacture polymer nanoparticles. A Design of Experiments (DoE) was set up to describe the effects of process and formulation variables (polymer and drug concentration, flow rate ratio (FRR)) involved in the microfluidic method on encapsulation efficiency and drug loading of the system to reduce drug loss. Then, a freeze-drying study has been performed to improve the long-term storage of microfluidic-prepared PLGA nanoparticles, using trehalose as a cryoprotectant to retain nanoparticle physicochemical properties. In this work, we demonstrated that the translation from nanoprecipitation to microfluidic leads to comparable formulations without alteration of nanosystem properties. Moreover, the drug content can be improved by controlling formulation and process parameters involved in the microfluidic process.

Key words: PLGA, nanoprecipitation, microfluidic, hydrophobic drug, DoE

Graphical abstract

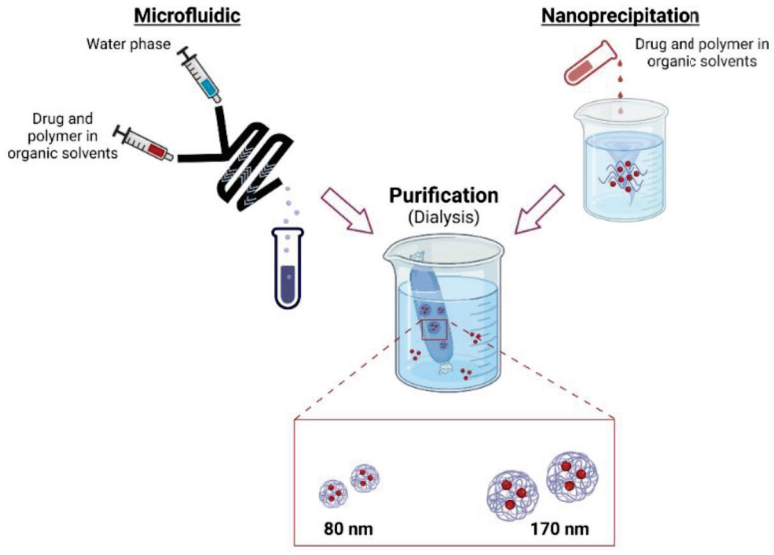

1. Introduction

Nanotechnologies in pharmaceutical fields have been developed to improve therapeutic applications of different water-insoluble drugs by enhancing their solubility and their protection against degradation, controlling drug release and overcoming pharmacokinetics issues [1–3]. Thus, several drug delivery strategies have been established by the design and synthesis of various biocompatible materials [4,5]. Among them, poly(lactic-*co*-glycolic acid) (PLGA) is an attractive material for biomedical uses thanks to its approval both by Food and Drug Administration (FDA) and European Medicines Agency (EMA) for human usage [6,7]. The application of PLGA has been widely studied for the delivery of small molecules [8], proteins and/or sub-structures [9], genetic materials [10,11] and imaging applications [12]. Despite its versatile role in the production of polymer nanoparticles (NPs) as drug delivery systems, the lack of reproducible and scalable processes limits the their clinical translation and commercial use [13,14]. Several methods of NP preparation influence the distribution of the drug into the polymer matrix and/or its absorption on the surface. Emulsification-solvent evaporation technique and nanoprecipitation are the most commonly used preparation techniques, chosen on the basis of the chemical characteristics of the drug molecule to encapsulate [6]. As literature reports, nanoprecipitation technique is described as a straightforward technique to entrap hydrophobic as well as hydrophilic compounds [14,15]. Nevertheless, for conventional production methods some drawbacks concerning batch-to-batch variability, scalability, and production in a continuous manner, make clinical translation of NPs challenging. Recently, to address the urgent need to standardize NP production, microfluidic technique has been used to produce NPs with well-controlled physicochemical properties [16]. The possibility to reach high reproducibility, easy scale-up of the process, continuous production and precisely controlled assembly enhanced the application of this technique [17,18]. The microfluidic-based procedure has been vastly applied for the production on a large scale of mRNA-loaded lipid NPs [19]. The Covid-19 pandemic highlighted the urgent need for a reproducible and conventional procedure to formulate NPs with more controlled physical properties than by bulk production methods [20,21]. Microfluidic-assisted nanoprecipitation requires devices useful to perform a very fast and controlled mixing of water phase and organic water-miscible solvents when injected in a sub-millimeter multilamination mixer [22]. Devices of different architectures have been developed for polymer and lipid delivery systems. Formulation and process parameters have to be adapted to modulate NP features, underlining the importance of these factors on NP manufacturing process. For example, the flow rate of each solution before being mixed is well tunable as a determinative factor in polymer NP size [23,24]. On these bases, in

our study we selected a small benzimidazole molecule as the model drug to compare the formulation of loaded-PLGA NPs by conventional bulk mixing nanoprecipitation technique and microfluidic process. The study aimed to translate the formulation from conventional method to a scalable process, evaluating all the variables involved in the process. In our investigation, to assess the influence of process parameters and formulation variables on drug-loaded PLGA NPs, a design of experiments (DoE) was exploited. The effect of polymer and drug concentration, and process parameters has been studied to modulate the size and the encapsulation efficiency of the system. To obtain a dried form and eliminate the solvent residual, a freeze-drying study has been set up, using trehalose as a cryoprotectant to retain the size and polydispersity of nanosuspensions.

2. Experimental section

2.1 Materials

PLGA 75:25 (Resomer® RG 752 H, M_w = 4-15 kDa) (analytical grade) and 378.3 g/mol D-(+)-trehalose dehydrate (trehalose) used for the freeze-drying study were purchased by Sigma-Aldrich® (St Quentin-Fallavier, France). Small benzimidazole derivative drug (molar mass, M_w = 431.87 g/mol) was ordered from Cliniscience® (Nanterre, France). Spectrum™ Spectra/Por™ Float-A-Lyzer™ G2 Dialysis devices (MWCO = 3.5-5 kDa) were provided by Fisher Scientific (Illkirch, France). Sodium silicotungstate used for staining in TEM was supplied from Agar Scientific (Parsonage Lane, Stansted, UK). Milli Q water was obtained using a Milli Q Academic System (Merk Millipore®, St Quentin-Fallavier, France).

2.2 Water solubility of model drug

A saturated solution of the model drug in Milli Q water was prepared. The solution was stirred at 750 rpm for 3 h at room temperature (RT) and left overnight to reach equilibrium. Then, the sample was centrifuged (14000 rpm, 15 min, RT) and the supernatant was analyzed by ultra-high-performance liquid chromatography (UHPLC).

2.3 Preparation of polymer nanoparticles by nanoprecipitation

Drug-loaded NPs were prepared by the nanoprecipitation technique [25]. Practically, to 6 mg of PLGA 75:25 dissolved in acetonitrile, an aliquot (200 µL) of a methanolic stock solution of drug molecule (5 mg/mL) was added until a total volume of 1 mL. This organic solution was then dropped into 2 mL of Milli Q water under magnetic stirring. Precipitation of NPs occurred

spontaneously. To remove the organic solvent and purify the NPs from the non-incorporated drug, drug-loaded NPs were dialyzed (Spectrum™ Spectra/Por™ Float-A-Lyzer™ G2 Dialysis devices (MWCO = 3.5-5 kDa)) against Milli Q water at room temperature for 1 h. Unloaded NPs, without adding drug molecule, were prepared as well. The water suspension was then stored at 4 °C.

2.4 Preparation of polymer nanoparticles by microfluidic technique

Drug-loaded PLGA NPs were also obtained by microfluidic technique using benchtop NanoAssemblr™ (Precision NanoSystem, Inc., Vancouver, Canada). Disposable cartridges with dimensions of 6.6 × 5.5 × 0.8 cm (w x d x h) with a specific toroidal micromixer were employed together with the automated NanoAssemblr™.

Briefly, to 6 mg of PLGA 75:25 dissolved in acetonitrile, an aliquot (200 µL) of a methanolic stock solution of drug molecule (5 mg/mL) was added until a total volume of 1 mL. The organic phase comprised of the polymer/drug solution was simultaneously injected to the aqueous phase at a 1:2 organic:aqueous flow rate ratio (FRR) and 12 mL/min total flow rate (TFR). To remove the organic solvent and purify the NPs from the non-incorporated drug, drug-loaded NPs were dialyzed against Milli Q water at RT for 1 h. Unloaded NPs were prepared as well. The particles were then stored as colloidal suspensions at 4 °C.

2.5 Physicochemical characterization of blank and loaded nanoparticles

The hydrodynamic diameter, polydispersity index (PDI) and surface potential of the prepared particles were analyzed by dynamic light scattering (DLS) using a Zetasizer Nano-ZS (Malvern Panalytical, Malvern, UK). The angle was set at 173° and measurements were carried out at 25 °C after dilution of the particulate suspension in Milli Q water. The surface charge of NPs was evaluated by zeta potential (ζ) measurements after appropriate dilution of the suspensions using the Nanosizer Nano Z. The physical stability of nanoparticle suspensions in the storage conditions (4 °C) was determined by evaluating at different interval times the mean diameter, the PDI and ζ . Each measurement was carried out in triplicate.

2.6 Morphology of nanoparticles using transmission electron microscopy

The morphology of NPs prepared by microfluidic technique was evaluated by transmission electron microscopy (TEM) analysis. TEM was performed with a Philips CM120 microscope at the Centre Technologique des Microstructures (CTµ) of the University Lyon 1 (Villeurbanne, France). The diluted samples (10 µL) were dropped onto a 200 mesh carbon/formavar

microscope grid (copper support coated with carbon), stained with a sodium silicotungstate aqueous solution, and slowly dried in the open air. The dry samples were observed by TEM under 120 kV acceleration voltage.

2.7 Determination of encapsulation efficiency

The amount of incorporated drug was determined by separating the non-encapsulated drug from loaded NPs by dialysis for 1 h against Milli Q water. The total amount of drug was determined from a fresh aliquot of organic phase used to formulate NPs. The encapsulation efficiency (EE) was calculated as follows (Eq. (1)):

Eq. 1:

$$E.E.(\%) = \frac{A}{B} * 100$$

where A is the amount of entrapped drug after NPs purification and B is the initial amount in the preparation of nanocarriers ×100. The drug loading (DL) was calculated as the ratio between the amount of entrapped drug and the total nanocarrier weight ×100. The amount of incorporated drug was determined by UHPLC. The nanosuspension was diluted with CH_3CN/water mixture 50/50 v/v, acidified by 0.1% TFA, vortexed and filtered through 0.22 µm Nylon filters (Agilent). The UHPLC system consisted of a quaternary pump (Waters™, quaternary solvent manager-R), autosampler (Waters™, sample manager FTN-R), and a multiple wavelength UV detector (Waters, 2998 PDA Detector). The data were processed using Empower 3 (Waters™). The analytical column was a Cortecs C18 column (50 × 4.6 mm, 2.7 µm; Waters) at 40 °C; the mobile phase consisted of waters 0.1% TFA (solvent A) and CH_3CN 0.1% TFA (solvent B) at a flow-rate of 0.5 mL/min with isocratic conditions: 40% A and 60% B. The column effluent was monitored at 254 nm. The quantification of the active molecule was done using calibration curves obtained with standard solution chromatographed in the same experimental conditions, with a concentration range of 0.25-200 µg/mL (R^2>0.995).

2.8 Nanoparticle optimization using a design of experiment (DoE)

A 2^3 full factorial design was used to investigate the effect of three experimental factors (PLGA and drug concentrations, and FRR) and their interactions on NP physicochemical characteristics. For each factor was defined the experimental domain whose lower and upper limits correspond to the coded levels -1 and +1, respectively. The center point corresponds to the coded level 0. As reported in Table 1, the polymer concentration (X_1) was varied from 5-10

mg/mL, FRR (X_2) from 1:2-1:5 and drug amount (X_3) from 0.7-1.4 mg/mL. The studied responses were the encapsulation efficiency (Y_1) and the drug loading (Y_2) as NP characteristics to be well-controlled.

Table 1 Selected experimental factors and their coded levels in the 2^3 full factorial design

Experimental factors	Coded levels		
	- 1	0	+ 1
PLGA conc. (mg/mL) (X_1)	5	7.5	10
FRR (X_2)	1:5	1:3.5	1:2
Drug conc. (mg/mL) (X_3)	0.7	1.1	1.4

The full factorial design consists in 2^3 runs defined as every possible combination of +1 and −1 levels selected in turn and allows calculating a synergistic model, as follows:

$$\hat{y}_i = b_0 + b_1X_1 + b_2X_2 + b_3X_3 + b_{12}X_1X_2 + b_{13}X_1X_3 + b_{23}X_2X_3 \quad \text{(Eq. 2)}$$

where $\hat{y}_i$ is the predicted response for experiment i, b_0 is the intercept, the coefficients b_i correspond to the main effects of the experimental factors (X_i) and the coefficients b_{ij} are the effects of the two-factor interactions.

Two center points were also added in order to estimate the variance of the experimental error and to evaluate the predictive performance of the developed models. The corresponding experimentation plan is presented in Table 3. Multiple linear regression calculations, statistical analysis and response contour plots were performed with Umetrics MODDE 12.0 software (Umetrics, Umeå, Sweden).

2.9 In vitro release study of drug-loaded nanoparticles

To evaluate the drug release from the suspensions, the formulations were incubated at pH 7.4 and 37 °C in phosphate-buffered saline (PBS) 10 mM, simulating physiological conditions. At different time points (0 min, 30 min, 1 h, 3 h, 5 h, 8 h, 24 h), 50 µL of each sample were collected and analyzed by UHPLC for drug quantification. The amount of released drug overtime was calculated from the difference between the initial total amount of the drug present in drug-loaded NPs and the amount of remaining drug in the dialysis bag at different time points. The experiments were performed for NPs prepared using both methods, in triplicate. The same experiment was performed by incubating the free drug in a dialysis bag in PBS at 37 °C.

2.10 Freeze-drying of drug-loaded nanoparticles

Microfluidic-prepared drug-loaded NPs were freeze-dried using the CRYONEXT pilot freeze dryer (Cryotec, Saint-Gély-du-Fesc, France). The suspension was prepared by diluting 1/5 with a solution of trehalose at a final concentration of 12% w/v. The freeze-drying process started reaching an initial cool temperature of -35 °C for 3 h. Then, the temperature of the shelf was increased to -20 °C for 10 h with a chamber pressure of 0.25 mBar to remove ice by sublimation (primary drying). Secondary drying was carried out for 5 h at 4 °C, with 0.1 mBar pressure. Finally, freeze-dried NPs were resuspended in 1 mL of Milli Q water and vortexed until complete dissolution of pellet. Size, PDI, ζ, encapsulation efficiency and storage physical stability at 4 °C of NPs were measured after resuspension. Also, morphological observations using TEM were performed.

2.11 Determination and quantification of organic solvent residuals

Considering two different methods to remove organic solvents, NPs were either dialyzed for 1 h against Milli Q water (Spectrum™ Spectra/Por™ Float-A-Lyzer™ G2 Dialysis devices (MWCO = 3.5-5 kDa)) or evaporated by rotary evaporation under reduced pressure (Rotavapor R-100, Buchi, Cornaredo, Italy). The quantifications of remaining acetonitrile were performed by ^{1}H NMR analysis. ^{1}H NMR spectra were recorded at the NMR technical facility "Centre Commun de RMN" of the University of Lyon on the liquid samples in 5 mm tubes with a liquid-state high-resolution Bruker AVL300 NMR spectrometer operating at 300 MHz under quantitative analysis conditions. The FID was recorded during an acquisition time of 5.5 s after a 90° radiofrequency pulse (14 µs). A delay of 60 s was applied between each scan for ensuring full relaxation of the FID. 8 scans were accumulated with conventional phase cycling. 500 µL of an aqueous suspension of NPs were added to 500 µL of deuterium oxide (D_2O) containing 2% v/v of acetone used as internal standard. Quantification of acetonitrile residuals was done from the integral of the acetonitrile peak at 1.98 ppm and that of the acetone reference peak at 2.15 ppm. The quantification of acetonitrile was performed on lyophilized samples as well.

3. Results and Discussion

3.1 Chemical properties of the drug molecule

The selected model drug is a small benzimidazole derivative, completely insoluble in water having a LogP of 5.6 (predicted). The molecule behavior depends on the presence of a benzimidazole and another acidic group which are both ionized at physiological pH, giving

zwitterion characteristics to the molecule. It was soluble in acetonitrile with a predicted LogP of 0 and very soluble in methanol characterized by a predicted LogP of -0.5. Its solubility increased in methanol due to the enhanced number of hydrogen bond donors compared to acetonitrile. Thus, it has been selected as a model hydrophobic drug for efficiently encapsulation in polymer NPs to overcome pharmacokinetic and pharmacodynamics issues related to *in vivo* administration [26].

3.2 Physicochemical characterization of nanoparticles

Particles were formulated *via* the nanoprecipitation method, using manual dropwise addition in bulk mixing and *via* automatized microfluidic technique. The polymer was dissolved in acetonitrile, the most common solvent used in nanoparticle formulation and tabulated in Class 2 as reported by ICH Q3C "Impurities: guidelines for residual solvents" [27]. The drug molecule was solubilized in methanol obtaining an organic phase mixture miscible with water. The diffusion of the organic mixture into the water phase suddenly decreases the solubility of the polymer and, as a response to this change of hydrophobicity, it immediately self-assemblies to form NPs. In this process, the hydrophobic drug concentrated in the core of the polymer matrix and most of the carboxylic groups of PLGA were exposed on the surface, conferring a negative zeta potential to NPs [8]. Ideally, the nanoprecipitation process should be robust and reproducible to control NPs properties [28]. However, batch-to-batch reproducibility and difficulties in controlling operative parameters limit translation into clinics of drug delivery systems. Microfluidic is an automatized technique that offers precise and homogeneous mixing of the organic solution with the aqueous phase. In our setup to translate the formulation from a conventional production process to a more controlled technique, a toroidal micromixer was connected to the syringes pumps to facilitate hydrodynamic flow focusing (Fig. 1) [16].

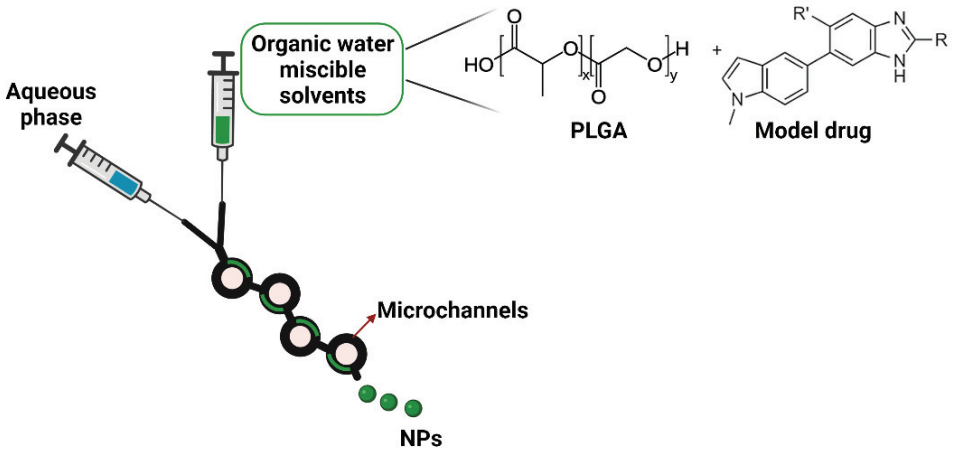

Fig. 1. Schematic representation of the microfluidic micromixer

The particle size is related to the mixing of the organic and aqueous phases. Generally, faster mixing and lower locally amount of organic solvent yield smaller NPs [29]. To evaluate the formulation of size-tailored NPs and investigate the influence on other physicochemical characteristics (*e.g.*, ζ, EE, DL and *in vitro* release), we compared the manual droplet addition in bulk mixing and microfluidic strategy. We formulated the NPs setting a total flow rate (TFR) of 12 mL/min and flow rate ratio (FRR) of 1:2 to obtain sub-100 nm NPs by microfluidics. The TFR is considered one of the microfluidic parameters to tune the size of PLGA NPs. Indeed, the high total combined speed at which the organic and aqueous phases are mixed together results in a faster mixing time which reduces the particle size [29,30]. To compare the microfluidic results with the nanoprecipitation method, we formulated PLGA NPs by manual addition of the organic phase into the aqueous phase under magnetic stirring. The results in Table 2 show the effect of the manufacturing technique on the physicochemical characteristics of nanocarriers. In the controlled-mixing process, we obtained particles in size of 70 or 81 nm, for blank and loaded NPs, respectively, with a slight diameter change in presence of the encapsulated drug. *Via* nanoprecipitation process, we achieved particles with a size above 150 nm (Tab. 2).

Table 2 Physicochemical characterization of blank and loaded PLGA NPs prepared by nanoprecipitation (N) and microfluidic technique (M). Values are given as mean ± SD (*n*=3). NPs nanoparticles; PDI: polydispersity index

Formulation	Size (nm ± SD)	PDI	Zeta Potential (mV ± SD)	EE % ± SD	DL% ± SD
Blank N	147 ± 3	0.05	- 30.5 ± 0.4	/	/
Loaded N	169 ± 15	0.10	- 46.4 ± 7.4	85.0 ± 12.0	10.9 ± 0.4
Blank M	70 ± 2	0.18	- 50.1 ± 1.9	/	/
Loaded M	81 ± 8	0.17	- 49.1 ± 10	75.1 ± 7.8	9.4 ± 1.0

All the preformed formulations yielded monodispersed NPs with the polydispersity index (PDI) in the range of 0.05-0.18.

The spontaneous encapsulation of the model drug occurred during the self-assembling of the particulate system, a classical approach to facilitate the administration in aqueous media of hydrophobic drugs [31]. During the formulation process, the organic solvent needs to be eliminated to avoid destabilization of the system and for *in vitro* and *in vivo* testing. Among the different methods for organic solvent elimination, which include rotary evaporation under pressure and ultracentrifugation, the dialysis method was exploited as an efficient strategy to both eliminate the organic solvent from nanosuspension and purify NPs from the unbound fraction of the drug. The solvent removal methods employed can influence the size and the distribution of the drug through the polymer matrix [32].

Compared to other procedures, dialysis led to a slight increase in the PDI due to the slow removal of the solvents which could facilitate particle growth. However, the dialysis method was selected as the solvent removal technique for its advantages. Indeed, solvent exchange by dialysis is considered a slower process that occurs under equilibrium conditions. This gentle procedure resulted in structural relaxation of the polymer and consequently increased entrapped drug molecules. Results of EE and DL of NPs prepared *via* nanoprecipitation or by microfluidic process showed no significant variation in drug encapsulation (Tab. 2). The dialysis led to the elimination of organic solvents and improved the association of the drug, removing its unentrapped fraction, still solubilized in the organic phase. Therefore, the determined EE referred to the completely encapsulated drug into the polymer matrix.

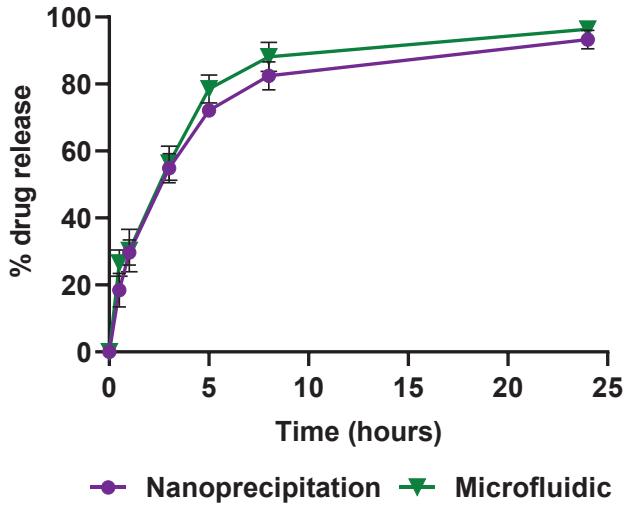

Fig. 2. Release profile of drug-loaded PLGA NPs in PBS medium at 37 °C

The effect of dialysis resulted in a controlled i*n vitro* release, as reported in Fig. 2. Normally, the presence of molecules on the surface of NPs determine an initial burst release, characterized by a complete loss of the drug in a few hours [33]. Purification by dialysis eliminated the fraction of drug adsorbed on the polymer surface leading to a better-controlled drug release profile. Generally, a combination of diffusion and erosion of the polymer matrix leads to drug release from PLGA. Water adsorption by the PLGA occurs immediately, increasing porosity and consequently diffusion of release medium, regardless of NP size. PLGA undergoes degradation by hydrolysis and starts to release the encapsulated drug. In our case, the encapsulation of the drug into the polymer matrix allowed a sustained release of the drug over 8 h in PBS at 37 °C (Fig. 2). After 6 h, 50% of the initial amount of drug was released from the polymer matrix and reached almost 100% after 24 h (Fig. 2). There are no important differences

in release kinetics for loaded nanosuspensions prepared using classical nanoprecipitation or microfluidic process.

To further characterize the nanocarrier prepared by the most reproducible microfluidic technique, a morphological study was performed by TEM microscopy. For blank and loaded NPs, the analysis confirmed the diameter found by DLS (Fig. 3). Moreover, the observed round shape was similar for both empty and loaded NPs, as already reported for PLGA-based nanosystems [34,35].

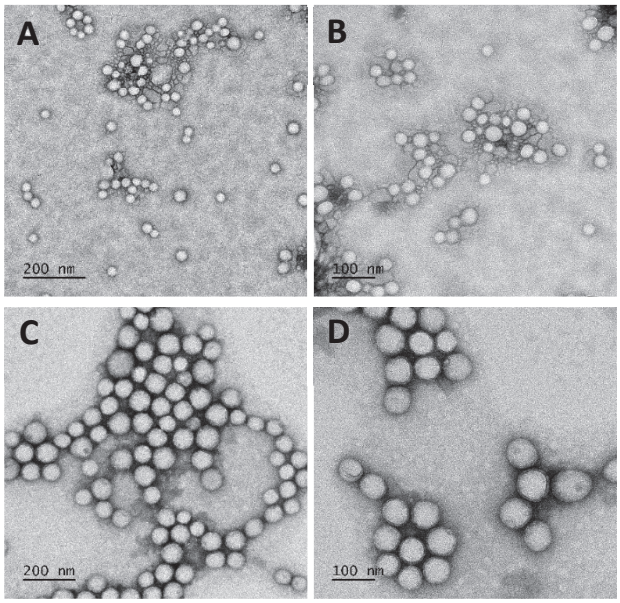

Fig. 3. TEM images of (A-B) PLGA NPs and (C-D) loaded NPs prepared by microfluidic technique

3.3 Design of experiments (DoE) for microfluidic translation

The translation from conventional bulk mixing nanoprecipitation technique to microfluidic was possible by controlling both formulation and process parameters which might affect NP characteristics [36]. For this purpose, a DoE was set up starting from the nanoprecipitated formulation in order to optimize a more effective and easily scalable preparation technique for drug-loaded NPs. FRR, polymer and drug concentration are critical parameters in the microfluidic procedure and were investigated considering the resulting effect on the effective amount of hydrophobic drug loaded into PLGA NPs (EE and DL). Each suspension was formulated by a constant volume of organic phase at different polymer and drug concentrations and varying the volume of aqueous phase by using different FRR. All experimental results in terms of physicochemical characteristics are reported in Table 3.

Table 3 Experimentation plan built according to a 2^3 full factorial design (runs 1 to 8) with two additional center points (runs 9 and 10) with the corresponding responses EE and DL

Run	PLGA (mg/mL)[a] (X_1)	FRR (v/v)[b] (X_2)	Drug (mg/mL)[c] (X_3)	Size (nm ± SD)	PDI	Zeta Potential (mV ± SD)	EE%	DL%
1	5	1:5	0.7	148 ± 11	0.28	- 32.8 ± 4.2	100.0	8.9
2	10	1:5	0.7	70 ± 1	0.20	- 43.8 ± 3.0	95.0	4.6
3	5	1:2	0.7	85 ± 6	0.11	- 50.0 ± 3.7	50.3	6.1
4	10	1:2	0.7	90 ± 1	0.07	- 50.5 ± 2.6	74.3	5.0
5	5	1:5	1.4	148 ± 1	0.16	- 40.5 ± 0.5	78.1	18.3
6	10	1:5	1.4	110 ± 3	0.21	- 47.1 ± 0.8	77.6	10.9
7	5	1:2	1.4	136 ± 1	0.14	- 46.6 ± 0.1	75.0	13.6
8	10	1:2	1.4	110 ± 1	0.04	- 43.8 ±2.5	86.4	9.5
9	7.5	1:3.5	1.1	129 ± 4	0.25	- 43.4 ± 9.8	85.9	10.8
10	7.5	1:3.5	1.1	128 ± 3	0.25	- 44.8 ± 0.2	92.5	11.3

[a] polymer concentration in the organic phase

[b] flow rate ratio (polymer-drug solution: aqueous phase)

[c] drug concentration in the organic phase

Compared to the conventional process, the microfluidic technique offers a more precise control over NP size during the formulation development. Working at a fixed TFR of 12 mL/min, we obtained NPs characterized by a mean diameter below 150 nm and PDI around 0.2 (Tab. 3), as reported in the literature for PLGA NPs working at high TFR (10-15 mL/min) [29,37]. The ζ of considered runs was ranged between -50 mV and -30 mV, suggesting that for hydrophobic drug-loaded PLGA NPs it is directly correlated to the presence of carboxylic groups on polymer chemical structure, regardless of modification of process parameters (Tab. 3) [38]. To reduce the waste of expensive drug molecules by maximizing the encapsulation into polymer nanosuspension, EE and DL were investigated by the means of a DoE. The experimental values of EE ranged from 50.3 up to 100% and DL evolved between 4.6 and 18.3% depending on the operating conditions (Tab. 3). The coefficients of Eq. 2 were determined for both EE and DL using least square linear regression (Tab. 4). The determination coefficients R^2 indicated the satisfactory adequacy of the developed models. Moreover, the residual error value of each experiment was calculated as the difference between the experimental response and the response predicted by the model (data not shown). Since these residual errors are almost all contained within the range of $2*SD_{exp}$ (Tab. 4), we can conclude that the developed models well explain each response.

Thus, the validated models were used to visualize the surface responses as a bi-dimensional plot of two factors (PLGA (X_1) and drug (X_3) concentrations), while keeping the third one (FRR (X_2)) constant (Fig. 4). In the case of EE, at a large volume of water compared to organic phase

(FRR 1:5), no significant influence of the polymer concentration was observed while the increase of drug concentration from 0.7 to 1.4 mg/mL led to a decrease of EE from 100% down to ~80%, probably due to high amount of drug compared to polymer amount. NPs reached a sort of limit of entrapment efficiency of the hydrophobic drug in a polymer matrix which determined a lower EE in presence of a high amount of polymer.

At the intermediate FRR 1:3.5, EE was slightly influenced by both drug concentrations. The main difference compared to FRR 1:5 was a decrease of EE from 100% down to 80-85% for 0.7 mg/mL of drug. At FRR 1:5, the larger amount of water compared to organic phase accelerated the solvent diffusion process and consequently allowed immediate NPs precipitation with higher amount of entrapped drug. At FRR 1:2 and 0.7 mg/mL of drug concentration, we observed a further decrease of EE that evolved between 55% and 70% as the polymer concentration ranged from 5 to 10 mg/mL. At FRR 1:2, corresponding to the lowest solvent diffusion rate, the amount of entrapped drug decreased. Moreover, EE was minimized at low polymer concentration since there was less polymer to entrap the active molecule. For 1.4 mg/mL of drug, we observed a similar trend since EE increased from ~70% to 90% by increasing the polymer concentration.

Concerning DL, Figure 4 shows similar results at FRR 1:5 and 1:3.5: the effect of drug amount on DL is more important than polymer concentration.

As expected, DL increased with the drug concentration and by decreasing the polymer amount. DL was slightly more influenced by the drug amount than the polymer concentration. Regarding the effect of FRR on DL, we observed a decrease of the maximal DL from 16-18% obtained at FRR 1:3.5 and 1:5 down to 12% at FRR 1:2. Once again, this result may be explained by the fast solvent diffusion process at FRR 1:5 that limited the drug loss [36]. The DL maximization was obtained for high drug amounts and low polymer ones (*i.e.,* 1.4 mg/mL drug and 5 mg/mL PLGA) but these operating conditions did not lead to optimal EE. EE was promoted at FRR 1:5 for low drug amount and at FRR 1:2 for high concentrations of both drug and polymer.

Thanks to these results, optimal operating conditions for the microfluidic process may be determined, but this needs to define specifications for a good compromise between EE, DL and the amount of wasted expensive drug.

Table 4 Coefficients of synergistic models (Eq. 2) for EE and DL with their corresponding R^2 and the estimation of the experimental standard deviation SDexp

Coefficients	EE (%) (Y1)	DL (%) (Y2)
b0	80.8	9.7
b1	3.9	-2. 1
b2	-8.9	-1.1
b3	0.1	3.5
b12	5.5	0.8
b13	9.8	-0.8
b23	-	-0.5
R^2	0.930	0.986
SDexp*	5.4 %	0.8%

*standard deviation of the experimental error determined from repeated runs (Degrees of Freedom=3)

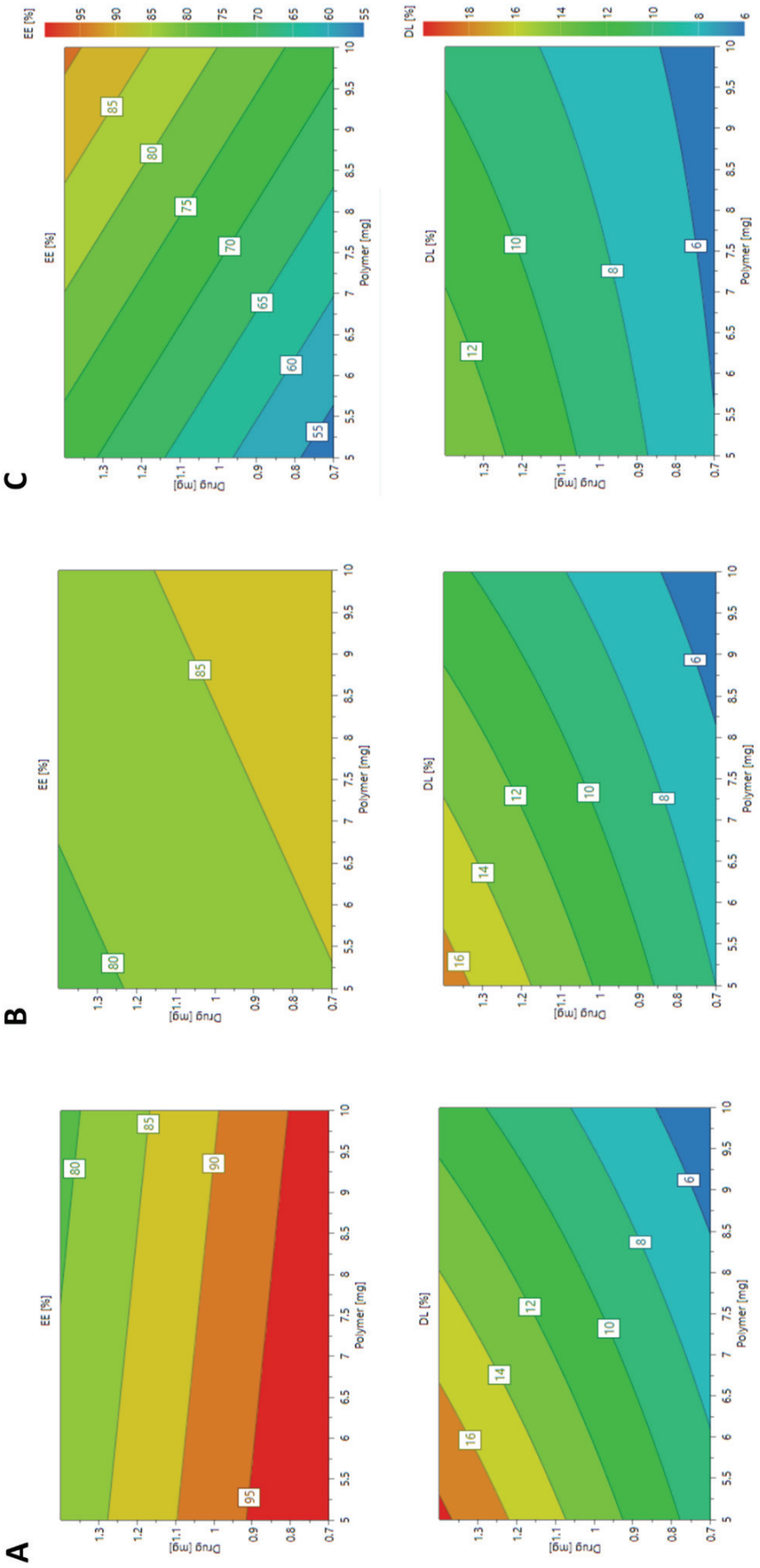

Fig. 4. Contour plots of the response surface for EE and DL at FRR 1:5 (A), 1:3.5 (B) and 1:2 (C)

3.4 Freeze-drying of loaded NPs

The stability of colloidal suspensions was evaluated at the storage condition (4 °C). For NPs prepared *via* nanoprecipitation, no appreciable size and ζ change and no precipitation or aggregation were observed. In microfluidic prepared NPs, the presence of the drug impacted the stability of the system. To understand the destabilization process, NMR analysis was performed to evaluate the presence of remaining organic solvents which could have an impact on PLGA formulation [39]. After the preparation of polymer NPs, rotary evaporation under pressure and dialysis against water were performed to eliminate acetonitrile. ^{1}H NMR spectra showed the presence of acetonitrile either using under-pressure evaporation or dialysis (data not shown). The fast destabilization of loaded systems could be partially ascribed to the presence of remaining acetonitrile. The effect was more evident in NPs prepared by microfluidic process, probably due to their smaller size (80 nm) to whom corresponded a faster degradation rate compared to nanoprecipitation-prepared NPs (170 nm) [40]. PLGA degradation and consequent destabilization of nanosystems can be ascribed to drug size or hydrophobicity, NP size and drug-polymer interactions [41]. During the formulation of the nanosuspension, organic solvents are required, but they must be eliminated (even the residual) for *in vitro* and *in vivo* testing. To guarantee a dry form of NPs with increased storage stability, a freeze-drying study was set up on NPs prepared by microfluidic technique. To not affect the physicochemical properties of NPs, trehalose 12% w/v was selected as a cryoprotectant agent, as already described for other polymer nanosystems [42]. Results shown in Tab. 5 demonstrate the retention of size, PDI, and ζ of lyophilized NPs after resuspension in Milli Q water.

Table 5 Physicochemical characterization of loaded-PLGA NPs prepared by microfluidic technique, before and after freeze-drying

Time	Size (nm ± SD)	PDI	Zeta Potential (mV ± SD)	Osmolarity
Before freeze-drying	81 ± 8	0.165	-49.1 ± 10	-
After freeze-drying	84 ± 18	0.190	-35.6 ± 2.9	0.286

Moreover, stability over time after NP resuspension was evaluated over 28 days at storage conditions (Fig. 5A). After reconstitution in water, the size of loaded NPs was retained by a monodispersed population (PDI<0.2) (Tab. 5) and their rounded shape did not register significant changes (Fig. 5B). By UHPLC analysis, we determined a drug association efficiency of 84% after reconstitution. As shown in Figure 5, the freeze-drying process, in combination with the cryoprotectant effect of trehalose, offered increased NP stability compared to the not-lyophilized formulation. The ζ was still negative and increased due to the presence of surface-

adsorbed sugar in the system [43]. The value around –35 mV allowed obtaining stable NPs thanks to the repulsion forces still present on the shell of PLGA NPs. Moreover, the ^{1}H NMR spectra demonstrated the complete elimination of acetonitrile after the freeze-drying process (data not shown). Lyophilization performed the double effect to increase the storage stability of loaded NPs and make the formulation suitable for *in vitro* and *in vivo* testing, by removing the organic solvent.

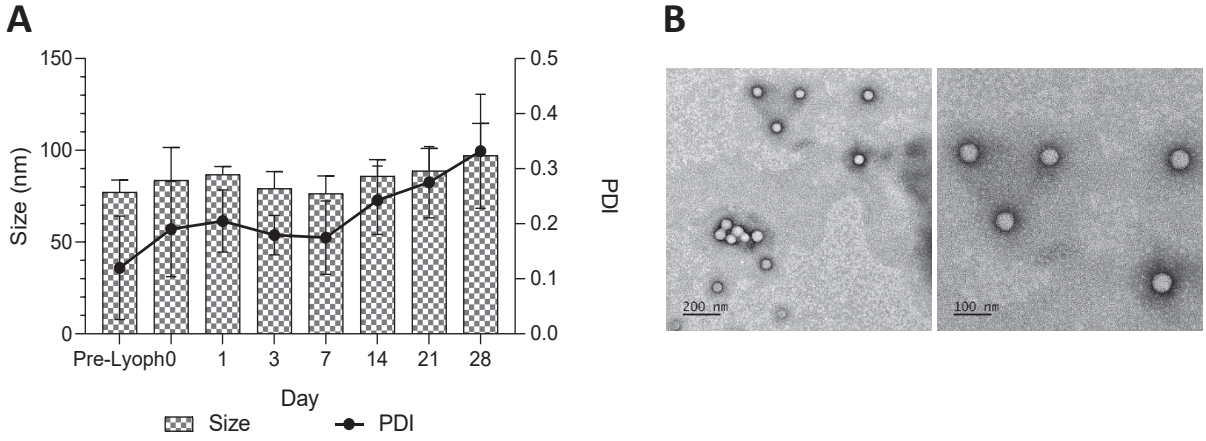

Fig. 5. Characterization of drug-loaded NPs after freeze-drying. (A) Stability study (size, and PDI) upon resuspension of loaded freeze-dried NPs. (B) TEM images of freeze-dried loaded-PLGA NPs after resuspension

4. Conclusions

The reported results confirm the useful application of microfluidic technique in the preparation of hydrophobic drug-loaded PLGA NPs. The translation from conventional bulk mixing to microfluidic technique is a key point to achieve a more effective and easily scalable preparation method. Notably, drug-loaded PLGA NPs were successfully manufactured by NanoAssemblr device, reducing the preparation time, and yielding suitable NP physicochemical characteristics (size, EE and DL). Indeed, starting from nanoprecipitation parameters, including polymer concentration, organic phase content and aqueous/organic phase ratio, the translation into microfluidic resulted in NPs with sub-100 nm size. The organic solvent elimination methods were investigated to obtain monodispersed nanosuspension with high EE. Among the most common methods, the dialysis technique led to NPs with PDI<0.2 with complete elimination of unencapsulated or surface-adsorbed drug. Thus, the drug content referred to the molecules efficiently encapsulated into the polymer matrix. In an effort to systematically investigate the impact on NP properties by changing the preparation methods, a DoE highlighted the crucial effect of polymer and drug concentrations, and FRR on NP features: in all the runs considered,

FRR set up at 1:5 enhanced the entrapment of the drug into polymer matrix at low drug concentration. However, the amount of drug improved EE and DL at FRR 1:2 up to a limit point which is characterized by the maximum entrapment capacity of PLGA NPs towards hydrophobic molecules. Microfluidic nanoprecipitation method has demonstrated to be a potential tool to ameliorate the size and EE of PLGA NPs loaded with a small hydrophobic model drug.

We can conclude that the translation from the conventional nanoprecipitation method to the microfluidic technique for polymer NPs has an ameliorating effect on NP features. However, the optimization of translated formulation needs to consider all the formulation and process parameters involved in microfluidic nanoprecipitation method.

References

1. Qiu, L.; Chen, T.; Öçsoy, I.; Yasun, E.; Wu, C.; Zhu, G.; You, M.; Han, D.; Jiang, J.; Yu, R.; et al. A Cell-Targeted, Size-Photocontrollable, Nuclear-Uptake Nanodrug Delivery System for Drug-Resistant Cancer Therapy. *Nano Lett* **2015**, *15*, 457–463, doi:10.1021/nl503777s.
2. Lv, Y.; Pan, Q.; Bligh, S.W.A.; Li, H.; Wu, H.; Sang, Q.; Zhu, L.-M. Core-Sheath Nanofibers as Drug Delivery System for Thermoresponsive Controlled Release. *J Pharm Sci* **2017**, *106*, 1258–1265, doi:10.1016/j.xphs.2016.12.031.
3. Park, H.; Otte, A.; Park, K. Evolution of Drug Delivery Systems: From 1950 to 2020 and Beyond. *Journal of Controlled Release* **2022**, *342*, 53–65, doi:10.1016/j.jconrel.2021.12.030.
4. Carton, F.; Chevalier, Y.; Nicoletti, L.; Tarnowska, M.; Stella, B.; Arpicco, S.; Malatesta, M.; Jordheim, L.P.; Briançon, S.; Lollo, G. Rationally Designed Hyaluronic Acid-Based Nano-Complexes for Pentamidine Delivery. *Int J Pharm* **2019**, *568*, 118526, doi:10.1016/j.ijpharm.2019.118526.
5. Kühne, M.; Lindemann, H.; Grune, C.; Schröder, D.; Cseresnyés, Z.; Godmann, M.; Koschella, A.; Figge, M.T.; Eggeling, C.; Fischer, D.; et al. Biocompatible Sulfated Valproic Acid-Coupled Polysaccharide-Based Nanocarriers with HDAC Inhibitory Activity. *J Control Release* **2021**, *329*, 717–730, doi:10.1016/j.jconrel.2020.10.006.
6. Danhier, F.; Ansorena, E.; Silva, J.M.; Coco, R.; Le Breton, A.; Préat, V. PLGA-Based Nanoparticles: An Overview of Biomedical Applications. *J Control Release* **2012**, *161*, 505–522, doi:10.1016/j.jconrel.2012.01.043.
7. Park, K.; Skidmore, S.; Hadar, J.; Garner, J.; Park, H.; Otte, A.; Soh, B.K.; Yoon, G.; Yu, D.; Yun, Y.; et al. Injectable, Long-Acting PLGA Formulations: Analyzing PLGA and Understanding Microparticle Formation. *J Control Release* **2019**, *304*, 125–134, doi:10.1016/j.jconrel.2019.05.003.
8. Stella, B.; Andreana, I.; Zonari, D.; Arpicco, S. Pentamidine-Loaded Lipid and Polymer Nanocarriers as Tunable Anticancer Drug Delivery Systems. *J Pharm Sci* **2020**, *109*, 1297–1302, doi:10.1016/j.xphs.2019.11.011.
9. Jaradat, A.; Macedo, M.H.; Sousa, F.; Arkill, K.; Alexander, C.; Aylott, J.; Sarmento, B. Prediction of the Enhanced Insulin Absorption across a Triple Co-Cultured Intestinal

Model Using Mucus Penetrating PLGA Nanoparticles. *Int J Pharm* **2020**, *585*, 119516, doi:10.1016/j.ijpharm.2020.119516.
10. Liu, Y.; Zhao, G.; Xu, C.-F.; Luo, Y.-L.; Lu, Z.-D.; Wang, J. Systemic Delivery of CRISPR/Cas9 with PEG-PLGA Nanoparticles for Chronic Myeloid Leukemia Targeted Therapy. *Biomater Sci* **2018**, *6*, 1592–1603, doi:10.1039/c8bm00263k.
11. Frede, A.; Neuhaus, B.; Klopfleisch, R.; Walker, C.; Buer, J.; Müller, W.; Epple, M.; Westendorf, A.M. Colonic Gene Silencing Using SiRNA-Loaded Calcium Phosphate/PLGA Nanoparticles Ameliorates Intestinal Inflammation in Vivo. *J Control Release* **2016**, *222*, 86–96, doi:10.1016/j.jconrel.2015.12.021.
12. Zhang, Y.; García-Gabilondo, M.; Grayston, A.; Feiner, I.V.J.; Anton-Sales, I.; Loiola, R.A.; Llop, J.; Ramos-Cabrer, P.; Barba, I.; Garcia-Dorado, D.; et al. PLGA Protein Nanocarriers with Tailor-Made Fluorescence/MRI/PET Imaging Modalities. *Nanoscale* **2020**, *12*, 4988–5002, doi:10.1039/C9NR10620K.
13. Langer, K.; Anhorn, M.G.; Steinhauser, I.; Dreis, S.; Celebi, D.; Schrickel, N.; Faust, S.; Vogel, V. Human Serum Albumin (HSA) Nanoparticles: Reproducibility of Preparation Process and Kinetics of Enzymatic Degradation. *Int J Pharm* **2008**, *347*, 109–117, doi:10.1016/j.ijpharm.2007.06.028.
14. Martínez Rivas, C.J.; Tarhini, M.; Badri, W.; Miladi, K.; Greige-Gerges, H.; Nazari, Q.A.; Galindo Rodríguez, S.A.; Román, R.Á.; Fessi, H.; Elaissari, A. Nanoprecipitation Process: From Encapsulation to Drug Delivery. *Int J Pharm* **2017**, *532*, 66–81, doi:10.1016/j.ijpharm.2017.08.064.
15. Yan, X.; Bernard, J.; Ganachaud, F. Nanoprecipitation as a Simple and Straightforward Process to Create Complex Polymeric Colloidal Morphologies. *Adv Colloid Interface Sci* **2021**, *294*, 102474, doi:10.1016/j.cis.2021.102474.
16. Shepherd, S.J.; Issadore, D.; Mitchell, M.J. Microfluidic Formulation of Nanoparticles for Biomedical Applications. *Biomaterials* **2021**, *274*, 120826, doi:10.1016/j.biomaterials.2021.120826.
17. Lou, G.; Anderluzzi, G.; Schmidt, S.T.; Woods, S.; Gallorini, S.; Brazzoli, M.; Giusti, F.; Ferlenghi, I.; Johnson, R.N.; Roberts, C.W.; et al. Delivery of Self-Amplifying MRNA Vaccines by Cationic Lipid Nanoparticles: The Impact of Cationic Lipid Selection. *J Control Release* **2020**, *325*, 370–379, doi:10.1016/j.jconrel.2020.06.027.
18. Shepherd, S.J.; Warzecha, C.C.; Yadavali, S.; El-Mayta, R.; Alameh, M.-G.; Wang, L.; Weissman, D.; Wilson, J.M.; Issadore, D.; Mitchell, M.J. Scalable MRNA and SiRNA Lipid Nanoparticle Production Using a Parallelized Microfluidic Device. *Nano Lett* **2021**, *21*, 5671–5680, doi:10.1021/acs.nanolett.1c01353.
19. Maeki, M.; Uno, S.; Niwa, A.; Okada, Y.; Tokeshi, M. Microfluidic Technologies and Devices for Lipid Nanoparticle-Based RNA Delivery. *Journal of Controlled Release* **2022**, *344*, 80–96, doi:10.1016/j.jconrel.2022.02.017.
20. Yang, R.; Deng, Y.; Huang, B.; Huang, L.; Lin, A.; Li, Y.; Wang, W.; Liu, J.; Lu, S.; Zhan, Z.; et al. A Core-Shell Structured COVID-19 MRNA Vaccine with Favorable Biodistribution Pattern and Promising Immunity. *Signal Transduct Target Ther* **2021**, *6*, 213, doi:10.1038/s41392-021-00634-z.
21. Naderi Sohi, A.; Kiani, J.; Arefian, E.; Khosrojerdi, A.; Fekrirad, Z.; Ghaemi, S.; Zim, M.K.; Jalili, A.; Bostanshirin, N.; Soleimani, M. Development of an MRNA-LNP Vaccine against SARS-CoV-2: Evaluation of Immune Response in Mouse and Rhesus Macaque. *Vaccines (Basel)* **2021**, *9*, 1007, doi:10.3390/vaccines9091007.
22. Riewe, J.; Erfle, P.; Melzig, S.; Kwade, A.; Dietzel, A.; Bunjes, H. Antisolvent Precipitation of Lipid Nanoparticles in Microfluidic Systems – A Comparative Study. *International Journal of Pharmaceutics* **2020**, *579*, 119167, doi:10.1016/j.ijpharm.2020.119167.

23. Zhao, X.; Bian, F.; Sun, L.; Cai, L.; Li, L.; Zhao, Y. Microfluidic Generation of Nanomaterials for Biomedical Applications. *Small* **2020**, *16*, 1901943, doi:10.1002/smll.201901943.
24. Roces, C.B.; Lou, G.; Jain, N.; Abraham, S.; Thomas, A.; Halbert, G.W.; Perrie, Y. Manufacturing Considerations for the Development of Lipid Nanoparticles Using Microfluidics. *Pharmaceutics* **2020**, *12*, 1095, doi:10.3390/pharmaceutics12111095.
25. Fessi, H.; Puisieux, F.; Devissaguet, J.Ph.; Ammoury, N.; Benita, S. Nanocapsule Formation by Interfacial Polymer Deposition Following Solvent Displacement. *International Journal of Pharmaceutics* **1989**, *55*, R1–R4, doi:10.1016/0378-5173(89)90281-0.
26. Olivier, S.; Foretz, M.; Viollet, B. Promise and Challenges for Direct Small Molecule AMPK Activators. *Biochem Pharmacol* **2018**, *153*, 147–158, doi:10.1016/j.bcp.2018.01.049.
27. Bramosanti, M.; Chronopoulou, L.; Grillo, F.; Valletta, A.; Palocci, C. Microfluidic-Assisted Nanoprecipitation of Antiviral-Loaded Polymeric Nanoparticles. *Colloids and Surfaces A: Physicochemical and Engineering Aspects* **2017**, *532*, 369–376, doi:10.1016/j.colsurfa.2017.04.062.
28. Todaro, B.; Moscardini, A.; Luin, S. Pioglitazone-Loaded PLGA Nanoparticles: Towards the Most Reliable Synthesis Method. *International Journal of Molecular Sciences* **2022**, *23*, 2522, doi:10.3390/ijms23052522.
29. Zhigaltsev, I.V.; Belliveau, N.; Hafez, I.; Leung, A.K.K.; Huft, J.; Hansen, C.; Cullis, P.R. Bottom-up Design and Synthesis of Limit Size Lipid Nanoparticle Systems with Aqueous and Triglyceride Cores Using Millisecond Microfluidic Mixing. *Langmuir* **2012**, *28*, 3633–3640, doi:10.1021/la204833h.
30. Gimondi, S.; Guimarães, C.F.; Vieira, S.F.; Gonçalves, V.M.F.; Tiritan, M.E.; Reis, R.L.; Ferreira, H.; Neves, N.M. Microfluidic Mixing System for Precise PLGA-PEG Nanoparticles Size Control. *Nanomedicine* **2021**, *40*, 102482, doi:10.1016/j.nano.2021.102482.
31. Phongpradist, R.; Chaiyana, W.; Anuchapreeda, S. Curcumin-Loaded Multi-Valent Ligands Conjugated-Nanoparticles for Anti-Inflammatory Activity. *International Journal of Pharmacy and Pharmaceutical Sciences* **2015**, *7*, 203–208.
32. Zhang, C.; Chung, J.W.; Priestley, R.D. Dialysis Nanoprecipitation of Polystyrene Nanoparticles. *Macromolecular Rapid Communications* **2012**, *33*, 1798–1803, doi:10.1002/marc.201200335.
33. Choi, J.-S.; Cao, J.; Naeem, M.; Noh, J.; Hasan, N.; Choi, H.-K.; Yoo, J.-W. Size-Controlled Biodegradable Nanoparticles: Preparation and Size-Dependent Cellular Uptake and Tumor Cell Growth Inhibition. *Colloids Surf B Biointerfaces* **2014**, *122*, 545–551, doi:10.1016/j.colsurfb.2014.07.030.
34. Ortiz de Solorzano, I.; Uson, L.; Larrea, A.; Miana, M.; Sebastian, V.; Arruebo, M. Continuous Synthesis of Drug-Loaded Nanoparticles Using Microchannel Emulsification and Numerical Modeling: Effect of Passive Mixing. *Int J Nanomedicine* **2016**, *11*, 3397–3416, doi:10.2147/IJN.S108812.
35. Jose, S.; A, C.T.; Sebastian, R.; H, S.M.; A, A.N.; Durazzo, A.; Lucarini, M.; Santini, A.; Souto, E.B. Transferrin-Conjugated Docetaxel-PLGA Nanoparticles for Tumor Targeting: Influence on MCF-7 Cell Cycle. *Polymers (Basel)* **2019**, *11*, E1905, doi:10.3390/polym11111905.
36. Chiesa, E.; Dorati, R.; Modena, T.; Conti, B.; Genta, I. Multivariate Analysis for the Optimization of Microfluidics-Assisted Nanoprecipitation Method Intended for the Loading of Small Hydrophilic Drugs into PLGA Nanoparticles. *Int J Pharm* **2018**, *536*, 165–177, doi:10.1016/j.ijpharm.2017.11.044.

37. Abstiens, K.; Goepferich, A.M. Microfluidic Manufacturing Improves Polydispersity of Multicomponent Polymeric Nanoparticles. *Journal of Drug Delivery Science and Technology* **2019**, *49*, 433–439, doi:10.1016/j.jddst.2018.12.009.
38. Shi, Y.; xue, J.; Jia, L.; Du, Q.; Niu, J.; Zhang, D. Surface-Modified PLGA Nanoparticles with Chitosan for Oral Delivery of Tolbutamide. *Colloids and Surfaces B: Biointerfaces* **2018**, *161*, 67–72, doi:10.1016/j.colsurfb.2017.10.037.
39. Shim, H.; Sah, H. Assessment of Residual Solvent and Drug in PLGA Microspheres by Derivative Thermogravimetry. *Pharmaceutics* **2020**, *12*, E626, doi:10.3390/pharmaceutics12070626.
40. Ge, Z.; Wang, Y. Estimation of Nanodiamond Surface Charge Density from Zeta Potential and Molecular Dynamics Simulations. *J. Phys. Chem. B* **2017**, *121*, 3394–3402, doi:10.1021/acs.jpcb.6b08589.
41. Mir, M.; Ahmed, N.; Rehman, A.U. Recent Applications of PLGA Based Nanostructures in Drug Delivery. *Colloids Surf B Biointerfaces* **2017**, *159*, 217–231, doi:10.1016/j.colsurfb.2017.07.038.
42. Fonte, P.; Araújo, F.; Seabra, V.; Reis, S.; van de Weert, M.; Sarmento, B. Co-Encapsulation of Lyoprotectants Improves the Stability of Protein-Loaded PLGA Nanoparticles upon Lyophilization. *Int J Pharm* **2015**, *496*, 850–862, doi:10.1016/j.ijpharm.2015.10.032.
43. Soares, S.; Fonte, P.; Costa, A.; Andrade, J.; Seabra, V.; Ferreira, D.; Reis, S.; Sarmento, B. Effect of Freeze-Drying, Cryoprotectants and Storage Conditions on the Stability of Secondary Structure of Insulin-Loaded Solid Lipid Nanoparticles. *Int J Pharm* **2013**, *456*, 370–381, doi:10.1016/j.ijpharm.2013.08.076.

Chapter V

AMPK activator encapsulation into polymer nanoparticles ameliorates muscle homeostasis in a pre-clinical mouse model of Duchenne muscular dystrophy

I. Andreana, S. Ben Larbi, A. Kneppers, A. Fessard, J. Sidi-Boumedine, S. Zilio, F. Tifni, D. Kryza, B. Chazaud, R. Mounier, G. Lollo, G. Juban

(In preparation)

AMP-protein kinase (AMPK) is a new emerging therapeutic target in the treatment of muscular myopathies. Small molecules can efficiently activate AMPK to reduce the production of pro-inflammatory and fibrosis mediators and positively affect the development of muscular dystrophies.

Main aim

The aim of this chapter was to exploit the nanotechnological strategy to overcome the drawback of *in vivo* administration of a potent AMPK activator molecule, called 991.

Specific objectives

- Test 991 efficacy *in vitro* and *in vivo* once loaded in PLGA-based nanoparticles (NPs)
- Study the internalization of PLGA NPs in bone marrow derived macrophages (BMDMs)
- Study the cellular viability for empty and loaded NPs on BMDMs
- Study the retained activity of loaded 991
- Study the *in vivo* pharmacokinetics and NPs uptake in diaphragm and gastrocnemius
- Study the *in vivo* efficacy of 991-loaded PLGA NPs

Highlights of the chapter

- Encapsulation of 991 in biodegradable and biocompatible PLGA NPs is a promising strategy for *in vivo* delivery.
- The internalization of PLGA NPs is very fast in BMDM without toxic effects. *In vitro* efficacy of 991, as potent activator of AMPK was retained. The evaluation of transforming growth factor- β ($TGF\beta_1$) expression confirmed a reduction in cells treated with 991, free or loaded in NPs.
- The biodistribution of NPs after i.v. injection in a superior Duchenne muscular dystrophy mouse model (D2.mdx) showed a 10% uptake in diaphragm and gastrocnemius cells.
- *In vivo* treatment of 991-loaded NPs over three weeks demonstrated a 10% fibrosis reduction in D2.mdx, suggesting promising results of 991 activity *in vivo*.
- Nanomedicine strategy allowed the *in vivo* delivery of 991, without evident side effects on mice.

AMPK activator encapsulation into polymer nanoparticles ameliorates muscle homeostasis in a pre-clinical mouse model of Duchenne muscular dystrophy

Ilaria Andreana[a,b], Sabrina Ben Larbi[c,], Anita Kneppers[c], Aurélie Fessard[c], Jaqueline Sidi-Boumedine[b], Serena Zilio[b], Federica Tifni[b], David Kryza[b], Bénédicte Chazaud[c], Rémi Mounier[c] [†], Giovanna Lollo[b,†,*], Gaëtan Juban[c,†,*].

[a] *Dipartimento di Scienza e Tecnologia del Farmaco, Università di Torino, Via P. Giuria 9, 10125, Torino, Italy*

[b] *Laboratoire d'Automatique, de Génie des Procédés et de Génie Pharmaceutique, Université Claude Bernard Lyon 1, CNRS UMR 5007, 43 bd 11 Novembre 1918, 69622, Villeurbanne, France*

[c] *Institut NeuroMyoGène, Laboratoire de Physiopathologie et Génétique du Neurone et du Muscle, University of Lyon, INSERM U1315, CNRS UMR 5261, Lyon, France*

[d] *Hospices Civils de Lyon, 69437 Lyon, France*

[†] These authors contributed equally to this work

*** Correspondance to :**

Giovanna Lollo. Postal address : Laboratoire d'Automatique, de Génie des Procédés et de Génie Pharmaceutique, Université Claude Bernard Lyon 1, CNRS UMR 5007, 43 bd 11 Novembre 1918, 69622, Villeurbanne, France. E-mail address: giovanna.lollo@univ-lyon1.fr

Gaëtan Juban. Postal address : Institut NeuroMyoGène, Laboratoire de Physiopathologie et Génétique du Neurone et du Muscle, University of Lyon, INSERM U1315, CNRS UMR 5261, 8 avenue Rockefeller, Lyon, France, France. E-mail address: gaetan.juban@univ-lyon1.fr

Abstract

Muscular dystrophies, such as Duchenne muscular dystrophy (DMD), are caused by permanent muscle injuries leading to a chronic inflammation, with macrophages harboring an altered inflammatory profile that contributes to fibrosis establishment through secretion of the TGFβ$_1$ profibrotic cytokine. AMP-activated protein kinase (AMPK) is an attractive therapeutic target for treating chronic inflammation and fibrosis in DMD as we previously showed that its indirect activation reduces TGFβ$_1$ secretion by macrophages and improves muscle homeostasis and muscle force in a mouse model of DMD. However, potent direct AMPK activators like compound 991 show strong adverse effects *in vivo* which prevent their use. Here, we encapsulated 991 into biodegradable poly(lactic-*co*-glycolic) acid (PLGA) nanoparticles to deliver it *in vivo* and overcome these toxicity issues. We demonstrate that 991-loaded PLGA nanoparticles retained drug activity on fibrotic bone marrow derived macrophages, by reducing the secretion of TGFβ$_1$ and preserving cellular viability *in vitro*. In the D2-mdx pre-clinical DMD mouse model, sub-100 nm nanoparticles accessed the gastrocnemius and diaphragm muscles, the most affected muscles in DMD mouse model, after chronic intravenous injections. Muscles exhibited a decreased inflammation associated with fibrosis reduction and increase in muscle mass, indicative of muscle homeostasis improvement. Our results suggest that nanomedicine is an efficient strategy to achieve direct AMPK activator molecules administration *in vivo*, to prevent their adverse effect and ameliorate dystrophic muscle phenotype.

Keywords: nanoparticles, macrophages, fibrosis, muscle homeostasis

Graphical abstract

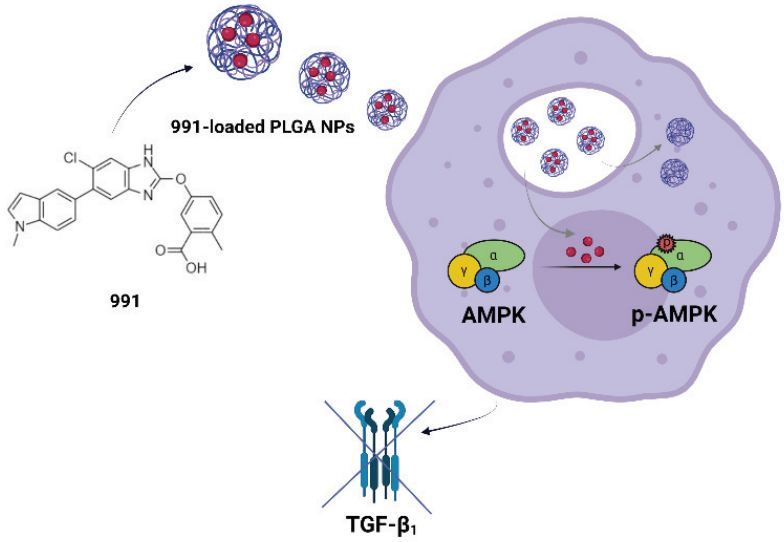

1. Introduction

Inflammation and fibrosis achieved important attention for their pathogenic role in several acute and chronic diseases, including cardiomyopathy, metabolic and autoimmune diseases, and genetic disorders [1,2]. The biological complexity of an inflamed and fibrotic environment made it difficult to develop anti-inflammatory therapies to improve tissue regeneration [3,4]. Therefore, the investigation of new approaches to reduce chronic inflammation and pathological fibrosis are of substantial interest to promote muscle homeostasis. Among several pathologies, Duchenne muscular dystrophy (DMD) is an X-linked genetic disorder, triggered by mutations in the dystrophin gene, in which inflammatory and fibrotic responses play a crucial role in disease progression [5]. Chronic inflammation contributes to persistent muscle damage and the progression of muscle weakness with high infiltration of immune cells. The first immune cells to invade the injured area are pro-inflammatory damage-associated macrophages which can establish fibrosis [6]. Existing data suggest that an appropriate balance of immune cells responses in dystrophic muscle is essential to ultimately restoring natural muscle physiology. Indeed, resolution of inflammation is characterized by phenotype changes of pro-inflammatory macrophages toward their anti-inflammatory phenotype. This process is promoted by different pathways, including the activation of AMP-protein kinase (AMPK) [7,8]. AMPK is a ubiquitously expressed serine/threonine kinase, considered a crucial protein in maintaining energy balance and homeostasis in skeletal muscles [9]. Activation of AMPK exhibited anti-inflammatory properties through the regulation of macrophages' inflammatory status, gaining much attention as a new therapeutic target. Since the discovery of AMPK as a druggable target, the effort to develop different compounds able to enhance protein activity, increased. Although the use of small molecules highlighted the importance of AMPK in the treatment of many human pathologies, challenges and drawbacks might limit their therapeutic applicability [10,11]. In dystrophic muscles, the activation of AMPK in immune cells, particularly in macrophages, causes the activation of the latent-TGF-β-binding protein (LTBP4) genetic pathway, which is a known modified gene in DMD patients. Consequently, kinase activation reduces the expression of LTBP4, reducing the amount of the pro-inflammatory cytokines transforming growth factor-β (TGFβ_1) production, crucial for muscle regeneration [12]. AMPK activator molecules have already found application in the treatment of diabetes type II. For example, metformin can enhance the activation of AMPK and improve glucose uptake, even in skeletal muscles to ameliorate muscle contractility [13–15].

In this frame, a potent activator AMPK molecule, namely 991 or EX229, was studied as a potential approach to reduce inflammation and associated fibrosis in a pre-clinical fibrotic mdx

mouse model [12,16,17]. However, in the literature, there is no information about the immediate side effects after intravenous (i.v.) injection of AMPK activator molecules. In the scientific community, it is known about the irreversible hemolytic effect and platelet aggregation after AMPK activator i.v. administration in mice. The growing interest in applying nanotechnology to therapeutic approaches is largely attributable to its uniquely appealing features for drug delivery, diagnosis, and imaging, synthetic vaccine development [18,19], and the treatment of muscular dystrophies [20]. Among the studied drug delivery systems, poly(lactic-*co*-glycolic) acid (PLGA), a biocompatible and biodegradable polymer, has attracted researchers for the ability to incorporate hydrophobic compounds [21]. In this study, we investigated nanomedicine as a possible strategy to administer an AMPK activator molecule *in vivo*. The working hypothesis was the use of PLGA nanoparticles to provide a huger concentration in the systemic circulation, avoiding its rapid clearance, increasing drug accumulation in inflamed tissues and reducing adverse effects [22]. The developed nanosystem is based on a biodegradable and biocompatible polymer whose metabolic monomers, lactic and glycolic acid, can be used by cells to maintain homeostasis [23,24]. PLGA is considered one of the most successfully biodegradable polymers and its features need to be considered in DMD treatment to prevent additional muscle degeneration of severely injured skeletal muscles [25].

In the present work, the ability of these nanoparticles to control inflammation and reduce fibrosis in the context of chronic inflammation was assessed. Their activity on fibrotic bone marrow derived macrophages (BMDMs) was investigated, by evaluating the ability of 991 to retain its activity even loaded into polymer nanocarriers. *In vivo* tests were then set up to evaluate a possible accumulation of biodegradable nanoparticles into dystrophic muscles, with a specific focus on gastrocnemius and diaphragm muscles, which are considered the most representative muscles of inflammation and fibrosis patterns in the pre-clinical mdx mouse model [26].

2. Experimental section

2.1 Materials

PLGA 75:25 (Resomer® RG 752 H, M_w = 4-15 kDa) and solvents (analytical grade) were purchased by Sigma-Aldrich® (St Quentin-Fallavier, France). 991 (M_w = 431.87 g/mol) was ordered from Cliniscience® (Nanterre, France) and 1,1′-dioctadecyl-3,3,3′,3′-tetramethylindodicarbocyanine, 4-chlorobenzenesulfonate salt (DiD) from Thermo Fisher

Scientific® (Waltham, Massachusetts, USA). Spectrum™ Spectra/Por™ Float-A-Lyzer™ G2 Dialysis devices (MWCO = 3.5-5 kDa) were provided by Fisher Scientific (Illkirch, France).
For the biological tests, Dulbecco's Modified Eagle Medium (DMEM), high glucose, Glutamax Supplement, pyruvate, was bought from Gibco® (Thermo Fisher Scientific®) and used for cell culture. Fetal bovine serum (FBS), penicillin/streptamycin and fungizone as DMEM supplements were supplied by Gibco®. TGF beta-1 Human/Mouse Uncoated ELISA Kit was supplied by Gibco®. Annexin V conjugated to Alexa Fluor 488 (ref A1, 1/20 dilution) was purchased by Molecular Probes (Eugene, Oregon). DAPI (1 µg/mL, ref 564907) was obtained from BD Biosciences (Grenoble, France). For immunostaining, cells were labeled with rabbit anti-laminin (ref. L9393, 1/200 dilution) from Sigma-Aldrich® and goat anti-type I collagen (ref 1310-01, 1/400 dilution) from Southern Biotech (Birmingham, Alabama, USA). For double immunolabeling, antibodies against F4/80 were purchased from Elabscience (France). Hoechst 33342 (1 µg/mL, ref 14533) for nuclei staining was purchased from Sigma-Aldrich®.

2.2 Nanoparticle preparation and characterization

991-loaded PLGA nanoparticles were produced using a benchtop NanoAssemblr™ (Precision NanoSystem, Inc., Vancouver, Canada), as already described (Chapter IV).
Briefly, for each preparation, to 6 mg of PLGA 75:25 dissolved in acetonitrile, an aliquot (200 µL) of a methanolic stock solution of 991 (5 mg/mL) was added until a total volume of 1 mL. The organic phase comprised of the polymer/drug solution was injected into one port of the NanoAssemblr™ instrument. The aqueous phase was simultaneously injected into the second port of the system to maintain a 1:2 organic:aqueous flow rate ratio (FRR) and 12 mL/min total flow rate (TFR). To remove the organic solvent and purify the nanoparticles from the non-incorporated drug, 991-loaded nanoparticles were dialyzed (Spectrum™ Spectra/Por™ Float-A-Lyzer™ G2 Dialysis devices (MWCO = 3.5-5 kDa)) against Milli Q water at room temperature for 1 h. Unloaded (*i.e.*, without adding 991) and DiD-loaded nanoparticles were prepared as well. The particles were then stored at 4 °C. Quantification of encapsulated 991 was determined by ultra high performance liquid chromatography (UHPLC) analysis, which has already been described (Chapter IV).

2.3 Hemolysis test

The hemolytic potential of free and encapsulated 991 was determined on erythrocytes. 10 mL of mice blood were taken and transferred into Vacutainer tubes. The blood was centrifuged (2229 rpm, 20 °C, 5 min) and the supernatant was discarded. The solid residue of erythrocytes

was redispersed with a sterile saline solution containing NaCl 150 mM and centrifuged three times; each time the supernatant was discarded and NaCl solution added. Then, the solid residue of erythrocytes was diluted with PBS (3% w/v) and stored at 4 °C. 150 µL of the erythrocyte stock dispersion was added to 150 µL of free 911 and loaded nanoparticle suspensions (50, 20 and 10 µM), and incubated at 37 °C for 1 h. A dispersion of erythrocytes in PBS was prepared as negative control and a solution of Triton X-100 20% v/v as a positive control. After incubation, samples were centrifuged (2229 rpm, 20 °C, 5 min) to separate the red blood cells and the supernatant. The absorption of the supernatant was measured by UV spectroscopy (λ = 570 nm). Results were set relative to negative control with 0% lysis (PBS) and positive control with 100% lysis (Triton X-100). The hemolytic percentage was calculated according to the equation (Eq. 1).

Eq. 1

$$\%\ Hemolysis = \frac{Abs(sample) - Abs\ (negative\ control)}{Abs\ (positive\ control) - Abs\ (negative\ control)} * 100$$

2.4 In vitro studies on BMDMs

2.4.1 Cell culture conditions

Macrophages were derived from murine bone marrow precursors as previously described [7]. Briefly, total bone marrow was obtained by flushing the femur and tibiae from wild-type C57BL/6J mice with DMEM. Cells were cultured in DMEM containing 20% heat-inactivated FBS, 30% of L929 cell-line derived conditioned medium (European Collection of Authenticated Cell Cultures; enriched in CSF-1), 1% of penicillin/streptamycin and 1% of fungizone for 6-7 days. Cells were cultured at 37 °C in a humidified atmosphere 5% CO_2. Macrophages were polarized toward 1 µg/mL of total protein lysate from fib-mdx mouse, in DMEM containing FBS 10% for at least 48 h.

2.4.2 Cell viability study

Fibrotic BMDMs treated with free 991, blank and 991-loaded nanoparticles (20 µM) for 24 h, were collected using cold PBS and suspended in PBS containing 1% FBS. After centrifugation, cells were resuspended in 1X binding buffer containing Annexin V-FITC and DAPI and incubated for 15 min at room temperature in the dark. Cells were then washed with 1X binding buffer. Staurosporine (2 µM) and cisplatin (50 µM) induced cells were used as positive controls. Cells were sorted using a FACSCanto II (BD Biosciences) apparatus.

2.4.3 Nanoparticles internalization by BMDMs

1.8-2.0×10^5 BMDMs obtained as previously described were cultured on a round coverslip in a 12-well plate. Cells were incubated with fluorescent PLGA nanoparticles at the final DiD concentration of 0.9 µg/mL for 2 h, 4 h and 24 h at 37 °C. As a control, untreated samples were used. After incubation, wells were washed with PBS three times for 5 min and fixed with 4% paraformaldehyde at 37 °C. Afterward, the cells were washed three times with PBS. Membranes were permeabilized with PBS 0.5% TritonX-100 and stained with 30 µL of a solution of primary antibody against F4/80 (ref E-AB.F0995A, 1/200 dilution) overnight at 4 °C. 30 µL diluted secondary antibody in PBS (1/2000 dilution) was added and incubated 2 h at 37 °C. The secondary antibody was coupled to Cy3 fluorophore. The nuclei were stained with Hoechst 33342. Samples were analyzed under a laser scanning confocal microscope (LEICA SP5 X) equipped with 2 lasers (405 nm/Diode laser and 470-670 nm/white laser), and the results were analyzed by Las X (Leica MICROSYSTEMS).

2.4.4 Protein extractions and western blotting

2×10^6 BMDMs were seeded in 6-well plates. The culture medium was replaced with DMEM without Phenol Red (Gibco®) supplemented with 10% charcoal-stripped FBS (Gibco®), and cells were treated with 10 and 20 µM of 991, PLGA nanoparticles and 991-loaded PLGA nanoparticles for 6 or 24 h. Proteins were isolated in lysis buffer containing 50 mM Tris-HCl (pH 7.5), 1 mM EDTA, 1 mM EGTA, 0.27 M sucrose, 1% Triton X-100, 20 mM glycerol-2-phosphate disodium, 50 mM NaF, 0.5 mM PMSF, 2 mM benzamidine, 1 mM Na_3VO_4 and 1% phosphate inhibitor cocktail 3 (Sigma-Aldrich®; P0044) for 30 min on ice and centrifuged for 10 min at 16.000 g to remove debris. Then, 10 µg of the protein was subjected to SDS-PAGE and transferred into a nitrocellulose membrane, which was probed with antibodies against acetyl-CoA carboxylase (ACC) (#3676S, 1:1000) and phosphorylated ACC (p-ACC; #3661S, 1:1000) or β-actine (A5316, Sigma-Aldrich®; 1:2000). Blots were analyzed on a Chemidoc imager (Bio-Rad) using SuperSignal West Femto Maximum Sensitivity Substrate (Thermo Fisher Scientific), and signal intensity was quantified using Image Lab Software (Bio-Rad).

2.4.5 Quantification of $TGF\beta_1$ by ELISA kit

1.5×10^5 BMDMs were seeded in 48-well plates and polarized as described above. Free 991, empty and loaded nanoparticles were incubated overnight at 10 µM concentration; cells were washed with PBS and cultured for 20 h in DMEM without FBS. The conditioned medium was

then harvested and centrifuged for 5 min at 2000 rpm. To quantify the total amount of $TGF\beta_1$, samples were subjected to heat denaturation followed by acidic treatment and neutralization according to the manufacturer's instructions. The level of active $TGF\beta_1$ was determined by ELISA (TGF beta-1 Human/Mouse Uncoated ELISA Kit, Invitrogen).

2.5 In vivo studies

2.5.1 Animal preparation

D2-mdx (D2.B10-Dmd^{mdx}/J) mice were purchased from The Jackson Laboratory. They were bred and used according to French legislation. The protocols were approved by the ACCeS Ethical committee from Université Claude Bernard Lyon 1 (project n°APAFIS#33920-2021092301268077v4). Experiments were conducted on males of 8-12 weeks of age.

2.5.2 Organs biodistribution

200 µL of fluorescent nanoparticles were administered to anesthetized mice by i.v. injection in the tail vein. At scheduled time points (30 min, 1 h, 24 h, 48 h, 72 h), anesthetized animals were fully imaged in a light-tight chamber where a controlled flow of 1.5% isoflurane in the air was administered to maintain anesthesia. Fluorescence images, as well as bright-field pictures of mice's whole body (ventral and prone view), were acquired *via* a back-thinned CCD-cooled camera ORCAIIBT-512G Deutschland GmbH (Herrsching am Ammersee, Germany) using a coloured glass long-pass RG 665 filter (Melles Griot, Voisins les Bretonneaux, France), which cuts off all excitation light. Optical excitation was carried out at 644 nm, and the emission wavelength was detected at 655 nm. At each time point, n = 3 mice for time point were sacrificed and tissues and organs (brain, heart, lungs, liver, kidney, spleen, GI, diaphragm, bone marrow, lymph nodes and muscles) were harvested for *ex vivo* imaging. Images were analyzed using the Wasabi software 1.5 (Hamamatsu Photonics Deutschland GmbH).

2.5.3 Treatment efficacy

Mice were randomly divided into three groups: 991-loaded PLGA nanoparticles, PLGA nanoparticles, and untreated (NT). Loaded and empty nanoparticles were administered one injection every other day (3.50 mg/kg of drug) during the 3 weeks.

2.5.4 Isolation of all cell populations from muscles

Diaphragm and gastrocnemius muscles were dissociated and digested in RPMI medium (Gibco #61870) containing 1 U/mL of Collagenase B (Gibco #17101015) for 1.5 h at 37°C with

agitation. Digested muscles were passed through a 30 μm strainer (Myltenyi Biotec #130-098-458), red blood cells were eliminated with ACK Lysing Buffer (Lonza #BP10-548E) and samples were incubated with anti-mouse FcR Blocking Reagent (Myltenyi Biotec #130-092-575) for 20 min at 4 °C in PBS 2% FBS. Cells were then stained with anti-CD45 (PE-(eBioscience #12-0451-82) or PE-Cy7-(eBioscience #25-0451-82)conjugated), anti-CD64 (FITC-(Biolegend #139316) or Alexa Fluor 647-(Biolegend #139321)conjugated), anti-Ly6C (PE-conjugated, eBioscience #12-5932-82), anti-CD163 (PE-Cy7-conjugated, Biolegend #155319), anti-CD206 (FITC-conjugated, eBioscience # 53-2061-82) and anti-Folate Receptor β (APC-conjugated, Biolegend #153306) antibodies for 30 min at 4 °C in PBS 2% FBS. After dead cells labeling with DAPI solution (BD Biosciences #564907), samples were analyzed on a FACSCanto II (BD Biosciences) apparatus. Cross-sectional area (CSA) was determined on whole muscle sections labeled by anti-laminin antibody using the Open-CSAM program, as previously described [27].

2.6 Data analysis

For *in vitro* and *in vivo* analysis, the results are reported as mean ± standard error mean (SEM) of replicate experiments. Statistical analyses were performed using Student's t test. P-value reported was considered as statistically significant for $^{**}p<0.01$, highly significant for $^{***}p<0.0005$. All graphs were prepared using GraphPad software.

3. Results

3.1 In vitro

In the current study, we hypothesized that the nanoformulation of 991-loaded PLGA nanoparticles might serve as a potential strategy to overcome the side effects of the free drug during *in vivo* administration. In our previous work, we described the formulation and optimization of 991-loaded nanoparticles by microfluidic technique.

The validation of the polymer nanosystem *in vitro* was investigated by culturing BMDMs rendered pro-fibrotic by treatment with fib-mdx muscle homogenates (Fig. 1A). The internalization of polymer nanoparticles was assessed by preparing fluorescence-labeled nanoparticles for confocal microscopy analysis. Our findings revealed a fast internalization as soon as 2h incubation time which lasted over 24 h (Fig. 1B). The internalization of polymer nanoparticles started very fast due to the biological nature of macrophages which are devoted to recognize external agents and phagocyte any external and "non-self" intruders [28,29].

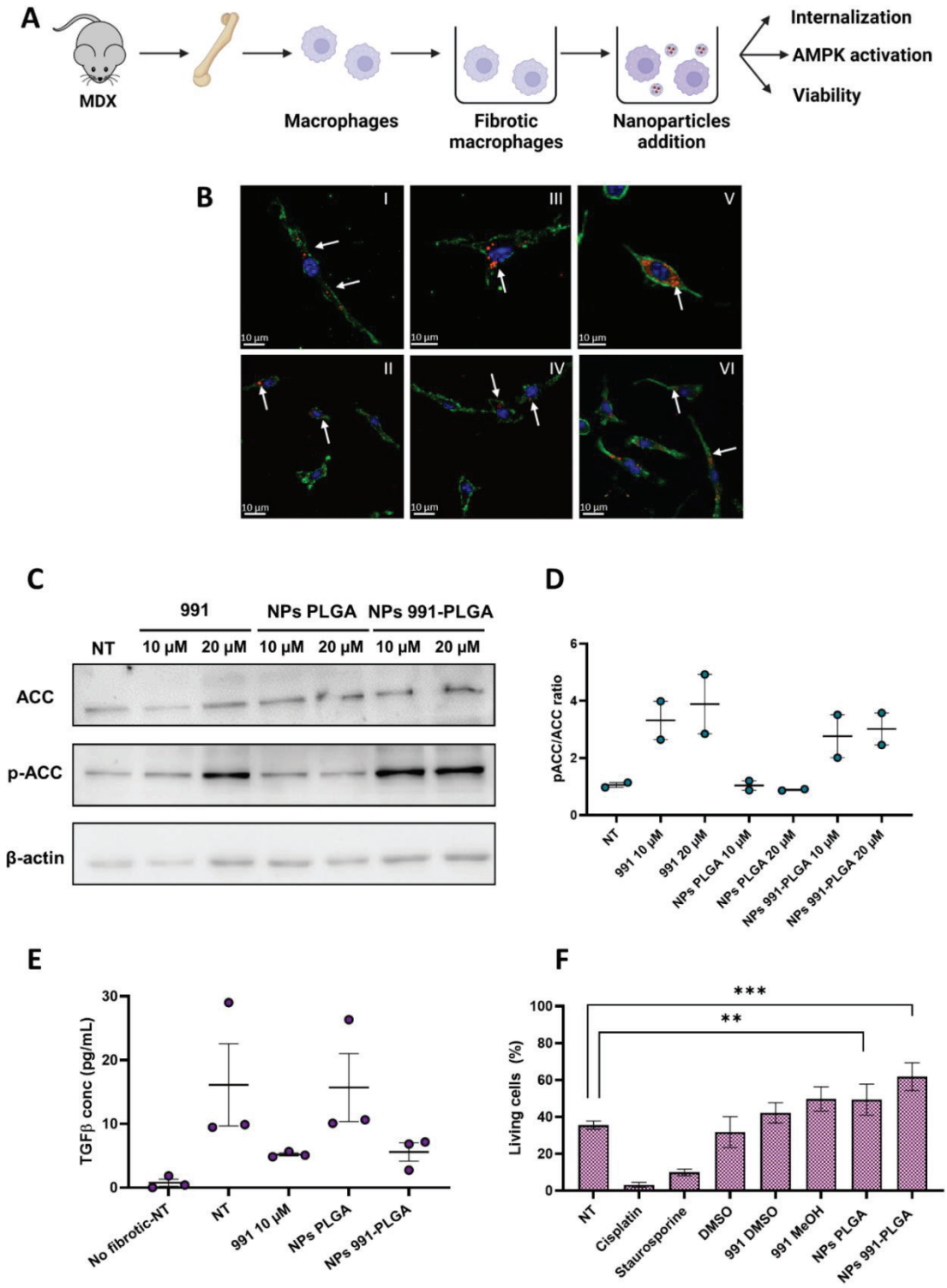

Fig. 1. (A) Scheme of the experimental design. (B) Intracellular uptake of PLGA nanoparticles in fibrotic BMDMs. Confocal fluorescence microscopy of BMDMs (I-VI) that have been incubated with nanoparticles for 2 h (I, II), 4 h (III, IV) and 24 h (V, VI). PLGA nanoparticles were loaded with DiD (red fluorescence) and cell membranes are counterstained with Cy3 fluorophore (green fluorescence). Hoechst 33258 (blue fluorescence) staining depicts nuclei. (C, D) BMDMs were treated with free and loaded 991 (NPs 991-PLGA) for 6 h, and the phosphorylation of ACC (p-ACC) was quantified by immunoblotting (C-D). (C) Representative immunoblots showing p-ACC, total ACC, and β-actin as a loading control (NT, non-treated). (D) Quantification of the ratio of phosphorylated and total ACC protein. (E) TGFβ_1 production of BMDMs incubated overnight with free drug, PLGA nanoparticles, and drug-loaded PLGA nanoparticles at a concentration of 10 µM. (F) Annexin V/DAPI staining of fibrotic BMDMs. The cells were incubated for 24 h with free 991 and 991-loaded nanoparticles at a concentration of 20 µM. Data are presented as means ± SEM. **p<0.01, *** p<0.0005

In an attempt to demonstrate that 991 encapsulation into nanoparticles did not alter drug properties, we evaluated the impact of 991-PLGA nanoparticles on phosphorylation of acetyl-CoA carboxylase (ACC), a major target of AMPK. Similarly to the treatment with 991 alone (68.1% and 72.3% for 10 and 20 μM concentration, respectively), treatment of fibrotic BMDMs with 991-loaded nanoparticles induced the phosphorylation of ACC (58.5% and 61.5% for 10 and 20 μM concentration, respectively) compared with untreated control (Fig. 1C-D), indicating AMPK activation. Next, we confirmed the retention of 991 activity once incorporated into the polymer matrix by assessing its capacity to inhibit TGFβ_1 secretion on fibrotic BMDMs, as previously described [12]. Treatment of fibrotic BMDMs by 991-loaded PLGA nanoparticles reduced their TGFβ_1 secretion (Fig. 1E, 65.0% as compared with PLGA) as efficiently as treatment by free 991 (Fig 1E, 67.8% as compared with NT). Importantly, these decrease in TGFβ_1 secretion was not due to a cytotoxic effect of PLGA-991 nanoparticles. Indeed, incubation of BMDMs with empty and loaded nanoparticles induced no significant reduction in cell viability after 24 h treatment compared with untreated control (Fig. 1F). The presence of PLGA as unloaded and loaded nanoparticles significantly increased cellular viability as compared with NT sample.

Furthermore, to preliminary characterize the behavior of loaded nanoparticles *in vivo*, hemolytic analysis was performed. The release of hemoglobin determined the membrane damage caused by the formulation assayed. The results showed that 991-loaded PLGA nanoparticles had no hemolytic effect at tested concentrations (10, 20 and 50 μM) when diluted with erythrocytes at 3% w/v, registering no detectable disturbance in the red blood cell membranes. Therefore, these results indicate that the encapsulation of 991 into polymer nanoparticles might counteract the hemolytic activity of free 991 even at high concentrations, providing a hemocompatible system. *In vitro* results evidenced fast nanoparticle internalization in pro-inflammatory macrophages, which phenotype can be switched toward anti-inflammatory cells by AMPK activation, preserving the activity of encapsulated 991. 991 loaded into PLGA nanoparticles showed biocompatibility and no toxic effects *in vitro*. Activation of AMPK cascade was induced after 991 release from polymer matrix, making 991 usable *in vivo*.

3.2 Organs biodistribution

Next, we evaluated the nanoparticulate system on the pre-clinical mouse model of DMD (D2.mdx), which exhibits strong inflammation, fibrosis and muscle alteration in the diaphragm and the gastrocnemius muscles [30,31]. To assess whether small-size PLGA nanoparticles, characterized by size below 100 nm, can accumulate in the diaphragm and skeletal muscles,

DiD-loaded nanoparticles were administered by i.v. injection to mice (Fig. 2A). At defined time points, all the organs and tissues were excised and imaged using IVIS® (Fig. 2B). The fluorescence intensity was quantified considering the areas of the whole organ. Our data confirmed that sub-100 nm nanoparticles administered by i.v. reached the main organs at a very shorter time point, meaning that they are immediately internalized and then re-distributed by blood circulation. In the liver, nanoparticle residence lasted over 72 h, but in the spleen and lung the fluorescence intensity decreased over time showing an initial uptake and then the complete elimination of nanosystem (Fig. 2C), as already reported for PLGA nanoparticles [32]. Interestingly, fluorescence was also detected in the diaphragm (Fig. 2D). Flow cytometry analysis showed that up to 10% of the cells in the diaphragm internalized the nanosystem after 30 min and 1 h (Fig. 2E). The nanosystem signal decreased over time until an elimination over 72 h (<5%). Although no fluorescence was detected in the gastrocnemius muscle by imaging, flow cytometry showed that around 5% of the cells internalized the nanosystems (Fig. 2F).
These results show that PLGA nanoparticles efficiently reach the diaphragm and gastrocnemius muscles in the D2.mdx pre-clinical model of DMD and represent a relevant strategy to deliver specific AMPK activators.

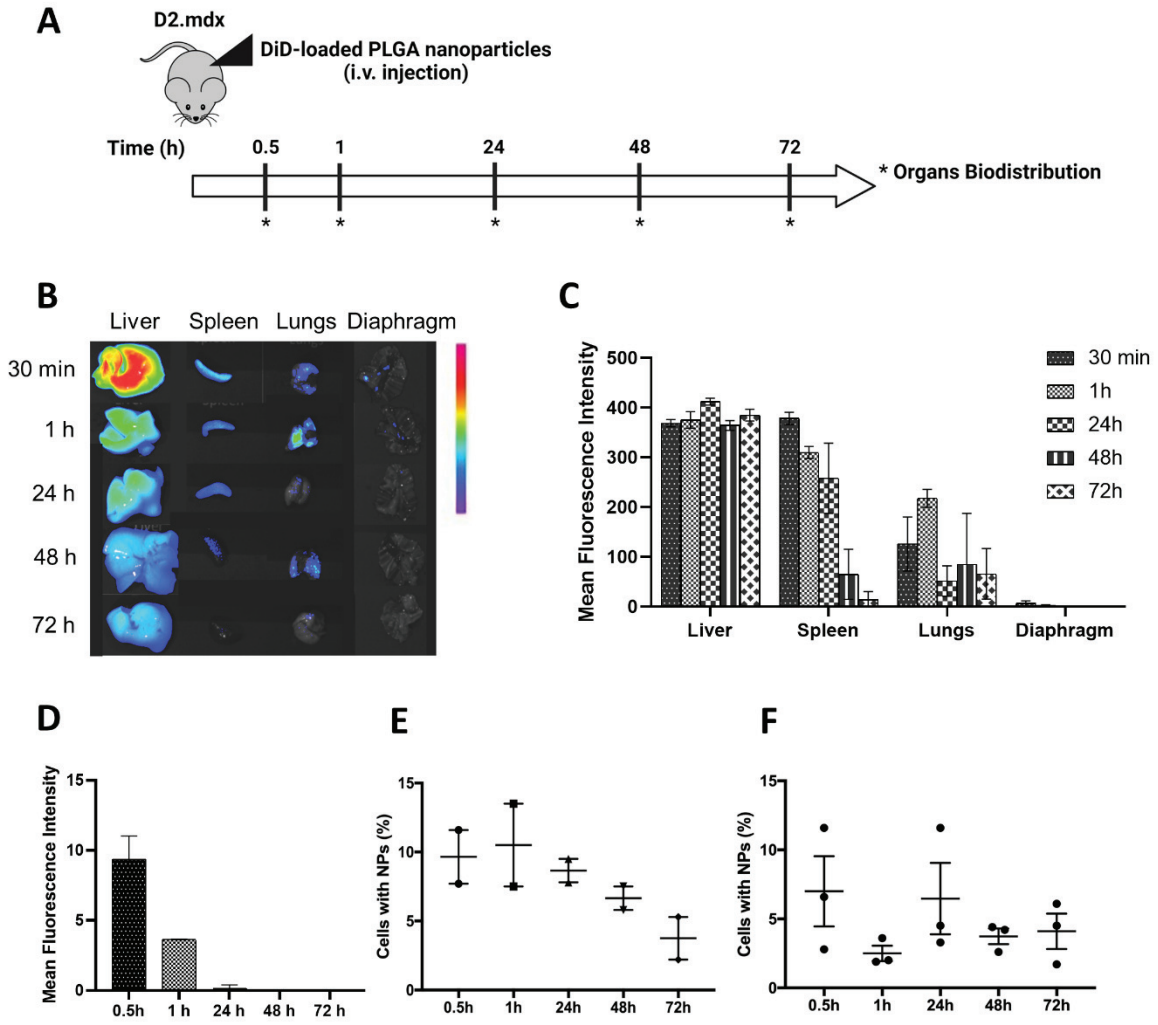

Fig. 2. (A) Scheme of the experimental design. (B) Organ *ex vivo* biodistribution of DiD-loaded PLGA nanoparticles, at selected time points. (C) Quantification of mean fluorescence intensity in fluorescent organs. (D) Quantification of mean fluorescence intensity in diaphragm. (E) Quantification of cells which internalized fluorescent-PLGA nanoparticles by FACS analysis in diaphragm cells. (F) Quantification of cells which internalized fluorescent-PLGA nanoparticles by FACS analysis in gastrocnemius cells. Data is shown as mean ± SEM (n =3).

3.3 991-loaded nanoparticles treatment improves muscle homeostasis

Finally, we used the D2.mdx mouse model to investigate the functional effect of loaded nanoparticles on dystrophic muscle homeostasis. To this aim, 991-loaded PLGA nanoparticles were chronically i.v. administered to mice for three weeks (Fig. 3A). In the first set of experiments, we evaluated the consequences of improvement in immune cell status by assessing the 991-PLGA nanoparticles treatment on dystrophic muscle features. 991 released from the polymer matrix was associated with a reduced macrophage infiltration in gastrocnemius compared to mice that received only the vehicle (Fig. 3B-C).

This effect was associated to a decrease in muscle fibrosis, as shown by a reduction in the area expressing collagen 1 (Coll1) in the diaphragm (Fig. 3D-E). Moreover, 991-loaded PLGA nanoparticles promoted muscle mass increasing of diaphragm and gastrocnemius in loaded nanoparticles-treated mice (Fig. 3F-G). This significant increase in muscle mass and reduced fibrosis are indicative of improved muscle homeostasis in D2.mdx mice after treatment with 991-PLGA nanoparticles.

Taken together, these results show that the modulation of inflammation and especially macrophages' phenotype upon 991-loaded PLGA nanoparticles treatment is associated with reduced fibrosis in the diaphragm and increased muscle mass, leading to improved muscle homeostasis.

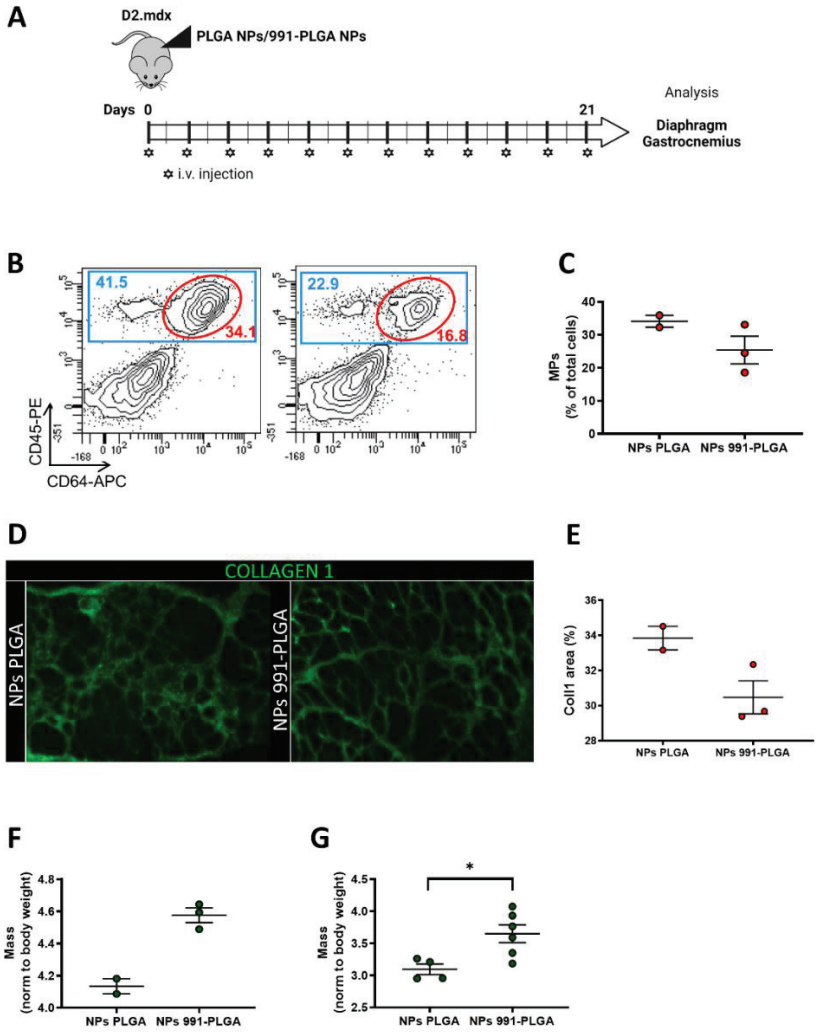

Fig. 3. 991-PLGA nanoparticles treatment ameliorates dystrophic muscle phenotype. (A-F) D2.mdx mice were treated every other day for three weeks, and diaphragm and gastrocnemius were harvested. (A) Scheme of the experimental design. (B-C) FACS analysis of the surface marker CD45+ and CD64+ in gastrocnemius for sample treated with PLGA nanoparticles (B, left) and 991-PLGA nanoparticles (B, right). (C) Percentage of positive macrophages in gastrocnemius. (D-E) Muscle sections were immunostained for Coll1. (D) Representative images of Coll1 immunostained in the diaphragm. (E) Percentage of Coll1 area in the diaphragm. (F-G) Muscle mass normalized to mouse body weight for diaphragm (F) and (G) gastrocnemius.

4. Discussion

The role of macrophages in fibrosis pattern is still not clear [33,34]. It has been demonstrated how macrophages infiltration is responsible for increased fibrosis in injured muscle [35,36]. These inflammatory macrophages produce high amount of pro-inflammatory cytokines, in particular TGFβ_1 amount through the expression of the latent-TGF-β-binding protein (LTBP4) genetic pathway. LTBP4 has been demonstrated to be involved in the pathological features of DMD patients [37] and its expression was directly controlled by AMPK activation. Consequently, activation of AMPK can improve muscle homeostasis in dystrophic muscle. However, *in vivo* administration of AMPK activator molecules can be challenging for their off-target effects [10]. In this study, encapsulation of 991 into PLGA nanoparticles has been proposed as potential strategy for using AMPK activator molecules *in vivo*. The effect of 991 encapsulated into polymer nanoparticles was assessed *in vitro* and *in vivo* to improve muscle homeostasis in pre-clinical DMD mouse model. We showed that the 991 can be efficiently encapsulated into PLGA nanoparticles, preserving its activity on AMPK activation. Our results indicates activation of AMPK by reduction of TGFβ_1 expression and activation of ACC in BMDMs by loaded nanoparticles, as already demonstrated in macrophages treated with free 991 [12]. At the same concentration of free 991, loaded nanoparticles promoted the activation of AMPK and consequently skewing of pro-inflammatory macrophages toward their anti-inflammatory phenotype. Encapsulation of the active molecule into drug delivery systems of different nature usually allows to preserve the pharmacological activity of drug, exerting its therapeutical efficacy [38]. The choice of specific nanocarriers is crucial to consider the delivery in dystrophic muscles. The potential toxic effect of nanoparticles was avoided by choosing PLGA to promote 991 activity *in vitro* and *in vivo*. PLGA is a biocompatible and biodegradable polymer, FDA-approved for humane usage [39] and widely used in nanomedicine field [40]. The effect of PLGA metabolites, in particular lactic acid, can positively participate in cell survival. Lactate has been recently investigated as fuel for cells and chemical messenger to enhance cellular viability [41,42]. The principal advantage of nanoparticles as drug carriers is their small size, which allows them to traverse biological barriers, enter various tissues and associate to specific cell populations. As already demonstrated for nanosystems of diverse natures, liver, spleen and lungs are the organs showing higher uptake [43]. For PLGA nanoparticles that have successfully delivered different therapeutic compounds, the biodistribution is usually affected by size [32]. Using IVIS and flow cytometry, 10% of sub-100 nanoparticles resulted in diaphragm after i.v. injection. The

discrepancy observed between IVIS analysis and flow cytometry in detecting nanoparticles into gastrocnemius can be likely due to the too low fluorescence intensity, hard to detect, compared to the most sensitive flow cytometry technique. Similar to tumor accumulation, the internalization of the nanoparticulate system by i.v. injection can reach around a 10-15% [44,45]. These results are useful to understand the ability of nanoparticles to be distributed by blood circulation. The alteration of vessel junctions and the enhanced permeation of vessels have demonstrated a higher accumulation of nanoparticles compared to physiological conditions, by the exploitation of the enhanced permeation and retention (EPR) effect [46]. By exploiting the inflammatory status of D2.mdx, we can enhance the permeation of blood vessels and increase the extravasation and then the accumulation of nanoparticles in inflamed tissues [47].

Here, incorporation of 991 into polymer nanoparticles allowed non-toxic distribution of the drug throughout the dystrophic muscles, providing a model to administer AMPK activator molecules *in vivo*. Formulation of colloidal nanosystems has been described to modulate inflammatory response in pre-clinical DMD mouse model, by providing anti-inflammatory cytokines and improving dystrophic muscle functions by intramuscular (i.m.) injection [48]. The more severe and chronic inflammatory and fibrosis nature of pre-clinical DMD mouse model suggests the need of a generalized delivery of nanoparticles to immediately target compromised organs and tissues, such as diaphragm, through i.v. administration [49].

991-loaded PLGA nanoparticle treatment significantly reduced macrophages infiltration in gastrocnemius muscle in DMD mouse model. I.v. nanoparticles injection for 3 weeks increased muscle mass of diaphragm and gastrocnemius (Fig. 3F-G), and reduced fibrosis in the diaphragm (Fig. 3E). Our promising results on reduced macrophages infiltration and increased muscle mass are consistent with previous finding of AMPK activation *in vivo* by agonist molecules. Activation of AMPK *in vivo* has already demonstrated to improve histological signs of pathology and improve contractile function in the mdx mouse model of DMD [50].

5. Conclusions

Here we propose a new biocompatible formulation of an AMPK activator molecule to make 991 usable *in vivo*. The study indicates that 991 encapsulated into polymer nanoparticles can be administered *in vivo* without evident toxic drug effects. The immune response mediated by pro-inflammatory macrophages can be shifted in chronically inflamed dystrophic muscle and ultimately promote improved muscle homeostasis. Although a huge number of unique mutations have been identified in muscular myopathies, chronic inflammation and fibrosis play

a significant role in the pathogenesis of DMD patients [51]. This study suggests that modulation of inflammation may slow disease progression and improve dystrophic muscle phenotype through AMPK activation.

References

1. Lafuse, W.P.; Wozniak, D.J.; Rajaram, M.V.S. Role of Cardiac Macrophages on Cardiac Inflammation, Fibrosis and Tissue Repair. *Cells* **2020**, *10*, E51, doi:10.3390/cells10010051.
2. Lee, Y.S.; Olefsky, J. Chronic Tissue Inflammation and Metabolic Disease. *Genes Dev* **2021**, *35*, 307–328, doi:10.1101/gad.346312.120.
3. Medzhitov, R. Origin and Physiological Roles of Inflammation. *Nature* **2008**, *454*, 428–435, doi:10.1038/nature07201.
4. Caja, L.; Dituri, F.; Mancarella, S.; Caballero-Diaz, D.; Moustakas, A.; Giannelli, G.; Fabregat, I. TGF-β and the Tissue Microenvironment: Relevance in Fibrosis and Cancer. *Int J Mol Sci* **2018**, *19*, E1294, doi:10.3390/ijms19051294.
5. Muntoni, F.; Torelli, S.; Ferlini, A. Dystrophin and Mutations: One Gene, Several Proteins, Multiple Phenotypes. *Lancet Neurol* **2003**, *2*, 731–740, doi:10.1016/s1474-4422(03)00585-4.
6. Hoyer, F.F.; Naxerova, K.; Schloss, M.J.; Hulsmans, M.; Nair, A.V.; Dutta, P.; Calcagno, D.M.; Herisson, F.; Anzai, A.; Sun, Y.; et al. Tissue-Specific Macrophage Responses to Remote Injury Impact the Outcome of Subsequent Local Immune Challenge. *Immunity* **2019**, *51*, 899-914.e7, doi:10.1016/j.immuni.2019.10.010.
7. Mounier, R.; Théret, M.; Arnold, L.; Cuvellier, S.; Bultot, L.; Göransson, O.; Sanz, N.; Ferry, A.; Sakamoto, K.; Foretz, M.; et al. AMPKα1 Regulates Macrophage Skewing at the Time of Resolution of Inflammation during Skeletal Muscle Regeneration. *Cell Metabolism* **2013**, *18*, 251–264, doi:10.1016/j.cmet.2013.06.017.
8. Saclier, M.; Ben Larbi, S.; My Ly, H.; Moulin, E.; Mounier, R.; Chazaud, B.; Juban, G. Interplay between Myofibers and Pro-Inflammatory Macrophages Controls Muscle Damage in Mdx Mice. *J Cell Sci* **2021**, *134*, jcs258429, doi:10.1242/jcs.258429.
9. Coccimiglio, I.F.; Clarke, D.C. ADP Is the Dominant Controller of AMP-Activated Protein Kinase Activity Dynamics in Skeletal Muscle during Exercise. *PLoS Comput Biol* **2020**, *16*, e1008079, doi:10.1371/journal.pcbi.1008079.
10. Olivier, S.; Foretz, M.; Viollet, B. Promise and Challenges for Direct Small Molecule AMPK Activators. *Biochem Pharmacol* **2018**, *153*, 147–158, doi:10.1016/j.bcp.2018.01.049.
11. Kim, J.; Yang, G.; Kim, Y.; Kim, J.; Ha, J. AMPK Activators: Mechanisms of Action and Physiological Activities. *Exp Mol Med* **2016**, *48*, e224, doi:10.1038/emm.2016.16.
12. Juban, G.; Saclier, M.; Yacoub-Youssef, H.; Kernou, A.; Arnold, L.; Boisson, C.; Ben Larbi, S.; Magnan, M.; Cuvellier, S.; Théret, M.; et al. AMPK Activation Regulates LTBP4-Dependent TGF-B1 Secretion by Pro-Inflammatory Macrophages and Controls Fibrosis in Duchenne Muscular Dystrophy. *Cell Rep* **2018**, *25*, 2163-2176.e6, doi:10.1016/j.celrep.2018.10.077.
13. Jiang, P.; Ren, L.; Zhi, L.; Yu, Z.; Lv, F.; Xu, F.; Peng, W.; Bai, X.; Cheng, K.; Quan, L.; et al. Negative Regulation of AMPK Signaling by High Glucose via E3 Ubiquitin Ligase MG53. *Mol Cell* **2021**, *81*, 629-637.e5, doi:10.1016/j.molcel.2020.12.008.

14. Yang, F.; Qin, Y.; Wang, Y.; Meng, S.; Xian, H.; Che, H.; Lv, J.; Li, Y.; Yu, Y.; Bai, Y.; et al. Metformin Inhibits the NLRP3 Inflammasome via AMPK/MTOR-Dependent Effects in Diabetic Cardiomyopathy. *Int J Biol Sci* **2019**, *15*, 1010–1019, doi:10.7150/ijbs.29680.
15. Bultot, L.; Jensen, T.E.; Lai, Y.-C.; Madsen, A.L.B.; Collodet, C.; Kviklyte, S.; Deak, M.; Yavari, A.; Foretz, M.; Ghaffari, S.; et al. Benzimidazole Derivative Small-Molecule 991 Enhances AMPK Activity and Glucose Uptake Induced by AICAR or Contraction in Skeletal Muscle. *Am J Physiol Endocrinol Metab* **2016**, *311*, E706–E719, doi:10.1152/ajpendo.00237.2016.
16. Xiao, B.; Sanders, M.J.; Carmena, D.; Bright, N.J.; Haire, L.F.; Underwood, E.; Patel, B.R.; Heath, R.B.; Walker, P.A.; Hallen, S.; et al. Structural Basis of AMPK Regulation by Small Molecule Activators. *Nat Commun* **2013**, *4*, 3017, doi:10.1038/ncomms4017.
17. Lai, Y.-C.; Kviklyte, S.; Vertommen, D.; Lantier, L.; Foretz, M.; Viollet, B.; Hallén, S.; Rider, M.H. A Small-Molecule Benzimidazole Derivative That Potently Activates AMPK to Increase Glucose Transport in Skeletal Muscle: Comparison with Effects of Contraction and Other AMPK Activators. *Biochem J* **2014**, *460*, 363–375, doi:10.1042/BJ20131673.
18. Huang, X.; Qiu, M.; Wang, T.; Li, B.; Zhang, S.; Zhang, T.; Liu, P.; Wang, Q.; Qian, Z.R.; Zhu, C.; et al. Carrier-Free Multifunctional Nanomedicine for Intraperitoneal Disseminated Ovarian Cancer Therapy. *Journal of Nanobiotechnology* **2022**, *20*, doi:10.1186/s12951-022-01300-4.
19. Lim, S.A.; Cox, A.; Tung, M.; Chung, E.J. Clinical Progress of Nanomedicine-Based RNA Therapies. *Bioactive Materials* **2022**, *12*, 203–213, doi:10.1016/j.bioactmat.2021.10.018.
20. Andreana, I.; Repellin, M.; Carton, F.; Kryza, D.; Briançon, S.; Chazaud, B.; Mounier, R.; Arpicco, S.; Malatesta, M.; Stella, B.; et al. Nanomedicine for Gene Delivery and Drug Repurposing in the Treatment of Muscular Dystrophies. *Pharmaceutics* **2021**, *13*, doi:10.3390/pharmaceutics13020278.
21. Macedo, L.B.; Nogueira-Librelotto, D.R.; Mathes, D.; de Vargas, J.M.; da Rosa, R.M.; Rodrigues, O.E.D.; Vinardell, M.P.; Mitjans, M.; Rolim, C.M.B. Overcoming MDR by Associating Doxorubicin and PH-Sensitive PLGA Nanoparticles Containing a Novel Organoselenium Compound—An In Vitro Study. *Pharmaceutics* **2022**, *14*, 80, doi:10.3390/pharmaceutics14010080.
22. Welc, S.S.; Flores, I.; Wehling-Henricks, M.; Ramos, J.; Wang, Y.; Bertoni, C.; Tidball, J.G. Targeting a Therapeutic LIF Transgene to Muscle via the Immune System Ameliorates Muscular Dystrophy. *Nat Commun* **2019**, *10*, 2788, doi:10.1038/s41467-019-10614-1.
23. Li, D.; Sun, H.; Jiang, L.; Zhang, K.; Liu, W.; Zhu, Y.; Fangteng, J.; Shi, C.; Zhao, L.; Sun, H.; et al. Enhanced Biocompatibility of PLGA Nanofibers with Gelatin/Nano-Hydroxyapatite Bone Biomimetics Incorporation. *ACS Appl Mater Interfaces* **2014**, *6*, 9402–9410, doi:10.1021/am5017792.
24. Almoustafa, H.A.; Alshawsh, M.A.; Chik, Z. Technical Aspects of Preparing PEG-PLGA Nanoparticles as Carrier for Chemotherapeutic agents by Nanoprecipitation Method. *International Journal of Pharmaceutics* **2017**, *533*, 275–284, doi:10.1016/j.ijpharm.2017.09.054.
25. Danhier, F.; Ansorena, E.; Silva, J.M.; Coco, R.; Le Breton, A.; Préat, V. PLGA-Based Nanoparticles: An Overview of Biomedical Applications. *J Control Release* **2012**, *161*, 505–522, doi:10.1016/j.jconrel.2012.01.043.
26. Hammers, D.W.; Hart, C.C.; Matheny, M.K.; Wright, L.A.; Armellini, M.; Barton, E.R.; Sweeney, H.L. The D2.Mdx Mouse as a Preclinical Model of the Skeletal Muscle Pathology Associated with Duchenne Muscular Dystrophy. *Sci Rep* **2020**, *10*, 14070, doi:10.1038/s41598-020-70987-y.

27. Desgeorges, T.; Liot, S.; Lyon, S.; Bouvière, J.; Kemmel, A.; Trignol, A.; Rousseau, D.; Chapuis, B.; Gondin, J.; Mounier, R.; et al. Open-CSAM, a New Tool for Semi-Automated Analysis of Myofiber Cross-Sectional Area in Regenerating Adult Skeletal Muscle. *Skelet Muscle* **2019**, *9*, 2, doi:10.1186/s13395-018-0186-6.
28. Gessain, G.; Blériot, C.; Ginhoux, F. Non-Genetic Heterogeneity of Macrophages in Diseases—A Medical Perspective. *Frontiers in Cell and Developmental Biology* **2020**, *8*.
29. Oishi, Y.; Manabe, I. Macrophages in Inflammation, Repair and Regeneration. *Int Immunol* **2018**, *30*, 511–528, doi:10.1093/intimm/dxy054.
30. McRae, N.L.; Addinsall, A.B.; Howlett, K.F.; McNeill, B.; McCulloch, D.R.; Stupka, N. Genetic Reduction of the Extracellular Matrix Protein Versican Attenuates Inflammatory Cell Infiltration and Improves Contractile Function in Dystrophic Mdx Diaphragm Muscles. *Sci Rep* **2020**, *10*, 11080, doi:10.1038/s41598-020-67464-x.
31. Gaglianone, R.B.; Bloise, F.F.; Lagrota-Candido, J.; Mermelstein, C.; Quirico-Santos, T. Persistent Mdx Diaphragm Alterations Are Accompanied by Increased Expression and Activity of Calcium and Muscle-Specific Proteins. *Histol Histopathol* **2021**, *36*, 775–783, doi:10.14670/HH-18-334.
32. Mandl, H.K.; Quijano, E.; Suh, H.W.; Sparago, E.; Oeck, S.; Grun, M.; Glazer, P.M.; Saltzman, W.M. Optimizing Biodegradable Nanoparticle Size for Tissue-Specific Delivery. *J Control Release* **2019**, *314*, 92–101, doi:10.1016/j.jconrel.2019.09.020.
33. Tidball, J.G.; Villalta, S.A. Regulatory Interactions between Muscle and the Immune System during Muscle Regeneration. *Am J Physiol Regul Integr Comp Physiol* **2010**, *298*, R1173-1187, doi:10.1152/ajpregu.00735.2009.
34. Kölbel, H.; Preuße, C.; Brand, L.; von Moers, A.; Della Marina, A.; Schuelke, M.; Roos, A.; Goebel, H.-H.; Schara-Schmidt, U.; Stenzel, W. Inflammation, Fibrosis and Skeletal Muscle Regeneration in LGMDR9 Are Orchestrated by Macrophages. *Neuropathol Appl Neurobiol* **2021**, *47*, 856–866, doi:10.1111/nan.12730.
35. Ueshima, E.; Fujimori, M.; Kodama, H.; Felsen, D.; Chen, J.; Durack, J.C.; Solomon, S.B.; Coleman, J.A.; Srimathveeravalli, G. Macrophage-Secreted TGF-B1 Contributes to Fibroblast Activation and Ureteral Stricture after Ablation Injury. *Am J Physiol Renal Physiol* **2019**, *317*, F52–F64, doi:10.1152/ajprenal.00260.2018.
36. Wen, Y.; Lu, X.; Ren, J.; Privratsky, J.R.; Yang, B.; Rudemiller, N.P.; Zhang, J.; Griffiths, R.; Jain, M.K.; Nedospasov, S.A.; et al. KLF4 in Macrophages Attenuates TNFα-Mediated Kidney Injury and Fibrosis. *J Am Soc Nephrol* **2019**, *30*, 1925–1938, doi:10.1681/ASN.2019020111.
37. Flanigan, K.M.; Ceco, E.; Lamar, K.-M.; Kaminoh, Y.; Dunn, D.M.; Mendell, J.R.; King, W.M.; Pestronk, A.; Florence, J.M.; Mathews, K.D.; et al. LTBP4 Genotype Predicts Age of Ambulatory Loss in Duchenne Muscular Dystrophy. *Annals of Neurology* **2013**, *73*, 481–488, doi:10.1002/ana.23819.
38. Pontes-Quero, G.M.; Benito-Garzón, L.; Pérez Cano, J.; Aguilar, M.R.; Vázquez-Lasa, B. Amphiphilic Polymeric Nanoparticles Encapsulating Curcumin: Antioxidant, Anti-Inflammatory and Biocompatibility Studies. *Mater Sci Eng C Mater Biol Appl* **2021**, *121*, 111793, doi:10.1016/j.msec.2020.111793.
39. Sartor, O. Eligard: Leuprolide Acetate in a Novel Sustained-Release Delivery System. *Urology* **2003**, *61*, 25–31, doi:10.1016/s0090-4295(02)02396-8.
40. Ding, D.; Zhu, Q. Recent Advances of PLGA Micro/Nanoparticles for the Delivery of Biomacromolecular Therapeutics. *Mater Sci Eng C Mater Biol Appl* **2018**, *92*, 1041–1060, doi:10.1016/j.msec.2017.12.036.
41. Descalzi, G.; Gao, V.; Steinman, M.Q.; Suzuki, A.; Alberini, C.M. Lactate from Astrocytes Fuels Learning-Induced MRNA Translation in Excitatory and Inhibitory Neurons. *Commun Biol* **2019**, *2*, 247, doi:10.1038/s42003-019-0495-2.

42. Lund, J.; Aas, V.; Tingstad, R.H.; Van Hees, A.; Nikolić, N. Utilization of Lactic Acid in Human Myotubes and Interplay with Glucose and Fatty Acid Metabolism. *Sci Rep* **2018**, *8*, 9814, doi:10.1038/s41598-018-28249-5.
43. Hong, C.; Alser, O.; Gebran, A.; He, Y.; Joo, W.; Kokoroskos, N.; Velmahos, G.; Olsen, B.D.; Hammond, P.T. Modulating Nanoparticle Size to Understand Factors Affecting Hemostatic Efficacy and Maximize Survival in a Lethal Inferior Vena Cava Injury Model. *ACS Nano* **2022**, *16*, 2494–2510, doi:10.1021/acsnano.1c09108.
44. Moss, J.I.; Barjat, H.; Emmas, S.-A.; Strittmatter, N.; Maynard, J.; Goodwin, R.J.A.; Storm, G.; Lammers, T.; Puri, S.; Ashford, M.B.; et al. High-Resolution 3D Visualization of Nanomedicine Distribution in Tumors. *Theranostics* **2020**, *10*, 880–897, doi:10.7150/thno.37178.
45. Guo, P.; Liu, D.; Subramanyam, K.; Wang, B.; Yang, J.; Huang, J.; Auguste, D.T.; Moses, M.A. Nanoparticle Elasticity Directs Tumor Uptake. *Nat Commun* **2018**, *9*, 130, doi:10.1038/s41467-017-02588-9.
46. Yu, J.; He, X.; Wang, Z.; Liu, S.; Hao, D.; Li, X.; Huang, Y. Combination of Starvation Therapy and Pt-NP Based Chemotherapy for Synergistic Cancer Treatment. *J Mater Chem B* **2021**, *9*, 6406–6411, doi:10.1039/d1tb01222c.
47. Shi, Y.; van der Meel, R.; Chen, X.; Lammers, T. The EPR Effect and beyond: Strategies to Improve Tumor Targeting and Cancer Nanomedicine Treatment Efficacy. *Theranostics* **2020**, *10*, 7921–7924, doi:10.7150/thno.49577.
48. Raimondo, T.M.; Mooney, D.J. Anti-Inflammatory Nanoparticles Significantly Improve Muscle Function in a Murine Model of Advanced Muscular Dystrophy. *Sci Adv* **2021**, *7*, eabh3693, doi:10.1126/sciadv.abh3693.
49. Crisp, A.; Yin, H.; Goyenvalle, A.; Betts, C.; Moulton, H.M.; Seow, Y.; Babbs, A.; Merritt, T.; Saleh, A.F.; Gait, M.J.; et al. Diaphragm Rescue Alone Prevents Heart Dysfunction in Dystrophic Mice. *Hum Mol Genet* **2011**, *20*, 413–421, doi:10.1093/hmg/ddq477.
50. Pauly, M.; Daussin, F.; Burelle, Y.; Li, T.; Godin, R.; Fauconnier, J.; Koechlin-Ramonatxo, C.; Hugon, G.; Lacampagne, A.; Coisy-Quivy, M.; et al. AMPK Activation Stimulates Autophagy and Ameliorates Muscular Dystrophy in the Mdx Mouse Diaphragm. *The American Journal of Pathology* **2012**, *181*, 583–592, doi:10.1016/j.ajpath.2012.04.004.
51. Tulangekar, A.; Sztal, T.E. Inflammation in Duchenne Muscular Dystrophy–Exploring the Role of Neutrophils in Muscle Damage and Regeneration. *Biomedicines* **2021**, *9*, 1366, doi:10.3390/biomedicines9101366.

Chapter VI

L-carnitine functionalization to increase muscular tropism of PLGA nanoparticles

I. Andreana, M.A. Lacavalla, M. Malatesta, V. Bincoletto, S. Arpicco, B. Stella

(In preparation)

Active targeting strategies can enhance the accumulation of drugs in target tissues or organs. Drug delivery systems, and particularly polymer nanoparticles (NPs), can be surface-functionalized by means of small molecules, proteins or antibodies to improve tropism toward specific therapeutic targets.

Main aim

The aim of this chapter was to exploit L-carnitine as an active targeting molecule to functionalize PLGA NPs and increase muscular tropism.

Specific objectives

- Formulation study to functionalize PLGA NPs with stearoyl-L-carnitine (SC)
- Evaluation of different amounts of targeting agent for a suitable target density
- *In vitro* evaluation of the uptake of targeted NPs
- *In vitro* cytotoxicity study of conjugated NPs

Highlights of the chapter

- The design and optimization of SC-associated PLGA NPs has been presented. 5% and 10% w/w of SC have been assessed to evaluate the most suitable target agent density on NP surface.
- SC-associated NPs were formulated with a fluorescent probe to evaluate the uptake of by muscular cells.
- Morphometric analysis was performed on C2C12 myotubes to number NPs in cells, showing preferential uptake of SC-associated NPs.

L-carnitine functionalization to increase muscular tropism of PLGA nanoparticles

Ilaria Andreana[a], Maria Assunta Lacavalla[b], Manuela Malatesta[b], Valeria Bincoletto[a], Silvia Arpicco[a], Barbara Stella[a,*]

[a] *Dipartimento di Scienza e Tecnologia del Farmaco, Università degli Studi di Torino, Via P. Giuria 9, 10125 Torino, Italy*

[b] *Dipartimento di Neuroscienze, Biomedicina e Movimento, Università di Verona, Strada Le Grazie 8, 37134, Verona, Italy*

***** Corresponding author at: Dipartimento di Scienza e Tecnologia del Farmaco, Università degli Studi di Torino, Via P. Giuria 9, 10125 Torino, Italy. E-mail address: barbara.stella@unito.it. Phone: +39.011.670.66.60.

Abstract

Muscular dystrophies are a group of rare genetic pathologies encompassing a variety of clinical phenotypes and mechanisms of disease. Several compounds have been proposed to treat compromised muscles, but pharmacokinetics and pharmacodynamics problems could occur; to solve these issues, nanocarriers could be used to allow controlled and targeted drug release. Therefore, the aim of this study was to prepare actively targeted drug-loaded PLGA nanoparticles for the treatment of muscular pathologies. By taking advantage of the specific expression of Na^+-coupled carnitine transporter (OCTN2) on muscular cells, nanoparticles have been actively targeted by associating them to an amphiphilic derivative of L-carnitine during nanoprecipitation. We obtained stable and monodispersed targeted nanoparticles; furthermore, pentamidine, an old drug repurposed for its positive effects on myotonic dystrophy type I, was incorporated into nanoparticles. Cell uptake studies have been performed on C2C12 myoblasts and myotubes by confocal microscopy and morphological analysis. The preliminary results showed an increased uptake for carnitine-nanoparticles if compared to nontargeted carriers, probably due to the interaction with OCTN2 receptor, preferentially expressed on myotubes.

Keywords: PLGA, L-carnitine, nanoparticles, active targeting, muscular cells

Graphical abstract

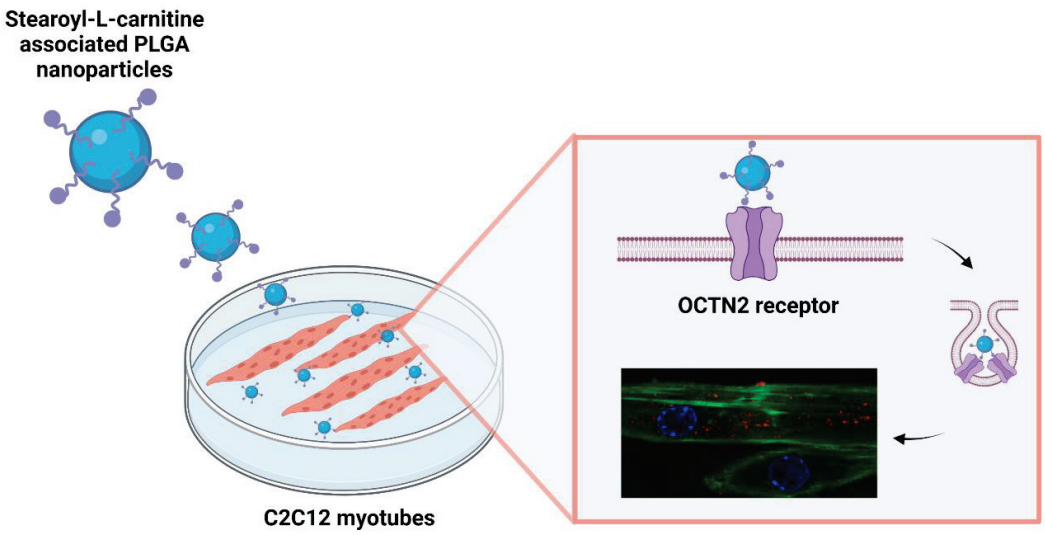

1. Introduction

For years, the enhanced permeation and retention (EPR) effect was the driven strategy for passive targeting, being largely studied for nanocarrier accumulation in tumor environment [1,2]. However, models used to study EPR effect often are not sufficiently accurate to describe the nanocarrier behavior in human body [3]. The active targeting approach is based on the identification of precise disease biomarkers to which specific ligands on nanocarrier surface are directed to increase organ or tissue tropism with great affinity and precision. Moreover, internalizing receptors can enhance nanocarrier uptake by cells [4].

Muscular dystrophies (MDs) are a group of chronic inherited genetic diseases which affect muscles, especially at skeletal level. Currently, no therapies are available to counteract their pathogenic causes and conventional treatments are based on glucocorticoids to mitigate symptoms [5]. Over the last years, drug delivery systems have been proposed for the treatment of MDs; however, *in vivo* delivery is challenging due to the presence of biological barriers: the complex architecture of skeletal muscle and its enveloping by extracellular matrix (ECM) made of fibrous-forming proteins are the main hurdles for drug delivery to skeletal muscles [6,7]. To restrict interactions with ECM, intravenous administration of nanocarriers appeared as a potential strategy to achieve muscle fibers by their dense blood capillary network. However, the treatment of MDs requires long-term administration, which makes biocompatibility and biodegradability of nanosystems important requirements. In this context, surface-engineered nanosystems have been designed to actively promote muscular targeting thanks to peptides anchored on nanocarrier surface [8,9]. In our work, we identified Na^+-coupled organic cation/carnitine transporter (OCTN) as a potential target for drug delivery at muscular level [10,11]. OCTN receptors constitute a subfamily of solute carrier SLC22 family, whose differences in amminoacid composition define two main classes, namely OCTN1 and OCTN2 receptors. Moreover, each member of SLC22 has differences in substrate affinity. In particular, OCTN2 has a high affinity for L-carnitine, which is a small zwitterion molecule synthetized endogenously by liver, kidney and brain [12]. L-Carnitine-associated polymer nanoparticles have been shown to be effective to increase drug delivery by oral administration: the insertion of a L-carnitine derivative, namely stearoyl-L-carnitine (SC), into the polymer matrix enhanced cellular uptake and intestinal absorption of drug molecules by OCTN2-mediated transport [13,14]. Furthermore, SC-conjugated PLGA nanoparticles have been described as novel potential tools for colon cancer cell-targeted drug delivery. Indeed, cancer cells express high levels of OCTN2 and $ATB^{0,+}$ receptors, both having high affinity for L-carnitine [15]. The same

approach can be exploited to target the respiratory epithelium of human trachea and bronchi, since the identification of OCTN transporters can play a significant role in the delivery of therapeutics molecules by nanomedicine approach [16,17].

On these bases, we propose the formulation of drug-loaded SC-associated PLGA nanoparticles to target OCTN2 receptor expressed on muscular cells. We tested two amounts of SC to efficiently functionalize the nanoparticles, which were then characterized. Preliminary *in vitro* tests were assessed to evaluate the cell viability in presence of targeted nanoparticles; then, the analysis of cellular uptake was performed by transmission electron microscopy (TEM) and confocal microscopy using fluorescent nanoparticles. In the frame of the repurposing approach, pentamidine (PTM) has been encapsulated into targeted nanoparticles for its proposed activity in the treatment of myotonic dystrophy type I.

2. Experimental section

2.1. Materials

PLGA 75:25 (Resomer® RG 752 H, M_w = 4-15 kDa) (analytical grade), SC, PVA (M_w=31-50 kDa, 98-99% hydrolyzed) and PTM isethionate (PTM-I) were purchased from Sigma-Aldrich (Milan, Italy). All the solvents used were of analytical grade and purchased from Carlo Erba Reagenti (Milan, Italy). Solvent evaporation was carried out using a rotating evaporator (Heidolph Laborota 400, Heidolph Instruments, Schwabach, Germany) equipped with a vacuum pump (Diaphragm Vacuum Pump DC-4). Lyophilization was performed with a LyoQuest-85® freeze drier (Azbil Telstar Technologies, Barcelona, Spain).

2.2. Preparation and characterization of free base form of PTM

Free base from of PTM (PTM-B) was obtained by dissolving PTM-I in distilled water and adding a 25% w/w NH_4OH solution at 4 °C. The obtained precipitate was filtered, washed with a 5% NH_4OH solution and dried under vacuum overnight. The conversion of PTM-I into PTM-B was confirmed by mass spectrometry analysis using electrospray ionization or by atmospheric pressure chemical ionization, in positive ion mode, on a Micromass ZQ spectrometer (Waters, Milan, Italy), as previously reported [18].

2.3. Preparation of SC-nanoparticles

SC-associated PLGA nanoparticles were prepared by the nanoprecipitation technique [19]. Practically, for each preparation, to 5 mg of PLGA 75:25 dissolved in acetone, an aliquot of a methanolic stock solution of SC (1 mg/mL), corresponding to SC 5% or 10% w/w, was added

until a total volume of 1 mL. The organic solution was then dripped into 5 mL of a 0.2% w/w PVA solution in MilliQ water under magnetic stirring. Precipitation of nanoparticles occurred immediately. After solvent evaporation under reduced pressure, an aqueous nanoparticle suspension was obtained. PTM-B-loaded SC-associated nanoparticles were prepared as well, adding an aliquot of a methanolic stock solution of PTM-B (2.5 mg/mL) to the organic solution containing PLGA and SC, for a maximum of 30 µg/mL PTM-B concentration in the final nanoparticle suspension. To purify the nanoparticles from nonincorporated drug, PTM-B-loaded SC-associated nanoparticles were extensively dialyzed against MilliQ water at 4 °C (Spectra/Por® 3500 MWCO dialysis membrane; Spectrum, Houston, TX). Unloaded and unconjugated nanoparticles, without PTM and/or SC, were prepared as well. Fluorescent nanoparticles were prepared adding 7 µg of a fluorescent probe (Nile Red)/mg of PLGA. The suspensions were then stored at 4 °C until further use.

2.4. Characterization of SC-nanoparticles

The mean hydrodynamic diameter and the polydispersity index (PDI) of all the nanoparticle samples were analyzed by dynamic light scattering (DLS) using a nanosizer (Zetasizer Nano Z, Malvern Inst., Malvern, UK). The selected angle was 173° and the measurements were carried out at 25 °C after dilution of the particulate suspensions in MilliQ® water. Each measurement was performed in triplicate.

The surface charge of the nanoparticles was evaluated by zeta potential measurements at 25 °C after appropriate dilution in MilliQ® water of the suspensions, using the Smoluchowski equation and the Nanosizer Nano Z. Each reported value is the average of three measurements. The physical colloidal stability of the nanoparticle suspensions in the storage conditions (4 °C) was monitored by evaluating at different interval times for 4 weeks mean diameter, PDI and zeta potential by DLS. Each measurement was carried out in triplicate.

The amount of incorporated PTM-B was determined spectrophotometrically (DU 730 UV-vis spectrophotometer, Beckman Coulter, Brea, CA) at 264 nm using a calibration curve. To this aim, each suspension was lyophilized for 24 h; then, the product was dissolved in dichloromethane. To the solution, methanol was added followed by centrifugation (6000 rpm for 15 min) to separate the precipitated polymer. The supernatants were then measured at 264 nm [20]. The concentration of the polymer in the suspension was based on dry weight analysis. Each sample was analyzed in triplicate. The results were expressed as encapsulation efficiency (EE) (calculated as the ratio between the amount of entrapped drug and the initial amount used

in the preparation of nanocarriers × 100) and drug loading (DL) (calculated as the ratio between the amount of entrapped PTM-B and the total nanocarrier weight × 100).

2.5. PTM-B release from nanoparticles

To evaluate the PTM-B release from 5% SC-nanoparticles, the suspension was incubated at 37 °C in 10 mM phosphate-buffered saline (PBS) buffer pH 7.4. Aliquots (1 mL) were withdrawn at predetermined time intervals (0, 1, 2, 4, 6, 8, 16, and 24 h) and, after purification by dialysis, the drug content was measured as previously described and compared with the initial value.

2.6. Cell culture and treatment

C2C12 myoblasts (an immortalized murine cell line purchased from ECACC 91031101) were cultured in 75 cm^2-plastic flasks using Dulbecco's modified Eagle medium (DMEM), supplemented with 10% (v/v) fetal bovine serum (FBS), 1% (w/v) glutamine, 0.5% (v/v) amphotericin B, 100 units/mL of penicillin-streptomycin (Gibco, Thermo Fisher Scientific, Waltham, MA, USA) and incubated at 37 °C with 5% CO_2. Cells were trypsinized in 0.05% EDTA in PBS and seeded in flat-bottom 96-well plates (3×10^3 cells/well) for MTT assay. Twenty-four hours after seeding, the cells were treated with 5% SC-nanoparticles for increasing times (2 h, 24 h, 24 h + 24 h recovery) and then processed for MTT assay. For the differentiation into myotubes, myoblasts were seeded (8×10^3 cells/well) onto glass-coverslips (12-mm diameter) in 24-multiwell plates. When cells were grown at confluence, differentiation medium (supplemented with 2% horse serum) was added for 7 days. The myotubes were processed for immunofluorescence analysis.

2.7. Cell viability tests

The MTT assay was used to assess the cytotoxicity of 5% SC-nanoparticles on myoblasts. To this aim, cells were seeded in flat-bottom 96-multiwell plates at the density of 3×10^3 cells/well. Then, cells were treated with different nanocarrier concentrations (from 47.35 to 284.14 µg/mL of PLGA) for 2 h, 24 h and 24 h + 24 h of recovery, selected based on their PTM-B entrapment capacity. At each incubation time, the medium was replaced by 100 µl of 0.5 mg/mL MTT solution (Thiazolyl Blue Tetrazolium Bromide, Sigma-Aldrich) (0.5 mg/mL in medium) and incubated for 4 h at 37 °C in a cell incubator. Then, MTT solution was removed and formazan crystals were dissolved in 100 µl of dimethyl sulfoxide (DMSO). The absorbance was measured at 570 nm using a ChroMate 4300 ELISA microplate reader (Awareness Technology Inc., Palm City, FL, USA). Experiments were performed in triplicate. Statistical comparisons between

control and experimental conditions were made by the Mann-Whitney pairwise test and significant difference was set at $p \leq 0.05$.

2.8. Immunofluorescence and transmission electron microscopy (TEM) analysis

Myotubes were fixed for fluorescence microscopy with 4% (v/v) paraformaldehyde in PBS pH 7.4 for 30 min at room temperature. Cells were then permeabilized in PBS containing 0.05% Tween 20 and 0.1% bovine serum albumin (BSA), and incubated with rabbit polyclonal antibody direct against Solute Carrier Family 22 Member 5 (Abcam ab180757) diluted 1:200, for 1 h at room temperature. Cells were washed with PBS and incubated with the secondary antibody (Alexafluor 488) diluted 1:200 in PBS, for 1 h at room temperature. After washing, cells were incubated with Phalloidin-Atto 594 (Sigma-Aldrich) diluted 1:50 in PBS, for 1 h at room temperature. Finally, cells were washed and mounted in 1:1 mixture of glycerol:PBS. For confocal microscopy (CFM), a Leica TCS SP5 AOBS system (Leica Microsystems Italia, Buccinasco, Italy) was used.

For TEM, myoblasts were incubated for 2 and 24 h with the 5% SC-nanoparticles at the same concentration used for MTT analysis (91.71 μg/mL). Then, cells were fixed with 2.5% (v/v) glutaraldehyde and 2% (v/v) paraformaldehyde in 0.1 M PBS pH 7.4 at 4 °C for 2 h, postfixed with 1% OsO4 at room temperature for 1 h, dehydrated with acetone and embedded in Epon. Ultrathin sections were observed unstained or after weak staining with uranyl acetate replacement stain (Electron Microscopy Science) (UAR-EMS). Observations were made in a Philips Morgagni TEM (FEI Company Italia Srl, Milan, Italy), operating at 80 kV and equipped with a Megaview II camera for digital image acquisition.

2.9. Nanoparticle distribution in myoblasts

For CFM, myoblasts were incubated for 2 and 24 h with Nile Red-labeled PLGA nanoparticles at concentrations found to be noncytotoxic by cell viability. At each incubation time, cells were fixed with 4% (v/v) paraformaldehyde in PBS pH 7.4, for 30 min at room temperature. To visualize the intracellular distribution of fluorescent nanocarriers, the cells were washed in PBS, incubated with either 0.1% Trypan blue (Gibco, Milan, Italy) or Phalloidin-Atto 594 or Phalloidin-Atto 488 (Sigma-Aldrich) diluted 1:20 in PBS, stained for DNA with Hoechst 33342 (1 μg/mL in PBS), rinsed in PBS, and finally mounted in 1:1 mixture of glycerol:PBS. To investigate nanocarrier uptake, live myoblasts were preincubated with either PKH26 Red Fluorescent Cell Linker or PKH67 Green Fluorescent Cell Linker (Sigma-Aldrich) to stain the plasma membrane, then incubated with the fluorescently labeled PLGA nanoparticles for 30

min (this short time is necessary to label early endosomes only [21]) and finally fixed and processed for CFM, as described above. This procedure allowed detecting possible co-localization of the fluorescence signals of the internalized vesicles and nanoparticles, irrespective of the type of the occurring endocytic process (*e.g.*, clathrin-mediated endocytosis, caveolin-mediated endocytosis, lipid-raft mediated endocytosis, phagocytosis, macro-pinocytosis), since cell internalization of nanoparticles depends on several factors and the mechanisms may be multiple [22–24]. For CFM, a Leica TCS SP5 AOBS system (Leica Microsystems Italia) was used: for fluorescence excitation, a diode laser at 405 nm for Hoechst 33342 and a He/Ne laser at 543 nm for Trypan blue, Nile Red were employed. Z-stack of 1 μm step sized images (1024 × 1024-pixel format) was collected.

3. Results and Discussion

3.1. Preparation and characterization of SC-nanoparticles

In this work, L-carnitine was exploited as an active targeting agent to increase nanoparticle muscular tropism and improve the therapeutical treatment of MDs. To promote the association to PLGA nanoparticles, we have chosen a commercial L-carnitine derivative, SC, in which the hydroxyl group of L-carnitine has been functionalized by a stearoyl moiety; during nanoparticle formulation, the SC long fatty chain anchors to PLGA matrix by hydrophobic interactions and exposes hydrophilic L-carnitine on nanoparticle surface (Fig. 1) [25]. A similar approach has been used to prepare functionalized nanoparticles by solvent extraction/evaporation to increase drug oral delivery by carnitine receptor-mediated uptake [14]. In this work, as a repurposed drug for potential applications in muscular dystrophy treatment by active targeting [26], PTM-B was encapsulated into SC-nanoparticles. The incorporation was allowed by the electrostatic interactions between the positively charged PTM-B and the negatively charged PLGA, as previously reported [20].

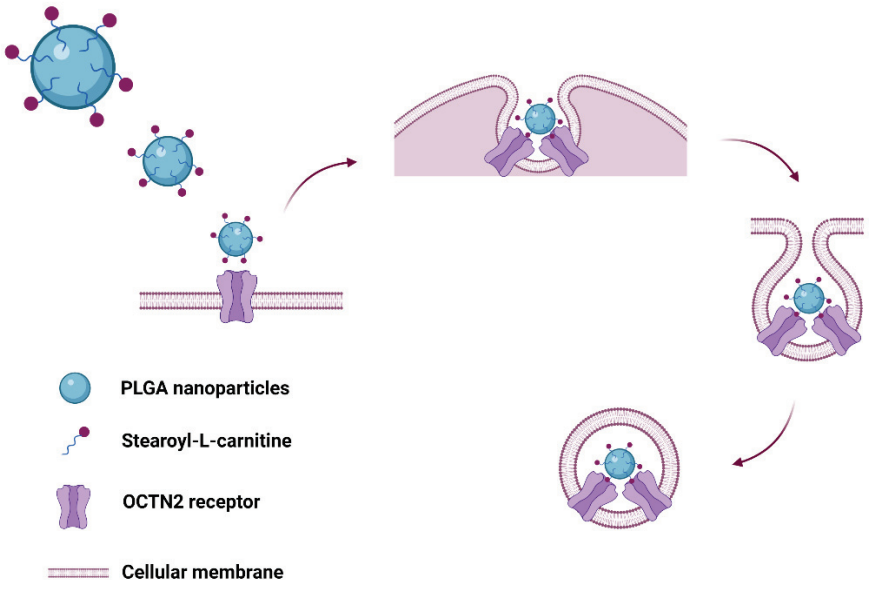

Fig. 1. Cellular uptake of SC-PLGA nanoparticles: functionalized nanoparticles bind to OCTN2 receptor on cell membrane, forming a complex that is then internalized into the cell.

All the nanoparticles were prepared by nanoprecipitation. However, the composite formulation required the presence of PVA in the aqueous phase as a stabilizer. In particular, different concentrations (from 0.1 to 1% w/v) of PVA were assessed to obtain stable nanoparticles, limiting, at the same time, PVA toxicity *in vitro*. Finally, a nontoxic 0.2% PVA concentration was used [27].

Nanoparticles were formulated at 5% and 10% SC to investigate the effect of ligand percentage on nanoparticle characteristics. As reported in Table 1, the nanoparticle mean diameter tends to diminish with the increase of SC percentage, probably as a consequence of the amphiphilic character of SC during nanoparticle formation. On the contrary, the incorporation of PTM-B into functionalized nanoparticles causes mean size and PDI to increase: this effect can be due to the more complex composition of the systems. Concerning the zeta potential, for SC-associated and PTM-B-loaded nanoparticles it is higher than that of blank nanocarriers. Indeed, the charged functional groups of SC and PTM-B interact with PLGA and modify the surface charge of the nanoparticles.

Table 1 Physicochemical characteristics (mean diameter, PDI and zeta potential) of nanoparticles.

Nanoparticle composition	Mean diameter (nm ± S.D.)	PDI	Zeta potential (mV ± S.D.)
PLGA	94 ± 1	0.170	-39.2 ± 1.8
5% SC-PLGA	82 ± 1	0.198	-23.7 ± 1.1
10% SC-PLGA	73 ± 1	0.184	-29.6 ± 1.0
5% SC-PTM-B-PLGA	98 ± 11	0.399	-18.4 ± 2.4
10% SC-PTM-B-PLGA	128 ± 10	0.222	-28.8 ± 3.3

After 4-week storage at 4 °C, no precipitation and/or aggregation occurred for 5% and 10% empty SC-nanoparticles. On the contrary, for PTM-B-loaded nanosystems, the mean particle size, PDI and zeta potential values were stable only for 5% SC-nanoparticles. On these bases, we selected the lower SC percentage for further EE and drug release tests.

5% SC-PTM-B-PLGA nanoparticles showed an EE of 65%, which was lower than that of untargeted nanoparticles (about 90%); this result is probably due to the interaction of the stearoyl chain of SC with the polymer matrix and the competition with PTM-B incorporation.

To evaluate PTM-B release from 5% SC-nanoparticles, the suspension was incubated for 24 h at 37 °C in PBS pH 7.4. At physiological pH, the drug is stably associated to the polymer matrix thanks to electrostatic interactions, as already demonstrated [20]: indeed, after 24 h, only 60% of PTM-B is released in these conditions (Fig. 2).

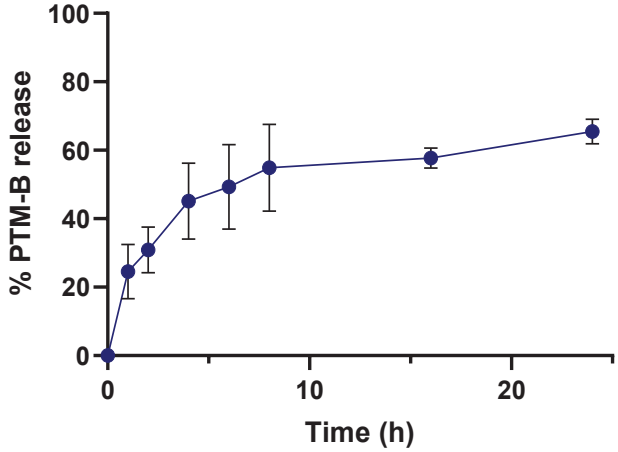

Fig. 2. PTM-B release from 5% SC-nanoparticles as a function of time after incubation in PBS pH 7.4 at 37 °C.

3.2. In vitro tests

C2C12 myoblasts were cultured and incubated for 2 h, 24 h and 24 h + 24 h of recovery with 5% SC-nanoparticles to evaluate cellular viability. The nanoparticle concentrations were 47.35, 94.71, and 284.14 μg/mL. Unconjugated nanoparticles were used as control at the same concentrations.

Cellular viability was similar in control samples and in samples exposed to any nanocarrier concentration after 2 h of incubation (Fig. 3A). Conversely, cell population viability decreased after 24 h in a dose-dependent manner (from 86% for lowest concentration to 62% for higher concentration) (Fig. 3B). A further step of experiments was performed at a longer incubation time of 24 h, followed by 24 h of recovery in culture medium. The cell viability showed similar values in control samples and in samples exposed to the lowest concentrations of 5% SC-

nanoparticles, while the highest concentration tested induced a decrease of 24% of cellular viability (Fig. 3C). Since PLGA is a biodegradable and biocompatible polymer without toxic effects *in vitro* and *in vivo* [28], the reduced cellular viability can be related to the presence of SC.

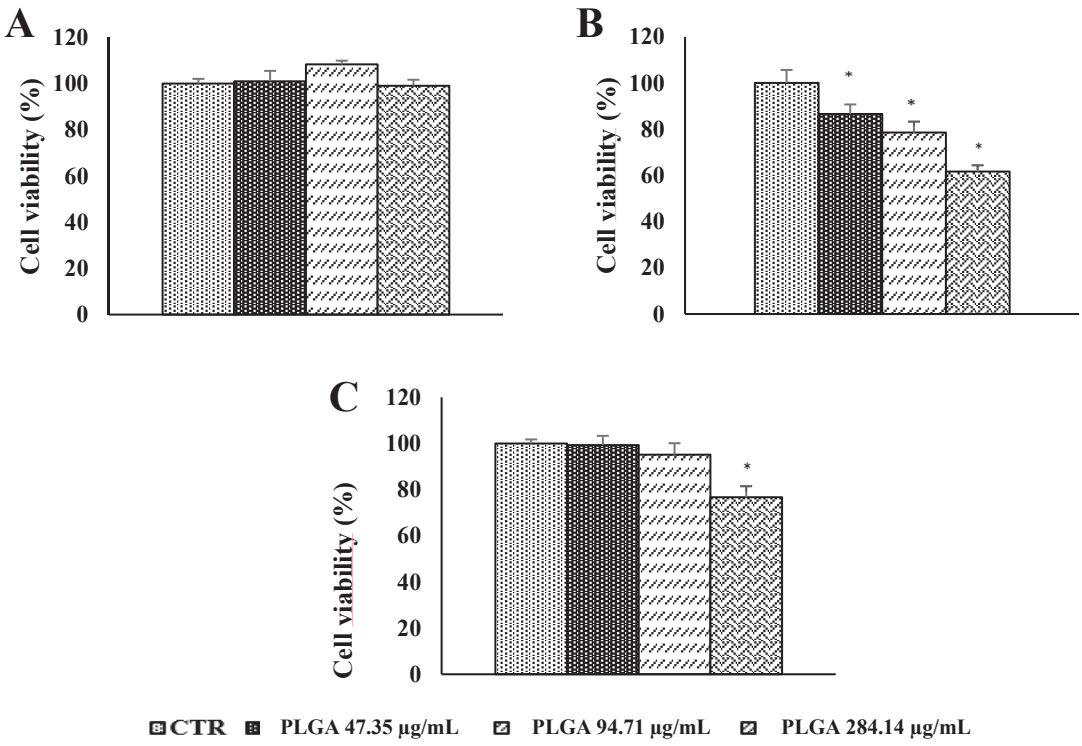

Fig. 3. C2C12 cell viability evaluated by MTT test after 2 h (A), 24 h (B), 24 h + 24 h recovery (C) treatment in presence of 5% SC-nanoparticles. Data are given as mean SEM, representative of three independent experiments. * $p < 0.03$ *vs* control (CTR) sample.

TEM analysis, performed to shed light on nanoparticle interaction with cells, confirmed the uptake of 5% SC-nanoparticles within the myoblasts (Fig. 4) at 2 h- and 24 h-incubation time. At TEM, nanoparticles showed a regular roundish shape and a moderate electron density. After 2 h of incubation, SC-nanoparticles entered the myoblasts by endocytosis (Fig. 4A) and a nanoparticle exhibited endosomal escape (Fig. 4B). After 24 h-incubation, nanoparticles were found free in the cytosol (Fig. 4C) and some residual bodies containing roundish moderately electro-dense structures accumulated in the cytoplasm and occurred in secondary lysosomes (Fig. 4D-E). Nanoparticles were never found inside the nucleus nor contacting cytoplasmatic organelles. No cell alteration or suffering occurred in myoblasts at any incubation time. The experimental evidence of TEM indicates that 5% SC-nanoparticles enter the myoblasts mostly by classical endocytosis or OCTN2-mediated endocytosis [14,29]. Consistent with observations on PLGA nanoparticle cell uptake [30], TEM confirmed that, in the myoblasts, nanoparticles,

after endocytosis, follow the endolytic pathway, always remaining outside the nucleus. However, their rapidly escape from endosomes, as already described for other polymer nanoparticles [31,32], and occur free in the cytosol. The large number of residual bodies can be ascribed to enzymatic degradation of nanoparticles. Moreover, C2C12 cells, treated with the nanocarrier concentration 94.71 μg/mL, did not show any sign of cell stress, thus confirming the biocompatibility of the nanosystem.

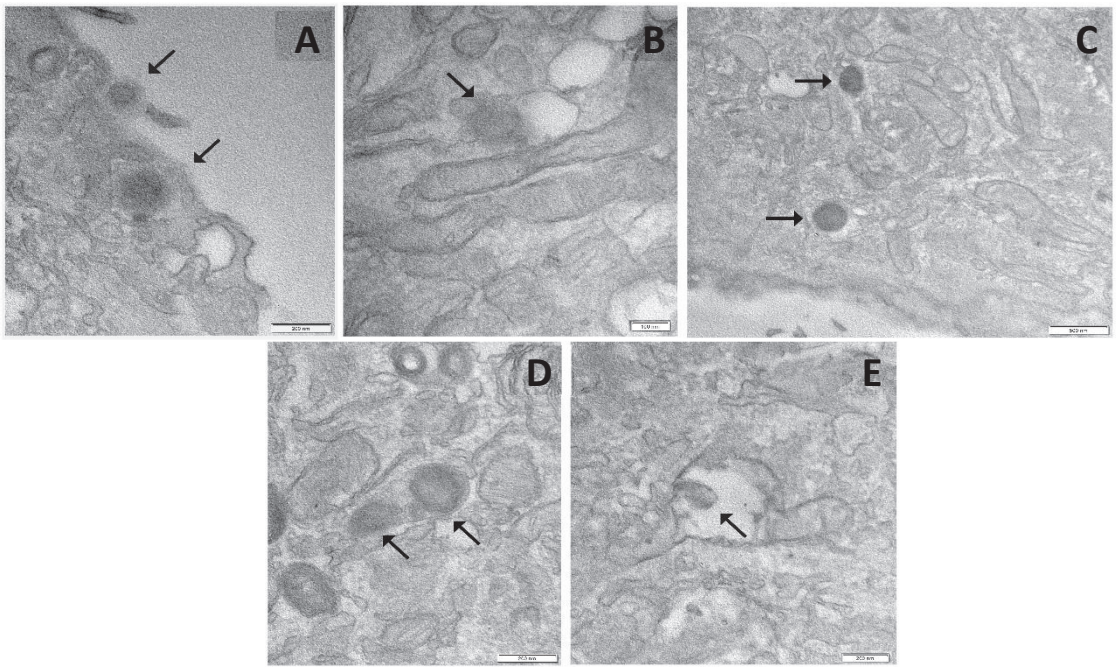

Fig. 4. TEM analysis of 5% SC-nanoparticles uptake and intracellular fate. TEM images of a C2C12 myoblast incubated for 2 h with 5% SC-nanoparticles (A-B). Two nanoparticles (arrows) are entering the cell by endocytosis (A). A nanoparticle (arrow) is escaping an endosome (B). TEM images of a C2C12 myoblast incubated for 24 h with 5% SC-nanoparticles (C-E). Two nanoparticles (arrows) occur free in the cytosol (C). Three nanoparticles (arrows) occur inside secondary lysosomes (D-E).

3.3. Cellular internalization

OCTN receptors belong to the larger family of solute carriers which are ubiquitously expressed in human body. OCTN2 is a sub-set of OCTN receptors and it is considered the principal plasma membrane carnitine transporter [12,33]. To detect the presence of OCTN2 receptor in myoblasts and myotubes to gain further insights into the possible role of the transporter, myoblasts and myotubes were labeled with the anti-OCTN2 antibody and evaluated by immunofluorescence. The presence of OCTN2 receptors was observed either on myoblasts or in myotubes. However, the high number of receptors is highlighted in the myotube (Fig. 5).

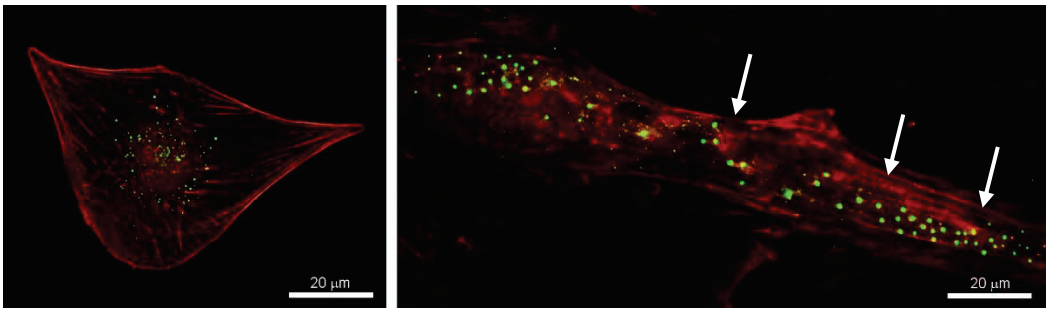

Fig. 5. Fluorescence microscopy micrographs of a myoblast (A) and a myotube (B) immunolabelled for OCTN2 (green); counterstaining with phalloidin (red). Note the high number of receptors in the myotube.

To visualize the cell internalization, Nile Red-loaded nanoparticles were prepared. Then, C2C12 myoblasts and myotubes were incubated 24 h in presence of fluorescent nanoparticles (5% SC-associated or untargeted). Confocal microscopy analysis did not show significant difference in nanoparticle uptake between SC-associated and untargeted nanoparticles, either in myoblasts or in myotubes (Fig. 6A).

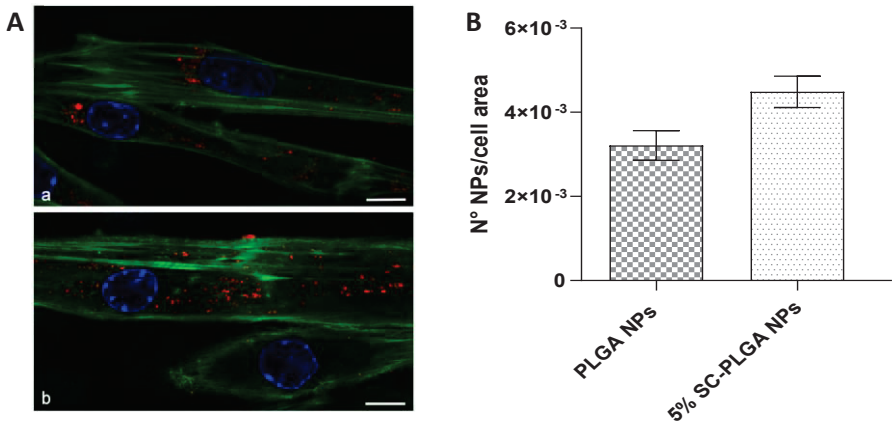

Fig. 6. (A) Confocal fluorescence microscopy analysis of myotubes that have been incubated with (A-a) untargeted nanoparticles and (A-b) 5% SC-conjugated PLGA nanoparticles. Nanoparticles are loaded with Nile Red (red fluorescence) and cells are counterstained with phalloidin conjugated with Alexa488 (green fluorescence). Hoechst 33342 (blue fluorescence) staining depicts cell nuclei. (B) Morphometric analysis of C2C12 myoblasts for nanoparticles (NPs).

Morphometric analysis was performed to number nanoparticles in each cell. Only in myotubes, 5% SC-nanoparticles resulted better internalized compared to untargeted nanoparticles (Fig. 6B). Probably, the enhanced uptake effect for targeted nanoparticles can be ascribed to an increased expression of OCTN2 receptors in myotubes than in myoblasts (Fig. 5).

4. Conclusions

To our knowledge, our preliminary results demonstrate for the first time that the association of L-carnitine to PLGA nanoparticles could allow nanosystem muscular tropism *via* the OCTN2 receptor-mediated endocytosis. Furthermore, we demonstrated that the cell differentiation stage affects the receptor expression and possibly influences the nanoparticle uptake. Finally, the developed nanosystems showed high biocompatibility to muscle cells, making these SC-nanoparticles potential candidates for delivering therapeutic agents against muscular pathologies.

Acknowledgments

The research was supported by the Italian Ministry of University and Research - University of Turin "Fondi Ricerca Locale (ex-60%)".

References

1. Ravi Kiran, A.V.V.V.; Kusuma Kumari, G.; Krishnamurthy, P.T.; Khaydarov, R.R. Tumor Microenvironment and Nanotherapeutics: Intruding the Tumor Fort. *Biomaterials Science* **2021**, *9*, 7667–7704, doi:10.1039/d1bm01127h.
2. Shi, Y.; van der Meel, R.; Chen, X.; Lammers, T. The EPR Effect and beyond: Strategies to Improve Tumor Targeting and Cancer Nanomedicine Treatment Efficacy. *Theranostics* **2020**, *10*, 7921–7924, doi:10.7150/thno.49577.
3. Danhier, F. To Exploit the Tumor Microenvironment: Since the EPR Effect Fails in the Clinic, What Is the Future of Nanomedicine? *J Control Release* **2016**, *244*, 108–121, doi:10.1016/j.jconrel.2016.11.015.
4. Pearce, A.K.; O'Reilly, R.K. Insights into Active Targeting of Nanoparticles in Drug Delivery: Advances in Clinical Studies and Design Considerations for Cancer Nanomedicine. *Bioconjug Chem* **2019**, *30*, 2300–2311, doi:10.1021/acs.bioconjchem.9b00456.
5. Mercuri, E.; Bönnemann, C.G.; Muntoni, F. Muscular Dystrophies. *Lancet* **2019**, *394*, 2025–2038, doi:10.1016/S0140-6736(19)32910-1.
6. Sleboda, D.A.; Stover, K.K.; Roberts, T.J. Diversity of Extracellular Matrix Morphology in Vertebrate Skeletal Muscle. *J Morphol* **2020**, *281*, 160–169, doi:10.1002/jmor.21088.
7. Engin, A.B.; Nikitovic, D.; Neagu, M.; Henrich-Noack, P.; Docea, A.O.; Shtilman, M.I.; Golokhvast, K.; Tsatsakis, A.M. Mechanistic Understanding of Nanoparticles' Interactions with Extracellular Matrix: The Cell and Immune System. *Part Fibre Toxicol* **2017**, *14*, 22, doi:10.1186/s12989-017-0199-z.
8. Huang, D.; Yue, F.; Qiu, J.; Deng, M.; Kuang, S. Polymeric Nanoparticles Functionalized with Muscle-Homing Peptides for Targeted Delivery of Phosphatase and Tensin Homolog Inhibitor to Skeletal Muscle. *Acta Biomater* **2020**, *118*, 196–206, doi:10.1016/j.actbio.2020.10.009.

9. Yu, C.-Y.; Yuan, Z.; Cao, Z.; Wang, B.; Qiao, C.; Li, J.; Xiao, X. A Muscle-Targeting Peptide Displayed on AAV2 Improves Muscle Tropism on Systemic Delivery. *Gene Ther* **2009**, *16*, 953–962, doi:10.1038/gt.2009.59.
10. Pochini, L.; Scalise, M.; Galluccio, M.; Indiveri, C. OCTN Cation Transporters in Health and Disease: Role as Drug Targets and Assay Development. *J Biomol Screen* **2013**, *18*, 851–867, doi:10.1177/1087057113493006.
11. Kou, L.; Sun, R.; Ganapathy, V.; Yao, Q.; Chen, R. Recent Advances in Drug Delivery via the Organic Cation/Carnitine Transporter 2 (OCTN2/SLC22A5). *Expert Opin Ther Targets* **2018**, *22*, 715–726, doi:10.1080/14728222.2018.1502273.
12. Juraszek, B.; Nałęcz, K.A. SLC22A5 (OCTN2) Carnitine Transporter-Indispensable for Cell Metabolism, a Jekyll and Hyde of Human Cancer. *Molecules* **2020**, *25*, doi:10.3390/molecules25010014.
13. He, C.; Jin, Y.; Deng, Y.; Zou, Y.; Han, S.; Zhou, C.; Zhou, Y.; Liu, Y. Efficient Oral Delivery of Poorly Water-Soluble Drugs Using Carnitine/Organic Cation Transporter 2-Mediated Polymeric Micelles. *ACS Biomaterials Science and Engineering* **2020**, *6*, 2146–2158, doi:10.1021/acsbiomaterials.0c00020.
14. Kou, L.; Yao, Q.; Sun, M.; Wu, C.; Wang, J.; Luo, Q.; Wang, G.; Du, Y.; Fu, Q.; Wang, J.; et al. Cotransporting Ion Is a Trigger for Cellular Endocytosis of Transporter-Targeting Nanoparticles: A Case Study of High-Efficiency SLC22A5 (OCTN2)-Mediated Carnitine-Conjugated Nanoparticles for Oral Delivery of Therapeutic Drugs. *Adv Healthc Mater* **2017**, *6*, doi:10.1002/adhm.201700165.
15. Kou, L.; Yao, Q.; Sivaprakasam, S.; Luo, Q.; Sun, Y.; Fu, Q.; He, Z.; Sun, J.; Ganapathy, V. Dual Targeting of L-Carnitine-Conjugated Nanoparticles to OCTN2 and ATB0,+ to Deliver Chemotherapeutic Agents for Colon Cancer Therapy. *Drug Deliv* **2017**, *24*, 1338–1349, doi:10.1080/10717544.2017.1377316.
16. Ingoglia, F.; Visigalli, R.; Rotoli, B.M.; Barilli, A.; Riccardi, B.; Puccini, P.; Dall'Asta, V. Functional Activity of L-Carnitine Transporters in Human Airway Epithelial Cells. *Biochim Biophys Acta* **2016**, *1858*, 210–219, doi:10.1016/j.bbamem.2015.11.013.
17. Rotoli, B.M.; Visigalli, R.; Barilli, A.; Ferrari, F.; Bianchi, M.G.; Di Lascia, M.; Riccardi, B.; Puccini, P.; Dall'Asta, V. Functional Analysis of OCTN2 and ATB0,+ in Normal Human Airway Epithelial Cells. *PLoS One* **2020**, *15*, e0228568, doi:10.1371/journal.pone.0228568.
18. Peretti, E.; Miletto, I.; Stella, B.; Rocco, F.; Berlier, G.; Arpicco, S. Strategies to Obtain Encapsulation and Controlled Release of Pentamidine in Mesoporous Silica Nanoparticles. *Pharmaceutics* **2018**, *10*, E195, doi:10.3390/pharmaceutics10040195.
19. Fessi, H.; Puisieux, F.; Devissaguet, J.Ph.; Ammoury, N.; Benita, S. Nanocapsule Formation by Interfacial Polymer Deposition Following Solvent Displacement. *International Journal of Pharmaceutics* **1989**, *55*, R1–R4, doi:10.1016/0378-5173(89)90281-0.
20. Stella, B.; Andreana, I.; Zonari, D.; Arpicco, S. Pentamidine-Loaded Lipid and Polymer Nanocarriers as Tunable Anticancer Drug Delivery Systems. *J Pharm Sci* **2020**, *109*, 1297–1302, doi:10.1016/j.xphs.2019.11.011.
21. Grecchi, S.; Malatesta, M. Visualizing Endocytotic Pathways at Transmission Electron Microscopy via Diaminobenzidine Photo-Oxidation by a Fluorescent Cell-Membrane Dye. *Eur J Histochem* **2014**, *58*, 2449, doi:10.4081/ejh.2014.2449.
22. Oh, N.; Park, J.-H. Endocytosis and Exocytosis of Nanoparticles in Mammalian Cells. *Int J Nanomedicine* **2014**, *9 Suppl 1*, 51–63, doi:10.2147/IJN.S26592.
23. Behzadi, S.; Serpooshan, V.; Tao, W.; Hamaly, M.A.; Alkawareek, M.Y.; Dreaden, E.C.; Brown, D.; Alkilany, A.M.; Farokhzad, O.C.; Mahmoudi, M. Cellular Uptake of Nanoparticles: Journey inside the Cell. *Chem Soc Rev* **2017**, *46*, 4218–4244, doi:10.1039/c6cs00636a.

24. Ding, L.; Zhu, X.; Wang, Y.; Shi, B.; Ling, X.; Chen, H.; Nan, W.; Barrett, A.; Guo, Z.; Tao, W.; et al. Intracellular Fate of Nanoparticles with Polydopamine Surface Engineering and a Novel Strategy for Exocytosis-Inhibiting, Lysosome Impairment-Based Cancer Therapy. *Nano Lett* **2017**, *17*, 6790–6801, doi:10.1021/acs.nanolett.7b03021.
25. Kou, L.; Yao, Q.; Sivaprakasam, S.; Luo, Q.; Sun, Y.; Fu, Q.; He, Z.; Sun, J.; Ganapathy, V. Dual Targeting Ofl-Carnitine-Conjugated Nanoparticles to Octn2 and Atb0,þ to Deliver Chemotherapeutic Agents for Colon Cancer Therapy. *Drug Delivery* **2017**, *24*, 1338–1349, doi:10.1080/10717544.2017.1377316.
26. Warf, M.B.; Nakamori, M.; Matthys, C.M.; Thornton, C.A.; Berglund, J.A. Pentamidine Reverses the Splicing Defects Associated with Myotonic Dystrophy. *Proc Natl Acad Sci U S A* **2009**, *106*, 18551–18556, doi:10.1073/pnas.0903234106.
27. Menon, J.U.; Kona, S.; Wadajkar, A.S.; Desai, F.; Vadla, A.; Nguyen, K.T. Effects of Surfactants on the Properties of PLGA Nanoparticles. *J Biomed Mater Res A* **2012**, *100*, 1998–2005, doi:10.1002/jbm.a.34040.
28. Wang, Q.; Shen, M.; Li, W.; Li, W.; Zhang, F. Controlled-Release of Fluazinam from Biodegradable PLGA-Based Microspheres. *J Environ Sci Health B* **2019**, *54*, 810–816, doi:10.1080/03601234.2019.1634971.
29. Costanzo, M.; Carton, F.; Marengo, A.; Berlier, G.; Stella, B.; Arpicco, S.; Malatesta, M. Fluorescence and Electron Microscopy to Visualize the Intracellular Fate of Nanoparticles for Drug Delivery. *Eur J Histochem* **2016**, *60*, 2640, doi:10.4081/ejh.2016.2640.
30. Palocci, C.; Valletta, A.; Chronopoulou, L.; Donati, L.; Bramosanti, M.; Brasili, E.; Baldan, B.; Pasqua, G. Endocytic Pathways Involved in PLGA Nanoparticle Uptake by Grapevine Cells and Role of Cell Wall and Membrane in Size Selection. *Plant Cell Rep* **2017**, *36*, 1917–1928, doi:10.1007/s00299-017-2206-0.
31. Kulkarni, S.A.; Feng, S.-S. Effects of Particle Size and Surface Modification on Cellular Uptake and Biodistribution of Polymeric Nanoparticles for Drug Delivery. *Pharm Res* **2013**, *30*, 2512–2522, doi:10.1007/s11095-012-0958-3.
32. Sun, J.; Zhang, L.; Wang, J.; Feng, Q.; Liu, D.; Yin, Q.; Xu, D.; Wei, Y.; Ding, B.; Shi, X.; et al. Tunable Rigidity of (Polymeric Core)–(Lipid Shell) Nanoparticles for Regulated Cellular Uptake. *Advanced Materials* **2015**, *27*, 1402–1407, doi:10.1002/adma.201404788.
33. Wu, X.; Huang, W.; Prasad, P.D.; Seth, P.; Rajan, D.P.; Leibach, F.H.; Chen, J.; Conway, S.J.; Ganapathy, V. Functional Characteristics and Tissue Distribution Pattern of Organic Cation Transporter 2 (OCTN2), an Organic Cation/Carnitine Transporter. *J Pharmacol Exp Ther* **1999**, *290*, 1482–1492.

Discussion

The present Ph.D. thesis has been co-tutored by the department of Drug Science and Technology, University of Turin, and the Laboratoire d'Automatique, de Génie des Procédés et de Génie Pharmaceutique, Université Claude Bernard Lyon 1. The research project is based on nanotechnological approaches for the formulation of active molecules to enhance their therapeutic applicability.

Over the years, the number of publications concerning nanomedicine importantly increased, due to its benefits [1]. Administration of potentially toxic compounds, molecule protection from degradation and drug rapid clearance are important challenges that nanomedicine strategy can overcome [2,3]. Indeed, the nanotechnological approach was highlighted as a powerful tool to ameliorate the therapeutic index and the chemical properties of drug molecules. For example, nanomedicine reached significant advances in antitumor therapy to limit the non-specific toxicity of anticancer agents [4,5]. Moreover, the innovative development of nanotechnology-enabled vaccines based on lipid nanoparticles (NPs) for mRNA delivery enhanced the importance of nanotechnological strategies in clinical applications [6]. However, limitations in production processes and difficulties to achieve the Good Manufacturing Practices (GMP) standards in terms of final product limit the translation from bench to the clinics of nanomedicine-based therapies [7].

In this research work, we exploited nanomedicine to design and characterize drug delivery systems (DDSs) for improving the pharmacokinetics and pharmacodynamics properties of old and new therapeutic compounds, repurposing their therapeutical applications. In particular, the aim of the present research has been the development of lipid and polymer colloidal carriers as DDSs for studying biomedical applications.

NPs, which include nanospheres and nanocapsules, are defined as colloidal DDSs characterized by a sub-micrometer size and chemically constituted by natural or synthetic polymers [8]. Compared to liposomes or inorganic nanocarriers, polymer sub-structures confer higher physical stability and tunable release profile to NPs [9]. Moreover, the surface of polymeric NPs can be easily modified to adapt the nanosystem to the therapeutic needs (*e.g.* PEGylation, active targeting agents) [10–12].

In this context, squalene (SQ) and poly(lactic-*co*-glycolic) acid (PLGA) have been selected as materials to develop biocompatible and biodegradable nanocarriers. SQ and PLGA-based NPs offer tremendous opportunities to design and obtain nanosystems with adaptable properties through simple preparation processes and versatility. Moreover, the consolidated experience with SQ and PLGA NPs from Italian and French labs was the driving force in the choice of this class of biocompatible nanosystems [13,14].

SQ and PLGA nanosystems were designed to efficiently encapsulate pentamidine (PTM), an antiprotozoal drug that recently has been repurposed for alternative applications [15,16]. Recently, its new clinical repositioning required technological approaches to improve its therapeutic efficacy and overcome off-target effects [17–19]. Indeed, PTM has been repurposed for its positive effects on cancer pathologies, muscular dystrophies, and brain disorders [16,20,21]. Furthermore, PTM anticancer activity was already tested in a collaborative study between the University of Turin and University of Lyon, resulted in an original scientific paper [22].

In this project, we first decided to assess nanocarriers of different nature for PTM delivery as anticancer molecule. In literature, several techniques have been reported as easy methods for the preparation of NPs. However, solvent displacement (nanoprecipitation) is considered the most suitable technique for lab-scale preparation. Indeed, nanoprecipitation has been adopted as an incorporation strategy both for lipophilic, and sometimes, hydrophilic compounds, which can be more challenging [23]. The choice of PLGA and a SQ derivative, as NP building polymers, was based on their chemical features. PLGA is a co-polymer of lactic and glycolic acids, which are biocompatible monomers for the human body [24]. On the same bases, SQ is an endogenous compound involved in cholesterol biosynthesis [25]. Moreover, both polymers can spontaneously self-assembly to form NPs and electrostatically interact with PTM free base (PTM-B) that is characterized by two amidine groups (pKa=12), positively charged at physiological pH (Fig. 1). In this contest, formulative studies of PTM-B-loaded NPs have been previously set up exploiting drug chemical structure: nanocomplexes of polyarginine and hyaluronic acid or functionalized-mesoporous silica NPs were described to efficiently interact with the positively charged amidine groups of PTM-B [22,26]. On the same bases, we proposed lipidic NPs to exploit the electrostatic and hydrophobic interactions between PTM-B and squalenic acid (SQ-COOH) [27]. As already described by P. Couvreur *et al*., formulation of SQ NPs is supported by the behavior of SQ derivatives to self-assembly and from NPs in aqueous media [28]. In this work, we evaluated different molar and charge ratios between SQ-COOH and PTM-B to significantly increase the drug loading (DL) of the nanosystems. A molecular modeling study showed the interactions among PTM-B and SQ-COOH molecules, considering the three SQ-COOH/PTM-B molar ratios (3:1, 4:1, 4.5:1) having the highest DL. SQ-COOH/PTM-B 3:1 and 4.5 are characterized by the same size of about 190 nm and a negative zeta potential (- 26 mV), which confers colloidal stability. Further experiments were performed on SQ-COOH/PTM-B 3:1 formulation which is characterized by the highest DL (17.5%) and colloidal stability. Investigations on organic/aqueous phases ratio (V_e/V_w) led to NPs with a

lower mean diameter (109 nm), PDI below 0.1 and increased drug loading (19%) (0.2:1 V_e/V_w). Moreover, as for other nanosystems based on ionic interactions, SQ-COOH/PTM-B NPs have a pH-responsive drug release [29]. Indeed, at pH 7.4 the ionizable groups of PTM-B and SQ-COOH are charged, occurring in strong ionic interactions that limit drug release. However, in the endosomal or tumor microenvironment (pH 5.0) [30], the balance between the positive charges of PTM-B and the negative charge of SQ-COOH is altered, enhancing PTM-B release. Moreover, since SQ has been reported to bind low-density lipoprotein receptor (LDLR) for its structural homology with cholesterol [31], cancer cells with different expressions of LDLR were selected to evaluate PTM-B anticancer activity and test the hypothesis of SQ as an indirect targeting agent (Fig. 1). Results showed that the anticancer activity of loaded NPs improved with increasing LDLR expression.

On the whole, the advantages of our system lay in: i) the possibility to electrostatically combine a biocompatible drug delivery system and the active molecule by the simple nanoprecipitation technique; ii) the pH-dependent release profile exploiting ionization of carboxylic and amidine groups; iii) the indirect targeting activity of a SQ derivative toward cells expressing LDLR.

The following step was to translate the nanotechnological formulation of PTM-B-loaded lipid NPs to polymer-based nanocarriers. A comparison between lipid and polymer systems was proposed by the formulative study of PLGA NPs for PTM-B encapsulation. We selected a PLGA acid-terminated (pKa=4.5) to which we associated PTM-B by ionic interactions. Nanosystems based on ionic forces highlighted the feasibility of these formulations that are based on strong interactions without any covalent linkage [32]. Indeed, establishment of ionic interactions between PLGA and PTM-B leads to a decrease in mean size from 135 nm for empty PLGA NPs to 120 nm for loaded nanosystems, with EE above 80%. Since numerous researches have demonstrated the possibility to modify PLGA NP surface [33–35], we prepared PEG_{2000}-functionalized NPs to increase the hydrophilicity of the surface by using a mixture of PLGA: PLGA-PEG_{2000} (1:2 w/w ratio), still maintaining a high EE (above 85%). Overall, the formulation process exploited the chemical properties of the polymers and the drug. Once again, the nanoprecipitation method has proven to be a simple preparation procedure, economically beneficial and environmentally friendly (thanks to the low amount of energy and time required). Moreover, the mutual stabilization between PLGA and PTM-B allowed us to avoid surfactant agents in the formulation. *In vitro* tests on human ovarian carcinoma cells (A2780) demonstrated that PTM-B retained its anticancer activity, even if delayed due to the gradual release from the NPs (Fig. 1).

The two mentioned formulative studies highlighted the interest in a positively charged small molecule, such as PTM-B, for the design of nano-sized carriers. Indeed, PTM-B chemical characteristics open the possibility to nanotechnological approaches exploiting a variety of nanocarriers that can overcome PTM-B-related issues and thus allowing its repurposing in the treatment of rare muscular diseases and brain disorders [36,37].

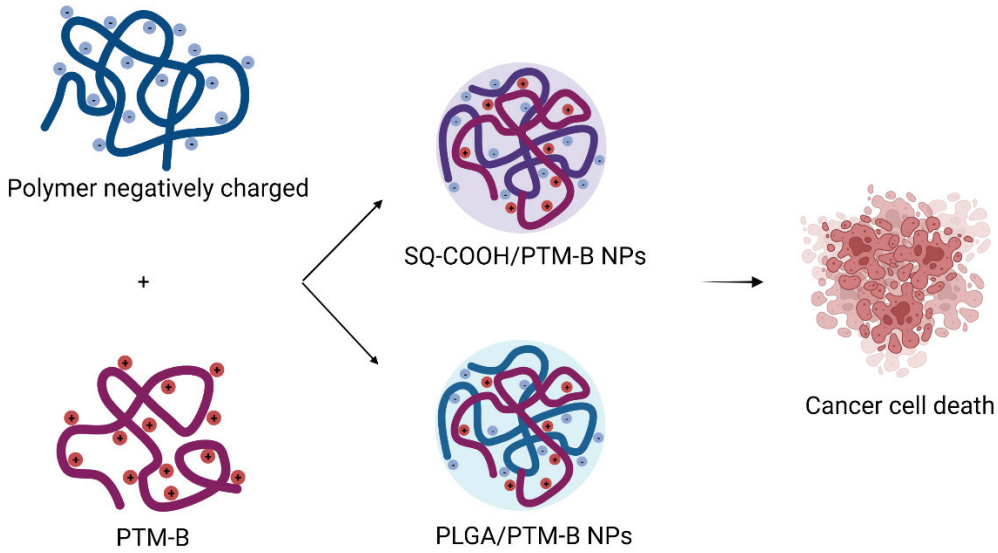

Fig. 1. Schematic representation of self-assembled NPs by electrostatic interactions

Although nanoprecipitation is considered the most simple and reproducible manufacturing process at lab-scale [38,39], scaling-up can be challenging. Thus, the second part of the work was focused on the translation study of PLGA formulation from the classical nanoprecipitation method to the microfluidic technique, evaluating the impact of formulative and operative parameters on nanosuspension (Fig. 2). We chose a hydrophobic model drug, called 991, to assess the microfluidic technique as a potential scalable process. The driving force of 991 choice was its importance in the treatment of inflammation in muscular diseases. However, *in vivo* administration of 991 is limited by its significant side effects. In collaboration with the Institut NeuroMyoGéné in Lyon, we developed 991-loaded PLGA NPs to challenge *in vivo* side effects of free 991 administration. Loaded PLGA NPs were prepared either by nanoprecipitation or microfluidic technique to determine the effects of process and operative parameters on the final formulation. By the nanoprecipitation technique, the hydrodynamic diameter increased from 147 nm for empty NPs to 170 nm after drug encapsulation. NP mean diameter was monodispersed (PDI<0.1) and the zeta potential was below -40 mV. To directly transpose it into microfluidic technique, flow rate ratio (FRR) (organic:aqueous phase) remained 1:2 and total flow rate (TFR) was set up to 12 mL/min. It has been reported that TFR

affects the size of the NPs, with a high TFR corresponding to smaller nanocarriers [40]. Microfluidic-prepared NPs showed a size of 80 nm compared to 170 nm for nanoprecipitation. The zeta potential of all preparations was highly negative. Encapsulation efficiency (EE) and DL were quite similar for both the manufacturing processes: EE was 75% and 85% for the microfluidic and nanoprecipitation process, respectively, and DL was around 9-10% for both the techniques. Even the drug release profile was comparable between the two formulations: indeed, a complete release of the drug was achieved over 24 h, without a burst release of , as usually reported for PLGA NPs [41].

The most important difference between the NPs prepared by nanoprecipitation and microfluidics was their stability at storage conditions. For the latter technique, the smaller size of loaded NPs determined a faster degradation and the destabilization of the system. Indeed, the determination of critical coagulation concentration (*CCC*) for NPs characterized by a size below 100 nm was lower compared to nanoprecipitated NPs, whose destabilization rate was slower. The importance of formulation and process parameters can be investigated by design of experiment (DoE) [42]. We set up a DoE to reduce drug loss and evaluate the importance of drug and polymer concentration and FRR used. At fixed FRR of 1:5, no significant influence of polymer concentration was evidenced on EE. We hypothesized a sort of limit of polymer matrix to encapsulate hydrophobic drugs. Conversely, at higher FRR the effect of polymer concentration was important, probably related to the higher polymer solubility in the high solvent content solution and longer time mixing between aqueous phase and organic solvents [43]. Indeed, EE and DL maximized at high drug amount and low polymer concentration, concluding that they are extensively influenced by FRR. With amphiphilic molecules, important changes in solvent polarity and viscosity drive the nucleation steps which determine the EE and drug loss.

In an effort to systematically unveil the interplay among formulation and process variables on translated drug-loaded PLGA NPs, we can conclude that drug loss can be controlled by playing with FRR which determined a significant effect on EE and DL. The aforementioned formulation study showed the possibility to formulate drug-loaded PLGA NPs *via* either nanoprecipitation or microfluidic technique. In particular, we evaluated the issues related to formulative translation toward microfluidic production and the effects over NPs stability. Finally, we applied DoE to determine the effects of microfluidic formulation and process parameters on EE and DL. The findings of the comparative study here reported can be helpful for the future design of drug-loaded nanosystems by nanoprecipitation and/or microfluidic process.

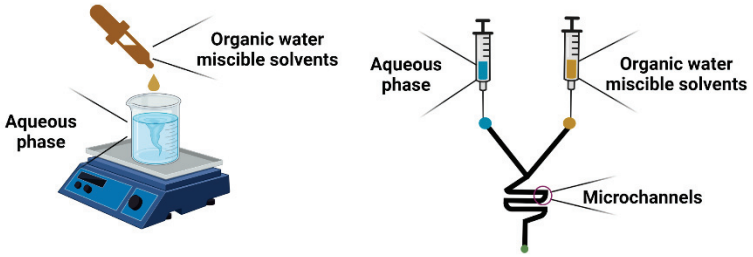

	Nanoprecipitation	Microfluidic
FORMULATION METHOD		
FORMULATIVE PARAMETERS	Polymer and drug concentration	Polymer and drug concentration, TFR, FRR
STABILITY	Lower degradation rate due to the higher size	Freeze-drying
PURPOSE	Preliminary formulation for translation in continuous production	Optimization for scaling-up

Fig. 2. Comparative analysis of nanoprecipitation and microfluidic technique

Further *in vitro* and *in vivo* studies aimed at assessing the biological activity of the formulation obtained by the microfluidic technique. Indeed, 991 belongs to a class of compounds which attracted the attention for the activity as AMPK activators [44]. AMPK is considered an interesting therapeutic target to enhance glucose uptake and regulate numerous metabolic pathways, maintaining cellular energy homeostasis [45]. It also emerged as a target to ameliorate inflammation and fibrosis in muscular cells by a negative regulation of transforming growth factor beta (TGFβ_1) production [46]. However, *in vivo* delivery of AMPK activator molecules is challenging due to significant side effects. PLGA NPs were easily and fast internalized by fibrotic bone marrow-derived macrophages (BMDMs), the most relevant immune cells in Duchenne muscular dystrophy (DMD), giving promises to the internalization of loaded NPs. The fast uptake was due to the macrophages' nature as cells devoted to recognize and phagocyte external and ‘’non-self’’ intruders [47]. The ability of PLGA NPs to efficiently encapsulate 991 gave interesting perspective for an *in vivo* delivery. Indeed, the biocompatibility and biodegradability of PLGA is crucial in perspective to treat muscular tissues already damaged. Furthermore, viability results on BMDMs showed no significant toxic effect on living cells, but a slight increase in the percentage of living cells resulted in the presence of PLGA. This effect is probably due to PLGA degradation and increased lactic acid content, considered as fuel for living cells [48]. By these results, the effect on inhibition of TGFβ_1 production was confirmed by its quantification in samples treated with free 991 and

encapsulated drug. Taken together, *in vitro* results gave promises for an *in vivo* administration. In inflamed tissues, as DMD affected muscles, the anatomical features of blood vessels are altered in presence of inflammatory mediators. The tight junctions become more permeable leading to easy extravasation of nanosystems, on the same concept as the well-known enhanced permeation and retention (EPR) effect exploited for tumor targeting [49]. On these bases, preliminary *in vivo* studies were carried out in a superior DMD mouse model (D2.mdx) [50]. In the new crossed mouse model, the diaphragm is the most representative organ for its inflammatory and fibrosis pattern, which affects its strength more than in gastrocnemius or tibialis anterior (TA) muscles, the main affected organs [51]. Biodistribution analysis of fluorescent NPs administered by intravenous injection (i.v.) resulted in high NPs accumulation in liver, spleen and lungs, as already described for polymer nanocarriers [52]. However, by FACS and fluorescence analysis, we demonstrated that 10% of diaphragm and gastrocnemius cells internalized NPs after 1 h injection, as promising results for distribution in muscles. Moreover, our system can be exploited to reach all muscular cells after i.v. injection. The therapeutical potential of loaded NPs can be maximized in inflamed tissues, exploiting the EPR effect. Following the preliminary biodistribution data, an efficacy study was assessed on D2.mdx mice to evaluate the feasibility of *in vivo* administration of encapsulated 991 and the consequent effectiveness on muscular fibrosis. At the end of the treatment, all mice were still alive and diaphragm and gastrocnemius were analyzed for pro- and anti-inflammatory markers, showing a reduction of pro-inflammatory immune cells in gastrocnemius. Moreover, mice treated with loaded 991 showed a 10% of fibrosis reduction in the diaphragm, compared to empty NPs administration. The fibrosis improvement paves the way for an *in vivo* administration of AMPK activators, confirming that nanotechnological approach can overcome the toxicity issues of AMPK activator molecules. The findings of this first study can be helpful to investigate different nanocarriers as tools to encapsulate AMPK activator molecules and promote their *in vivo* delivery. A screening of several nanosystems could ameliorate the targeting toward macrophages and reduce inflammation and fibrosis in DMD models.

Given the difficulties to develop therapeutic approaches for muscular diseases, active targeting strategies could improve nanocarrier uptake by target cells [53,54]. Thus, in the third part of the research project, preliminary results were collected about the surface functionalization of PLGA NPs by an active targeting agent to increase the nanomedicine tropism toward muscle cells. In the context of muscular targeting, L-carnitine, a small zwitterion molecule, has been selected as a potential targeting agent to increase muscular tropism [55]. Skeletal muscle has a complex organization of structures and sub-structures, which makes drug delivery hard and

complex. It is composed of long cylindrical post-mitotic multinucleated myofibers, rounded by connective tissue [56]. To gain skeletal muscle selectivity, some recognition elements are required. We hypothesized to improve NPs muscular tropism by L-carnitine binding to OCTN2 receptors on muscular cells [57]. To this aim, PLGA NPs were functionalized with a lipophilic derivative of L-carnitine, stearoyl-L-carnitine (SC), in different amounts to achieve an appropriate density on NPs surface [58]. Unfortunately, the presence of SC on NPs determined a lower *in vitro* myoblasts viability at longer incubation times. Then, the detection of OCTN2 receptor was assessed on myoblasts and myotubes, confirming its presence in multinucleate cells. Demonstration of SC-NPs internalization in myoblasts by TEM images confirmed the ability of PLGA NPs to enter cells by classical or OCTN2-mediated endocytosis, as previously demonstrated for SC-conjugated NPs across the blood brain barriers or intestinal barriers [59,60]. Moreover, PTM-B can be efficiently encapsulated into SC-PLGA NPs and repurposed to improve delivery in muscular dystrophy transfected cells. Indeed, PTM has potential effect in the treatment of myotonic dystrophy type I (DM1). DM1 is characterized by splicing defect on DMPK gene, leading to accumulation of expanded RNA-protein aggregates, namely primarily nuclear foci. Research studies demonstrated the potential activity of PTM in reducing the accumulation of nuclear foci and improving physiopathology of DM1 [61]. These preliminary results need further investigations to uncover the possibilities of these formulations. To conclude, active targeting of muscular cells by surface-modified nanocarriers can be a powerful tool to improve muscular uptake, challenging its biological complex structure by enhancing the permeation and therapeutic efficacy of drug.

References

1. Taina-González, L.; de la Fuente, M. The Potential of Nanomedicine to Unlock the Limitless Applications of MRNA. *Pharmaceutics* **2022**, *14*, 460, doi:10.3390/pharmaceutics14020460.
2. Yokel, R.A. Direct Nose to the Brain Nanomedicine Delivery Presents a Formidable Challenge. *Wiley Interdisciplinary Reviews: Nanomedicine and Nanobiotechnology* **2022**, *14*, doi:10.1002/wnan.1767.
3. Joseph, X.; Akhil, V.; Arathi, A.; Mohanan, P. Nanobiomaterials in Support of Drug Delivery Related Issues. *Materials Science and Engineering: B* **2022**, *279*, 115680, doi:10.1016/j.mseb.2022.115680.
4. Li, T.; Shi, W.; Yao, J.; Hu, J.; Sun, Q.; Meng, J.; Wan, J.; Song, H.; Wang, H. Combinatorial Nanococktails via Self-Assembling Lipid Prodrugs for Synergistically Overcoming Drug Resistance and Effective Cancer Therapy. *Biomaterials Research* **2022**, *26*, doi:10.1186/s40824-022-00249-7.
5. Chen, X.; Zheng, R.; Zhao, L.; Kong, R.; Yang, N.; Liu, Y.; Chen, A.; Wang, C.; Cheng, H.; Li, S. Photodynamic Therapy Initiated Immunotherapy of Self-Delivery Re-Educator by Inducing Immunogenic Cell Death and Macrophage Polarization. *Chemical Engineering Journal* **2022**, *435*, doi:10.1016/j.cej.2022.134783.
6. Chung, Y.H.; Beiss, V.; Fiering, S.N.; Steinmetz, N.F. COVID-19 Vaccine Frontrunners and Their Nanotechnology Design. *ACS Nano* **2020**, *14*, 12522–12537, doi:10.1021/acsnano.0c07197.
7. Đorđević, S.; Gonzalez, M.M.; Conejos-Sánchez, I.; Carreira, B.; Pozzi, S.; Acúrcio, R.C.; Satchi-Fainaro, R.; Florindo, H.F.; Vicent, M.J. Current Hurdles to the Translation of Nanomedicines from Bench to the Clinic. *Drug Delivery and Translational Research* **2022**, *12*, 500–525, doi:10.1007/s13346-021-01024-2.
8. Wang, C.-P.J.; Byun, M.J.; Kim, S.-N.; Park, W.; Park, H.H.; Kim, T.-H.; Lee, J.S.; Park, C.G. Biomaterials as Therapeutic Drug Carriers for Inflammatory Bowel Disease Treatment. *Journal of Controlled Release* **2022**, *345*, 1–19, doi:10.1016/j.jconrel.2022.02.028.
9. Gentile, P.; Chiono, V.; Carmagnola, I.; Hatton, P.V. An Overview of Poly(Lactic-Co-Glycolic) Acid (PLGA)-Based Biomaterials for Bone Tissue Engineering. *International Journal of Molecular Sciences* **2014**, *15*, 3640–3659, doi:10.3390/ijms15033640.
10. El-Hammadi, M.M.; Arias, J.L. Recent Advances in the Surface Functionalization of PLGA-Based Nanomedicines. *Nanomaterials (Basel)* **2022**, *12*, 354, doi:10.3390/nano12030354.
11. Maddahfar, M.; Wen, S.; Hosseinpour Mashkani, S.M.; Zhang, L.; Shimoni, O.; Stenzel, M.; Zhou, J.; Fazekas de St Groth, B.; Jin, D. Stable and Highly Efficient Antibody-Nanoparticles Conjugation. *Bioconjug Chem* **2021**, *32*, 1146–1155, doi:10.1021/acs.bioconjchem.1c00192.
12. Zhong, Y.; Meng, F.; Deng, C.; Zhong, Z. Ligand-Directed Active Tumor-Targeting Polymeric Nanoparticles for Cancer Chemotherapy. *Biomacromolecules* **2014**, *15*, 1955–1969, doi:10.1021/bm5003009.
13. Dosio, F.; Reddy, L.H.; Ferrero, A.; Stella, B.; Cattel, L.; Couvreur, P. Novel Nanoassemblies Composed of Squalenoyl-Paclitaxel Derivatives: Synthesis, Characterization, and Biological Evaluation. *Bioconjug Chem* **2010**, *21*, 1349–1361, doi:10.1021/bc100154g.
14. Turino, L.N.; Stella, B.; Dosio, F.; Luna, J.A.; Barresi, A.A. Nanoparticles Obtained by Confined Impinging Jet Mixer: Poly(Lactide-Co-Glycolide) vs. Poly-ε-Caprolactone. *Drug Dev Ind Pharm* **2018**, *44*, 934–941, doi:10.1080/03639045.2017.1421662.

15. Katte, R.H.; Dowarha, D.; Chou, R.-H.; Yu, C. S100P Interacts with P53 While Pentamidine Inhibits This Interaction. *Biomolecules* **2021**, *11*, 634, doi:10.3390/biom11050634.
16. Wu, Y.; Zhang, Z.; Kou, Z. Pentamidine Inhibits Ovarian Cancer Cell Proliferation and Migration by Maintaining Stability of PTEN in Vitro. *Drug Design, Development and Therapy* **2021**, *15*, 2857–2868, doi:10.2147/DDDT.S311187.
17. Kennedy, P.G. Clinical Features, Diagnosis, and Treatment of Human African Trypanosomiasis (Sleeping Sickness). *Lancet Neurol* **2013**, *12*, 186–194, doi:10.1016/S1474-4422(12)70296-X.
18. Arino, T.; Karakawa, S.; Ishiwata, Y.; Nagata, M.; Yasuhara, M. Effect of Cimetidine on Pentamidine Induced Hyperglycemia in Rats. *Eur J Pharmacol* **2012**, *693*, 72–79, doi:10.1016/j.ejphar.2012.07.043.
19. Prabhavalkar, S.; Masengu, A.; O'Rourke, D.; Shields, J.; Courtney, A. Nebulized Pentamidine-Induced Acute Renal Allograft Dysfunction. *Case Reports in Transplantation* **2013**, *2013*, e907593, doi:10.1155/2013/907593.
20. Baroni, A.; Neaga, I.; Delbosc, N.; Wells, M.; Verdy, L.; Ansseau, E.; Vanden Eynde, J.J.; Belayew, A.; Bodoki, E.; Oprean, R.; et al. Bioactive Aliphatic Polycarbonates Carrying Guanidinium Functions: An Innovative Approach for Myotonic Dystrophy Type 1 Therapy. *ACS Omega* **2019**, *4*, 18126–18135, doi:10.1021/acsomega.9b02034.
21. Angelopoulou, E.; Paudel, Y.N.; Piperi, C. Emerging Role of S100B Protein Implication in Parkinson's Disease Pathogenesis. *Cellular and Molecular Life Sciences* **2021**, *78*, 1445–1453, doi:10.1007/s00018-020-03673-x.
22. Carton, F.; Chevalier, Y.; Nicoletti, L.; Tarnowska, M.; Stella, B.; Arpicco, S.; Malatesta, M.; Jordheim, L.P.; Briançon, S.; Lollo, G. Rationally Designed Hyaluronic Acid-Based Nano-Complexes for Pentamidine Delivery. *Int J Pharm* **2019**, *568*, 118526, doi:10.1016/j.ijpharm.2019.118526.
23. Arpicco, S.; Battaglia, L.; Brusa, P.; Cavalli, R.; Chirio, D.; Dosio, F.; Gallarate, M.; Milla, P.; Peira, E.; Rocco, F.; et al. Recent Studies on the Delivery of Hydrophilic Drugs in Nanoparticulate Systems. *Journal of Drug Delivery Science and Technology* **2016**, *32*, 298–312, doi:10.1016/j.jddst.2015.09.004.
24. Han, F.Y.; Thurecht, K.J.; Whittaker, A.K.; Smith, M.T. Bioerodable PLGA-Based Microparticles for Producing Sustained-Release Drug Formulations and Strategies for Improving Drug Loading. *Frontiers in Pharmacology* **2016**, *7*.
25. Ačimovič, J.; Rozman, D. Steroidal Triterpenes of Cholesterol Synthesis. *Molecules* **2013**, *18*, 4002–4017, doi:10.3390/molecules18044002.
26. Peretti, E.; Miletto, I.; Stella, B.; Rocco, F.; Berlier, G.; Arpicco, S. Strategies to Obtain Encapsulation and Controlled Release of Pentamidine in Mesoporous Silica Nanoparticles. *Pharmaceutics* **2018**, *10*, E195, doi:10.3390/pharmaceutics10040195.
27. Maksimenko, A.; Dosio, F.; Mougin, J.; Ferrero, A.; Wack, S.; Reddy, L.H.; Weyn, A.-A.; Lepeltier, E.; Bourgaux, C.; Stella, B.; et al. A Unique Squalenoylated and Nonpegylated Doxorubicin Nanomedicine with Systemic Long-Circulating Properties and Anticancer Activity. *Proc Natl Acad Sci U S A* **2014**, *111*, E217-226, doi:10.1073/pnas.1313459110.
28. Desmaële, D.; Gref, R.; Couvreur, P. Squalenoylation: A Generic Platform for Nanoparticular Drug Delivery. *J Control Release* **2012**, *161*, 609–618, doi:10.1016/j.jconrel.2011.07.038.
29. Cunningham, A.J.; Robinson, M.; Banquy, X.; Leblond, J.; Zhu, X.X. Bile Acid-Based Drug Delivery Systems for Enhanced Doxorubicin Encapsulation: Comparing Hydrophobic and Ionic Interactions in Drug Loading and Release. *Mol Pharm* **2018**, *15*, 1266–1276, doi:10.1021/acs.molpharmaceut.7b01091.

30. Ko, M.; Quiñones-Hinojosa, A.; Rao, R. Emerging Links between Endosomal PH and Cancer. *Cancer Metastasis Rev* **2020**, *39*, 519–534, doi:10.1007/s10555-020-09870-1.
31. Yesylevskyy, S.O.; Ramseyer, C.; Savenko, M.; Mura, S.; Couvreur, P. Low-Density Lipoproteins and Human Serum Albumin as Carriers of Squalenoylated Drugs: Insights from Molecular Simulations. *Mol Pharm* **2018**, *15*, 585–591, doi:10.1021/acs.molpharmaceut.7b00952.
32. Li, Y.-X.; Liu, Y.; Wang, H.; Li, Z.-T.; Zhang, D.-W. Water-Soluble Porphyrin-Based Nanoparticles Derived from Electrostatic Interaction for Enhanced Photodynamic Therapy. *ACS Appl. Bio Mater.* **2022**, *5*, 881–888, doi:10.1021/acsabm.1c01262.
33. Gu, P.; Wusiman, A.; Wang, S.; Zhang, Y.; Liu, Z.; Hu, Y.; Liu, J.; Wang, D. Polyethylenimine-Coated PLGA Nanoparticles-Encapsulated Angelica Sinensis Polysaccharide as an Adjuvant to Enhance Immune Responses. *Carbohydr Polym* **2019**, *223*, 115128, doi:10.1016/j.carbpol.2019.115128.
34. Bondioli, L.; Costantino, L.; Ballestrazzi, A.; Lucchesi, D.; Boraschi, D.; Pellati, F.; Benvenuti, S.; Tosi, G.; Vandelli, M.A. PLGA Nanoparticles Surface Decorated with the Sialic Acid, N-Acetylneuraminic Acid. *Biomaterials* **2010**, *31*, 3395–3403, doi:10.1016/j.biomaterials.2010.01.049.
35. Song, X.; Wang, J.; Xu, Y.; Shao, H.; Gu, J. Surface-Modified PLGA Nanoparticles with PEG/LA-Chitosan for Targeted Delivery of Arsenic Trioxide for Liver Cancer Treatment: Inhibition Effects Enhanced and Side Effects Reduced. *Colloids and Surfaces B: Biointerfaces* **2019**, *180*, 110–117, doi:10.1016/j.colsurfb.2019.04.036.
36. Chakraborty, M.; Selma-Soriano, E.; Magny, E.; Couso, J.P.; Pérez-Alonso, M.; Charlet-Berguerand, N.; Artero, R.; Llamusi, B. Pentamidine Rescues Contractility and Rhythmicity in a Drosophila Model of Myotonic Dystrophy Heart Dysfunction. *Dis Model Mech* **2015**, *8*, 1569–1578, doi:10.1242/dmm.021428.
37. Cirillo, C.; Capoccia, E.; Iuvone, T.; Cuomo, R.; Sarnelli, G.; Steardo, L.; Esposito, G. S100B Inhibitor Pentamidine Attenuates Reactive Gliosis and Reduces Neuronal Loss in a Mouse Model of Alzheimer's Disease. *Biomed Res Int* **2015**, *2015*, 508342, doi:10.1155/2015/508342.
38. Hernández-Giottonini, K.Y.; Rodríguez-Córdova, R.J.; Gutiérrez-Valenzuela, C.A.; Peñuñuri-Miranda, O.; Zavala-Rivera, P.; Guerrero-Germán, P.; Lucero-Acuña, A. PLGA Nanoparticle Preparations by Emulsification and Nanoprecipitation Techniques: Effects of Formulation Parameters. *RSC Adv.* **2020**, *10*, 4218–4231, doi:10.1039/C9RA10857B.
39. Huang, W.; Zhang, C. Tuning the Size of Poly(Lactic-Co-Glycolic Acid) (PLGA) Nanoparticles Fabricated by Nanoprecipitation. *Biotechnology Journal* **2018**, *13*, 1700203, doi:10.1002/biot.201700203.
40. Roces, C.B.; Lou, G.; Jain, N.; Abraham, S.; Thomas, A.; Halbert, G.W.; Perrie, Y. Manufacturing Considerations for the Development of Lipid Nanoparticles Using Microfluidics. *Pharmaceutics* **2020**, *12*, 1095, doi:10.3390/pharmaceutics12111095.
41. Czapka, A.; Grune, C.; Schädel, P.; Bachmann, V.; Scheuer, K.; Dirauf, M.; Weber, C.; Skaltsounis, A.-L.; Jandt, K.D.; Schubert, U.S.; et al. Drug Delivery of 6-Bromoindirubin-3'-Glycerol-Oxime Ether Employing Poly(d,l-Lactide-Co-Glycolide)-Based Nanoencapsulation Techniques with Sustainable Solvents. *Journal of Nanobiotechnology* **2022**, *20*, doi:10.1186/s12951-021-01179-7.
42. Chiesa, E.; Dorati, R.; Modena, T.; Conti, B.; Genta, I. Multivariate Analysis for the Optimization of Microfluidics-Assisted Nanoprecipitation Method Intended for the Loading of Small Hydrophilic Drugs into PLGA Nanoparticles. *Int J Pharm* **2018**, *536*, 165–177, doi:10.1016/j.ijpharm.2017.11.044.
43. Terada, T.; Kulkarni, J.A.; Huynh, A.; Chen, S.; van der Meel, R.; Tam, Y.Y.C.; Cullis, P.R. Characterization of Lipid Nanoparticles Containing Ionizable Cationic Lipids Using

Design-of-Experiments Approach. *Langmuir* **2021**, *37*, 1120–1128, doi:10.1021/acs.langmuir.0c03039.
44. Kim, J.; Yang, G.; Kim, Y.; Kim, J.; Ha, J. AMPK Activators: Mechanisms of Action and Physiological Activities. *Exp Mol Med* **2016**, *48*, e224, doi:10.1038/emm.2016.16.
45. Olivier, S.; Foretz, M.; Viollet, B. Promise and Challenges for Direct Small Molecule AMPK Activators. *Biochem Pharmacol* **2018**, *153*, 147–158, doi:10.1016/j.bcp.2018.01.049.
46. Juban, G.; Saclier, M.; Yacoub-Youssef, H.; Kernou, A.; Arnold, L.; Boisson, C.; Ben Larbi, S.; Magnan, M.; Cuvellier, S.; Théret, M.; et al. AMPK Activation Regulates LTBP4-Dependent TGF-B1 Secretion by Pro-Inflammatory Macrophages and Controls Fibrosis in Duchenne Muscular Dystrophy. *Cell Rep* **2018**, *25*, 2163-2176.e6, doi:10.1016/j.celrep.2018.10.077.
47. Gessain, G.; Blériot, C.; Ginhoux, F. Non-Genetic Heterogeneity of Macrophages in Diseases—A Medical Perspective. *Frontiers in Cell and Developmental Biology* **2020**, *8*.
48. Chereddy, K.K.; Vandermeulen, G.; Préat, V. PLGA Based Drug Delivery Systems: Promising Carriers for Wound Healing Activity. *Wound Repair Regen* **2016**, *24*, 223–236, doi:10.1111/wrr.12404.
49. Kang, H.; Rho, S.; Stiles, W.R.; Hu, S.; Baek, Y.; Hwang, D.W.; Kashiwagi, S.; Kim, M.S.; Choi, H.S. Size-Dependent EPR Effect of Polymeric Nanoparticles on Tumor Targeting. *Adv Healthc Mater* **2020**, *9*, e1901223, doi:10.1002/adhm.201901223.
50. Coley, W.D.; Bogdanik, L.; Vila, M.C.; Yu, Q.; Van Der Meulen, J.H.; Rayavarapu, S.; Novak, J.S.; Nearing, M.; Quinn, J.L.; Saunders, A.; et al. Effect of Genetic Background on the Dystrophic Phenotype in Mdx Mice. *Hum Mol Genet* **2016**, *25*, 130–145, doi:10.1093/hmg/ddv460.
51. Hammers, D.W.; Hart, C.C.; Matheny, M.K.; Wright, L.A.; Armellini, M.; Barton, E.R.; Sweeney, H.L. The D2.Mdx Mouse as a Preclinical Model of the Skeletal Muscle Pathology Associated with Duchenne Muscular Dystrophy. *Sci Rep* **2020**, *10*, 14070, doi:10.1038/s41598-020-70987-y.
52. Mandl, H.K.; Quijano, E.; Suh, H.W.; Sparago, E.; Oeck, S.; Grun, M.; Glazer, P.M.; Saltzman, W.M. Optimizing Biodegradable Nanoparticle Size for Tissue-Specific Delivery. *J Control Release* **2019**, *314*, 92–101, doi:10.1016/j.jconrel.2019.09.020.
53. Andreana, I.; Repellin, M.; Carton, F.; Kryza, D.; Briançon, S.; Chazaud, B.; Mounier, R.; Arpicco, S.; Malatesta, M.; Stella, B.; et al. Nanomedicine for Gene Delivery and Drug Repurposing in the Treatment of Muscular Dystrophies. *Pharmaceutics* **2021**, *13*, doi:10.3390/pharmaceutics13020278.
54. Passaro, F.; Tocchetti, C.G.; Spinetti, G.; Paudice, F.; Ambrosone, L.; Costagliola, C.; Cacciatore, F.; Abete, P.; Testa, G. Targeting Fibrosis in the Failing Heart with Nanoparticles. *Advanced Drug Delivery Reviews* **2021**, *174*, 461–481, doi:10.1016/j.addr.2021.05.004.
55. Furuichi, Y.; Sugiura, T.; Kato, Y.; Takakura, H.; Hanai, Y.; Hashimoto, T.; Masuda, K. Muscle Contraction Increases Carnitine Uptake via Translocation of OCTN2. *Biochem Biophys Res Commun* **2012**, *418*, 774–779, doi:10.1016/j.bbrc.2012.01.101.
56. Bottinelli, R.; Reggiani, C. Human Skeletal Muscle Fibres: Molecular and Functional Diversity. *Prog Biophys Mol Biol* **2000**, *73*, 195–262, doi:10.1016/s0079-6107(00)00006-7.
57. Pochini, L.; Scalise, M.; Galluccio, M.; Indiveri, C. OCTN Cation Transporters in Health and Disease: Role as Drug Targets and Assay Development. *J Biomol Screen* **2013**, *18*, 851–867, doi:10.1177/1087057113493006.
58. Elias, D.R.; Poloukhtine, A.; Popik, V.; Tsourkas, A. Effect of Ligand Density, Receptor Density, and Nanoparticle Size on Cell Targeting. *Nanomedicine* **2013**, *9*, 194–201, doi:10.1016/j.nano.2012.05.015.

59. Kou, L.; Yao, Q.; Sun, M.; Wu, C.; Wang, J.; Luo, Q.; Wang, G.; Du, Y.; Fu, Q.; Wang, J.; et al. Cotransporting Ion Is a Trigger for Cellular Endocytosis of Transporter-Targeting Nanoparticles: A Case Study of High-Efficiency SLC22A5 (OCTN2)-Mediated Carnitine-Conjugated Nanoparticles for Oral Delivery of Therapeutic Drugs. *Adv Healthc Mater* **2017**, *6*, doi:10.1002/adhm.201700165.
60. Kou, L.; Hou, Y.; Yao, Q.; Guo, W.; Wang, G.; Wang, M.; Fu, Q.; He, Z.; Ganapathy, V.; Sun, J. L-Carnitine-Conjugated Nanoparticles to Promote Permeation across Blood-Brain Barrier and to Target Glioma Cells for Drug Delivery via the Novel Organic Cation/Carnitine Transporter OCTN2. *Artif Cells Nanomed Biotechnol* **2018**, *46*, 1605–1616, doi:10.1080/21691401.2017.1384385.
61. Warf, M.B.; Nakamori, M.; Matthys, C.M.; Thornton, C.A.; Berglund, J.A. Pentamidine Reverses the Splicing Defects Associated with Myotonic Dystrophy. *Proc Natl Acad Sci U S A* **2009**, *106*, 18551–18556, doi:10.1073/pnas.0903234106.

Conclusions and perspectives

In this thesis work, we proposed formulative studies of active molecules for different therapeutic applications; lipid and polymer nanocarriers were chosen as the building blocks to encapsulate these therapeutic compounds. Drug repurposing strategy was the driving force for selecting therapeutical candidates to ameliorate their pharmacokinetics issues.

In the first part, nanosystems based on biocompatible squalenic acid (SQ-COOH) and PLGA were formulated with pentamidine free base (PTM-B) to reduce its toxic effects *in vitro* and *in vivo*. We presented two formulation studies based on the molecular structure of PLGA and SQ-COOH, which exploited their negatively charged groups to incorporate PTM-B through ionic interactions with its positively charged amidine groups. A comprehensive characterization of the nanosystems was described. For both the formulations, the preliminary studies performed *in vitro* suggested that encapsulated PTM-B can display anticancer activity. Moreover, SQ-COOH has been assessed as a possible indirect targeting agent: cancer cells with high expression of low-density lipoprotein receptor (LDLR) showed enhanced PTM-B activity. Thus, we confirmed that squalene can efficiently interact with LDL and indirectly improve drug uptake. Future tests will be devoted to evaluate the cellular trafficking of SQ-COOH/PTM-B nanoparticles thanks to the association of a fluorescent dye. The first part of the work also showed that nanoparticles based on ionizable groups could offer pH-responsive release that can be exploited to improve drug accumulation in an acidic environment, such as the tumor interstitium. In these studies, the nanoprecipitation technique, a simple and environment-friendly procedure, found easy applicability to formulate nanocarriers based on electrostatic interactions. This is an important advantage for a future scale-up of these formulations, which have all the pre-requisites for translation in the microfluidic technique.

The second part of the work, aimed to design PLGA nanoparticles for the encapsulation of a novel hydrophobic drug, highlighted the importance of the microfluidic technique and the problems related to transposing polymer nanocarrier formulation from conventional nanoprecipitation technique to high-controlled microfluidic process. In this frame, we prepared drug-loaded PLGA nanoparticles by both techniques and evaluated the process and formulative parameters to improve encapsulation efficiency and drug loading. Although microfluidic technique offers the possibility to tune the physicochemical characteristics of polymer nanoparticles, the translation process is hard to achieve and many variables need to be considered. Nevertheless, this technique allowed a small benzimidazole drug, namely 991, interesting in the treatment of Duchenne muscular dystrophy, to be efficiently encapsulated, preventing its *in vivo* toxic effects. The system was cytocompatible with bone marrow-derived macrophages and had a positive impact on reducing inflammatory and fibrosis mediators in

biological tests. *In vivo*, we were able to administer 991 without visible toxic effects on D2.mdx mice, promoting a 10% reduction of muscular fibrosis. Further studies will be devoted to confirm the fibrosis reduction in diaphragm and gastrocnemius in a large number of animals. Moreover, the encapsulation of 991 into polymer nanocarriers paves the way to the encapsulation of AMPK activator molecules into nanosystems of different nature.

The third part of the thesis describes preliminary results to promote an active targeting strategy toward muscular cells. To this aim, PLGA nanoparticles were functionalized with stearoyl-L-carnitine to exploit specific uptake mediated by OCTN2 receptors. Further tests will be focused on the characterization of the internalization process to confirm a preferential uptake in presence of the active targeting agent.

The findings of this work can serve the domain from different perspectives. From a technological point of view, they offer a better understanding of the formulation process for polymer-based nanocarriers obtained by either nanoprecipitation or microfluidic technique, highlighting the importance of a rational design to obtain nanocarriers with appropriate physicochemical and morphological characteristics. Indeed, although the two techniques are based on the same principle, changing the process can modify the nanoparticle features. Moreover, the encapsulation of hydrophobic drugs, either by electrostatic interactions or *via* hydrophobic forces, is a difficult process that requires formulative considerations in terms of organic solvents, volume ratio and molecular proportions. From a biological point of view, we showed that our biodegradable and biocompatible drug delivery systems might improve the efficacy of the tested active molecules. Further investigations are highly recommended to uncover the possibilities of these formulations. Finally, the drug-repurposing strategy offers the possibility to re-collocate old or new drugs in the treatment of different rare pathologies that often do not have a cure.

In conclusion, considering the multidisciplinary aspect of the research, the combination of technical and scientific skills and tools available to each group resulted to be crucial for the realization of the project itself and for obtaining the expected scientific results. The collaboration through the co-tutored Ph.D. thesis allowed the involved research groups to enhance and strengthen the synergy of skills perfectly complementary and guarantees for further developments in the formulation and active targeting of repurposed drugs.

Résumé substantiel

Des problèmes de pharmacocinétique et de pharmacodynamique peuvent entraver les applications cliniques de plusieurs molécules actives. La nanomédecine propose une stratégie potentielle pour pallier aux inconvénients de certains médicaments et améliorer leur utilisation thérapeutique en utilisant des systèmes d'administration de médicaments (DDSs). Les DDSs ont été largement étudiés pour la conception de traitements plus efficaces et plus sûrs, avec des applications importantes, notamment dans le domaine du cancer [1,2], et maladies immunitaires [3]. L'un des principaux obstacles au développement des DDSs réside dans leur éventuelle toxicité. Sur cette base, l'acide poly(lactique-*co*-glycolique) (PLGA) et les dérivés du squalène sont des composants biodégradables et biocompatibles capables de s'auto-assembler pour former des nanoparticules (NPs). Plusieurs méthodes de préparation des NPs sont décrites dans la littérature [4]. La méthode de nanoprécipitation est un processus simple en une seule étape, principalement utilisée pour l'encapsulation de molécules hydrophobes [5]. Une solution organique du polymère et molécule active est ajoutée goutte à goutte à la phase aqueuse, qui peut être de l'eau ou un tampon aqueux. Ainsi, le NPs se forment immédiatement. Cependant, cette méthode présente un certain nombre d'inconvénients pour la production de NPs, tels que la variabilité entre différents échantillons, le manque de contrôle précis sur les caractéristiques des NPs à obtenir et la difficulté de produire de grands volumes. Ces questions ont accru l'intérêt de la recherche scientifique pour le développement de méthodes de production nouvelles et innovantes. Au cours de ces dernières années, les dispositifs à micro-échelle ont été optimisés pour produire des NPs avec un meilleur contrôle des caractéristiques chimiques et physiques du système [6]. Ce travail de thèse comprend la formulation de DDSs à base de polymères et lipides pour améliorer la pharmacocinétique et la pharmacodynamique de molécules d'intérêt thérapeutique. Une étude comparative est présentée pour souligner l'importance des paramètres et des variables du processus dans la détermination des caractéristiques physico-chimiques des NPs. Deux molécules actives ont été étudiées dans ce travail et ont été sélectionnées en tenant compte de leur possible repositionnement dans des applications cliniques (*drug repurposing*).
La première partie de ce travail de thèse décrit une stratégie de formulation pour incorporer la base libre de la pentamidine (PTM-B) dans des NPs d'un dérivé du squalène, notamment l'acide squalénique (SQ-COOH), qui a été choisi en raison de sa structure chimique caractéristique, présentant un acide carboxylique terminal (pKa=4,5) chargé négativement au pH physiologique. Les dérivés du squalène ont la capacité de s'auto-assembler pour former des suspensions colloïdales en milieu aqueux [7]. La PTM-B, qui possède deux groupes amidine chargés positivement (pKa=12), est capable d'établir des liaisons ioniques avec le groupe carboxylique du SQ-COOH pour former une suspension colloïdale stable. Dans cette partie du

travail, il a été possible d'optimiser la capacité de charge du système, appelée charge médicamenteuse (DL). Les NPs ont été préparées en utilisant la technique de nanoprécipitation [8], en évaluant l'impact des variables de formulation, telles que le rapport molaire SQ-COOH/PTM-B et le rapport des volumes des phases organique et aqueuse, sur les caractéristiques du système. Une étude de dynamisme moléculaire a permis de décrire l'interaction entre la PTM-B et le SQ-COOH à différents rapports molaires SQ-COOH/PTM-B (3:1, 4:1 et 4,5:1). Étant donné que pour les différents rapports molaires considérés les différences en termes de caractéristiques physico-chimiques étaient négligeables, le rapport molaire SQ-COOH/PTM-B 3:1 a été sélectionné pour maximiser la DL de la formulation. L'effet du rapport entre le volume de la phase organique et le volume de la phase aqueuse (V_e/V_a) utilisé pour la formulation des NPs a été étudié et mis en relation avec le diamètre moyen et la DL des nanoparticules. En travaillant à un V_e/V_a de 0,2:1, les NPs présentaient un diamètre moyen d'environ 110 nm et une DL maximale de 19%. Il a été démontré précédemment que les dérivés du squalène sous forme de NPs s'associent *in vivo* aux lipoprotéines de basse densité (LDL) par analogie avec le cholestérol, dont le squalène est un intermédiaire endogène de la synthèse [9]. Ce phénomène permet au dérivé du squalène de cibler indirectement le récepteur des LDL (LDLR), qui est surexprimé à la surface de certaines cellules cancéreuses. Sur cette base, des essais *in vitro* ont été réalisés sur des lignées de cellules cancéreuses présentant différents degrés d'expression du récepteur, démontrant l'internalisation des NPs par le LDLR. Toujours sur la base d'interactions électrostatiques, la PTM-B a été incorporée dans des NPs de PLGA. La formulation a été optimisée en testant différents types de PLGA (50:50 et 75:25, ratio acide lactique/acide glycolique) et différentes quantités de PTM-B. Les suspensions colloïdales ont été caractérisées par un diamètre moyen de 120 nm et un potentiel zêta négatif d'environ -25 mV. L'efficacité d'encapsulation (EE) du médicament dans la matrice polymère par le biais d'interactions électrostatiques était élevée et supérieure à 80%. Les méthodes classiques de formulation des NPs, notamment la nanoprécipitation, peuvent poser des problèmes lors de la production à grande échelle, car le processus de translation peut entraîner des modifications des propriétés du nanosystème [10]. Pour surmonter ces inconvénients, la technologie microfluidique est utilisée pour produire des DDSs et mieux contrôler les caractéristiques chimiques et physiques de la suspension colloïdale [11,12]. Afin d'étudier l'impact des variables de processus et de formulation pour la production à grande échelle de NPs polymériques, une étude comparative entre la méthode de production classique et la microfluidique a été optimisée. Un dérivé de benzimidazole, appelée 991, a été choisie comme médicament modèle dans la formulation de NPs de PLGA pour la nanoprécipitation et

la microfluidique. Les paramètres de *total flow rate* (TFR) et de *flow rate ratio* (FRR) corrélés au processus de microfluidique ont été étudiés pour transposer la synthèse des NPs en microfluidique. En travaillant à un TFR de 12 mL/min et à un FRR de 1:2 (rapport phase organique/phase aqueuse), il a été constaté que les NPs chargées de 991 avaient un diamètre moyen d'environ 80 nm, comparé aux 170 nm obtenus par nanoprécipitation. Une fois dialysé pour éliminer la fraction de médicament non incorporée, l'EE et la DL des formulations ont été étudiées. Les formulations ont montré une EE similaire entre 75% et 85%, respectivement pour celles produites par microfluidique et celles obtenues par nanoprécipitation, correspondant à 9-10% de DL. La purification par dialyse a permis d'obtenir des NPs dans lesquelles le médicament est efficacement incorporé dans la matrice polymère, ce qui a également été confirmé par l'absence de libération soudaine dans des conditions physiologiques (PBS, pH 7,4). Cependant, les NPs préparées par microfluidique ont montré une moindre stabilité à 4 °C que celles préparées par nanoprécipitation classique. Probablement, le diamètre moyen inférieur à 100 nm entraine une concentration critique de coagulation (*CCC*) plus faible et donc une déstabilisation plus rapide. La formulation a été convertie en forme solide par lyophilisation, en utilisant 12% p/v de tréhalose comme cryoprotecteur. Après lyophilisation, les NPs remises en suspension ont conservé leur diamètre moyen initial d'environ 80 nm. Le passage de la technique classique de nanoprécipitation à la microfluidique peut entraîner une modification des caractéristiques de la formulation, ce qui constitue un inconvénient majeur. Par conséquent, le processus de translation microfluidique des NPs a été optimisé à l'aide d'un plan d'expériences (DoE), permettant d'évaluer l'influence du FRR, de la concentration du polymère et du médicament dans la phase organique sur EE et DL. L'EE et la DL ont été maximisées pour une concentration élevée de médicament et une faible concentration de polymère, ce qui permet de conclure que ces deux valeurs sont largement influencées par le FRR. Les résultats de l'étude comparative sont utiles pour la conception future de nanosystèmes chargés de médicaments afin de passer de la méthode de production classique au processus microfluidique. La troisième partie de ce projet était l'évaluation biologique des NPs chargées. Le 991 est un puissant activateur de l'AMP-protéine kinase (AMPK), qui participe à la réduction de l'inflammation et de la fibrose dans la Dystrophie Musculaire de Duchenne (DMD). L'activation de l'AMPK entraîne une régulation négative du facteur de croissance transformant-β (TGFβ_1), une cytokine pro-inflammatoire [13]. Cependant, l'utilisation clinique du 991 est entravée par ses effets secondaires importants. Des macrophages fibrotiques dérivés de la moelle osseuse (BMDM) ont été utilisés pour évaluer l'activation de l'AMPK et, par conséquent, la réduction du TGFβ_1. Les résultats ont montré que les NPs sont rapidement internalisées par

les macrophages et ont entraîné à une réduction du TGFβ_1 en présence de 991, à la fois sous forme de médicament libre et chargé dans les NPs de PLGA. L'évaluation du comportement du système *in vivo* a été la dernière étude de l'évaluation biologique. Nous nous sommes concentrés sur l'absorption des NPs de PLGA au niveau du diaphragme car il est considéré comme l'organe le plus représentatif pour son profil inflammatoire et fibrotique [14]. Des études préliminaires ont évalué le profil pharmacocinétique des NPs après administration intraveineuse (i.v.) dans un modèle supérieur de DMD (D2.mdx). Après 1 h, une 10% des cellules dans le diaphragme et le muscle gastrocnémien avaient internalisés des NPs. En outre, des NPs chargées de 991 ont été injectées par voie i.v. pour évaluer la réduction de la fibrose chez les souris D2.mdx. Après trois semaines de traitement, une réduction de 10% de la fibrose a été obtenue dans ce modèle animal, un résultat prometteur pour l'amélioration de l'homéostasie musculaire *in vivo*. La dernière partie du projet explique le développement préliminaire d'une stratégie de ciblage actif pour augmenter le tropisme musculaire de NPs. Compte tenu de la présence de récepteurs spécifiques sur les cellules musculaires, en particulier le transporteur organique/cationique Na^+ 2 (OCTN2) [15], la L-carnitine a été utilisée pour cibler sur les cellules musculaires. L'agent de ciblage est dérivé de la fonctionnalisation de la L-carnitine par l'acide stéarique pour obtenir la stéaroyl-L-carnitine (SC). La SC a été choisi car l'acide stéarique peut interagir efficacement avec la matrice polymère et exposer la carnitine à la surface des NPs. Deux concentrations différentes de SC (5% et 10% p/p) ont été évaluées pour trouver la densité équilibrée du ligand [16]. Les nanoparticules étaient caractérisées par un diamètre moyen inférieur à 100 nm pour les deux pourcentages de SC testés, et un potentiel zêta négatif autour de -20 mV. La viabilité cellulaire a été évaluée sur des myoblastes de la lignée cellulaire C2C12 traités avec des NPs conjuguées à 5% de SC. Après 2 h d'incubation aucun changement n'a été observé dans les échantillons traités avec des NPs marquées par SC par rapport au contrôle. Cependant, après 24 heures d'incubation et plus, la viabilité cellulaire a diminué de manière significative. L'expression du récepteur OCTN2 sur les myoblastes et les myotubes a été évaluée par immunomarquage en microscopie confocale. Les myotubes ont montré une présence plus élevée du récepteur OCTN2, par rapport aux myoblastes. Ces données préliminaires démontrent la possibilité de développer une stratégie de ciblage active et d'améliorer le tropisme musculaire sans effets de véhicule toxiques. Globalement, ce projet de thèse a démontré les applications potentielles des systèmes d'administration de médicaments dans divers domaines biologiques. Du point de vue de la formulation, la nanoprécipitation représente le procédé de fabrication de nanoparticules polymères le plus simple et le plus respectueux de l'environnement, facilement transposable en microfluidique.

References

1. Xiao, Y.; Chen, J.; Zhou, H.; Zeng, X.; Ruan, Z.; Pu, Z.; Jiang, X.; Matsui, A.; Zhu, L.; Amoozgar, Z.; et al. Combining P53 MRNA Nanotherapy with Immune Checkpoint Blockade Reprograms the Immune Microenvironment for Effective Cancer Therapy. *Nature Communications* **2022**, *13*, doi:10.1038/s41467-022-28279-8.
2. Nakamura, T.; Kawakami, K.; Nomura, M.; Sato, Y.; Hyodo, M.; Hatakeyama, H.; Hayakawa, Y.; Harashima, H. Combined Nano Cancer Immunotherapy Based on Immune Status in a Tumor Microenvironment. *J Control Release* **2022**, *345*, 200–213, doi:10.1016/j.jconrel.2022.03.026.
3. Parayath, N.N.; Hao, S.; Stephan, S.B.; Koehne, A.L.; Watson, C.E.; Stephan, M.T. Genetic in Situ Engineering of Myeloid Regulatory Cells Controls Inflammation in Autoimmunity. *J Control Release* **2021**, *339*, 553–561, doi:10.1016/j.jconrel.2021.08.040.
4. Rocha, C.V.; Gonçalves, V.; da Silva, M.C.; Bañobre-López, M.; Gallo, J. PLGA-Based Composites for Various Biomedical Applications. *International Journal of Molecular Sciences* **2022**, *23*, doi:10.3390/ijms23042034.
5. Cordt, C.; Meckel, T.; Geissler, A.; Biesalski, M. Entrapment of Hydrophobic Biocides into Cellulose Acetate Nanoparticles by Nanoprecipitation. *Nanomaterials (Basel)* **2020**, *10*, E2447, doi:10.3390/nano10122447.
6. Sun, Y.; Lee, R.J.; Meng, F.; Wang, G.; Zheng, X.; Dong, S.; Teng, L. Microfluidic Self-Assembly of High Cabazitaxel Loading Albumin Nanoparticles. *Nanoscale* **2020**, *12*, 16928–16933, doi:10.1039/C9NR10941B.
7. Desmaële, D.; Gref, R.; Couvreur, P. Squalenoylation: A Generic Platform for Nanoparticular Drug Delivery. *J Control Release* **2012**, *161*, 609–618, doi:10.1016/j.jconrel.2011.07.038.
8. Fessi, H.; Puisieux, F.; Devissaguet, J.Ph.; Ammoury, N.; Benita, S. Nanocapsule Formation by Interfacial Polymer Deposition Following Solvent Displacement. *International Journal of Pharmaceutics* **1989**, *55*, R1–R4, doi:10.1016/0378-5173(89)90281-0.
9. Sobot, D.; Mura, S.; Rouquette, M.; Vukosavljevic, B.; Cayre, F.; Buchy, E.; Pieters, G.; Garcia-Argote, S.; Windbergs, M.; Desmaële, D.; et al. Circulating Lipoproteins: A Trojan Horse Guiding Squalenoylated Drugs to LDL-Accumulating Cancer Cells. *Mol Ther* **2017**, *25*, 1596–1605, doi:10.1016/j.ymthe.2017.05.016.
10. Fabozzi, A.; Sala, F.D.; Gennaro, M. di; Solimando, N.; Pagliuca, M.; Borzacchiello, A. Polymer Based Nanoparticles for Biomedical Applications by Microfluidic Techniques: From Design to Biological Evaluation. *Polymer Chemistry* **2021**, *12*, 6667–6687, doi:10.1039/D1PY01077H.
11. Maeki, M.; Uno, S.; Niwa, A.; Okada, Y.; Tokeshi, M. Microfluidic Technologies and Devices for Lipid Nanoparticle-Based RNA Delivery. *Journal of Controlled Release* **2022**, *344*, 80–96, doi:10.1016/j.jconrel.2022.02.017.
12. Gimondi, S.; Guimarães, C.F.; Vieira, S.F.; Gonçalves, V.M.F.; Tiritan, M.E.; Reis, R.L.; Ferreira, H.; Neves, N.M. Microfluidic Mixing System for Precise PLGA-PEG Nanoparticles Size Control. *Nanomedicine* **2021**, *40*, 102482, doi:10.1016/j.nano.2021.102482.
13. Juban, G.; Saclier, M.; Yacoub-Youssef, H.; Kernou, A.; Arnold, L.; Boisson, C.; Ben Larbi, S.; Magnan, M.; Cuvellier, S.; Théret, M.; et al. AMPK Activation Regulates LTBP4-Dependent TGF-B1 Secretion by Pro-Inflammatory Macrophages and Controls Fibrosis in Duchenne Muscular Dystrophy. *Cell Rep* **2018**, *25*, 2163-2176.e6, doi:10.1016/j.celrep.2018.10.077.

14. Hammers, D.W.; Hart, C.C.; Matheny, M.K.; Wright, L.A.; Armellini, M.; Barton, E.R.; Sweeney, H.L. The D2.Mdx Mouse as a Preclinical Model of the Skeletal Muscle Pathology Associated with Duchenne Muscular Dystrophy. *Sci Rep* **2020**, *10*, 14070, doi:10.1038/s41598-020-70987-y.
15. Pochini, L.; Scalise, M.; Galluccio, M.; Indiveri, C. OCTN Cation Transporters in Health and Disease: Role as Drug Targets and Assay Development. *J Biomol Screen* **2013**, *18*, 851–867, doi:10.1177/1087057113493006.
16. Elias, D.R.; Poloukhtine, A.; Popik, V.; Tsourkas, A. Effect of Ligand Density, Receptor Density, and Nanoparticle Size on Cell Targeting. *Nanomedicine* **2013**, *9*, 194–201, doi:10.1016/j.nano.2012.05.015.

Sintesi sostanziale

Alcuni aspetti di farmacocinetica e farmacodinamica limitano l'applicazione clinica di numerose molecole terapeutiche. La nanomedicina si propone come una possibile strategia per migliorare l'efficacia terapeutica di sostanze farmacologicamente attive. Il termine "nanomedicina" si riferisce alla formulazione di nanosistemi, chiamati generalmente sistemi di rilascio di farmaci (*drug delivery systems* – DDSs). I DDSs sono stati largamente studiati per sviluppare approcci terapeutici più efficaci, con notevoli risultati nel trattamento dei tumori [1,2] e di malattie autoimmuni [3]. Uno dei maggiori problemi che si riscontra nella formulazione di sistemi di rilascio di farmaci è la possibile tossicità del veicolo. In questo contesto, l'acido poli(lattico-*co*-glicolico) (PLGA) e i derivati squalenici, come l'acido squalenico (SQ-COOH), sono tra i candidati per formulare dei DDSs, grazie alla loro biocompatibilità e biodegradabilità. In presenza di un mezzo acquoso, questi materiali hanno la capacità di auto-assemblarsi per formare delle nanoparticelle (NPs) dell'ordine dei nanometri. La preparazione delle NPs può avvenire mediante diversi metodi [4]. Il metodo della nanoprecipitazione è considerato un processo semplice, che viene prevalentemente utilizzato per incorporare farmaci idrofobici in matrici polimeriche [5]. Una soluzione organica di polimero e molecola terapeuticamente attiva viene aggiunta goccia a goccia nella fase acquosa, costituita da acqua oppure tampone acquoso. In questo modo le NPs si formano istantaneamente. Tuttavia, esistono diversi svantaggi nell'utilizzo di questo metodo per la produzione di NPs, come la variabilità tra campioni diversi, la mancanza di un preciso controllo sulle caratteristiche delle NPs e la difficoltà di una produzione in grandi volumi. Queste problematiche hanno rivolto l'interesse della ricerca scientifica allo sviluppo di innovativi metodi di produzione. Negli ultimi anni sono stati ottimizzati dei dispositivi su microscala per produrre NPs con un maggiore controllo delle caratteristiche chimico-fisiche del sistema [6]. Questo lavoro di tesi descrive la formulazione di DDSs a base di polimeri e lipidi per migliorare l'efficacia e diminuire la tossicità di molecole ad interesse terapeutico. Viene inoltre presentato uno studio comparativo che sottolinea l'importanza dei parametri e delle variabili di processo nel determinare le caratteristiche chimico-fisiche delle NPs. Le due molecole attive presentate in questo lavoro sono state selezionate considerando il loro possibile riposizionamento nelle applicazioni cliniche (*drug repurposing*).

La prima parte della tesi descrive una strategia formulativa per incorporare la pentamidina base libera (PTM-B) in NPs squaleniche. Lo SQ-COOH è stato selezionato come veicolo per la sua struttura chimica, che presenta un acido carbossilico terminale (pKa=4,5), carico negativamente a pH fisiologico. Inoltre, come molti derivati squalenici, anche lo SQ-COOH ha la capacità di auto-assemblarsi per formare delle sospensioni colloidali in mezzo acquoso [7]. La PTM-B

presenta due gruppi amidinici carichi positivamente (pKa=12), che instaurano dei legami ionici con il gruppo carbossilico dello SQ-COOH, formando una sospensione colloidale stabile. In questa parte di lavoro è stato possibile ottimizzare la capacità di carico del sistema, definita *drug loading* (DL). Le NPs sono state preparate con la tecnica della nanoprecipitazione [8], valutando l'impatto delle variabili formulative, come il rapporto molare SQ-COOH/PTM-B e il rapporto tra i volumi della fase organica e della fase acquosa, sulle caratteristiche del sistema. Uno studio di dinamica molecolare ha inoltre permesso di descrivere l'interazione tra PTM-B e SQ-COOH a differenti rapporti molari di SQ-COOH/PTM-B (3:1, 4:1 e 4,5:1). Dal momento che per i vari rapporti molari considerati le differenze chimico-fisiche delle NPs risultavano trascurabili, è stato selezionato il rapporto molare SQ-COOH/PTM-B 3:1 per massimizzare il DL della formulazione. L'effetto del rapporto tra i volumi di fase organica e fase acquosa (V_e/V_a) utilizzato per la formulazione delle NPs è stato studiato in relazione al diametro medio e al DL. Con un V_e/V_a di 0,2:1 le NPs presentano un diametro medio di circa 110 nm e un DL massimo del 19%. E' stato precedentemente dimostrato che i derivati squalenici sotto forma di NPs si associano *in vivo* alle lipoproteine a bassa densità (LDL) per analogia con il colesterolo, della cui sintesi lo squalene è intermedio endogeno [9]. Questo fenomeno consente un direzionamento indiretto da parte del derivato squalenico verso il recettore delle LDL (LDLR), che è overespresso sulla superficie di alcune cellule tumorali. Su queste basi, i test *in vitro* sono stati condotti su linee cellulari tumorali con diversi gradi di espressione del LDLR, dimostrando un'internalizzazione delle NPs mediata dallo stesso recettore. Basandosi sulle interazioni elettrostatiche tra farmaco e polimero, la PTM-B è stata incorporata anche in NPs di PLGA. La formulazione è stata ottimizzata testando diversi tipi di PLGA (50:50 e 75:25, rapporto acido lattico: acido glicolico) e diverse quantità di PTM-B: le sospensioni colloidali hanno mostrato un diametro medio di 120 nm e un potenziale zeta negativo di circa -25 mV. L'efficacia di incorporazione (EE) del farmaco nella matrice polimerica è risultata elevata e superiore all'80%. I metodi classici di formulazione delle NPs, tra cui la nanoprecipitazione, presentano delle difficoltà nella produzione su larga scala, poiché il processo di traslazione può determinare il cambiamento delle proprietà del nanosistema [10]. Per superare questi inconvenienti, nella formulazione di NPs è stata proposta la tecnologia della microfluidica, che permette di controllare meglio le caratteristiche chimico-fisiche della sospensione colloidale [11,12]. Con lo scopo di studiare l'impatto delle variabili di processo per una produzione su larga scala di NPs polimeriche, è stato effettuato uno studio comparativo tra la metodica classica di produzione e la microfluidica. Un derivato benzimidazolico, chiamato 991, è stato selezionato come farmaco idrofobico modello nella formulazione di NPs di PLGA mediante

nanoprecipitazione e microfluidica. Per traslare la preparazione delle NPs in microfluidica, sono stati impostati i parametri di *total flow rate* (TFR) and *flow rate ratio* (FRR): lavorando a TFR 12 mL/min e FRR 1:2 (rapporto fase organica/fase acquosa), le NPs caricate con 991 hanno mostrato un diametro medio di circa 80 nm, minore rispetto ai 170 nm ottenuti per nanoprecipitazione. Le preparazioni sono state dializzate per eliminare la frazione non incorporata di farmaco e determinare così l'EE e il DL. L'EE è risultata essere compresa tra 75% e 85%, rispettivamente per quelle prodotte in microfluidica e quelle ottenute mediante nanoprecipitazione, cui corrisponde un DL di 9-10%. La purificazione ha permesso di ottenere delle NPs in cui il farmaco è efficacemente incorporato nella matrice polimerica, confermato anche dal mancato *burst release* in 4 h in condizioni fisiologiche (PBS, pH 7,4). Tuttavia, le NPs preparate per microfluidica hanno dimostrato una minore stabilità a 4 °C rispetto a quelle preparate con la nanoprecipitazione classica. Probabilmente, il diametro medio inferiore ai 100 nm determina una minore concentrazione di coagulazione critica (*CCC*) e pertanto una destabilizzazione più rapida. La formulazione è stata convertita in forma solida mediante processo di liofilizzazione, utilizzando trealosio al 12% p/v come crioprotettore. Dopo liofilizzazione, le NPs risospese hanno mantenuto il loro iniziale diametro medio di circa 80 nm. Come detto, il passaggio dalla tecnica convenzionale di nanoprecipitazione alla microfluidica può determinare una modifica delle caratteristiche della formulazione. Pertanto, il processo di translazione in microfluidica delle NPs è stato ottimizzato utilizzando un disegno sperimentale (DoE), che permette di valutare l'influenza di FRR e della concentrazione sia del polimero sia di farmaco nella fase organica sull'EE e DL. EE e DL sono stati massimizzati per un'alta concentrazione di farmaco e una bassa concentrazione di polimero, portando alla conclusione che entrambi i valori sono largamente influenzati dall'FRR. I risultati dello studio comparativo sono utili per la progettazione futura di nanosistemi contenenti farmaci, passando dal metodo di produzione classico al processo di microfluidica.

La terza parte di questo progetto ha riguardato la valutazione biologica delle NPs-991. Il 991 è un potente attivatore della AMP-proteina chinasi (AMPK), coinvolta nella riduzione di infiammazione e fibrosi nella distrofia muscolare di Duchenne (DMD). L'attivazione di AMPK si traduce in una minore produzione del fattore di crescita trasformante-β ($TGF\beta_1$), una citochina pro-infiammatoria [13]. Tuttavia, l'applicabilità clinica del 991 è impedita dai suoi significativi effetti collaterali. I macrofagi fibrotici derivati dal midollo osseo (BMDMs) sono stati utilizzati per valutare l'attivazione di AMPK e, di conseguenza, la riduzione di $TGF\beta_1$. Si è osservato che le NPs vengono velocemente internalizzate dai macrofagi e portano ad una riduzione del $TGF\beta_1$ in presenza del 991, sia come farmaco libero sia caricato nelle NPs di

PLGA. La valutazione del comportamento del sistema *in vivo* è stato l'ultimo studio della valutazione biologica. Ci siamo concentrati sull'assorbimento di NPs di PLGA da parte del diaframma, considerato l'organo più rappresentativo per il suo modello infiammatorio e fibrotico [14]. Studi preliminari hanno permesso di valutare il profilo farmacocinetico delle NPs dopo la somministrazione endovenosa (i.v.) in un modello superiore di DMD (D2.mdx). Dopo 1 h è stato registrato un assorbimento del 10% delle NPs nel diaframma e nel muscolo gastrocnemio. Successivamente le NPs contenenti 991 sono state iniettate per i.v. per valutare la riduzione della fibrosi nei topi D2.mdx. Dopo tre settimane di trattamento è stata osservata una riduzione del 10% della fibrosi nel modello animale, un risultato promettente per il miglioramento dell'omeostasi muscolare *in vivo*.

L'ultima parte della tesi descrive lo sviluppo preliminare di una strategia di direzionamento attivo per aumentare il tropismo muscolare delle NPs. Data la presenza di recettori specifici sulle cellule muscolari, in particolare il trasportatore organico/cationico Na^+ 2 (OCTN2) [15], abbiamo selezionato la L-carnitina per direzionare le NPs di PLGA verso le cellule muscolari. A questo scopo è stata utilizzata la stearoil-L-carnitina (SC), in cui l'agente di *targeting* è stato legato all'acido stearico per favorire l'associazione con la matrice polimerica ed esporre la L-carnitina sulla superficie delle NPs. Due diverse concentrazioni di SC (5% e 10% p/p) sono state testate per ottimizzare la densità del ligando [16]. Le NPs risultano essere caratterizzate da un diametro medio inferiore a 100 nm per entrambe le percentuali di SC e da un potenziale zeta negativo intorno a -20 mV. La vitalità cellulare è stata valutata per le NPs con il 5% di SC sui mioblasti della linea cellulare C2C12. Un tempo di incubazione di 2 ore non ha mostrato alcuna variazione di vitalità nei campioni trattati con NPs direzionate rispetto al controllo. Tuttavia, dopo 24 ore di incubazione la vitalità delle cellule è diminuita significativamente. L'espressione del recettore OCTN2 su mioblasti e miotubi è stata valutata mediante microscopia confocale utilizzando un anticorpo anti-OCTN2. I miotubi hanno mostrato una maggiore espressione del recettore OCTN2 rispetto ai mioblasti. Questi dati preliminari dimostrano la possibilità di sviluppare una strategia di direzionamento attivo e migliorare il tropismo muscolare.

In conclusione, questo progetto di tesi ha confermato le potenziali applicazioni dei sistemi di *drug delivery* in diversi campi terapeutici. Da un punto di vista formulativo, lo studio ha permesso di valutare l'utilizzo della nanoprecipitazione in diverse condizioni sperimentali, confermandone l'utilità nella preparazione di NPs polimeriche e la sua applicabilità in microfluidica.

References

1. Xiao, Y.; Chen, J.; Zhou, H.; Zeng, X.; Ruan, Z.; Pu, Z.; Jiang, X.; Matsui, A.; Zhu, L.; Amoozgar, Z.; et al. Combining P53 MRNA Nanotherapy with Immune Checkpoint Blockade Reprograms the Immune Microenvironment for Effective Cancer Therapy. *Nature Communications* **2022**, *13*, doi:10.1038/s41467-022-28279-8.
2. Nakamura, T.; Kawakami, K.; Nomura, M.; Sato, Y.; Hyodo, M.; Hatakeyama, H.; Hayakawa, Y.; Harashima, H. Combined Nano Cancer Immunotherapy Based on Immune Status in a Tumor Microenvironment. *J Control Release* **2022**, *345*, 200–213, doi:10.1016/j.jconrel.2022.03.026.
3. Parayath, N.N.; Hao, S.; Stephan, S.B.; Koehne, A.L.; Watson, C.E.; Stephan, M.T. Genetic in Situ Engineering of Myeloid Regulatory Cells Controls Inflammation in Autoimmunity. *J Control Release* **2021**, *339*, 553–561, doi:10.1016/j.jconrel.2021.08.040.
4. Rocha, C.V.; Gonçalves, V.; da Silva, M.C.; Bañobre-López, M.; Gallo, J. PLGA-Based Composites for Various Biomedical Applications. *International Journal of Molecular Sciences* **2022**, *23*, doi:10.3390/ijms23042034.
5. Cordt, C.; Meckel, T.; Geissler, A.; Biesalski, M. Entrapment of Hydrophobic Biocides into Cellulose Acetate Nanoparticles by Nanoprecipitation. *Nanomaterials (Basel)* **2020**, *10*, E2447, doi:10.3390/nano10122447.
6. Sun, Y.; Lee, R.J.; Meng, F.; Wang, G.; Zheng, X.; Dong, S.; Teng, L. Microfluidic Self-Assembly of High Cabazitaxel Loading Albumin Nanoparticles. *Nanoscale* **2020**, *12*, 16928–16933, doi:10.1039/C9NR10941B.
7. Desmaële, D.; Gref, R.; Couvreur, P. Squalenoylation: A Generic Platform for Nanoparticular Drug Delivery. *J Control Release* **2012**, *161*, 609–618, doi:10.1016/j.jconrel.2011.07.038.
8. Fessi, H.; Puisieux, F.; Devissaguet, J.Ph.; Ammoury, N.; Benita, S. Nanocapsule Formation by Interfacial Polymer Deposition Following Solvent Displacement. *International Journal of Pharmaceutics* **1989**, *55*, R1–R4, doi:10.1016/0378-5173(89)90281-0.
9. Sobot, D.; Mura, S.; Rouquette, M.; Vukosavljevic, B.; Cayre, F.; Buchy, E.; Pieters, G.; Garcia-Argote, S.; Windbergs, M.; Desmaële, D.; et al. Circulating Lipoproteins: A Trojan Horse Guiding Squalenoylated Drugs to LDL-Accumulating Cancer Cells. *Mol Ther* **2017**, *25*, 1596–1605, doi:10.1016/j.ymthe.2017.05.016.
10. Fabozzi, A.; Sala, F.D.; Gennaro, M. di; Solimando, N.; Pagliuca, M.; Borzacchiello, A. Polymer Based Nanoparticles for Biomedical Applications by Microfluidic Techniques: From Design to Biological Evaluation. *Polymer Chemistry* **2021**, *12*, 6667–6687, doi:10.1039/D1PY01077H.
11. Maeki, M.; Uno, S.; Niwa, A.; Okada, Y.; Tokeshi, M. Microfluidic Technologies and Devices for Lipid Nanoparticle-Based RNA Delivery. *Journal of Controlled Release* **2022**, *344*, 80–96, doi:10.1016/j.jconrel.2022.02.017.
12. Gimondi, S.; Guimarães, C.F.; Vieira, S.F.; Gonçalves, V.M.F.; Tiritan, M.E.; Reis, R.L.; Ferreira, H.; Neves, N.M. Microfluidic Mixing System for Precise PLGA-PEG Nanoparticles Size Control. *Nanomedicine* **2021**, *40*, 102482, doi:10.1016/j.nano.2021.102482.
13. Juban, G.; Saclier, M.; Yacoub-Youssef, H.; Kernou, A.; Arnold, L.; Boisson, C.; Ben Larbi, S.; Magnan, M.; Cuvellier, S.; Théret, M.; et al. AMPK Activation Regulates LTBP4-Dependent TGF-B1 Secretion by Pro-Inflammatory Macrophages and Controls Fibrosis in Duchenne Muscular Dystrophy. *Cell Rep* **2018**, *25*, 2163-2176.e6, doi:10.1016/j.celrep.2018.10.077.

14. Hammers, D.W.; Hart, C.C.; Matheny, M.K.; Wright, L.A.; Armellini, M.; Barton, E.R.; Sweeney, H.L. The D2.Mdx Mouse as a Preclinical Model of the Skeletal Muscle Pathology Associated with Duchenne Muscular Dystrophy. *Sci Rep* **2020**, *10*, 14070, doi:10.1038/s41598-020-70987-y.
15. Pochini, L.; Scalise, M.; Galluccio, M.; Indiveri, C. OCTN Cation Transporters in Health and Disease: Role as Drug Targets and Assay Development. *J Biomol Screen* **2013**, *18*, 851–867, doi:10.1177/1087057113493006.
16. Elias, D.R.; Poloukhtine, A.; Popik, V.; Tsourkas, A. Effect of Ligand Density, Receptor Density, and Nanoparticle Size on Cell Targeting. *Nanomedicine* **2013**, *9*, 194–201, doi:10.1016/j.nano.2012.05.015.

Annexes

List of publications

- Bohr A, Tsapis N, **Andreana I**, Chamarat A, Foged C, Delomenie C, Noiray M, El Brahmi N, Majoral JP, Mignani S, Fattal E. Anti-Inflammatory effect of anti-TNF-α siRNA cationic phosphorus dendrimer nanocomplexes administered intranasally in a murine acute lung injury model. Biomacromolecules. 2017 Aug 14;18(8):2379-2388. doi: 10.1021/acs.biomac.7b00572. PMID: 28639789.
- Stella B, **Andreana I**, Zonari D, Arpicco S. Pentamidine-loaded lipid and polymer nanocarriers as tunable anticancer drug delivery systems. J Pharm Sci. 2020 Mar;109(3):1297-1302. doi: 10.1016/j.xphs.2019.11.011. PMID: 31751563.
- Bosca F, Foglietta F, Gimenez A, Canaparo R, Durando G, **Andreana I**, Barge A, Peira E, Arpicco S, Serpe L, Stella B. Exploiting lipid and polymer nanocarriers to improve the anticancer sonodynamic activity of chlorophyll. Pharmaceutics. 2020 Jun 30;12(7):605. doi: 10.3390/pharmaceutics12070605. PMID: 32629767; PMCID: PMC7408081.
- Bohr A, Tsapis N, Foged C, **Andreana I**, Yang M, Fattal E. Treatment of acute lung inflammation by pulmonary delivery of anti-TNF-α siRNA with PAMAM dendrimers in a murine model. Eur J Pharm Biopharm. 2020 Nov;156:114-120. doi: 10.1016/j.ejpb.2020.08.009. PMID: 32798665; PMCID: PMC7425770.
- **Andreana I**, Repellin M, Carton F, Kryza D, Briançon S, Chazaud B, Mounier R, Arpicco S, Malatesta M, Stella B, Lollo G. Nanomedicine for Gene Delivery and Drug Repurposing in the Treatment of Muscular Dystrophies. Pharmaceutics. 2021 Feb 19;13(2):278. doi: 10.3390/pharmaceutics13020278. PMID: 33669654; PMCID: PMC7922331.
- **Andreana I**, Bincoletto V, Milla P, Dosio F, Stella B, Arpicco S. Nanotechnological approaches for pentamidine delivery. Drug Deliv Transl Res. 2022 Feb 25:1–17. doi: 10.1007/s13346-022-01127-4. PMID: 35217992; PMCID: PMC8880300.
- Cannito S, Bincoletto V, Turato C, Pontisso P, Scupoli MT, Ailuno G, **Andreana I**, Stella B, Arpicco S, Bocca C. Hyaluronated and PEGylated liposomes as a potential drug-delivery strategy to specifically target liver cancer and inflammatory cells. Molecules. 2022 Feb 4;27(3):1062. doi: 10.3390/molecules27031062. PMID: 35164326; PMCID: PMC8840578.

List of communications

The work included in this thesis was presented during international and national conferences as poster or oral communications:

Poster presentations

- **Andreana I**, Gazzano E, Piatti G, Riganti C, Arpicco S, Stella B. (2019) "Self-assembled nanoparticles obtained by electrostatic interactions" 13th Annual Meeting A.It.U.N., Castelraimondo, 13th-14th June, n. 2, p. 29
- Bosca F, **Andreana I**, Barge A, Peira E, Serpe L, Arpicco S, Stella B. (2019) "Biocompatible chlorophyll-loaded nanovectors for anticancer therapy" 46th Annual Meeting & Exposition of the Controlled Release Society, Valencia - Spain, 21st - 24th July, n. 625
- **Andreana I**, Stella B, Arpicco S. (2019) "Pentamidine-loaded lipid and polymer nanocarriers as tunable anticancer drug delivery systems", CRS Italy Chapter Annual Workshop "Steering the clinical translation of delivery systems for drugs and health products", Catania - Italy, 7th - 9th November 2019, cited in Pignatello R, Matricardi P. Steering the clinical translation of delivery systems for drugs and health products. *Pharmaceutics*.2020;12(4). doi:10.3390/pharmaceutics12040350
- **Andreana I**, Costanzo M, Malatesta M, Bincoletto V, Arpicco S, Stella B. (2021) "Surface functionalization of PLGA nanoparticles to increase muscular tropism" CRS Virtual Annual Meeting, 25th - 29th July
- **Andreana I**, Juban G, Mounier R, Chazaud B, Arpicco S, Stella B, Kryza D, Lollo G. (2021) "Biodegradable nanoparticles loaded with novel anti-inflammatory drug to treat muscular dystrophies" SFNano, Angers - France, 6th - 8th December
- **Andreana I**, Bordes C, Chevalier Y, Arpicco S, Kryza D, Stella B, Lollo G. (2022) "Manufacturing translation of polymeric nanoparticles: from conventional batch to microfluidic process" ESCDD, Egmond aan zee - Holland, 13th – 15th April

Oral communications

- **Andreana I**, Gazzano E, Piatti G, Riganti C, Arpicco S, Stella B. (2020) "Self-assembled nanoparticles obtained by electrostatic interactions" 25th journée EDISS, 12th November
- **Andreana I**, Juban G, Mounier R, Chazaud B, Stella B, Kryza D, Lollo G. (2021) "PLGA-based nanoparticles as emerging delivery tool for AMPK activator molecules" Journées des Jeunes Chercheuses et Chercheurs, Lyon - France, 28th June and 2nd July

Conferences participations and seminars

1. CRS Italy Chapter Annual Workshop "Advances in Drug Delivery and Biomaterials: facts and vision", Padova, 18th-20th October 2018
2. Formulation Days 2019, Lyon, Université Claude Bernard Lyon1, 10th-11th January 2019
3. 13th Annual Meeting A.It.U.N., Castelraimondo, 13th-14th June 2019
4. Summer School 2019 'Emergence and Organization of Life', Bardonecchia, 20th-21th June 2019
5. 46th Annual Meeting & Exposition of the Controlled Release Society", Valencia, 21st-24th July 2019
6. Seminar "Organic Carbonates in chlorine-free chemistry: state of the art and future perspective", Torino, 1st February 2019
7. Seminar "Functionalized Polymeric Platform for drug Delivery: Versatile Synthesis and Miniaturized Formulation", Torino, 5th February 2019
8. 19th Advanced School in Pharmaceutical Technology, Soverato (CZ),09th- 12th September 2019
9. 2° SCI-Convegno Nazionale della Divisione di Tecnologia Farmaceutica, Soverato (CZ),12th- 13th September 2019
10. CRS Italy Chapter Annual Workshop "Steering the Clinical Translation of Delivery Systems for Drugs and Health Products", Catania, 7th-9th November 2019
11. School of Nanomedicine, Trieste, 11th-13th December 2019
12. MI-TO: a journey between nanomedicine and drug management, Milano-Torino, 13th- 14th February 2020
13. Virtual Annual Meeting: 2020 Vision for Global Impact, Controlled Release Society, Las Vegas, June 29th- July 2nd, 2020
14. 25th journée EDISS, Lyon, 12th November 2020
15. CRS BeNeLux & France Local Chapter, Virtual Local Chapter Meeting, 4th March 2021
16. Journées des Jeunes Chercheuses et Chercheurs, LAGEPP, Lyon, 28th June and 2nd July 2021
17. CRS Virtual Annual Meeting, Controlled Release Society, 25th -29th July 2021
18. SFNano, Angers, 6th-8th December 2021
19. European Symposium of Controlled Drug Delivery (ESCDD), Egmond aan Zee, The Netherlands, 12th – 15th April 2022